University College London

Novel Genetic Causes of Cerebral and Systemic Vasculopathies

Annette Ai Lin Keylock

Thesis submitted for PhD

Infection, Inflammation and Rheumatology Section,

UCL GOS Institute of Child Health

I, Annette Ai Lin Keylock confirm that the work presented in this thesis is my own. Where information has been derived from other sources, I confirm that this has been indicated in the thesis.

Acknowledgements

I would like to thank my supervisors: Dr Despina Eleftheriou, Professor Paul Brogan and Professor Pete Scambler. Thank you Despina for being such a dedicated, tireless and all round amazing supervisor. You have been supportive, helpful and always responded to my emails regardless of how small the question was. I really appreciate everything you have done for me these past 4 or so years. Thank you Paul for your support, encouragement and enthusiasm. Your positivity and optimism was always much appreciated. Thank you Pete for chatting to me and giving me advice throughout my PhD. I would like to acknowledge the wonderful friends I have made at ICH: Ying Hong, Ebun Omoyinmi, Sira Nanthapisal, Claire Murphy/Walker, Elena Moraitis, Charris Papadopoulou and Sonia Melo-Gomes. Thank you Ying for being my lifesaver in so many ways, you are a truly special person and you underestimate how much you mean to so many people. Thank you for listening to me, advising me, keeping me company and being my friend. I honestly could not have done this PhD without your love and support. Ebun, thank you also for your expertise and love throughout this degree. You always listened to my complaints and rants and your smile and cheery disposition are beautiful qualities. Thank you Sira and Claire for being you, I definitely could not have got through this without you. You two are some of the most kind, generous, funny and warm people I know. Thank you for looking after me so well through the lab work, writing up and both pregnancies. I miss you both. Lastly, I would like to thank my family. Thank you to my in-laws for all the hours of babysitting and walks to the park over the past year. They were invaluable. Thank you to my parents who have been so supportive throughout the whole process. Mum and Dad you have always been there to talk me through things, provide financial, mental and emotional support as well as giving up so much of your time to look after Joel. I could not have completed this PhD so easily without you. My final thanks goes to my husband, Daniel. There are not really words to express how much you have done for me throughout this degree. Suffice to say you are my best friend and I love you.

Abstract

Vasculopathies are a varied group of disorders that affect the vascular tree resulting in arterial stenosis or dilatation causing multi-organ ischaemia and significant cardiac and cerebral circulation complications. Commonly, vasculopathies present in infancy and segregate within families so a genetic cause is often suspected but not always identified by the current routinely available genetic tests in the UK National Health Service (NHS). Due to the overlapping phenotypes of these disorders genetic sequencing is required for accurate diagnosis and appropriate clinical intervention.

In this thesis, a cohort of children with cerebral and systemic vasculopathies was subject to next-generation genetic sequencing. Several discoveries were made and various families are discussed herein. Firstly, a novel heterozygous mutation in *MYH11*, a gene affecting smooth muscle myosin heavy chain, was identified in a child with a moyamoya-like cerebrovascular disease and renal artery stenosis. This expanded the vasculopathic phenotype associated with *MYH11,* which previously was associated with familial aortopathy. Secondly, multiple members of three families diagnosed with a moyamoya arteriopathy were studied and were all found to have heterozygous mutations in *c-CBL*, an E3 ubiquitin ligase that down regulates various receptor tyrosine kinases. Detailed *in vitro* functional expression studies were undertaken in the patients with mutations in *c-CBL* showing impaired CBL-mediated degradation of cell-surface receptors in a dominant negative fashion. These results were compatible with dysregulated intracellular signaling through RAS. Lastly, three families with systemic vasculopathies associated with heterozygous mutations in *RNF213* were also studied. This protein possesses both ubiquitin ligase and ATPase activity and adversely affects endothelial cell function. For the first time I showed that heterozygous mutations in *RNF213* cause a vasculopathy that is not confined to the cerebral circulation.

Impact statement

The observations I made during this PhD project suggest several new genetic-phenotypic associations regarding vasculopathic disorders and a novel mechanism for the aetiopathogenesis of moyamoya arteriopathy. The primary beneficiaries of this project will be patients with early onset cerebral and systemic vasculopathies. Commonly, vasculopathies present in infancy and segregate within families so a genetic cause is often suspected but not always identified by the current routinely available genetic tests in the UK National Health Service (NHS). Due to the overlapping phenotypes of these disorders genetic sequencing is required for accurate diagnosis and appropriate clinical intervention.

The major way in which patients with this disease will benefit from this study are summarised below:

(i) Highlighting the need for a broader than previously suggested vascular surveillance in patients with mutations in *MYH11* to also include the cerebrovascular circulation. In addition, patients with established *MYH11* mutations should be screened for cerebrovascular involvement and vascular surveillance should extend beyond the aorta. In this study, I expanded the phenotype associated with heterozygous mutations in *MYH11* to include cerebrovascular disease similar to moyamoya arteriopathy. Up until this point *MYH11* has been solely associated with familial thoracic aortic aneurysm.

(ii) Understanding the pathways involved in moyamoya arteriopathy development. I identified a number of *c-CBL* germline mutations in several patients diagnosed with a cerebrovascular disease similar to a moyamoya arteriopathy. I started to delineate the mechanism behind how these mutations could contribute to the observed phenotype. I have informed future research on the fact that the occlusive vasculopathic phenotype of moyamoya arteriopathy may be the result of aberrant receptor tyrosine kinase signaling due to reduced E3 ubiquitin ligase activity of c-CBL which provides interesting clues for

the underlying pathophysiology of the disease in addition to possible therapeutic targets. My findings also provide evidence that children with arterial ischaemic stroke and vasculopathy should be screened for mutations in *c-CBL* particularly those with early onset moyamoya arteriopathy.

(iii) Identifying the potential need for patients with *RNF213* mutations who have early onset moyamoya arteriopathy to have broad vascular imaging to look for other vascular bed involvement.

Some of the data generated in this PhD has been publicised through open access peer review journals whilst the remainder is soon to be publicised hence contributing to significant knowledge enhancement and scientific advancement about the genetic causes of cerebral and systemic vasculopathies for academic beneficiaries in the field. This project also contributes to worldwide academic advancement to address issues of importance such as the pathogenesis of vasculopathic syndromes. Lastly, this PhD fellowship enabled my training as a highly skilled researcher and facilitated my academic career progress. I have developed expertise and knowledge in this multidisciplinary area and collaborative environment. My project also contributes towards the health of the rheumatology/neurology academic discipline with publications and presentations.

Abbreviations

AAV	ANCA associated vasculitis
ACA	Anterior cerebral artery
ACTA2	Actin alpha 2
ADA2	Adenosine deaminase 2
AGS	Aicardi-Goutières syndrome
ANCA	Antineutrophil cytoplasmic antibody
BCA	Bicinochoninic acid
CAD	Coronary artery disease
CADASIL	Cerebral Autosomal-Dominant Arteriopathy with Subcortical Infarcts and Leukoencephalopathy
CARASIL	Cerebral Autosomal-Recessive Arteriopathy with Subcortical Infarcts and Leukoencephalopathy
CANDLE	*C*hronic *a*typical *n*eutrophilic *d*ermatosis with *l*ipodystrophy and *e*levated temperature
c-CBL	Casitas B-lineage lymphoma
CECR1	Cat eye syndrome chromosome region, candidate 1
CGH	Comparative genomic hybridization
cPAN	Cutaneous polyarteritis nodosa
CSF	Cerebral spinal fluid
CT	Computed tomography
CTA	Computed tomography angiography
DADA2	Deficiency of adenosine deaminase 2
dd	Double distilled
DMEM	Dulbecco's modified eagle medium
DNA	Deoxyribnucleic acid
ECIC	Extra-cranial to intra-cranial
EDS	Ehlers-Danlos syndrome
EGFR	Epidermal growth factor receptor
EGPA	Eosinophilic granulomatosis with polyangiitis
EDTA	Ethylendiaminetetraacetic acid
ENT	Ear, nose and throat
EULAR	European league against rheumatism
FACS	Fluorescence-activated cell sorting
FBS	Foetal bovine serum
gDNA	Genomic DNA
GOSH	Great Ormond Street Hospital for Children NHS Foundation
GRB2	Growth factor receptor-bound protein 2
GPA	Granulomatosis with polyangiitis
GWAS	Genome wide association study
HDFC	Human dermal fibroblast cell
HS	High sensitivity
HSP	Henoch-Schönlein purpura
HUVEC	Human umbilical vein endothelial cell
ICA	Internal carotid artery
Ig	Immunoglobulin
IHC	In-house control
JAK	Janus kinase
JMML	Juvenile myelomonocytic leukeamia
LDS	Loeys-Dietz syndrome
KD	Kawasaki Disease

MAPK	Mitogen activated protein kinase
MCA	Middle cerebral artery
MHC	Major histocompatibility
MMD	Moyamoya disease
MPA	Microscopic polyangiitis
MRA	Magnetic resonance angiogram
MRI	Magnetic resonance imaging
MYH11	Smooth muscle myosin heavy chain 11
NF1	Neurofibromatosis type 1
NGS	Next-generation sequencing
NO	Nitric oxide
OR	Odds ratio
PAEC	Porcine aortic endothelial cell
PAN	Polyarteritis nodosa
PBMC	Peripheral blood mononuclear cell
PDA	Patent ductus arteriosus
PDGF	Platelet-derived growth factor
PDGFR	Platelet-derived growth factor receptor
PFA	Paraformaldehyde
PLCγ1	Phospholipase Cγ1
P-MAPK	Phosphorylated MAPK
PRES	Paediatric Rheumatology European Society
PRINTO	Paediatric Rheumatology International Trials Organisation
PSV	Primary systemic vasculitis
qPCR	Quantitative polymerase chain reaction
RIPA	Radioimmunoprecipitation assay
RTK	Receptor tyrosine kinase
SAgs	Superantigens
SAVI	STING-associated vasculitis of infancy
sGC	Soluble guanylate cyclase
SM-MHC	Smooth muscle myosin heavy chain
SMC	Smooth muscle cell
SNV	Single nucleotide variant
STING	Stimulator of interferon genes
TA	Takayasu arteritis
TAAD	Thoracic aortic aneurysm and dissection
TGFβ2	Type II transforming growth factor β
TGFβR2	Type II transforming growth factor β receptor
TICA	Terminal internal carotid artery
TKB	Tyrosine kinase binding
Ub	Ubiquitin
VEGFR-2	Vascular endothelial growth factor receptor 2
VSMC	Vascular smooth muscle cell
WES	Whole exome sequencing
WGS	Whole genome sequencing
WR	Working reagent

Table of Contents

Acknowledgements **3**

Abstract **4**

Impact statement **5**

Abbreviations **7**

Table of Contents **9**

List of tables **16**

Table of figures **18**

Chapter 1 Introduction **22**

1.1 Vasculopathy **22**

1.1.1 Inflammatory vasculopathy 22

1.1.2 Aetiopathogenesis of primary systemic vasculitis 28

1.1.3 Non-inflammatory vasculopathy 33

1.1.4 Vasculopathies with predominant aortic involvement 35

1.1.5 Cerebral arteriopathies 39

1.2 Discovering novel genetic causes of vasculopathies **45**

1.2.1 Next-generation sequencing 46

1.3 Summary **49**

1.4 Hypothesis **49**

Chapter 2 Materials and General Methods **51**

2.1 Subjects **51**

2.1.1 Patients 51

2.1.2 Healthy controls 52

2.2 Reagents for blood collection **52**

2.3 Tissue culture media **52**

2.4 Tissue culture reagents **53**

2.5 Sample collection **53**

2.6 DNA extraction **53**

2.6.1 DNA extraction from whole blood 53

2.6.2 DNA extraction from saliva 54

2.7 Nucleic acid quantification **55**

2.8 Preparation of peripheral blood mononuclear cells (PBMCs) **55**

2.8.1 Counting of cells 55

2.9 Other primary human cells **56**

2.10 Freezing and thawing of cells **56**

2.11 Passaging, plating and harvesting of cells **56**

2.12 RNA extraction from peripheral mononuclear blood cells and human umbilical vein endothelial cells **57**

2.13 cDNA synthesis **57**

2.14 Quantitative polymerase chain reaction (qPCR) **58**

2.15 Sanger sequencing **59**

2.15.1 Primer design 59

2.15.2 Amplification of DNA 59

2.15.3 Sequencing of DNA 61

2.15.4 DNA fragment size quantitation 62

2.16 Whole exome sequencing 62

2.16.1 DNA quantification and normalisation 62

2.16.2 Whole exome library preparation 62

2.16.3 Quantitation and sizing of whole exome libraries 63

2.16.4 Sequencing of whole exome libraries 64

2.16.5 *In silico* analysis 65

2.17 Protein extraction 71

2.18 Protein quantification 71

2.19 Western blotting 72

2.20 Fluorescence-activated cell sorting (FACS) 75

2.20.1 Analysis 75

2.21 Statistical analysis 76

Chapter 3 Moyamoya-like cerebrovascular disease associated with a novel mutation in *MYH11* 77

3.1 Summary 77

3.2 Introduction 77

3.3 Family tree for family A 78

3.4 Clinical presentation **79**

3.5 Identifying a causal allele: Whole Exome Sequencing **82**

3.5.1 Verification of candidate gene variants 82

3.6 Discussion **85**

3.7 Conclusion **89**

Chapter 4 Moyamoya-like cerebrovascular disease associated with heterozygous mutations in *c-CBL* **90**

4.1 Summary **90**

4.2 Introduction **91**

4.3 c-CBL function and structure **91**

4.4 Ubiquitin E3 ligase mechanism **93**

4.5 c-CBL and regulation of EGFR and PDGFR **95**

4.6 EGFR and induction of the Ras-Raf-mitogen activated protein kinase pathway **97**

4.7 c-CBL and regulation of PLCγ1 ..... **98**

4.8 Family tree for family B **98**

4.9 Clinical presentation of B-II-3 ..... **99**

4.10 Family tree for family C **102**

4.11 Clinical presentation of C-III-2 ..... **102**

4.12 Family tree for family D **108**

4.13 Clinical presentation of D-II-6 ..... **108**

4.14 Methods **111**

4.14.1 Human dermal fibroblast cell transdifferentiation 111

4.14.2 siRNA transfection in human umbilical vein endothelial cells 111

4.14.3 Cell stimulation 112

4.14.4 Immunoprecipitation 112

4.14.5 Ubiquitination 112

4.14.6 Vasculogenesis assay 113

4.14.7 FACS analysis of EGFR, MAPK and phosphorylated-MAPK expression in PBMCs, HUVECs and HDFCs 114

4.14.8 Analysis of FACS assays to explore the RAS signaling pathway 116

4.15 Identifying a causal allele: Whole Exome Sequencing 119

4.15.1 Verification of candidate gene variants 119

4.16 Effect of p.370_371del *c-CBL* variant on protein and RNA levels 124

4.16.1 Protein expression of wild-type c-CBL 124

4.16.2 c-CBL variant does not affect protein or mRNA expression levels in B-II-3. 126

4.17 Functional effect of p.370_371del *c-CBL* variant in PBMCs 128

4.17.1 Reduced EGF-induced EGFR degradation 128

4.17.2 No detectable ubiquitination activity after EGF stimulation 131

4.18 Functional effect of siRNA *c-CBL* in HUVECs 132

4.19 Additional patients 137

4.20 Functional effect of *c-CBL* mutations in HDFCs and SMC-myofibroblasts 138

4.20.1 Sustained PDGF-induced activation of the MAPK pathway....138

4.21 Discussion....141

4.22 Conclusion....145

Chapter 5 Systemic and cerebral vasculopathy associated with heterozygous mutations in *RNF213*....147

5.1 Summary....147

5.2 Introduction....147

5.3 Family tree for family E....148

5.4 E-III-2 clinical presentation....148

5.5 Family tree for family F....149

5.6 F-II-1 clinical presentation....150

5.7 Family tree for family G....151

5.8 G-II-1 clinical presentation....151

5.9 Identifying a causal allele: Whole Exome Sequencing....152

5.9.1 E-III-2....152

5.9.2 F-II-1....153

5.9.3 G-II-1....154

5.10 Discussion....154

5.11 Conclusion....157

Chapter 6 General discussion....158

6.1 Future work....160

6.2 Publications 161

References 162

Appendix 194

Appendix 1 Stroke protocol investigations 194

Appendix 2 VIP2 gene list 196

List of tables

Table 1-1 Childhood vasculitis subtype categorized by vessel size based on Paediatric Rheumatology European Society (PRES)/European League Against Rheumatism (EULAR)/Paediatric Rheumatology International Trials Organization (PRINTO) criteria. (Ruperto et al., 2010, Ozen et al., 2006, Ozen et al., 2010) 24

Table 1-2 Monogenic causes of non-inflammatory vasculopathies.....33

Table 2-1 QuantiTect primer assays for qPCR. 58

Table 2-2 Generic qPCR program using QuantiTect primers.....59

Table 2-3 Parameters specified for design in Exon Primer.....60

Table 2-4 Touchdown PCR program, 62°C to 57°C. 60

Table 2-5 Generic PCR program for FastStart™ PCR Master (Roche). 61

Table 2-6 Sequencing PCR thermocycler program. 61

Table 2-7 Candidate gene list for vasculopathies and monogenic vasculitides. ..69

Table 2-8 Recipe for RIPA buffer.....71

Table 2-9 Recipe for 1 x 7.5% and 12.5% running gel and 1 x 4% stacking gel for western blotting. 73

Table 2-10 Recipe for 5x SDS loading buffer. 73

Table 2-11 Recipe for 10x running buffer. 73

Table 2-12 Recipe for 10x transfer buffer.....73

Table 2-13 Dilution factors for antibodies used for western blots.....74

Table 2-14 PBAC recipe 75

Table 3-1 Primer sequences used for Sanger sequencing. 83

Table 4-1 Ubiquitylation assay reagents 113

Table 4-2 FACS antibodies used to examine the RAS pathway in different cell types. 115

Table 4-3 Primer sequences used for Sanger sequencing. 119

Table 4-4 Adjusted protein expression of c-CBL relative to actin in EBV transformed B cells, jurkat cells and human dermal fibroblast cells. 125

Table 4-5 Adjusted protein expression of c-CBL relative to actin. 127

Table 4-6 Adjusted protein expression of ubiquitinated EGFR relative to c-CBL. 132

Table 5-1 Primer sequences used for Sanger sequencing 153

Table of figures

Figure 2-1 Per base sequence quality output from FastQC for a proband from one of the families studied in this thesis. This graph shows the read quality for each base pair position within the read. Acceptable read quality score ≥20; reads<20 are trimmed. 67

Figure 2-2 Profile peaks generated by ImageJ to determine western blot band density. 74

Figure 3-1 Family tree for family A. 78

Figure 3-2 Brain Magnetic resonance imaging (MRI) for index case of family A. 80

Figure 3-3 Catheter and visceral digital subtraction angiography for index case of family A. 81

Figure 3-4 Sanger sequencing chromatogram for the parents (A-II-8 and A-II-9), proband (A-III-3) and a sibling (A-III-1). 84

Figure 4-1 The domain structure of c-CBL. Adapted from references (Schmidt and Dikic, 2005, Polo, 2012). 93

Figure 4-2 c-CBL interacts with many different signaling proteins. Adapted from reference (Thien and Langdon, 2001). 95

Figure 4-3 EGFR downregulation via c-CBL mediated ubiquitination. 96

Figure 4-4 Schematic representation of MAPK/ERK signaling pathway. Adapted from reference (Carlomagno and Chiariello, 2014). 97

Figure 4-5 c-CBL and PLCγ1 activation by VEGFR2 and c-CBL mediated ubiquitination of PLCγ1 and involvement of c-CBL in angiogenesis. Adapted from reference (Rahimi, 2009). 98

Figure 4-6 Family tree for family B 99

Figure 4-7 Brain magnetic resonance imaging (MRI) and cerebral catheter angiography images for B-II-3. 101

Figure 4-8 Family tree for family C 102

Figure 4-9 Brain MRI and catheter cerebral angiography images of the cerebral circulation for C-III-2 during initial presentation. 104

Figure 4-10 Follow up brain MRI for C-III-2. 105

Figure 4-11 Brain MRI and catheter angiography of the cerebral circulation for C-III-1. 106

Figure 4-12 Brain MRI and MRA images for C-II-2. 107

Figure 4-13 Family tree for family D 108

Figure 4-14 Brain MRI and catheter angiography of the cerebra circulation images for D-II-6. 110

Figure 4-15 Human umbilical vein endothelial cell (HUVEC) capillary network (tubule) formation on matrigel. 114

Figure 4-16 Flow diagram of staining method for PBMCs, HUVECs and transformed HDFCs for FACS assays to explore the RAS signaling pathway. 116

Figure 4-17 Flow cytometry gating strategy for monocyte EGFR and phosphorylated-MAPK staining. 117

Figure 4-18 Flow cytometry gating strategy for phosphorylated-PLCγ1 staining on HUVECs. 118

Figure 4-19 Flow cytometry gating strategy for phosphorylated-MAPK staining on HDFCs. 118

Figure 4-20 Sanger sequencing chromatogram of MYH11 for the parents (B-I-1 and B-I-2) and proband (B-II-3) of family B. 121

Figure 4-21 Sanger sequencing chromatogram of COL5A2 for the parents (B-I-1 and B-I-2) and proband (B-II-3) of family B. 122

Figure 4-22 Sanger sequencing chromatogram of c-CBL for the parents (B-I-1 and B-I-2) and proband (B-II-3) of family B. 123

Figure 4-23 Sanger sequencing chromatogram of c-CBL for the parents (B-I-1 and B-I-2) and proband (B-II-3) of family B. 124

Figure 4-24 c-CBL protein expression. 125

Figure 4-25 c-CBL protein expression in control and B-II-3 PBMCs. 126

Figure 4-26 c-CBL mRNA expression in PBMCs from B-II-3 and healthy controls. 127

Figure 4-27 Fold change in relative EGFR expression in permeabilised PBMCs from B-II-3 and healthy controls. 129

Figure 4-28 Fold change in relative phosphorylated-MAPK expression in permeabilised PBMCs from B-II-3 and healthy controls. 130

Figure 4-29 Ubiquitination assay using PBMCs from B-I-1 (Father) and B-II-3 (Proband). 131

Figure 4-30 c-CBL mRNA expression in HUVECs transfected with lipofectamine, SCR c-CBL siRNA and c-Cbl siRNA. 133

Figure 4-31 Fold change in relative phosphorylated-PLCγ1 expression in siRNA c-CBL transfected HUVECs. HUVECs were transfected with siRNA targeting c-CBL or a negative control (SCR). 135

Figure 4-32 siRNA c-CBL HUVEC tubule formation using a matrigel assay. . 136

Figure 4-33 Human umbilical vein endothelial cell (HUVEC) capillary network (tubule) formation on matrigel for SCR c-CBL siRNA and c-CBL siRNA transfected HUVECs. 136

Figure 4-34 Agarose gel image of amplified c-CBL cDNA. 137

Figure 4-35 Relative expression of ACTA2 in HDFCs and SMC-myofibroblasts derived from B-II-3 patient. 138

Figure 4-36 Fold change in relative phosphorylated-MAPK expression in B-II-3, C-III-1 and control HDFCs. 140

Figure 4-37 Phosphorylated-MAPK expression in B-II-3, C-III-1, C-III-2 and control SMC-myofibroblasts. 141

Figure 5-1 Family tree for family E 148

Figure 5-2 Family tree for family F. 150

Figure 5-3 Family tree for family G. 151

Figure 5-4 Mutation in RNF213 identified by VIP targeted gene panel and confirmed by Sanger sequencing. Adapted from reference (Omoyinmi et al., 2017) 152

Figure 5-5 Sanger sequencing chromatogram of RNF213 for the proband (F-II-1). 154

Figure 5-6 The domain structure of RNF213. Adapted from reference (Zhou et al., 2016). 157

Chapter 1 Introduction

1.1 Vasculopathy

The term vasculopathy is a general term to describe any pathology that affects the vascular tree (Berlit, 1994). Vasculopathies often result in structural vessel wall changes such as stenosis, and/or dilatation, that may cause impaired blood flow and, therefore, ischaemia to major organs (Markovic, 2012). Clinical consequences may include myocardial infarction, ischaemic strokes, arterial hypertension, cutaneous lesions, and renal and intestinal failure (Berlit, 1994). These conditions are therefore associated with significant morbidity and mortality (Hoffman and Calabrese, 2014). In terms of aetiopathogenesis, vasculopathies can be divided into two broad categories: inflammatory and non-inflammatory and can affect both children and adults.

1.1.1 Inflammatory vasculopathy

Inflammatory vasculopathies, otherwise known as vasculitides, present with a broad spectrum of clinical features and usually affect more than one organ system (Hoffman and Calabrese, 2014). The clinical presentation may be affected by the size of the affected blood vessel and the organ system(s) involved (Waller et al., 2013). The inflammatory process targets blood vessels with histopathologic evidence of mononuclear and/or neutrophilic infiltrate, which can lead to vessel wall destruction, thrombosis, tissue ischaemia and, ultimately, organ failure and/or death in severe cases (Carlson and Chen, 2006). In addition to vascular inflammation there is usually, but not invariably, evidence of systemic inflammation (Carlson and Chen, 2007). Vasculitis can be classified as either primary or secondary depending on its developmental history (Suresh, 2006). Secondary vasculitis, as the name suggests, occurs secondary to other upstream processes such as infection, drug exposure or malignancy (Carlson and Chen, 2006). Primary vasculitis, on the other hand, is not associated with such factors and is usually regarded as a primary autoimmune and/or autoinflammatory condition.

Excluding the fairly common vasculitides such as Henoch-Schönlein Purpura (HSP) and Kawasaki Disease (KD), the majority of the primary vasculitic syndromes are rare in children. Classification criteria for childhood vasculitis have, until recently, been based on modified adult classification criteria (Waller et al., 2013, Ozen et al., 2010, Ruperto et al., 2010, Ozen et al., 2006). It should be noted that these criteria are not the same as diagnostic criteria. Classification criteria are standardized definitions primarily intended to create well-defined, relatively homogenous cohorts for clinical research. The current classification criteria for vasculitides in children are based on the Paediatric Rheumatology European Society (PRES)/European League Against Rheumatism (EULAR)/Paediatric Rheumatology International Trials Organization (PRINTO) criteria (Ozen et al., 2010, Ruperto et al., 2010) which, in line with adult classification criteria, use vessel size as the distinguishing feature (Ozen et al., 2006) (Table 1-1). The classification criteria for paediatric vasculitides were first proposed in 2005 (Ozen et al., 2006) and modified and validated, in 2008, using an international web-based registry (Ozen et al., 2010). Classification criteria for KD were not included, as they were not validated in the aforementioned study (Ozen et al., 2010). Instead, the American Heart Association diagnostic criteria are commonly used in clinical studies of KD (McCrindle et al., 2017). It should be noted that the PRES/EULAR/PRINTO criteria did not review certain genetic vasculitides that have been subsequently identified such as deficiency of adenosine deaminase type 2 (DADA2) (Ozen, 2017).

The subtypes of vasculitis are described in more detail below.

Table 1-1 Childhood vasculitis subtype categorized by vessel size based on Paediatric Rheumatology European Society (PRES)/European League Against Rheumatism (EULAR)/Paediatric Rheumatology International Trials Organization (PRINTO) criteria. *(Ruperto et al., 2010, Ozen et al., 2006, Ozen et al., 2010)*

Vessel size	Vasculitis subtype
Large	Takayasu arteritis
Medium	Childhood polyarteritis nodosa
	Cutaneous polyarteritis nodosa
	Kawasaki disease
Small (Granulomatous)	Granulomatosis with polyangiitis (formerly known as Wegener's granulomatosis)
	Eosinophilic granulomatosis with polyangiitis (formerly known as Churg Strauss)
Small	Microscopic polyangiitis
(Non-granulomatous)	Henoch-Schönlein purpura
	Cutaneous leucocytoclastic vasculitis
	Hypocomplementaemic urticarial vasculitis
Other	Behçet's disease
	Vasculitis secondary to infection, malignancies, and drugs, including hypersensitivity vasculitis
	Isolated vasculitis of the central nervous system
	Cogan syndrome
	Unclassified vasculitis

1.1.1.1 Henoch-Schönlein purpura or IgA vasculitis

Henoch-Schönlein purpura (HSP), also referred to as IgA vasculitis, is a small vessel vasculitis with immunoglobulin (Ig) A-dominant immune deposits (Jennette et al., 1994). Classification criteria are: palpable purpura with a lower limb predominance and at least 1 of the following 4: diffuse abdominal pain; biopsy showing IgA deposition; arthritis and/or arthralgia; haematuria and/or proteinuria. Patients may develop glomerulonephritis, gastrointestinal haemorrhage and abdominal pain (Punnoose et al., 2012, Brogan and Eleftheriou, 2017). It is the most common vasculitis in children under 17 years of

age affecting 13-20 per 100,000 (Yang et al., 2005, Gardner-Medwin et al., 2002). Gastrointestinal involvement accounts for early morbidity whilst renal involvement results in morbidity later on as well as being the important determinant of a poor outcome (Eleftheriou et al., 2015a).

1.1.1.2 Antineutrophil cytoplasmic autoantibody associated vasculitides

Antineutrophil cytoplasmic antibody (ANCA)-associated vasculitis (AAV) include the following diseases: granulomatosis with polyangiitis (GPA), microscopic polyangiitis (MPA) and eosinophilic granulomatosis with polyangiitis (EGPA) (Brogan et al., 2010).

GPA is a necrotizing vasculitis characterised by granulomatous inflammation of the respiratory tract and glomerulonephritis (Brogan et al., 2010). The median age of disease onset is 14 years. All organs can be affected with the most frequently involved systems being ear, nose and throat (ENT); respiratory; renal; musculoskeletal; nervous; eyes; and skin (Belostotsky et al., 2002). Clinically it can be useful to think of GPA as having two presentations: a mainly granulomatous form, which is localized and chronic; and a florid, acute small vessel vasculitic form with patients susceptible to severe pulmonary haemorrhage and/or rapidly progressive vasculitis. These two forms can co-exist or develop sequentially.

MPA is a systemic, necrotizing vasculitis that affects the small vessels without clinical or pathological evidence of granulomatous inflammation. A number of systems are involved in the majority of patients: renal (75%), gastrointestinal (58%), musculoskeletal (52%) and cutaneous (52%) (Cabral et al., 2016). Other commonly observed features include rapidly progressive glomerulonephritis (94%) and pulmonary capillaritis (44%) (Jennette et al., 1994, Cabral et al., 2016). Now a recognised and distinct disease, MPA was initially thought of as the ‘microscopic’ form of childhood polyarteritis nodosa (PAN) with several symptoms resembling those of PAN (Jennette et al., 1994). The mean age of disease onset is 10.8 years with a predominance of patients being female (73%) (Cabral et al., 2016). This is in contrast to adult populations where the majority of patients are male (55-60%) (Mohammad et al., 2007, Guillevin et al., 1999).

EGPA is defined as an eosinophil-rich granulomatous inflammation involving the respiratory tract and a necrotizing vasculitis affecting small and medium-sized vessels (Jennette et al., 1994). Most patients have significant peripheral blood eosinophilia and asthma as well as the involvement of various other systems: renal (83%), pulmonary (74%), upper airways/ENT (70%) and musculoskeletal (65%) (Zwerina et al., 2009, Cabral et al., 2016). A recent case series from the UK indicated that the presence of cardiomyopathy is associated with increased mortality (Zwerina et al., 2009).

1.1.1.3 Kawasaki disease

Kawasaki disease (KD) is an acute, self-limiting vasculitis that predominantly affects infants and children and nowadays is regarded as the commonest cause of acquired heart disease in children (Pinna et al., 2008). KD is much more common in Asian countries compared to the rest of the world (Park et al., 2005, Newburger et al., 2004, Newburger and Fulton, 2004, Chang et al., 2004). The highest incidence rate, observed in Japanese children under the age of 5, is estimated at 134/100,000 (Newburger et al., 2004), whilst incidence in the UK is reported to be 4.55/100,000 (Tulloh et al., 2016). Additional characteristic symptoms include prolonged fever, which is unresponsive to antibiotics; bilateral non-purulent conjunctivitis; gastroenteritis; arthritis; aseptic meningitis; cervical lymphadenopathy; polymorphous rash; and erythema of the oral mucosa, lips, tongue, palms and soles (Eleftheriou et al., 2015a). The cardiovascular features of KD are secondary to widespread vasculitis, which causes formation of coronary artery aneurysms (Newburger et al., 2004). There is currently no diagnostic test for KD, which hampers efficient diagnosis and treatment. To further complicate matters, KD can be mistaken for other common childhood illnesses such as scarlet fever or viral infections. Nevertheless, it is essential to diagnose and treat KD to prevent lifelong coronary consequences (Eleftheriou et al., 2015a).

1.1.1.4 Childhood polyarteritis nodosa

Childhood polyarteritis nodosa (PAN) is a necrotizing systemic vasculitis affecting medium size muscular arteries and presents with skin; gastrointestinal

tract; and musculoskeletal and renal system involvement (Ozen et al., 2004). The peak age of onset for childhood PAN is ~9 – 10 years of age with males and females being equally affected (Ozen et al., 2004, Eleftheriou et al., 2013). Although estimated annual incidence in adults is 2 – 9 per million, this figure is likely to be lower in children (Eleftheriou et al., 2015a). Regardless of this fact, PAN is still regarded as the most common systemic vasculitis in children after HSP and KD (Ozen et al., 2004, Ozen et al., 2007). Characteristic symptoms include fever (87%), myalgia (83%), weight loss (10%), livedo racemosa or reticularis (88%), hypertension, necrotizing glomerulonephritis (19%), polyneuritis (10%) and ischaemic cardiac disease (Eleftheriou et al., 2013). A monogenic form of PAN has been recently identified and is discussed in more detail below.

1.1.1.5 Cutaneous polyarteritis nodosa

Cutaneous polyarteritis nodosa (cPAN) can be described as PAN limited to the skin. Although the predominant clinical manifestations are cutaneous, such as livedo reticularis, ulcers, petechiae, purpura and cutaneous necrosis, extra-cutaneous symptoms may include fever, malaise, neuropathy, arthralgia and myalgia (Morgan and Schwartz, 2010). An essential distinction between PAN and its cutaneous counterpart is that multi-organ involvement is not observed in cPAN (Morgan and Schwartz, 2010).

1.1.1.6 Takayasu arteritis

Takayasu arteritis (TA) is a chronic granulomatous large vessel vasculitis that predominantly affects the aorta and its main branches. TA can affect patients up to 50 years of age with a significant proportion of them being female (80 – 90%) (Chatterjee et al., 2014). The typical age of onset is between 10 – 40 years although cases as young as 18 months have been reported (Singh et al., 2013). Initially considered to be a disease that affected predominantly Asian women, cases all over the world have now been reported (Richards et al., 2010, Maksimowicz-McKinnon and Hoffman, 2007). In Japan, where the disease was first described (Takayasu, 1908), there is an unusually high prevalence rate: 40 cases per million (Toshihiko, 1996). The prevalence rate around the rest of the

world is lower with the UK, for example, reporting 4.7 cases per million (Watts et al., 2009).

Vascular inflammation initially causes thickening of the arterial wall, which can lead to stenosis, fibrosis, dilatation, and thrombus formation (Kerr et al., 1994). In severe acute cases the inflammatory process can destroy the arterial media causing aneurysm formation (Numano et al., 2000). There are two phases to the illness: an initial florid inflammatory phase followed by a fibrotic phase (Eleftheriou et al., 2015b, Morales et al., 1991, Brunner et al., 2010). Due to symptoms being non-specific there is often a significant diagnostic delay, sometimes spanning many years. At initial presentation, patients may suffer from non-specific symptoms such as fever, anorexia, malaise and myalgia (Kerr et al., 1994, Maksimowicz-McKinnon et al., 2007, Johnston et al., 2002, Mason, 2010, Freitas et al., 2012). As the vascular lesions progress more characteristic features may emerge such as limb claudication, vascular bruits, absent peripheral pulses, hypertension and discrepancies in blood pressure between limbs (Kerr et al., 1994, Maksimowicz-McKinnon et al., 2007, Johnston et al., 2002, Mason, 2010, Freitas et al., 2012). Fatal consequences may eventually develop including heart failure, vessel occlusion and aortic rupture (Rav-Acha et al., 2007, Watson et al., 2014).

1.1.2 Aetiopathogenesis of primary systemic vasculitis

The cause of most childhood primary systemic vasculitides (PSV) is unknown but it is likely be the consequence of a complex interaction between environmental triggers, such as infectious pathogens, and the genetic predisposition of the affected host. Increasingly, monogenic causes of inflammatory vasculitis are recognized, due to the more widespread use of next-generation genetic sequencing technology.

Due to the seasonal variation associated with some types of PSV (KD and HSP) it is possible that these diseases are infection-related (Yang et al., 2005, Kim and Dedeoglu, 2005). Various pathogens (viruses, fungi and bacteria) are known to either directly cause or potentially trigger pathogenesis of primary systemic

vasculitis (Pagnoux et al., 2006). For example, the hepatitis B virus has a well-known causal relationship with PAN whilst parvovirus B19 results in a vasculitis reminiscent of HSP (Pagnoux et al., 2006). Other suggested causative agents include Staphylococcus *aureus* but only in relation to GPA and superantigens (SAgs), a group of immune-stimulatory agents of viral or bacterial origin that have the ability to stimulate a large proportion of the T cell population (Li et al., 1998, Brogan et al., 2004, Popa and Tervaert, 2003). The most convincing evidence relating to SAgs and vasculitis is that bacterial SAgs potentially trigger KD (Yamashiro et al., 1996, Leung et al., 1995, Curtis et al., 1995). Finally ANCAs have been established as directly pathogenic resulting in small vessel vasculitis. The most accepted theory as to how they cause disease is that the ANCAs activate neutrophils, which in turn damage endothelial cells, and trigger an inflammatory response with mononuclear cell recruitment (Pendergraft and Nachman, 2015, Jennette et al., 2006, Morgan et al., 2006).

Over the last two decades identification of familial and early onset cases of PSV have raised questions as to the genetic component of these disorders (Mason et al., 1994, Manganelli et al., 2003, Dergun et al., 2005). Due to developments in technology and increased sample sizes, significant advances have been made in elucidating their genetic basis. One of the first studies to be published regarding the genetics of vasculitis was a genome-wide linkage analysis study conducted on a KD Japanese cohort and their families (Onouchi et al., 2007). It identified ten chromosomal regions (4q35, 5q34, 6q27, 7p15, 8q24, 12q24, 18q23, 19q13, Xp22 and Xq27) with the most significant being 12q24 (Onouchi et al., 2007). Six subsequent genome wide association studies (GWAS), in different populations (including Japanese, European, Korean, Taiwanese, and Han Chinese), corroborated some of the findings from the original linkage study as well as identifying several new loci (Tsai et al., 2011, Onouchi et al., 2012, Lee et al., 2012, Kim et al., 2011, Khor et al., 2011, Burgner et al., 2009, Onouchi et al., 2008). Of interest were five loci that reached genome-wide significance level and have been replicated in subsequent studies. They are: inositol 1,4,5-triphosphate 3-kinase C (*ITPKC,* a regulator of T-cell activation), caspase 3 (*CASP3*, which is involved in cellular apoptosis), Fc gamma receptor 2A (*FCGR2A,* which encodes a cell-surface protein of the immunoglobulin

superfamily), B lymphoid tyrosine kinase (*BLK,* plays a role in B-cell receptor signaling and B-cell development) and cluster domain 40 (*CD40,* functions as a receptor on antigen-presenting cells) (Onouchi et al., 2012, Lee et al., 2012, Khor et al., 2011, Kuo et al., 2011a, Kuo et al., 2011b, Onouchi et al., 2010, Onouchi et al., 2008). Several additional associations that have been observed but not confirmed include *N*-acetylated alpha-linked acidic dipeptidase-like 2 (*NAALADL2,* unknown function), zinc finger homeobox 3 (*ZFHX3*, a transcription factor that regulates myogenic differentiation), Dab reelin signal transducer homolog 1 (*DAB1*, plays a role in brain development) and pellino E3 ubiquitin protein ligase 1 (*PELI1*, involved in toll like receptor and interferon signaling) (Burgner et al., 2009, Kim et al., 2011).

In comparison to the wealth of GWAS data on KD only a handful of GWAS have been conducted in AAV populations (Xie et al., 2013, Lyons et al., 2012, Iwahashi et al., 2017, Kawasaki et al., 2017). Nevertheless they have significantly increased current knowledge on the genetic aspect of AAV. Two studies have revealed significantly associated loci within the major histocompatibility (MHC) class II region, the most significant one being *HLA-DPB1* (Lyons et al., 2012, Xie et al., 2013). Outside of this region serpin peptidase inhibitor, clade A (alpha-1 antiproteinase, antitrypsin), member 1 (*SERPINA1*, a serine protease inhibitor), proteinase 3 (*PRTN3*) and semaphorin 6A (*SEMA6A,* which has potential involvement in vasculogenesis, cardiogenesis and immune regulation) are associated with proteinase 3-ANCA associated vasculitis (Lyons et al., 2012, Carmona et al., 2015, Xie et al., 2013). This provides preliminary evidence that the type of human leukocyte antigen determines the type of AAV (Lyons et al., 2012, Xie et al., 2013). More recent studies have revealed an association between a *TNFSF4* polymorphism and proteinase 3-ANCA vasculitis and an *ETS1* polymorphism and GPA (Iwahashi et al., 2017, Kawasaki et al., 2017).

Lastly, the genetic component of TA has been partly elucidated after the publication of various Immunochip studies: a study that performed genome scanning and GWAS (Terao et al., 2013, Saruhan-Direskeneli et al., 2013, Renauer et al., 2015). The most consistent genetic risk factor across all three

studies was *HLA-B*5201* which was observed in several different populations, including Japanese, Turkish and North American populations (Terao et al., 2013, Saruhan-Direskeneli et al., 2013, Renauer et al., 2015). Outside of the MHC region the most pertinent loci with a genome-wide level of significance were interleukin 12B (*IL12B*, a cytokine) (Terao et al., 2013, Saruhan-Direskeneli et al., 2013), *FCGR2A* (Saruhan-Direskeneli et al., 2013), interleukin 6 (*IL6*, a cytokine) (Renauer et al., 2015) and ribosomal protein S9/leukocyte immunoglobulin-like receptor, subfamily B, member 3 (*RPS9/LILRB3*) (Renauer et al., 2015). The mechanisms linking these potential genetic components and the disease have yet to be discovered.

1.1.2.1 Monogenic vasculitides

As demonstrated above the systemic vasculitides were largely considered sporadic diseases, but more recently monogenic forms have been described. Firstly, a new group of Mendelian disorders known as type I interferonopathies some of which are associated with vasculitis have started to emerge (Liu et al., 2014, Jeremiah et al., 2014, Rice et al., 2007, Crow et al., 2006a) and secondly, the first true cases of monogenic PAN were recently discovered (Navon Elkan et al., 2014, Zhou et al., 2014).

In 2014 two separate studies investigated PAN patients, of different ancestries (European and Georgian Jewish), using whole exome sequencing (Navon Elkan et al., 2014, Zhou et al., 2014). Both independently discovered deleterious mutations in the cat eye syndrome chromosome region candidate 1 gene (*CECR1*) (Navon Elkan et al., 2014, Zhou et al., 2014). All the Georgian Jewish patients from one study and three patients from the other study were found to be homozygous for the same damaging mutation (p.G47R) (Navon Elkan et al., 2014, Zhou et al., 2014). Out of the remaining patients eleven were confirmed as compound heterozygous for eleven mutations in *CECR1* (Navon Elkan et al., 2014, Zhou et al., 2014). All mutations resulted in the loss-of-function of *CECR1*, which encodes adenosine deaminase 2 (ADA2). The functional consequence was a significantly reduced level of ADA2 activity in the haematopoietic stem cell populations of patients (Navon Elkan et al., 2014, Zhou et al., 2014). The disease now termed deficiency of ADA2 (DADA2) was shown

to lead to cerebral and systemic vasculitis by affecting the adenosine inflammatory-response pathway (Navon Elkan et al., 2014, Zhou et al., 2014). DADA2 is thus the first example of a monogenic disease causing PAN, a systemic vasculitis previously considered to be polygenic (Navon Elkan et al., 2014, Zhou et al., 2014). Since the initial discovery a number of studies have identified additional novel mutations in *CECR1* (Garg et al., 2014, Caorsi et al., 2017, Batu et al., 2015, Nanthapisal et al., 2016). For example, an 11-year-old Caucasian female, originally diagnosed with PAN, was found to harbour a novel *CECR1* deletion (c.144delG) resulting in a frameshift and insertion of a premature stop codon (Nanthapisal et al., 2016). The proband was found to have low enzymatic function of serum ADA2 and low *CECR1* mRNA expression (Nanthapisal et al., 2016).

The new group of Mendelian diseases termed type I interferonopathies are a growing group characterised by defective regulation of type I interferons and include diseases such as stimulator of interferon genes (STING)-associated vasculitis of infancy (SAVI); *C*hronic *a*typical *n*eutrophilic *d*ermatosis with *l*ipodystrophy and *e*levated temperature (CANDLE) syndrome; and Aicardi-Goutieres syndrome (AGS) (Volpi et al., 2016). SAVI is caused by sporadic dominant mutations in the transmembrane protein 17 gene (*TMEM17*). It has characteristic cutaneous features (vasculitic rash on the nose, cheeks and peripheries) as well as systemic involvement and interstitial lung disease (Liu et al., 2014). Therapeutic options are limited due to the disease's heterogeneity but treatment targeting the interferon pathway (e.g. Janus Kinase (JAK) inhibitors) is currently the best hope for individuals suffering from these conditions (Volpi et al., 2016).

Taking into account that several other forms of systemic vasculitis present early on in life and segregate within families, similarly to PAN and diseases such as SAVI and CANDLE, it is likely that several monogenic causes of primary systemic vasculitides exist and are yet to be identified (Morishita et al., 2011, Singh et al., 2013, Watson et al., 2014).

1.1.3 Non-inflammatory vasculopathy

Non-inflammatory vasculopathies have a significantly different mechanism to inflammatory vasculopathies but may present clinically in a similar way with features such as myocardial infarction, skin changes, renal and cerebral involvement (Callewaert et al., 2008, Scott and Smith, 2009, Hara et al., 2009, Loeys et al., 2006). Changes such as increased myofibroblast proliferation in the sub-endothelial layer or defective synthesis and secretion of an extracellular microfibril constitutive element can lead to occlusive thickening or weakening of the vessel walls, respectively (Callewaert et al., 2008, Scott and Smith, 2009, Hara et al., 2009, Loeys et al., 2006). Examples of non-inflammatory vasculopathies include a number of monogenic aortopathies such as Marfan syndrome, Loeys-Dietz syndrome and Ehlers-Danlos syndrome type IV; as well as several cerebral arteriopathies like fibromuscular dysplasia, moyamoya disease (MMD) and Cerebral Autosomal-Dominant/Recessive Arteriopathy with Subcortical Infarcts and Leukoencephalopathy (CARASIL and CADASIL), to name but a few (Callewaert et al., 2008, Scott and Smith, 2009, Hara et al., 2009, Loeys et al., 2006). Characteristic features of such diseases include large arterial aneurysms; dilation; tortuosity of the aorta and its major branches; and arterial stenosis (Callewaert et al., 2008, Scott and Smith, 2009, Hara et al., 2009, Loeys et al., 2006). Unlike the systemic inflammatory vasculitides, the majority of the non-inflammatory vasculopathies are monogenic (see Table 1-2). Table 1-2 details the genetic defects that have been identified, to date, in association with various non-inflammatory vasculopathies. Taking into account the disease pathogenesis of non-inflammatory vasculopathies, more than half of the reported genes are involved in collagen homeostasis, smooth muscle function and growth factor signaling (Table 1-2). The more common diseases and associated mechanisms are described in more detail below.

Table 1-2 Monogenic causes of non-inflammatory vasculopathies

Disease	Phenotype	Genes
Familial thoracic aortic aneurysm and dissection (TAAD)	Aneurysm or dissection of the aorta due to medial necrosis. Aortic stenosis.	*ACTA2* (Guo et al., 2007), *MFAP5* (Barbier et al., 2014), *MYH11* (Zhu et al.,

		2006), *MYLK* (Wang et al., 2010), *PRKG1* (Guo et al., 2013) and *TGFBR2* (Pannu et al., 2005)
Marfan syndrome	Mitral valve prolapse, mitral regurgitation, dilatation of the aortic root and aortic regurgitation. Aortic aneurysm and dissection. Tall and slender, arachnodactyly, scoliosis/kyphosis and myopia.	*FBN1*(Lee et al., 1991)
Loeys-Dietz syndrome (LDS)	Arterial tortuosity, enlarged aorta and aortic aneurysm. Hypertelorism, bifid uvula, cleft palate and craniosynostosis.	*SMAD3* (Regalado et al., 2011, van de Laar et al., 2011), *TGFB2* (Boileau et al., 2012), *TGFB3* (Rienhoff et al., 2013), *TGFBR1* (Loeys et al., 2006, Loeys et al., 2005*)* and *TGFBR2* (Loeys et al., 2006, Loeys et al., 2005)
Ehlers Danlos syndrome (EDS) type IV	Spontaneous rupture of large arteries. Hypermobililty and stretchy skin.	*COL3A1* (Tsipouras et al., 1986, Superti-Furga et al., 1988, Milewicz et al., 1993, Leistritz et al., 2011)
Congenital contractural arachnodactyly	Dilatation of the aortic root, mitral valve prolapse and mitral regurgitation. Contractures, arachnodactyly, scoliosis and crumpled ears.	*FBN2* (Putnam et al., 1995)
Moyamoya disease (MMD)	Bilateral intracranial carotid artery occlusion. Hemiplegia, epileptic seizures and subarachnoid bleeding.	*ACTA2* (Guo et al., 2009), *GUCY1A3* (Herve et al., 2014) and *RNF213* (Liu et al., 2011, Kamada et al., 2011).
CARASIL syndrome	Progressive encephalopathy. Spastic ataxia, generalised rigidity, hyper-reflexia and dementia.	*HTRA1* (Hara et al., 2009)
CADASIL syndrome	Progressive encephalopathy. Migraine, recurrent stroke and cognitive impairment.	*NOTCH3* (Joutel et al., 1997)

Other cerebral arteriopathy	Aneurysms. Cerebral palsy, migraine, cataracts, nephropathy and renal cysts.	*COL4A1*(Shah et al., 2010)
Aicardi-Goutières syndrome (AGS)	Occlusive or aneurysmal cerebral arteriopathy. Epilepsy, basal ganglia calcification, leukoencephalopathy, moderate to severe developmental delay, agenesis/digenesis of corpus callosum and chorioretinal lacunae.	*ADAR1* (Rice et al., 2012), *IFIH1* (Rice et al., 2014), *RNASEH2B* (Crow et al., 2006b), *RNASEH2C* (Crow et al., 2006b), *RNASEH2A* (Crow et al., 2006b), *SAMHD1* (Rice et al., 2009) and *TREX1* (Crow et al., 2006a)
Pulmonary venoocclusive disease	Pulmonary artery hypertension, occlusion of pulmonary veins, occult alveolar haemorrhage.	*BMPR2* (Runo et al., 2003)
Juvenile polyposis/hereditary hemorrhagic telangiectasia syndrome	Arteriovenous malformations of the lungs, liver, brain and gastrointestinal tract. Teleangiectases of the skin and epistaxis. Polyps in the gastrointestinal tract.	*SMAD4* (Gallione et al., 2006)
Supravalvar aortic stenosis	Stenosis of the aorta.	*ELN* (Ewart et al., 1994)
Aortic valve disease	Bicuspid aortic valve. Valve calcification.	*NOTCH1 (Garg et al., 2005)*
Shprintzen Goldberg syndrome	Valve regurgitation, aortic root dilation, aneurysm. Hypertelorism, exophthalmos and micrognathia. Long slender fingers and limbs, scoliosis.	*SKI* (Doyle et al., 2012)

1.1.4 Vasculopathies with predominant aortic involvement

1.1.4.1 Ehlers-Danlos syndrome

Ehlers-Danlos syndrome (EDS) is a connective tissue disorder that has been subcategorized into thirteen subtypes: classical, classical-like, cardiac-valvular, hypermobile, vascular, kyphoscoliotic, arthrochalasia, dermatosparaxis, brittle cornea syndrome, spondylodysplastic, musculocontractural, myopathic and periodontal (Malfait et al., 2017). All types share the common features of

hyperextensibility, articular hypermobility and tissue fragility (Malfait et al., 2017). The most relevant type of EDS for this report is the vascular type. Unlike the other types of EDS, vascular EDS is potentially life threatening as there is the risk of spontaneous vessel rupture due to severe tissue fragility. Vessels at risk of rupture include the aorta, splenic, iliac and renal arteries. Other phenotypic traits include translucent skin with abnormally visible veins, increased tendency to bruise, varicosities and characteristic facial features (thin face, large eyes, thin lips, thin nose) (Germain and Herrera-Guzman, 2004, Malfait et al., 2017).

Mutations in the pro-alpha1 chain of type III collagen gene (*COL3A1*) are well documented as causing vascular EDS, which is an autosomal dominantly inherited disease (Tsipouras et al., 1986, Superti-Furga et al., 1988, Milewicz et al., 1993, Leistritz et al., 2011). Shortened pro-alpha1 chains lead to decreased molecular stability, impaired collagen fibril formation and inefficient procollagen secretion (Superti-Furga et al., 1988). More than 600 *COL3A1* pathogenic variants have been recorded with the null mutations having reduced penetrance compared to the missense or splice-site mutations (Leistritz et al., 2011, Pepin et al., 1993). Individuals harbouring null mutations have an extended life span where the age at which the first complication is observed is delayed by 15 years compared to those with protein altering mutations (Leistritz et al., 2011).

1.1.4.2 Marfan syndrome

Marfan syndrome is a fibrous connective tissue disorder mainly affecting the skeletal, ocular and cardiovascular systems (Gray and Davies, 1996). Skeletal features include increased height, long limbs, joint laxity and a highly arched palate leading to overcrowding of the teeth (Gray and Davies, 1996). Ocular findings consist of myopia and subluxation of the lens (Gray and Davies, 1996). The cardiovascular traits include mitral valve prolapse, mitral regurgitation, dilatation of the aortic root and aortic regurgitation (Gray and Davies, 1996). Life threatening cardiovascular complications may arise such as aortic aneurysm and dissection.

Marfan syndrome is an autosomal dominant disorder caused by mutations in the fibrillin-1 (*FBN1*) gene, 27% of which are spontaneous mutations (Lee et al.,

1991). Fibrillin-1 is a glycoprotein, which is the major component of microfibrils in the extracellular matrix. Microfibrils are involved in elastic fiber homeostasis and structural integrity providing the scaffold onto which elastin is deposited (Whiteman et al., 2006, Ross and Bornstein, 1969). Individuals suffering from Marfan syndrome have been documented to have defects in fibrillin synthesis, secretion and extracellular matrix formation (Milewicz et al., 1992).

1.1.4.3 Loeys-Dietz syndrome

Loeys-Dietz syndrome (LDS) is an aortic aneurysm syndrome with extensive systemic involvement (Loeys et al., 2005). The characteristic features are hypertelorism; bifid uvula or cleft palate; and arterial tortuosity and aneurysms. Other systemic findings include craniosynostosis, mental retardation, congenital heart disease and structural brain abnormalities (Loeys et al., 2005).

To date five genes, all involved in TGF-β signalling, have been identified in association with LDS: type I transforming growth factor β receptor (*TGFBR1*) (Loeys et al., 2006, Loeys et al., 2005), type II transforming growth factor β receptor (*TGFBR2*) (Loeys et al., 2006, Loeys et al., 2005), type II transforming growth factor β (*TGFB2*) (Boileau et al., 2012), type III transforming growth factor β (*TGFB3*) (Rienhoff et al., 2013) and SMAD family member 3 (*SMAD3*) (Regalado et al., 2011). Heterozygous mutations in *TGFBR1* and *TGFBR2* are suggested to enhance TGF-β signaling ultimately affecting cell performance during tissue development and homeostasis (Loeys et al., 2005). Affected individuals appear to have increased expression of connective tissue growth factor (Loeys et al., 2005). Regarding *TGFB2,* causative mutations resulting in haploinsufficiency have been observed (Boileau et al., 2012). Reduced levels of TGFβ2 disrupt several developmental processes including the epithelial-to-mesenchymal transition and differentiation of neural-crest derived tissues (Boileau et al., 2012). This affects a wide range of cells/tissues in particular vascular smooth muscle cell (VSMC) differentiation from neural crest cells (Boileau et al., 2012, Guo and Chen, 2012). De novo mutations in *TGFB3* have been shown to lead to a non-functional TGFβ3 ligand (Loeys et al., 2005). Similarly to TGFβ2, a reduced level of TGF-β signalling may affect crucial embryonic developmental stages such as myogenesis (Loeys et al., 2005). Lastly,

SMAD3 is a key regulator of the TGF-β pathway with heterozygous *SMAD3* mutations affecting its ability to relay TGF-β signals (van de Laar et al., 2011). Dysregulation of the pathway could be further enhanced by alternative or compensatory mechanisms being activated (van de Laar et al., 2011).

1.1.4.4 Familial thoracic aortic aneurysm

Individuals with familial thoracic aortic aneurysm and/or aortic dissection (TAAD) develop aneurysms or dissections of the aorta due to degenerative changes in the aortic wall (Hanley and Jones, 1967). Aortic tissue has a histological appearance termed 'medial necrosis' where the elastic fibers have degenerated and fragmented, smooth muscle cells are lost and there is an accumulation of basophilic ground substance (Hanley and Jones, 1967). Although thoracic aortic aneurysms can occur in other connective tissue disorders like Marfan syndrome and EDS, they are more commonly observed in the absence of any identifiable syndrome (Regalado et al., 2011).

TAAD is inherited in an autosomal dominant fashion with several genes identified as being causative: smooth muscle myosin heavy chain 11 (*MYH11*), actin alpha 2 (*ACTA2*), myosin light chain kinase (*MYLK*), protein kinase CGMP-dependent type 1 (*PRKG1*), and transforming growth factor beta receptor 2 (*TGFBR2*) (Pannu et al., 2005). Of these genes, three encode smooth muscle cell (SMC) contractile proteins (*ACTA2, MYH11* and *MYLK*) indicating the importance of the SMC contractile unit in vascular integrity, especially in the aorta. The first SMC contractile protein to be identified in association with TAAD was MYH11. Mutations in *MYH11* are responsible for <2% of cases (Pannu et al., 2007) and affect the C-terminal region of MYH11 (Zhu et al., 2006). The mutations cause a conformational change of the α-helical coiled-coil structure, which affects its stability and thus assembly of myosin thick filaments resulting in aortic stiffness. On the back of identifying *MYH11* as a causative gene *ACTA2* mutations were then reported to be associated with TAAD (Guo et al., 2007). Accounting for 14% of cases *ACTA2* mutations are the most common cause of TAAD (Guo et al., 2007). Abnormalities in ACTA2 filament assembly or stability result in dysfunctional SMC contraction (Guo et al., 2007). Interestingly, in some cases *ACTA2* mutations are also associated with livedo

reticularis, indicating a potential occlusive vascular phenotype (Guo et al., 2007). The most recent SMC contractile protein to be identified is *MYLK* (Wang et al., 2010). *MYLK* encodes myosin light chain kinase (MLCK) that phosphorylates the regulatory light chain of smooth muscle myosin II leading to smooth muscle contraction. Heterozygous loss-of-function mutations in *MYLK* cause decreased contractile function of SMCs such that the aorta is unable to withstand the biomechanical forces imposed on it over an individual's lifetime. Mutations in *TGFBR2* account for 5% of TAAD and result in the dysregulation of TGF-β signaling although the precise pathogenic mechanism has yet to be elucidated (Pannu et al., 2005). The last gene associated with TAAD is *PRKG1*: a gain-of-function missense mutation (Guo et al., 2013). This mutation increases the activity of the encoded PRK-1α protein, which in turn increases dephosphorylation of the SMC regulatory light chain and consequently decreases SMC contractility (Guo et al., 2013).

1.1.5 Cerebral arteriopathies

Cerebral arteriopathy is a recognised cause of childhood arterial ischaemic stroke and is a strong predictor of recurrent episodes (Amlie-Lefond et al., 2009). There are various subtypes of arteriopathy defined by the International Paediatric Stroke Study such as focal cerebral arteriopathy, sickle cell disease arteriopathy and post-varicella angiopathy (Amlie-Lefond et al., 2009). For the purposes of this introductory overview, I will be focusing on arteriopathies with identified genetic causes.

1.1.5.1 Cerebral Autosomal-Dominant/Recessive Arteriopathy with Subcortical Infarcts and Leukoencephalopathy (CARASIL/CADASIL)

CARASIL/CADASIL are non-hypertensive cerebral small vessel arteriopathies. CARASIL is characterised by alopecia, spondylosis, and progressive motor dysfunction and dementia (Hara et al., 2009) whilst CADASIL is characterised by migraine, recurrent stroke and progressive cognitive impairment (Markus et al., 2002). CARASIL is associated with mutations in HtrA serine peptidase 1

(*HTRA1*) (Hara et al., 2009) and CADASIL with *NOTCH3* (Joutel et al., 1996). *HTRA1* is involved in the inhibition of TGF-β signaling with mutant *HTRA1* resulting in an increase in TGF-β signaling (Hara et al., 2009). However, how the disinhibition of TGF-β signaling specifically leads to the CARASIL phenotype is as yet unknown (Hara et al., 2009). CADASIL is associated with mutations in *NOTCH3* although the pathogenic mechanism has yet to be elucidated (Joutel et al., 1997, Haritunians et al., 2002, Cleves et al., 2010, Granild-Jensen et al., 2009).

1.1.5.2 Aicardi-Goutieres syndrome

Aicardi-Goutieres syndrome (AGS) is characterised by progressive early-onset encephalopathy with significant mental and physical disabilities (Goutieres, 2005). Typical clinical features are microcephaly, dystonia and spasticity, hepatosplenomegaly, sterile pyrexias and chilblain lesions (Crow, 1993). Neuroimaging displays distinctive traits such as basal ganglia calcifications, cerebral atrophy, bilateral striatal necrosis and intracerebral vasculopathy (Crow, 1993). There is also a specific cerebral spinal fluid (CSF) phenotype: CSF leukocytosis, high levels of α-interferon and increased neopterin concentration (Goutieres, 2005).

AGS is a genetically heterogeneous disorder caused by mutations in a number of different genes. There are seven forms of AGS (Livingston and Crow, 2016) each caused by mutations in a different gene: AGS1 is caused by *TREX1* (Crow et al., 2006a); AGS2 by *RNASEH2B* (Crow et al., 2006b); AGS3 by *RNASEH2C* (Crow et al., 2006b); AGS4 by *RNASEH2A* (Crow et al., 2006b); AGS5 by *SAMHD1* (Rice et al., 2009); AGS6 by *ADAR1* (Rice et al., 2012); and AGS7 by *IFIH1* (Oda et al., 2014). However, only one form is associated with a vasculopathic phenotype: AGS5 caused by mutations in SAM domain and HD domain 1 (*SAMHD1*) (Xin et al., 2011, Thiele et al., 2010, Ramesh et al., 2010, du Moulin et al., 2011). Patients with AGS5 display intracerebral large artery disease, which causes cerebral artery stenosis and aneurysms, as well as cutaneous vasculopathic features (Xin et al., 2011, Thiele et al., 2010, Ramesh et al., 2010, du Moulin et al., 2011). The mechanistic pathways causing AGS are described as follows. *TREX1* encodes a three prime repair exonuclease which

when dysfunctional is thought to result in the accumulation of unwanted intracellular DNA that triggers a viral-like innate immune response (Crow et al., 2006a). Three of the causative genes for AGS encode components of the ribonuclease H enzyme complex that catalyses cleavage of RNA from RNA:DNA complexes (Crow et al., 2006b). Reduced activity of this complex may affect cellular processes but how this causes an immunological response is as yet unknown (Crow et al., 2006b). The mechanism behind *SAMHD1* is thought to prevent self-activation of innate immunity and abrogation of this leads to AGS5 (Rice et al., 2009). Its role in vasculopathy development is not clear but it may be related to the dysregulation of the primary inflammatory stress response in fibroblasts (Thiele et al., 2010). Similarly to the aforementioned genes, *ADAR1* is hypothesised to affect interferon (IFN) regulation through aberrant editing of dsRNA (Rice et al., 2012) whilst mutated *IFIH1* is unable to detect nucleic acids leading to their inappropriate accumulation (Rice et al., 2014).

1.1.5.3 Moyamoya disease

Moyamoya disease (MMD) is a progressive vaso-occlusive disease characterized by stenosis of the distal internal carotid arteries (ICAs) and their major branches (Scott and Smith, 2009, Kuroda and Houkin, 2008). To compensate for the reduced cerebral blood flow and resulting ischaemia numerous small collateral vessels develop in the bottom of the cerebrum (Kuroda and Houkin, 2008). When visualized on cerebral angiography the mesh of tiny collateral vessels look like ‘a puff of smoke’, which in Japanese is referred to as ‘moyamoya’ (Suzuki and Takaku, 1969).

The angiographic pattern of stenosis and subsequent basal collateral vascular development in MMD is unfortunately not exclusive to this disease. In some cases, a moyamoya-like vasculopathy develops in patients with previously diagnosed diseases or syndromes (Kuroda and Houkin, 2008). In these instances, the disorder is termed moyamoya syndrome, as opposed to MMD, as alternative diseases can contribute to the pathogenesis of the cerebral vasculopathy. There are several moyamoya syndrome-associated diseases, some more common than others. The more common ones include neurofibromatosis type 1, Down

syndrome (trisomy 21), thyroid disease and sickle cell anaemia (Scott and Smith, 2009, Kuroda and Houkin, 2008, Dowling and Kirkham, 2017). The disease generally involves bilateral hemispheres but in some cases arterial stenosis is only evident in one hemisphere; in this case it is referred to as unilateral moyamoya syndrome (Kuroda and Houkin, 2008). The consensus definition of MMD, therefore, is based on its fundamental anatomic characteristics: bilateral, idiopathic vascular occlusion of the circle of Willis (Scott and Smith, 2009, Kuroda and Houkin, 2008).

There are two peak ages of onset for MMD: one at ~40 years of age which commonly presents as intracranial haemorrhage, and another at around 5 years of age which typically presents as arterial ischaemic stroke (Wakai et al., 1997). Severity is directly related to age of onset: the younger the child the more severe the presentation (Kim et al., 2004) with one study demonstrating that MMD has a poor prognosis in patients under the age of 4 (Papavasiliou et al., 2007). The incidence of MMD varies between countries. MMD has a higher incidence rate in Eastern Asian countries, such as Japan, Korea and China, compared to the rest of the world (Uchino et al., 2005, Kim, 2016). In Japan incidence is as high as 3-10 cases per 100,000 whilst in the USA it is 0.09 per 100,000 (Fukui et al., 2000).

Three genes have been linked to MMD: ring finger protein 213 (*RNF213*) (Liu et al., 2011, Kamada et al., 2011, Miyatake et al., 2012b, Miyatake et al., 2012a); guanylate cyclase 1, soluble, alpha 3 (*GUCY1A3*) (Herve et al., 2014); and *ACTA2* (Guo et al., 2009).

RNF213 was first identified as a susceptibility gene for MMD in a Japanese patient cohort (Kamada et al., 2011). The mutation that was discovered (p.R4859K) was thought to be a founder mutation due to the high carrier frequency in Japan (1/72) and complete absence in a large Caucasian control population (Kamada et al., 2011). This theoretcially explains the higher incidence rate in Japanese, and potentially also other Eastern Asian populations. A further 10 mutations were subsequently identified in East Asian and Caucasian cases (Liu et al., 2011). The variants discovered were significantly associated with MMD conferring disease risk with an odds ratio (OR) ranging from 236-

338.9 (Miyatake et al., 2012a, Liu et al., 2011). To determine functional relevance of *RNF213*, knockdown in zebrafish using morphilinos resulted in severely abnormal vessel sprouting in the head region, in addition to irregularly sized large vessels (lateral dorsal aorta and basilar artery) with aberrant sprouting (Liu et al., 2011). The morphant phenotype suggested that *RNF213* was somehow involved in intracranial angiogenesis, but the exact mechanism was not elucidated.

Deleterious mutations in *GUCY1A3* were identified in association with an autosomal recessive disease characterised by severe MMD and early-onset achalasia (Herve et al., 2014). Patients were homozygous for different variants, which all resulted in loss-of-function of the α1 subunit of soluble guanylate cyclase (sGC), a receptor for nitric oxide (NO) and an abundant protein in the vascular system (Herve et al., 2014). Although it is not known how loss of sGC causes MMD, it is hypothesized that abnormal vascular remodeling may result from changes to the NO-sGC pathway (Herve et al., 2014).

Mutations in *ACTA2,* which encodes alpha smooth muscle actin, were first found to be associated with familial thoracic aortic aneurysm (Guo et al., 2007). The mutations affected aortic integrity by disrupting actin filament structure and stability (Guo et al., 2007). Since then *ACTA2* has also been associated with a variety of other vascular diseases including coronary artery disease, stroke, and MMD (Guo et al., 2009, Milewicz et al., 2010). Vascular analysis has indicated that *ACTA2* contributes to a vascular occlusive phenotype, like MMD, via increased SMC proliferation, which is directly modulated by alpha actin (Guo et al., 2009). However, patients where an *ACTA2* mutation was observed and who were classified as having MMD did not actually display the characteristic hallmarks of MMD since they had absence of a basal collateral network (Munot et al., 2012). This would suggest that the cerebral arteriopathy associated with *ACTA2* has a different radiographic phenotype to MMD (Munot et al., 2012).

1.1.5.4 Neurofibromatosis type 1

Neurofibromatosis type 1 (NF1) is an autosomal dominant disease caused by mutations in the neurofibromin gene (*NF1*) (Boyd et al., 2009). Due to the high

rate of spontaneous mutations in this gene the causative mutations can range from complete gene deletions to insertions and splice mutations. Although not defined as a cerebral arteriopathy per se, 6-7.4% of individuals diagnosed with NF1 display cerebral arterial stenosis (Rea et al., 2009, D'Arco et al., 2014). It should be noted, however, that occlusive or aneurysmal disease can potentially affect any artery in the body in patients with NF1 (Lie, 1998). Aside from cerebral arteriopathy, abdominal coarctation of the aorta and renal artery stenosis are the other most frequently observed vasculopathies in NF1 patients (Lie, 1998). Other characteristic phenotypic traits include plexiform neurofibromas as well as cutaneous and subcutaneous fibromatous tumors; café-au-lait spots; intertriginous freckles; Lisch nodules in the eye; and optic gliomas (Szudek et al., 2003).

NF1 belongs to a group of Mendelian diseases termed RASopathies, which harbour mutations in genes involved in the RAS/mitogen-activated protein kinase (MAPK) pathway. Other syndromes that belong to this group include Noonan syndrome, capillary malformation–arteriovenous malformation syndrome, cardiofaciocutaneous syndrome, Legius syndrome and Costello syndrome to name a few (Rauen, 2013). Ras proteins are small guanosine nucleotide-bound GTPases that function as an essential signalling hub (Wennerberg et al., 2005). They are activated by growth factors binding to receptor tyrosine kinases (RTKs) that in turn activate various critical downstream signalling pathways. One of these is the MAPK pathway, which is essential to normal cell development and controlling processes such as cell cycle regulation, differentiation, growth and cell senescence (Tidyman and Rauen, 2009). *NF1* encodes a GTPase activating protein that negatively regulates Ras. Loss-of-function mutations in *NF1* reduce RASGTPase activity thus increasing Ras/MAPK pathway signalling and causing aberrant cell regulation, growth and proliferation (Tidyman and Rauen, 2009, Bollag et al., 1996). Another gene associated with a disease that displays similar phenotypic traits to NF1, Noonan, Costello, cardiofaciocutaneous, and Legius syndromes is c-*CBL* (Niemeyer et al., 2010). Patients with mutations in *c-CBL* displayed traits such as café-au-lait spots, cardiomyopathy, cryptorchism, hypertension, developmental delay,

hearing loss, optic atrophy and vasculitis in addition to increased susceptibility to juvenile myelomonocytic leukaemia (Niemeyer et al., 2010).

1.2 Discovering novel genetic causes of vasculopathies

As highlighted previously, patients with either vasculitis or non-inflammatory vasculopathy display a wide range of clinical symptoms and complications depending on which vascular beds are affected (Eleftheriou et al., 2015a). Despite the clear-cut differences in the pathogenesis of vasculitis versus non-inflammatory vasculopathy, the initial clinical presentation can be similar causing clinical differentiation for individual patients to be challenging (Moritani et al., 2004, Berlit, 1994). Nevertheless, it is essential to differentiate vasculitis from non-inflammatory vasculopathy since the former are treated with aggressive immunosuppression, which would be ineffective and even harmful to patients with the latter (Jayne, 2010). That said, non-inflammatory vasculopathy is also associated with significant cardiovascular and cerebrovascular morbidity and mortality (Berlit, 1994); a timely genetic diagnosis is therefore essential to allow prognostication, avoid inappropriate immunosuppression, facilitate genetic counseling, and relieve the "burden of unknowing" for families afflicted with these diseases.

As illustrated above, the list of monogenic vasculopathies is growing highlighting the importance of understanding the genetic basis of disease for many of these syndromes. The genetic mutations associated with the vasculopathies can affect a whole range of mechanisms such as disrupting an artery's structure during key developmental time points; interfering with homeostasis; or being triggered by environmental stress (Whiteman et al., 2006, Guo et al., 2013, Wang et al., 2010, Herve et al., 2014). Due to the overlapping phenotypes presented by these disorders, genetic sequencing is often required for accurate diagnosis and appropriate clinical intervention. Notably, technological advances have led to a revolution in the understanding of the genetics of some of these vasculopathic disorders (Milewicz et al., 2014).

High-throughput "next-generation" sequencing (NGS) is a fairly recent methodological innovation that allows rapid and affordable identification of mutations in genes associated with genetic disorders (Metzker, 2010), therefore can impact significantly on clinical care. NGS assays that are targeted to genomic regions that have been associated with previously identified pathogenic mutations offer several advantages over traditional sequencing methods such as lower sequencing cost, and the ability to rapidly assess a large number of regions (Metzker, 2010). Using such technologies, it is perhaps unsurprising that a number of genes have been identified in association with vasculopathic diseases (summarized above in Table 1-2). A major example of how understanding the genetic basis of a disease can lead to treatment is demonstrated by LDS. Identifying mutations in genes encoding components of the TGF-β signaling pathway led to treatment with the angiotensin II type 1 receptor antagonist losartan that restores SMAD2 phosphorylation and TGF-β1 expression thus significantly slowing the arteriopathy progression (Habashi et al., 2006, Gallo et al., 2014). At present a large proportion of patients with severe genetic vasculopathies do not have a causative mutation identified in any one of the known genes associated with vasculopathy. NGS however may provide a rapid way of discovering novel genetic causes for these diseases. Next generation sequencing techniques are described in more detail below.

1.2.1 Next-generation sequencing

Next-generation sequencing is the term given to non-Sanger-based high-throughput DNA sequencing technologies (Reis-Filho, 2009). This technology allows billions of DNA strands to be sequenced in parallel, resulting in a significantly higher throughput and reducing the need for fragment-cloning methods (Reis-Filho, 2009). Several different next-generation methods for DNA sequencing were developed in the late 1990s and applied in commercial DNA sequencers by 2000. Over the past 15 years, the cost of sequencing has dramatically dropped as technology has advanced in leaps and bounds. In September 2001, it cost $95,263,072 to sequence a genome or $5,292.39 per Mb. Today, a genome costs just $4211 or $0.05 per Mb to sequence (Wetterstrand). NGS provides an unbiased approach to assessing genetic variants in an

individual's genome or exome (Marian, 2012). Clinical phenotypes are determined by a combination of genetic and environmental factors and it is this genetic component that can potentially be delineated using NGS methods (Marian, 2012). There are three well recognised next generation sequencing methods: whole genome sequencing (WGS), whole exome sequencing (WES) and targeted enrichment of a set of genes (gene panels). The aim of each technique is to identify and analyse rare variants, which might have a large effect size and therefore be potentially pathogenic.

1.2.1.1 Whole genome sequencing

Whole genome sequencing (WGS) provides the most comprehensive analysis of an individual's genetic variation capturing rare variants as well as providing insight into structural anomalies and changes (e.g. copy number variants). WGS used to be prohibitively expensive but as sequencing costs have fallen WGS has become a more likely choice when it comes to identifying novel mutations. However, analysis of the copious amounts of data generated per individual is a significant hurdle as the time needed to determine which variants are meaningful or not could prove limiting (Ng and Kirkness, 2010, Sun et al., 2015).

WGS is being used within the NHS at the moment. In 2012 the 100,000 Genomes Project was launched in the UK, which aims to sequence 100,000 genomes from 70,000 patients diagnosed with rare diseases and their families and patients with cancer. The aim is to use the sequence data to provide patients with diagnoses and potentially develop new and more effective treatments.

1.2.1.2 Whole exome sequencing

WES was first proposed by Ng et al. (2009) as a feasible method to identify disease-causing genes. It assesses genetic variants in the protein-coding part of the genome: ~1% of the total genome (Rabbani et al., 2014). Unsurprisingly, such an approach is cheaper and simpler than WGS in terms of execution and analysis.

Although WES does carry the fundamental caveat that it does not sequence non-coding genomic regions, it is still a well-justified strategy for discovering rare genetic variants in Mendelian diseases, and potentially even in complex situations, for two main reasons (Rabbani et al., 2014). Firstly, the majority of known Mendelian diseases are due to disruptions in the protein-coding sequences (Stenson et al., 2009); and secondly, a significant proportion of protein-altering mutations, like non-synonymous substitutions and insertion/deletions, are predicted to have a deleterious effect on the resulting protein structure and function (Kryukov et al., 2007). The exome is, therefore, an ideal source of potential rare causative variants for as yet unexplained diseases. Any findings through WES and subsequent analyses may, however, need to be confirmed using Sanger sequencing due to reduced accuracy of reads (Reis-Filho, 2009). As such WES and Sanger sequencing can be viewed as complementary approaches.

There are two main challenges associated with employing WES in a clinical context: technical issues and data interpretation. Firstly, due to the size of the human exome, the error rate of allele calling is fairly significant with a false positive rate of ~5%. This equates to approximately 50,000 erroneous variants for every one million variants called. In addition, at the moment WES is only able to provide adequate coverage for 80-90% of exons leaving the possibility of missed diagnoses (Kiezun et al., 2012). Secondly, identifying the true causal allele from the vast number of harmless variants present in any one individual is extremely difficult.

1.2.1.3 Targeted enrichment of a set of genes (Gene panels)

Gene panels capture a nominated set of genes or gene regions that are associated with the disease/s under investigation. They provide a cheaper alternative to WES and WGS and limit the possibility of incidental findings. In addition, due to the increased depth-of-coverage somatic mosaic mutations can be identified even if the allelic fraction is only 3% (Omoyinmi et al., 2017). The one caveat is that the disease-causing gene must be included on the panel (Sun et al., 2015). The panel can of course be altered after the fact to include additional genes as they are identified as knowledge accrues over time (Sun et al., 2015).

1.3 Summary

Vasculopathies are a varied group of disorders that affect the vascular tree resulting in arterial stenosis or dilatation and causing multi-organ ischaemia including a prominent cardiac and cerebral involvement (Markovic, 2012, 2009). Because these diseases commonly present in infancy and segregate within families a genetic cause is often suspected but not always identified with the current routinely available genetic tests (Pannu et al., 2007, Milewicz et al., 2010). However, due to the overlapping phenotypes presented by these disorders genetic sequencing is required for accurate diagnosis and appropriate clinical intervention. At present a large proportion of patients with severe genetic vasculopathies do not have a causative mutation identified in any one of the known genes associated with vasculopathy (Carmona et al., 2015). Subsequently children may wait months or even years before receiving a diagnosis and can accrue organ injury or even die in this pre-diagnostic phase. Obtaining a rapid and definitive genetic diagnosis would therefore enable improved prognostic evaluation, genetic counseling, and treatment in these cases (Bersano et al., 2012).

In this project, I investigated the genetic basis of childhood vasculopathies in order to facilitate genetic diagnosis and elucidate major disease pathways and potential novel treatment targets.

1.4 Hypothesis

My project explored the following hypothesis:

Using state of the art genetic mapping and NGS techniques, namely whole exome sequencing, it is possible to discover novel monogenic diseases resulting in pathological undefined vasculopathic syndromes.

The aims of my project were therefore:

1. To identify the disease causing mutation for undefined vasculopathic syndromes using next generation sequencing technologies.
2. Once potential disease causing mutations were identified, to begin to elucidate some of the pathogenic mechanisms in these conditions using a series of functional experiments.

Chapter 2 Materials and General Methods

This section predominantly contains the materials and general methods that were used in more than one chapter. Methods that were applicable to only one chapter will be discussed in detail in the relevant chapter.

2.1 Subjects

2.1.1 Patients

The majority of patients were seen at Great Ormond Street Hospital for Children NHS Foundation trust (GOSH) either at the vasculitis clinic (Dr Eleftheriou/Prof Brogan) or the neurovascular service (Dr Ganesan). Additional informative cases were identified through international collaborations via vasculitis research networks (international collaborations with Professors Ozen (Ankara, Turkey); and Dolezalova (Prague, the Czech Republic); and Dr Kamphuis (Rotterdam, the Netherlands). Ethical approval for this study was given by Bloomsbury ethics committee (ethics number: 08/H0713/82), to which all patients were subsequently enrolled. Informed written consent/assent was obtained from all parents/subjects included in the study.

Index cases with a severe and unusual vasculopathic phenotype were studied. I specifically focussed on recruiting patients who developed disease early in life and/or those with a family history (with or without consanguineous parents). Sporadic cases were also considered on an individual case basis. The clinical presentation and relevant family histories are described in detail in the respective results chapters.

2.1.2 Healthy controls

Healthy adult controls were fully consented volunteer staff members from within the Infection, Inflammation and Rheumatology Department at the UCL Great Ormond Street Institute of Child Health. Healthy children controls (median age 17 years) were recruited through the Arthritis Research UK Centre for adolescent rheumatology. Informed consent was obtained with local ethics approval (REC 11/LO/0330). Volunteers had no medical history of acute or chronic illnesses and specifically no symptoms of current infection at time of sampling.

2.2 Reagents for blood collection

After blood was collected, it was aliquoted into one of two collection tubes depending on use: either 100 µl of 1% Ethylendiaminetetraacetic acid (EDTA; International specific supplies) per 1 ml of blood or 10 units of preservative free sodium heparin (CP pharmaceuticals Ltd, 1000U/ml) per 1 ml of blood.

2.3 Tissue culture media

Culture media for Jurkat cells consisted of RPMI with 10% foetal bovine serum (FBS) and 100U/ml Penicillin and 100µg/ml Streptomycin (Thermo Fisher Scientific).

Culture media for human dermal fibroblast cells (HDFCs) consisted of basal medium (Ham's F10 Nutrient Mix) supplemented with 10% FBS and 100U/ml Penicillin and 100µg/ml Streptomycin (LifeTechnologies).

Culture media for peripheral blood mononuclear cells (PBMCs) consisted of RPMI with 10% FBS and 100U/ml Penicillin and 100µg/ml Streptomycin (Thermo Fisher Scientific).

Culture media for human umbilical vein endothelial cells (HUVECs) consisted of endothelial cell growth medium 2 (EGM-2) (Promocell) with 2% FBS. Supplements were added according to the manufacturer's instructions.

Quiescent human umbilical vein endothelial cell (HUVEC) media consisted of EGM2 (Promocell) with 0.05% FBS and no additional supplements.

2.4 Tissue culture reagents

Trypsin-EDTA (Promo cell) and trypsin neutralizing solution/TNS (0.05% trypsin inhibitor, 0.1% BSA; Promo cell) were used for detachment of HUVECs and HDFCs from culture.

2.5 Sample collection

Blood was collected from patients and immediate family members (at least case-parent trios), where possible, in EDTA tubes for deoxyribonucleic acid (DNA) extraction. A further sample was collected in a 50 ml falcon tube, containing 1 µl of preservative free sodium heparin (CP Pharmaceuticals) per 1 ml blood, for the extraction of PBMCs. If blood could not be obtained from family members saliva was collected in DNA Genotek Oragene saliva pots. Blood samples for DNA extraction were stored at -20°C unless extraction was done immediately. Saliva pots were stored at room temperature.

2.6 DNA extraction

DNA was extracted from either blood or saliva samples provided by the proband and their family members.

2.6.1 DNA extraction from whole blood

DNA was extracted using the Qiagen Gentra Puregene blood kit. Samples were defrosted at room temperature if frozen. In brief, 900 µl of red blood cell lysis solution was added to 300 µl whole blood and inverted 10 times. After incubating at room temperature for 1 minute, the white blood cells were pelleted by spinning at 13,000 x *g* for 20 seconds. The supernatant was discarded and the pellet was resuspended in 10 µl of the remaining supernatant by vigorous

vortexing. A total of 300 µl of cell lysis solution and 100 µl of protein precipitation solution was added and vortexed vigorously. After centrifugation (13,000 x *g* for 1 minute), the supernatant was poured into a clean eppendorf and 300 µl of isopropanol was added. The eppendorf was inverted 50 times until the DNA became visible. The DNA was pelleted by centrifugation (13,000 x *g* for 1 minute) and the supernatant discarded. The DNA pellet was washed with 300 µl of 70% ethanol and centrifuged (13,000 x *g* for 1 minute). The supernatant was discarded and the pellet air-dried for 5 minutes. 100 µl of nuclease free water was added to the pellet and the sample was briefly vortexed. To ensure the DNA was fully resuspended the sample was incubated at 65°C for 5 minutes and then left shaking at room temperature overnight.

Some patient and family DNA was previously extracted by the clinical lab in Great Ormond Street Hospital NHS Foundation trust (York House) as part of their routine clinical care. They used 3 methods:

1. Autogen, which is a DNA automator. The method used is a modified version of salting-out.
2. QuickGene-610L, which is a semiautomator. This method is membrane-based.
3. EZ1 which uses magnetic bead technology.

2.6.2 DNA extraction from saliva

DNA was extracted using the DNA Genotek prepIT®L2P kit. The saliva pot was inverted several times and incubated at 50°C in a water bath for 1 hour. In an eppendorf, 500 µl of saliva was added to 20 µl of PT-L2P and vortexed. It was incubated on ice for 10 minutes and centrifuged (15,000 x *g* for 5 minutes). The supernatant was kept and mixed with 600 µl of 100% ethanol by inverting the eppendorf 10 times. After incubating at room temperature for 10 minutes, it was centrifuged (15,000 x *g* for 2 minutes). The supernatant was removed and the pellet washed with 250 µl of 70% ethanol. After removing the ethanol, 100 µl of nuclease free water was added to resuspend the pellet. To ensure complete rehydration the resuspended pellet was incubated at room temperature overnight.

2.7 Nucleic acid quantification

DNA was quantified using a Nanodrop (Thermo Fisher Scientific). DNA purity was measured by a ratio of the absorbance at 260 and 280nm ($A_{260/280}$). For pure DNA $A_{260/280}$ is ~1.8, and for pure RNA it is ~2. Nucleic acid concentration was also recorded.

2.8 Preparation of peripheral blood mononuclear cells (PBMCs)

PBMCs were isolated from whole blood within 2 hours of the blood being collected (see section 2.5).

Blood was diluted with an equal volume of RPMI and gently layered over an equal volume of Lymphoprep™ (Axis-Shield). Samples were centrifuged (800 x *g* for 20 minutes) leaving the PBMCs in a diffuse interface between the plasma and Lymphoprep™. The cells were carefully transferred into a new falcon tube and topped up to 50 ml with RPMI and centrifuged (800 x *g* for 10 minutes). The supernatant was removed and the pellet resuspended in RPMI for counting.

2.8.1 Counting of cells

10 µl of the cell/RPMI suspension was mixed with 10 µl of 0.4% trypan blue. 10 µl of the mix was pipetted into a Neubauer counting chamber. Unstained live cells were counted within a specified 25-box field and the total calculated according to the formula below:

$$unstained\ cells \times dilution\ factor \times 10^4 = viable\ cells/ml$$

2.9 Other primary human cells

Jurkat cells were purchased from ATCC®. They were grown in RPMI. Media was changed every 2-3 days and cells were split once they reached ~70% confluency.

HDFCs from a healthy control were gifted from the laboratory of Dr Wei-Li Di. They were grown in DMEM. Media was changed every 2-3 days and cells were split once they reached ~70% confluency.

HDFCs from patients were grown from skin punch biopsies in the GOSH clinical laboratory. They were transferred to our laboratory at passage 4.

HUVECs were purchased from Promocell. They were grown in EGM-2. Media was changed every 2-3 days and cells were split once they reached ~70% confluency. They were only used for 8 passages.

2.10 Freezing and thawing of cells

Cells were centrifuged (250 x *g* for 7 minutes) and the supernatant was discarded. The cells were resuspended in freezing medium (Bambanker) at a concentration of 5-10x10^6 per ml and aliquotted into cryovials. To facilitate slow cooling, the cryovials were placed at -80°C overnight in a freezing pot filled with isopropanol, and transferred to liquid nitrogen after 24 hours for long term storage. Cells were rapidly thawed by resuspending them in 2 ml/l of warm 37°C FBS.

2.11 Passaging, plating and harvesting of cells

Cells were washed twice in sterile PBS. An appropriate volume of 0.05% trypsin-EDTA (Thermo Fisher Scientific) was added and left for 5 minutes to allow the cells to detach from the flask/plate. An equal volume of trypsin neutralizer solution (TNS) (Thermo Fisher Scientific) was added. For passaging and plating, cells were plated at an appropriate density in their relevant media.

Media was changed the following day. For harvesting, cells were transferred into 1.5 ml eppendorfs and centrifuged (12,000 x *g* for 4 mins) to pellet.

2.12 RNA extraction from peripheral mononuclear blood cells and human umbilical vein endothelial cells

RNA was extracted using the Qiagen RNeasy Mini Kit. Cells were pelleted and 350 µl of buffer RLT was added to lyse the cells, followed by 350 µl of 70% ethanol. This solution was mixed thoroughly by pipetting and transferred to an RNeasy Mini spin column placed in a 2 ml collection tube. After centrifugation (15,000 x *g* for 30 sec), the flow-through was discarded and 700 µl of buffer RW1 was added. This step was repeated with the addition of 500 µl of buffer RPE instead. After another centrifugation (15,000 x *g* for 30 sec) and removal of the flow through, a final 500 µl of buffer RPE was added and the tube was centrifuged at 15,000 x *g* for 2 minutes. The RNeasy spin column was placed in a new collection tube and 50 µl RNase-free water was added. This was centrifuged (15,000 x *g* for 1 minute) to elute the RNA.

2.13 cDNA synthesis

RNA input was 1000 ng for a standard (used to generate a standard curve) and 400 ng for a sample. The Applied Biosystems high capacity cDNA reverse transcription kit was used. Each reaction required 2 µl 10x RT buffer, 0.8 µl dNTP mix, 2 µl 10x RT random primers, 1 µl MultiScribe reverse transcriptase and 4.2 µl in double distilled (dd) H_2O. To this mastermix was added either 400 ng (sample) or 1000 ng (standard) of RNA made up to a volume of 10 µl using ddH_2O.

2.14 Quantitative polymerase chain reaction (qPCR)

For each sample a target gene and a housekeeping gene were run in triplicate. To ensure consistency and accuracy within the triplicate a 3.5x mastermix was made up per sample: 3.5 µl cDNA, 7 µl primer, 35 µl SYBR® Green and 24.5 µl ddH_2O. QuantiTect primers (Qiagen) were used and are listed in Table 2-1. After thorough mixing, 20 µl of each sample mastermix was pipetted, in triplicate, into 100 µl qPCR strip tubes. Everything was carried out on ice.

Table 2-1 QuantiTect primer assays for qPCR.

Gene name	Product name	ID number
Actin beta	Hs_ACTB_2_SG	NM_001101
Cbl proto-oncogene, E3 ubiquitin protein ligase	Hs_CBL_1_SG	NM_005188

Samples were run on the Rotorgene 6000. The qPCR program is detailed in Table 2-2. For each primer a standard curve was generated using cDNA extracted from healthy control PBMCs. The curve dilutions were 1, 1/5, 1/25, 1/125 and 1/625. The target PCR efficiency for each standard curve was 90-110% and R^2, which represents the coefficient of correlation, was >0.99. A melt curve analysis was also completed for each gene studied to ensure that the reaction produced a single, specific product. After generating a standard curve for each primer the threshold Ct value could be used to evaluate subsequent samples.

The delta delta Ct (*ΔΔCt*) method was used to determine the relative quantification of gene expression. The following formula was used:

$$Ct\ target\ gene - Ct\ housekeeping\ gene = \Delta Ct$$

$$\Delta Ct\ sample - \Delta Ct\ calibrator = \Delta\Delta Ct$$

$$Expression\ fold\ change = 2^{-\Delta\Delta Ct}$$

Table 2-2 Generic qPCR program using QuantiTect primers.

Temperature (°C)	Time (s)	Number of cycles
	60	
	30	
	30	x 35
	60	
	5min	
	∞	

2.15 Sanger sequencing

2.15.1 Primer design

Forward and reverse primers were designed using ExonPrimer provided by the Institute of Human Genetics at Helmholtz Center Munich (https://ihg.gsf.de/ihg/ExonPrimer.html). The parameters are outlined in Table 2-3. Primers were ordered from Sigma-Aldrich®, resuspended in ddH_2O to a stock solution of 100 µM and diluted to a working solution of 5 µM for PCR.

2.15.2 Amplification of DNA

DNA was diluted to a concentration of 50 ng/µl with ddH_2O. To each well of a 96 well PCR plate was added: 1 µl of DNA, 2 µl of both the forward and reverse primers and 11 µl of FastStart™ PCR Master (Roche). Most exons were amplified using a touchdown PCR program, 62°C to 57°C (

Table 2-4). In some cases a single annealing temperature was used (Table 2-5). Annealing temperature was varied to optimize specific primer binding.

Table 2-3 Parameters specified for design in Exon Primer.

Parameter		Reason for parameter
Minimal distance between primer and exon/intron boundary	50 bp	Ensures sequencing of splice junctions
Primer region	70 bp	Location from exon-intron boundary
Maximal target (exon) size	500 bp	Allows good sequencing reads
Annealing temperature	60°C ± 5°C	Ensures a balance between specificity and template binding
GC clamp	Yes	Promotes specificity
Primer size	Minimum: 18 bp Optimum: 20 bp Maximum: 23 bp	Good specificity
Maximum length of a mononucleotide repeat	4	Reduces mispriming.
Masking	Human, score 300	Avoids interspersed repeats

Table 2-4 Touchdown PCR program, 62°C to 57°C.

Temperature (°C)	Time (s)	Number of cycles
95	5min	
95	15	
62	15	x 10
72	60	
95	15	x 16
62	15	62°C decreases 0.3°C per cycle
72	60	
95	15	
57	15	x 14
72	60	
72	7min	
4	∞	

Table 2-5 Generic PCR program for FastStart™ PCR Master (Roche).

Temperature (°C)	Time (s)	Number of cycles
95	60	
95	30	
60	30	x 35
72	60	
72	5min	
4	∞	

2.15.3 Sequencing of DNA

PCR product was cleaned in a MinElute 96 UF PCR purification plate using 80 µl of ddH_2O (per well) and a vacuum manifold. Once dry the products were resuspended with 20 µl ddH_2O (per well) and shaken at 150 rpm for 15 minutes. Cleaned products were transferred to a new 96 well PCR plate.

To each well of the new 96 well PCR plate was added: 5 µl cleaned amplification product, 0.75 µl of either forward or reverse primer, 0.5 µl BigDye® Terminator v3.1 Ready Reaction Mix (Applied Biosystems), 2 µl BigDye® 5x sequencing buffer and 8 µl ddH_2O. For the sequence reaction forward and reverse primers were placed in separate wells. The plate was run on a thermocycler according to the program shown in Table 2-6.

Table 2-6 Sequencing PCR thermocycler program.

Temperature (°C)	Time (s)	Number of cycles
96	60	
96	10	
50	5	x25
60	240	
4	∞	

Sanger sequencing was performed using the Applied Biosystems 3730 DNA Analyzer and calls were made using Applied Biosystem 5.2 software. Reads were aligned and visualized using CodonCode Aligner 5.1.

2.15.4 DNA fragment size quantitation

A 2% gel was made using 2 g of agarose dissolved in 100 ml 1x Tris-Borate EDTA (Sigma). The mixture was melted in the microwave and pre-stained using 10 µl/100 ml of gel red before the gel was poured into a cassette and left to cool. DNA was loaded with 5x Qiagen loading dye in a 1:4 ratio. DNA ladder was loaded into the first well. The gel was run at 120 V and visualized under a UV light.

2.16 Whole exome sequencing

2.16.1 DNA quantification and normalisation

DNA was quantified using a Qubit® dsDNA High Sensitivity kit and a Qubit® 2.0 fluorometer. Two standards were used as calibrators. Sample concentrations were measured in triplicate. The DNA was subsequently normalised in Tris HCl 10mM pH 8.5 to a final volume of 10 µl at 5 ng/µl.

2.16.2 Whole exome library preparation

The libraries for WES were prepared using the Nextera Rapid Capture Exome Enrichment Kit following the protocol provided by Illumina. Twelve exome libraries were prepared in parallel for each WES run. Below is a brief explanation of each step.

2.16.2.1 Tagmentation of genomic DNA

Using the transponsase Tn5 enzyme, genomic DNA (gDNA) was sheared into fragments of ≥300 bp with adapters ligated onto the ends of each fragment (i.e.

tagmented). The adapters enabled additional sequences, such as sequencing index primers, to be added in later stages.

2.16.2.2 Clean up and amplification of tagmented genomic DNA

The tagmented gDNA was cleaned using magnetic purification beads and 80% ethanol. After the addition of two sequencing primer-binding sites (which are a pair of indices and regions complementary to flow cell oligonucleotides) the gDNA was amplified and cleaned in the aforementioned manner. This produced a PCR-amplified library.

2.16.2.3 Hybridisation and capture of probes

The libraries were pooled and hybridised with biotinylated exon-specific capture probes. Probes hybridised to exonic regions were captured using magnetic streptavidin beads. Hybridisation and capture steps were repeated to enrich the exome library further. The final exon-enriched library was cleaned using magnetic purification beads and amplified by PCR.

2.16.3 Quantitation and sizing of whole exome libraries

At several points during the preparation of the whole exome library the Agilent Bioanalyser 2100 was used to assess the size, quality and quantity of gDNA fragments. Two Agilent chips were used: DNA1000 and DNA High Sensitivity (HS). The HS chip was used to verify the size of fragments produced after tagmentation (i.e. ≥300 bp) whilst the DNA1000 chip was used to assess both the initial PCR-amplified library and to validate the final exon-enriched library.

The chips were primed and loaded similarly. Firstly, a gel-dye mix was prepared. For the DNA1000 chip 25 µl of gel dye was added to the gel matrix and for the HS chip 15 µl of gel dye was added to the gel matrix. The gel-dye mix was centrifuged (2240 x *g* for 15 minutes). A chip was inserted into the priming station and 9 µl of the gel-dye mix pipetted into the syringe gel-dye well. The syringe was set to 1 ml and the priming station closed. The syringe was depressed and held by a clip for 1 minute before being released and reset at 1 ml.

9 µl of gel dye was added to the indicated wells and 5 µl of marker to any remaining wells. 1 µl of DNA ladder was pipetted into the ladder well and 1 µl of sample or deionized water was pipetted into the sample wells. The chip was shaken on the IKA vortex mixer for 60 sec at 2400 rpm and loaded and run on the Agilent Bioanalyser immediately.

2.16.4 Sequencing of whole exome libraries

Libraries were sequenced on a NextSeq500 sequencer. The premise for high-throughput sequencers is as follows.

Sequencing occurs within flow cells that are covered in oligonucleotides complementary to the adapters, which are ligated onto the gDNA during tagmentation. The oligonucleotides are a mixture of sequences complementary to either the 3' or 5' ends of the single stranded library fragments and enable the fragments to bind to the inside of a flow cell. These fragments then undergo solid-phase bridge amplification. Briefly, each bound fragment or strand is folded over to bind the alternate oligonucleotide, to that which it is already bound to, on the flow cell surface forming a bridge. A polymerase amplifies the strand to form a double stranded bridge, which is subsequently denatured into two single strands. This process is simultaneously repeated over and over to all the bound fragments resulting in millions of dense DNA clusters. After amplification, the reverse strands are removed and the residual 3' oligonucleotides attached to the flow cell surface are blocked to prevent unwanted priming.

Extension of the first sequencing primer starts the sequencing reaction off. During each sequencing cycle, four fluorescently labeled reversible terminator nucleotides are added and one is incorporated to extend the sequence according to Watson-Crick complementarity. Laser excitation causes fluorescence to be emitted by the nucleotide, which is captured and the base identified and recorded. The number of sequencing cycles determines the length of the read and in this case for the NextSeq500 it is 150. After 150 cycles of sequencing the forward strand is complete and the process is repeated to sequence the reverse

strand, the only differences being that the forward strand is removed and the second sequencing primer initiates the sequencing reaction.

Finally, to differentiate the twelve libraries from each other the indices, added during initial library amplification, are sequenced as well. Specific index primers are added and the reads are sequenced as above.

2.16.5 *In silico* analysis

2.16.5.1 Analysis of whole exome sequence data

Whole exome sequence data was analysed using the free web based genome analysis tool: Galaxy (Giardine et al., 2005, Goecks et al., 2010, Blankenberg et al., 2010) and wANNOVAR (an online functional annotation tool). In summary, WES produces millions of 300 bp reads that need to be accurately mapped to the human exome. Once mapped, variations from the reference sequence are assessed for clinical significance and highlighted for further investigation.

2.16.5.2 Dataset concatenation

All samples were run across four flow cell lanes using the NextSeq500 resulting in four forward and four reverse sequences per sample. Sequences were concatenated to produce one forward and one reverse sequence.

2.16.5.3 Quality control and trimming of reads

The quality of the concatenated sequences was assessed using the FastQC tool (Simon Andrews, Babraham Institute). The FastQC tool produces an output for each of the following:

- Basic Statistics
- Per base sequence quality
- Per sequence quality scores
- Per base sequence content
- Per base GC content
- Per sequence GC content

- Per base N content
- Sequence Length Distribution
- Sequence Duplication Levels
- Overrepresented sequences
- Kmer Content

Each output assesses different quality aspects of the reads. It should be noted that FastQC is designed to analyse whole genome data and therefore is based on the assumption that the sequenced library is random and diverse. However, for whole exome libraries the exonic regions in the genome have been enriched violating the aforementioned assumption. As a result, certain outputs have to be interpreted with caution: sequence duplication levels, overrepresented sequences and kmer content deviate from expected values and GC content per base and sequence are higher than expected due to exome enrichment (Lander et al., 2001). One of the most informative outputs is the per base sequence quality (Figure 2-1). Each bp position is allocated a score based on the probability that the position has been incorrectly called. A higher score indicates a more confident call. Bases with a score of <20 are deemed to be of too low a quality and need to be trimmed. A score of <20 is indicative of less than a 1 in 100 chance of being called correctly. To facilitate alignment low quality base calls are trimmed off (Figure 2-1).

Figure 2-1 Per base sequence quality output from FastQC for a proband from one of the families studied in this thesis. This graph shows the read quality for each base pair position within the read. Acceptable read quality score ≥20; reads<20 are trimmed.

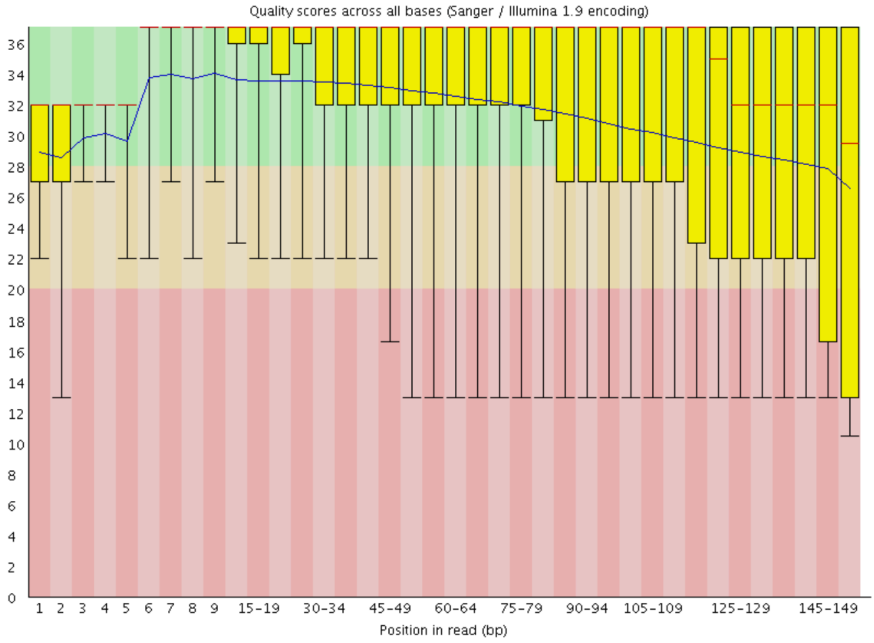

The per sequence quality scores highlight whether a subset of sequences within the WES library are of universally low quality. If a proportion of sequences are found to have a low quality score it may indicate a systematic error during library preparation or the sequencing process.

2.16.5.4 Alignment of reads

Trimmed reads were aligned to the Genome Reference Consortium build 37 of the human genome (GRCh37) using the Burrows-Wheeler Alignment algorithm (BWA) for Illumina.

2.16.5.5 Variant calling and annotation

Variant calling was performed using the GATK unified genotyper tool in Galaxy. It identified sites where the aligned sample sequence differed to that of the reference sequence. The subsequent dataset was annotated using wANNOVAR. Annotations for each identified variant included the base change, type of variant, genomic co-ordinates, functional prediction and population frequency. Types of variant include frameshift insertion and deletion, non-

frameshift insertion and deletion, non-synonymous single nucleotide variant (SNV), stopgain, stoploss and synonymous SNV.

2.16.5.6 Filtering of datasets

The raw data for each proband was subjected to four broad filters: a candidate gene list for vasculopathies and vasculitides, allele frequency, pathogenicity prediction, and variation type i.e. synonymous. The data was firstly compared to a known candidate gene list before any further filters were applied. These genes are already associated with a vasculopathy and it is thus prudent to eliminate any variants in them before further analysis. For this project the candidate gene list consisted of all the genes that have been identified to date in relation to vasculopathies, vasculitis and other pertinent diseases (Table 2-7). After identification of any possible candidate genes the remainder of the dataset was filtered based on frequency and variant type. Any variant that was synonymous and/or had a frequency of >0.01 in the general population databases (1000 genomes and the Exome Sequencing Project) were excluded from further analysis. A synonymous variant results in no change to the amino acid and therefore no functional effect. A variant with a frequency of >0.01 was classified as a polymorphism and therefore unlikely to be pathogenic, as a significant proportion of healthy people will carry the variant (although a notable exception to this rule is the aforementioned issue of founder effect resulting in higher frequency of true mutations in select populations, as highlighted by *RNF213* mutation on the Japanese). The remaining variants were compared to our 80 in-house controls (IHCs) to further exclude unlikely causative variants/genes. These IHCs were patients and their families that have been sequenced by our research group. I made sure that any patients with similar phenotypes were excluded.

The assumed model of inheritance determined how the proband dataset was compared to the IHC dataset. For a dominant model all heterozygous or homozygous variants in the IHCs that matched the heterozygote variants in the proband were excluded as causative. For a recessive model all homozygous variants in the IHCs that matched the homozygous variants in the proband were excluded. For a compound heterozygous model the method was more complicated. Assumptions as set out previously were used (Kamphans et al.,

2013). When parental data was not available the heterozygote variants in the proband were excluded if present in a homozygous state in the IHCs.

Table 2-7 Candidate gene list for vasculopathies and monogenic vasculitides.

Gene symbol	Gene name	Disease
ACTA2	Actin, alpha 2, smooth muscle	Familial thoracic aortic aneurysm and dissection, moyamoya disease, Multisystemic smooth muscle dysfunction syndrome
ADAR1	Adenosine deaminase, RNA specific	Aicardi Goutieres syndrome
BMPR2	Bone morphogenetic protein receptor, type II	Pulmonary venooclusive disease 1
CBL	Cbl proto-oncogene, E3 ubiquitin protein ligase	Noonan syndrome-like disorder with or without juvenile myelomonocytic leukemia
CBS	Cystathionine-beta-synthase	Homocystinuria, Thrombosis – hyperhomocysteinemic
CD40LG	CD40 ligand	Immunodeficiency
CECR1	Cat eye syndrome chromosome region, candidate 1	Polyarteritis nodosa
COH1	Vascular protein sorting 13 homolog B (yeast)	Cohen syndrome
COL3A1	Collagen type III, alpha 1	Ehlers-Danlos syndrome type III and IV
COL4A1	Collagen type IV, alpha 1	Other cerebral arteriopathy
COL5A1	Collagen V, alpha 1	Ehlers-Danlos syndrome classic type
COL5A2	Collagen type V, alpha 2	Ehlers-Danlos syndrome classic type
ELN	Elastin	Supravalvar aortic stenosis
FBN1	Fibrillin 1	Marfan syndrome, Aortic aneurysm ascending and dissection
FBN2	Fibrillin 2	Contractural arachnodactyly, Macular degeneration
GLA	Galactosidase, alpha	Fabry disease
GUCY1A3	Guanylate cyclase 1, soluble, alpha 3	Moyamoya 6 with achalasia
HFE	Hemochromatosis	Hemochromatosis

HTRA1	HtrA serine peptidase 1	CARASIL syndrome
IFIH1	Interferon-induced helicase C domain containing protein 1	Aicardi Goutieres syndrome
MFAP5	Microfibrillar associated protein 5	Familial thoracic aortic aneurysm and dissection
MYH11	Myosin, heavy chain 11, smooth muscle	Familial thoracic aortic aneurysm and dissection
MYLK	Myosin light chain kinase	Familial thoracic aortic aneurysm and dissection
NF1	Neurofibromin 1	Neurofibromatosis type 1
NOD2	Nucleotide-binding oligomerisation domain containing 2	Blau syndrome
NOTCH1	Notch 1	Aortic valve disease, Adams-Oliver syndrome
NOTCH3	Notch 3	CADASIL
PLOD1	Procollagen-lysine, 2-oxoglutarate 5-dioxygenase 1	Ehlers-Danols syndrome type IV
PRKG1	Protein kinase, cGMP-dependent, type 1	Familial thoracic aortic aneurysm and dissection
PSMB8	Proteasome subunit beta-type, 8	CANDLE
RNASEH2A	Ribonuclease H2, subunit A	Aicardi Goutieres syndrome
RNASEH2B	Ribonuclease H2, subunit B	Aicardi Goutieres syndrome
RNASEH2C	Ribonuclease H2, subunit C	Aicardi Goutieres syndrome
RNF213	Ring finger protein 213	Moyamoya disease
SAMHD1	SAM domain and HD domain 1	Aicardi-Goutieres syndrome
SKI	SKI proto-oncogene	Shprintzen-Goldberg syndrome
SLC2A10	Solute carrier family 2 (facilitate glucose transporter), member 10	Arterial tortuosity syndrome
SMAD3	SMAD family member 3	Loeys-Dietz syndrome type 3
SMAD4	SMAD family member 4	Juvenile polyposis/hereditary hemorrhagic telangiectasia syndrome, Myhre syndrome
TGFB2	Transforming growth factor, beta 2	Loeys-Dietz syndrome type 4
TGFB3	Transforming growth factor, beta 3	Loeys-Dietz syndrome type 5
TGFBR1	Transforming growth factor, beta	Loeys-Dietz syndrome type 1

	receptor 1	
TGFBR2	Transforming growth factor, beta receptor 2	Loeys-Dietz syndrome type 2
TMEM173	Transmembrane protein 173	STING-associated vasculopathy
TREX1	Three prime repair exonuclease 1	Vasculopathy, retinal, with cerebral leukodystrophy, Aicardi-Goutieres syndrome

Any interesting candidate gene variants were validated using Sanger sequencing (see above in section 2.15).

2.17 Protein extraction

Protein was extracted from HUVECs and PBMCs in 6 and 12 well plates respectively. Prior to protein extraction, cells were washed twice with PBS to remove all FBS. Protein was extracted by adding 100 µl ice-cold radioimmunoprecipitation (RIPA) buffer (Table 2-8) and 1 µl proteinase inhibitor (Sigma) to each well. Wells were scraped and the cell/RIPA suspension placed in a 1.5 ml eppendorf. To ensure complete lysis, the cells were kept on ice for 30 minutes and vortexed every 10 minutes or frozen at -20°C overnight.

Table 2-8 Recipe for RIPA buffer.

Reagent	**Quantity**
Sodium chloride	150 mM
NP-40 or Triton X-100	1.0 %
Sodium deoxycholate	0.5 %
SDS (sodium dodecyl sulphate)	0.1 %
Tris buffer pH 8.0	50 mM

2.18 Protein quantification

Protein concentration from cell lysate was measured with the Pierce™ bicinochoninic acid (BCA) protein assay kit (Thermo Fisher Scientific). Working

reagent (WR) was made up by diluting 50:1 BCA reagents A:B. 200 µl of WR was added to 25 µl of sample in a flat bottomed 96 well plate. A standard curve was produced using a dilution series of a BSA standard; BSA was diluted in RIPA buffer. The plate was incubated at 37°C for 30 minutes and read at 450 nM on a plate reader.

2.19 Western blotting

Gels used were either precast (BioRad) or cast using the recipes in Table 2-9. Samples were centrifuged (18,000 x g for 15 minutes at 4°C) and the supernatant removed to a new 1.5 ml eppendorf. Next, 5x SDS loading buffer (Table 2-10) was added to the protein samples at a 1:4 ratio. Samples were boiled at 95°C for 5 minutes to denature the protein. 7 µl of Amersham ECL Full-Range Rainbow weight marker was loaded into the first well and up to 40 µl of sample was added to subsequent wells. The volume of each sample was dependent on protein concentration; an equal amount of protein was loaded into each well. The gel was run, in running buffer, for 30 minutes at 90 V, which was increased to 120 V for an additional 2 hours (Table 2-11). A nitrocellulose membrane was activated by being soaked in cold methanol for 5 minutes, rinsed with distilled water and equilibrated in transfer buffer (Table 2-12). The gel was also equilibrated in transfer buffer for 1 minute. The transfer was run at 200 mA for 1 hour or until the ladder was visibly transferred onto the membrane. The membrane was blocked in PBS-Tween and 5 % milk for 1 hour. The primary antibody was added in 5 % milk, according to the concentrations in Table 2-13 and rolled overnight at 4°C. Before adding the secondary antibody in 5 % milk, the membrane was washed at room temperature with PBS-Tween: 3 x 10 minute washes. The secondary antibody was rolled for 1 hour at room temperature. It was washed a further three times before development. The image was developed using Amersham ECL prime western blotting detection reagent and Amersham hyperfilm ECL.

Table 2-9 Recipe for 1 x 7.5% and 12.5% running gel and 1 x 4% stacking gel for western blotting.

Reagent	7.5% separating gel (25ml)	12.5% separating gel (25ml)	4% stacking gel (10.06ml)
30% stock acrylamide	6.25 ml	10.0 ml	1.70 ml
1.5M Tris-HCl (pH 8.0)	6.25 ml	6.25 ml	-
0.5M Tris-HCl (pH 6.8)	-	-	1.25 ml
10% SDS	250 µl	250 µl	100 µl
APS (10%)	250 µl	250 µl	100 µl
Distilled water	11.0 ml	8.25 ml	6.80 ml
TEMED	10 µl	10 µl	10 µl

Table 2-10 Recipe for 5x SDS loading buffer.

Bromophenol blue dye was added and 1 ml aliquots were frozen at -20°C.

Reagent	Percentage	Per 20 ml
B-Mercaptoethanol	25%	Per 20 ml
Glycerol	50%	5 ml
SDS	10%	10 ml
0.25M Tris HCl pH6.8	15%	2 g
		To 20 ml

Table 2-11 Recipe for 10x running buffer.

Dilute to 1x in ddH_2O.

Reagent	Quantity per 1L
Tris	30 g
Glycine	144 g
SDS	10 g
ddH_2O	To 1L

Table 2-12 Recipe for 10x transfer buffer.

Prior to use 100 ml is added to 700 ml of ddH_2O and 200 ml of methanol and chilled at 4°C.

Reagent	Quantity per 1L
Tris	30 g
Glycine	144 g
ddH_2O	To 1L

Developed western blot films were scanned and the band densities of each lane quantified by densitometry using ImageJ. Peaks were generated corresponding to the bands on the film (Figure 2-2). The 'straight-line' tool was used to close off the base of each peak and the area under the curve was measured. The relative density of each band was then normalised to the loading control i.e. actin or vinculin.

Table 2-13 Dilution factors for antibodies used for western blots

Antibody	Clone	Type	Conc.
Actin	Mouse monoclonal	Primary	1:5000
Cbl	Mouse monoclonal	Primary	1:2500
Myh11	Mouse monoclonal	Primary	1:2500
EGFR	Rabbit monoclonal	Primary	1:1000
p44/42 MAPK	Rabbit polyclonal	Primary	1:1000
Phospho-p44/42 MAPK	Rabbit polyclonal	Primary	1:1000
PLCγ1	Rabbit polyclonal	Primary	1:1000
Phospho-PLCγ1	Rabbit polyclonal	Primary	1:1000
Vinculin	Mouse monoclonal	Primary	1:250,000
HRP conjugated	Goat anti-Mouse polyclonal	Secondary	1:5000
HRP conjugated	Goat anti-Rabbit polyclonal	Secondary	1:5000

Figure 2-2 Profile peaks generated by ImageJ to determine western blot band density.

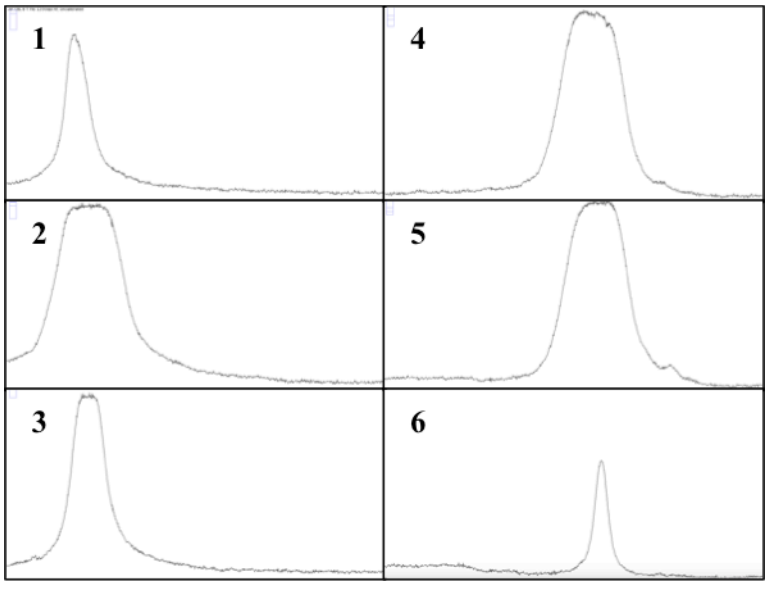

2.20 Fluorescence-activated cell sorting (FACS)

The general method is outlined here. The specific buffers and antibodies used in each experiment are mentioned in the relevant chapters. Cells were harvested (see 2.11), resuspended and washed in PBS. After centrifugation (14,000 x *g* for 4 minutes), the PBS was removed, cells were resuspended and 70 µl of a wash buffer was added to each sample. From each sample, 20 µl was removed and transferred to two separate eppendorfs: 10 µl for a non-staining control and 10 µl for a non-specific control. If required, cells were fixed and permeabilised before addition of the primary antibody. Primary antibodies were added at a concentration of 1:50 and incubated at room temperature on a shaker (200 rpm) for 15 minutes. No primary antibody was added to either control. Samples were then washed in 1 ml of wash buffer and centrifuged (14,000 x *g* for 4 minutes). The supernatant was removed, cells were resuspended in 50 µl of the wash buffer and a fluorophore-conjugated secondary antibody was added at a 1:200 concentration. Secondary antibody was added to the non-specific control. Samples were covered in foil and incubated at room temperature on a shaker (200 rpm) for 15 minutes before a final wash and centrifugation step (14,000 x *g* for 4 minutes). After removing the supernatant, cells were resuspended in 200 µl 4% paraformaldehyde (PFA) and analysed using a BD FACSCalibur™.

Table 2-14 PBAC recipe

Reagent	Per 1 L
Sodium azide	1 ml
Sodium citrate	6 ml
BSA	1 g
PBS	To 1 L

2.20.1 Analysis

Samples were analysed using FlowJo. For PBMC samples, gating of the monocyte population was carried out before relative fluorescence intensity was analysed. For HUVECs and transformed HDFCs, gating was done to separate live cells from dead ones. Gating parameters are outlined in the relevant

chapters. After gating, median fluorescence intensity was calculated for all samples.

2.21 Statistical analysis

All *in vitro* experiments were performed in triplicate unless otherwise stated, and values were presented as mean ± SEM unless otherwise specified. Statistical differences for *in vitro* experiments between groups were determined by unpaired two-tailed *t* test. $P<0.05$ was regarded as significant.

Chapter 3 Moyamoya-like cerebrovascular disease associated with a novel mutation in *MYH11*

3.1 Summary

Heterozygous mutations in the *MYH11* gene have been described to cause thoracic aortic aneurysm or aortic dissection (TAAD) and patent ductus arteriosus (PDA). The mutations affect the C-terminal coiled-coil region of the smooth muscle myosin heavy chain, a contractile protein of smooth muscle cells (SMCs). In this chapter, I employed whole exome sequencing (WES) to identify the genetic cause of a systemic vasculopathy affecting the renal and cerebral circulation in a 2 year old of non-consanguineous descent. I identified a missense alteration, R1535Q, in exon 33 of the *MYH11* gene that is likely to affect the communication between the motor domain and the coiled-coil tail of the SM-MHC-11 protein. I therefore expanded for the first time the phenotype associated with *MYH11* mutations to include a moyamoya-like cerebrovascular disease. My findings emphasize the systemic nature of the vasculopathy associated with *MYH11* mutations and the need for broader than previously suggested vascular surveillance to include the cerebrovascular circulation. The contribution of *MYH11* mutations to isolated cerebral arteriopathy and childhood stroke remains to be established.

3.2 Introduction

This chapter focuses on a patient under the care of the neurovascular service at GOSH (lead clinician Dr Ganesan) with an unclassified vasculopathy characterised by moyamoya arteriopathy and renal artery stenosis. For the purposes of this thesis I will refer to this family as Family A.

3.3 Family tree for family A

Index case of family A was a Jordanian/Moroccan female from non-consanguineous parents, referred to as A-III-3 from now on (Figure 3-1).

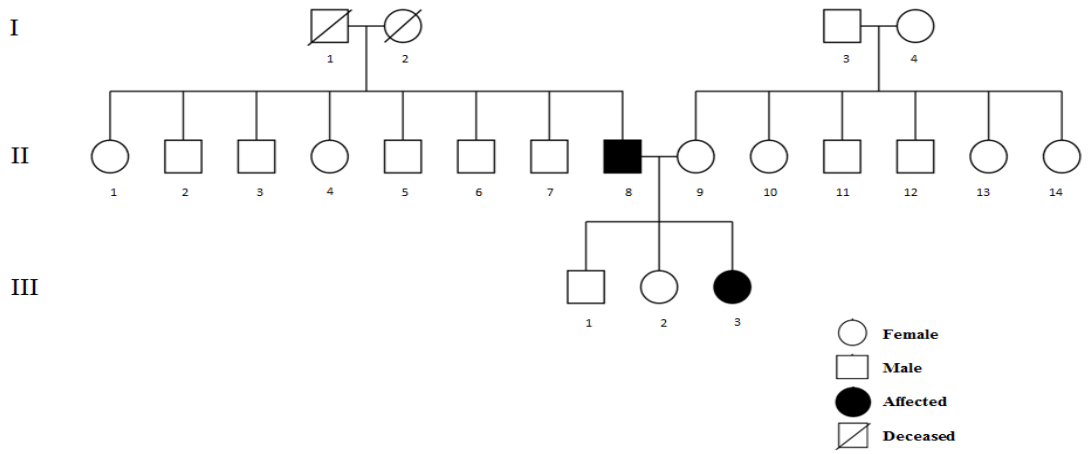

Figure 3-1 Family tree for family A.

3.4 Clinical presentation

The initial presentation of the index case of family A was at the age of 2 years old when she was found to have persistent weakness of the left arm. This was, at the time, attributed to slow recovery from a greenstick fracture of the humerus and reluctance to use that hand. Six months later she developed right-sided hemiparesis, aphasia, right hemianopia and right conjugate gaze palsy (Figure 3-2). There were no clear precipitants (recent infections or injury) prior to this episode. She reported no fever, skin rashes, articular, gastrointestinal or respiratory symptoms and blood tests revealed no acute phase response or systemic symptoms (C reactive protein < 5 mg/L, normal range < 10 mg/L; Erythrocyte Sedimentation Rate, ESR 5 mm/h, normal range < 10 mm/h). Brain magnetic resonance imaging (MRI) revealed left anterior and middle cerebral artery territory (ACA/MCA) infarction and a previous infarct in the right ACA/MCA territory (Figure 3-2) likely relating to the reluctance to use the left hand from years ago.

Catheter angiography of the cerebral arteries showed a pattern of bilateral terminal stenoses of the internal carotid arteries (ICAs) and MCAs with a collateralisation pattern consistent with moyamoya arteriopathy in addition to anterior and middle cerebral artery stenotic changes (Figure 3-3 A-F). Visceral digital subtraction angiography revealed narrowing of the mid-aorta and bilateral renal artery stenosis (Figure 3-3 G). Echocardiography revealed a small patent ductus arteriosus (PDA).

Extensive investigations for rheumatological, infectious and metabolic causes for this presentation were negative. On clinical examination she had two cutaneous café-au-lait spots. Of note genetic screening of *NF1* for neurofibromatosis type 1 was negative and array comparative genomic hybridization (CGH) did not detect any copy number variants. She was considered to have an unclassified generalized vasculopathy with a prominent cerebral involvement and underwent bilateral extracranial-intracranial (ECIC) bypass whilst being maintained on aspirin (antiplatelet dose 5mg/kg per day). Four years after the bypass there was radiological arteriopathy progression: a new right frontal lobe infarction, increased stenosis of the right ICA/MCA and occlusion of the left terminal ICA (TICA) with more basal collaterals (Figure 3-3 D-F). At the time of writing this report she was normotensive with normal cardiac and renal

function but had an asymmetric non-progressive tetraparesis and pseudobulbar palsy. Relevant family history included a paternal grandmother with a history of arterial ischaemic strokes from the age of 42 years old in the context of significant arterial hypertension who died in her mid 60s; a paternal cousin (9 years old) with arterial hypertension, possible thrombosis to a blood vessel in the neck and congenital heart disease; and a paternal uncle who had coronary artery bypass surgery at a young age.

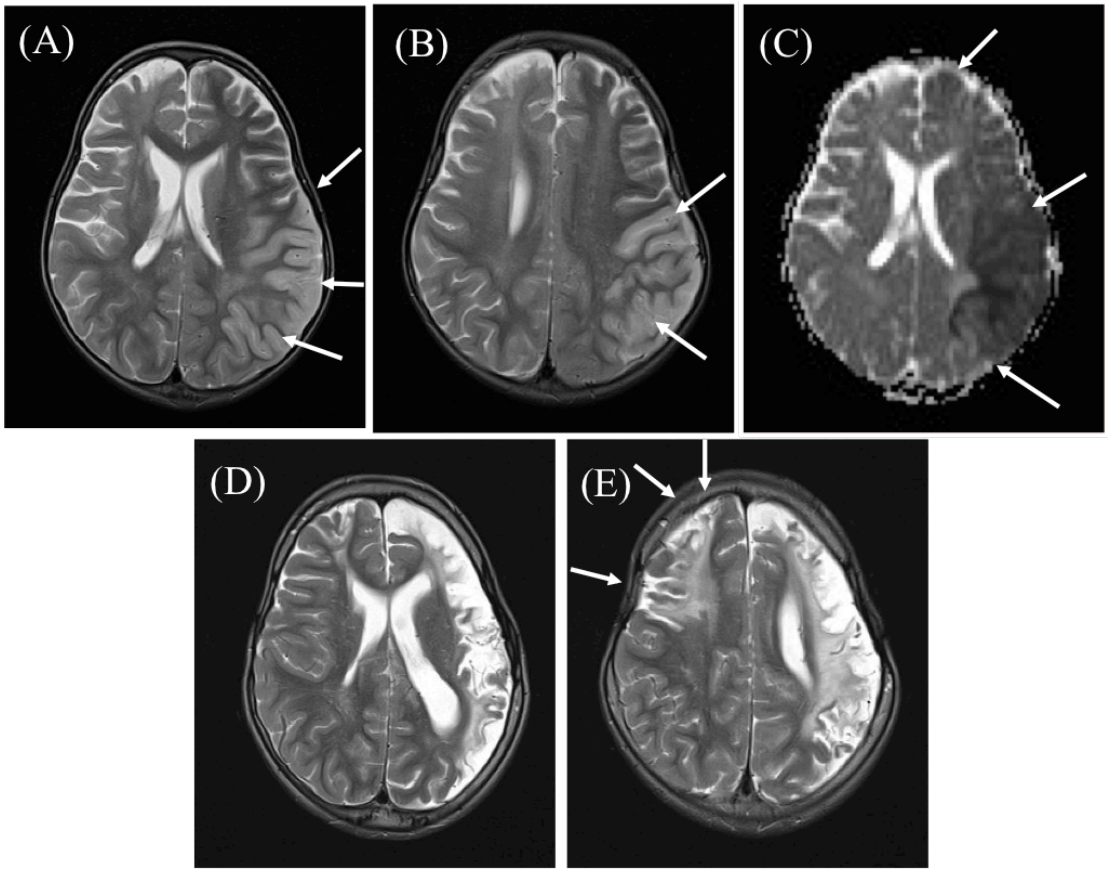

Figure 3-2 Brain Magnetic resonance imaging (MRI) for index case of family A.

(A, B) Axial T2 weighted MRI scans through the lateral ventricles and the top of the lateral ventricles at presentation show a largely cortical acute left ACA and MCA territory infarct (arrows) and a mature right MCA infarction involving the cortex, white matter and basal ganglia. (C) The ADC map corresponding to the slice in (A) confirms the left sided infarct is acute – dark on ADC map (arrows). (D, E) Axial T2-weighted MRI 6 years later demonstrates maturation of the left MCA infarct and extension of the right MCA infarct (arrows). ACA = anterior cerebral artery, MCA = middle cerebral artery, ADC = apparent diffusion coefficient.

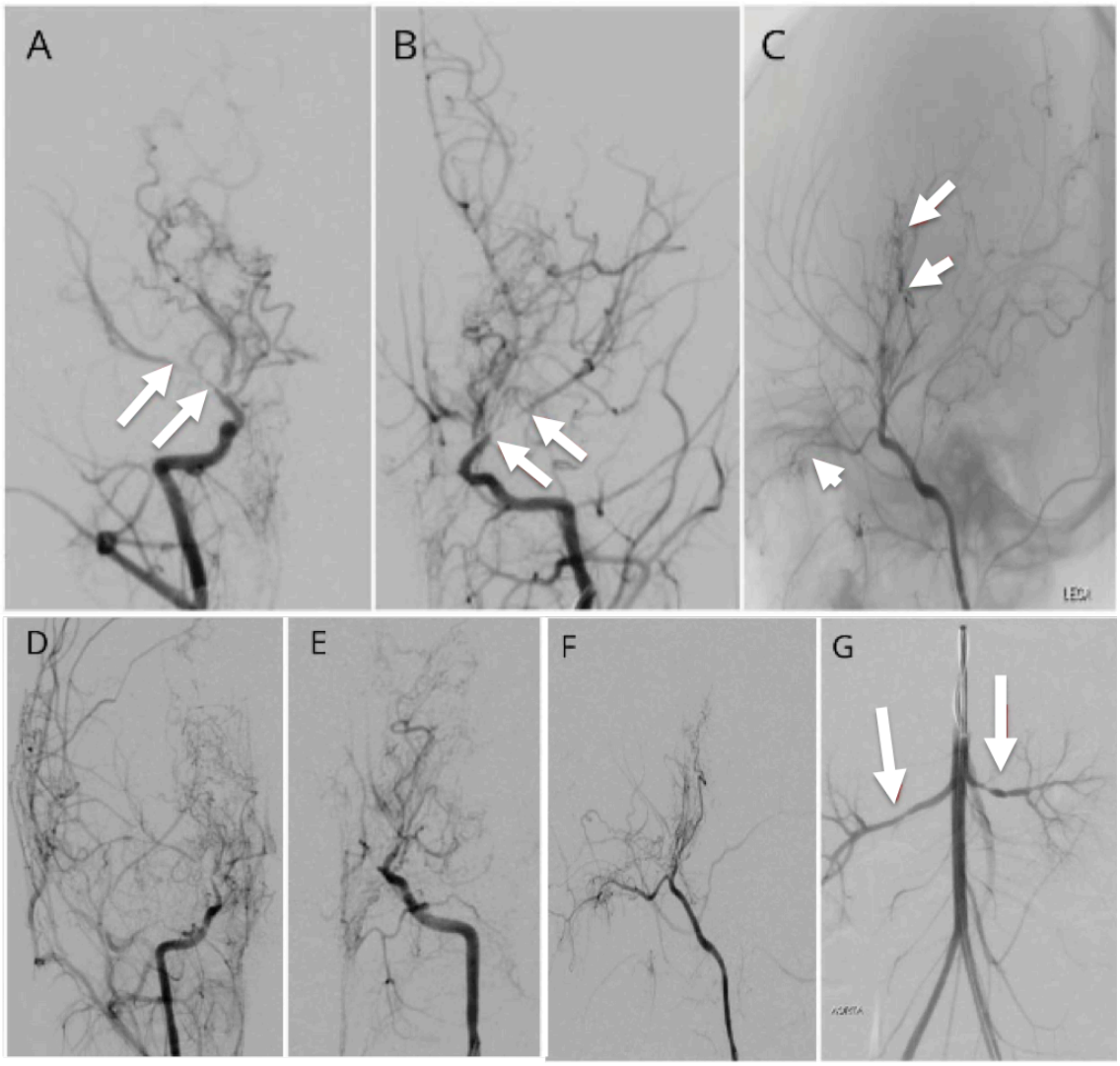

Figure 3-3 Catheter and visceral digital subtraction angiography for index case of family A.

(A) Right and (B) left AP projections of the ICA injections of the cerebral angiogram at presentation demonstrates narrowing of the tICA and straight and long segment narrowing of the M1 and A1 segments of the MCA (between arrows) and ACAs bilaterally. Moyamoya collaterals are present on the initial angiogram. (C) Lateral projection of the left ICA injection demonstrates the presence of basal and moyamoya collaterals (short arrows). 4 years later following progression of the arteriopathy is seen with (D) further narrowing of the right M1 segment of the MCA and (E,F) occlusion of the left tICA with absent filling of the terminal ACA and MCA arteries. (F) The number of basal and moyamoya collaterals has increased. The pial collaterals in (C) are a result of the pial synangiosis. (G) Bilateral narrowing of the renal arteries seen on digital subtraction renal angiography. AP = anteroposterior, ACA = anterior cerebral artery, MCA = middle cerebral artery, tICA = terminal internal carotid artery.

3.5 Identifying a causal allele: Whole Exome Sequencing

WES was performed on A-III-3 and her mother (see General methods and materials section 2.16). As only A-III-3 was affected a dominant heterozygous model was assumed as the possible mode of inheritance. WES identified 26,679 variants. As a first filter the WES output was initially compared to the vasculopathy candidate gene list (Table 2-7). Variants were found in three candidate genes: *MYH11, MYLK* and *NOTCH1*. These were investigated further.

3.5.1 Verification of candidate gene variants

These candidate genes were sequenced using Sanger sequencing (see General methods and materials section 2.15). The primers used are listed in Table 3-1. The variants in *MYLK* and *NOTCH1* were found to be false positives; however, the variant in *MYH11* was confirmed to be a novel heterozygous missense mutation NM_002474:c.4604G>A (p.R1535Q) presented in the index case (Figure 3-4). The variant was predicted to be deleterious by the SIFT, MutationTaster and PolyPhen-2 programs. The non-synonymous substitution resulted in an amino acid change from arginine to glutamine (p.R1535Q).

The p.R1535Q mutation in *MYH11* was not detected in the mother or sibling but was present in the father (Figure 3-4). The father was found to have a family history of arterial ischaemic stroke and early onset coronary artery disease in young adult life. He underwent baseline echocardiography and cardiac MRI and MRA, which showed mild narrowing of the aorta indicative of early signs of an evolving vasculopathy affecting the aorta.

I therefore expanded the phenotype associated with *MYH11* mutations to include moyamoya-like cerebrovascular disease. My findings also had implications for the proband's father, for whom annual cardiovascular monitoring was initiated and early changes suggestive of a vasculopathy were detected.

Table 3-1 Primer sequences used for Sanger sequencing.

Primer name	Primer sequence
MYLK exon 17a F	AGCAGGCCCTCCTACCTG
MYLK exon 17a R	AAGCCTGCTGAGACCCTG
MYLK exon 17b F	CTTTGCTAGCGGATTTCAGG
MYLK exon 17b R	GAGACCTCCTGGGGAAGAAG
MYLK exon 17c F	CAGACACAGTCTTTGGCTTCAC
MYLK exon 17c R	GCCTCTCACCAATGTTCCC
MYH11 exon 9 F	AGCCAGCTCGGGTTACTTG
MYH11 exon 9 R	CAGTGCACAACCTGCACC
MYH11 exon 33 F	CTGAGGCAGGAGGTGGAG
MYH11 exon 33 R	CAGTCGAGGATGGGTCTGAG
NOTCH1 exon 18 F	ATGTCTGGACTCAATGCAGC
NOTCH1 exon 18 R	GAAAGGCTGGGCTGTCC
NOTCH1 exon 19 F	ACCGGCTGCTCAGATCC
NOTCH1 exon 19 R	ACTGGCCTCCCTGGGTC

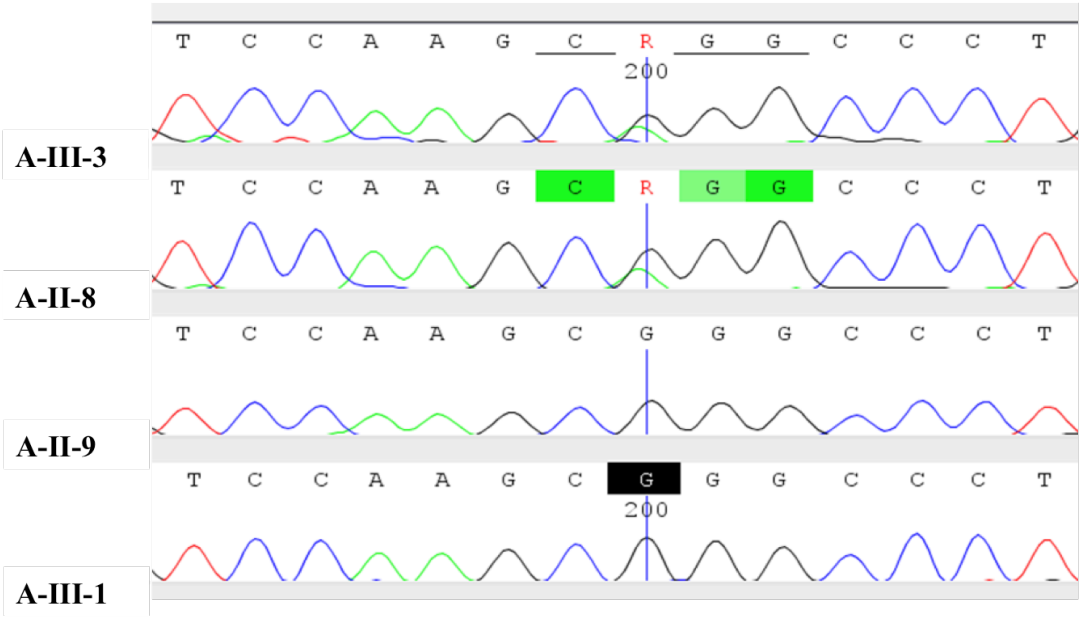

Figure 3-4 Sanger sequencing chromatogram for the parents (A-II-8 and A-II-9), proband (A-III-3) and a sibling (A-III-1).

Aligned to reference sequence exon 33 of MYH11 (NM_002474). Blue line indicates a heterozygous non-synonymous missense substitution present in the A-III-3 and A-II-8 but not in the A-II-9 or A-III-1 (c.4604G>A:p.R1535Q).

3.6 Discussion

The *MYH11* gene encodes smooth muscle myosin heavy chain (SM-MHC) and is predominantly expressed in smooth muscle cells. SM-MHC is a subunit of the hexameric myosin protein, which consists of two heavy chain subunits and two pairs of non-identical light chain subunits. Interaction between the myosin protein and actin filaments, powered by ATP hydrolysis, results in smooth muscle cell (SMC) shortening and contractile force generation (Vale and Milligan, 2000, Dillon et al., 1981). Each myosin molecule has two globular heads and a tail. The tail is formed from the dimerization of the C-terminal portions of the heavy chains and harbours an α-helical coiled-coil domain. The globular heads are the N-terminals of the heavy chains and each contains two major domains: the motor domain, which has both ATP- and actin-binding sites, and the regulatory domain, which is stabilized by a pair of light chains. The regulatory domain, which acts as a lever arm, connects to the coiled-coil domain and oligomerizes to form the myosin thick filament (Howard, 1997). Motility occurs when the globular myosin heads form cross-bridges with the actin filament and, through a 'rowing motion', move along the actin filaments.

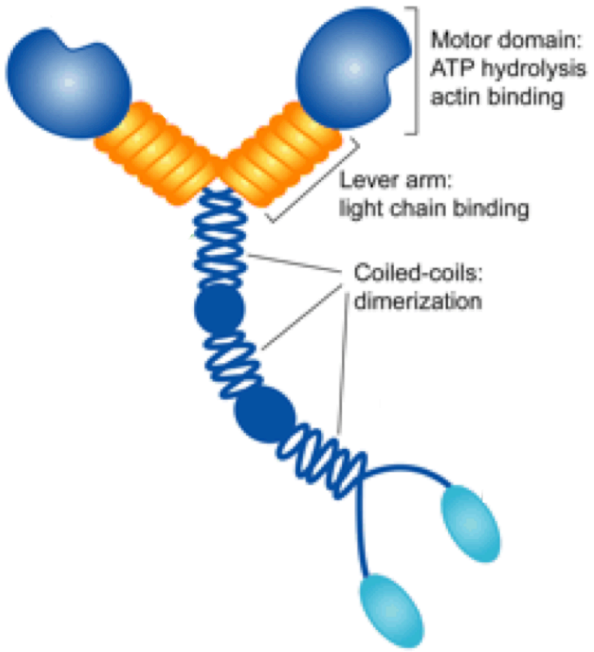

Figure 3-5 Schematic representation of MYH11. *Adapted from reference (Toth et al., 2005).*

To delineate the specific role that *MYH11* plays in the contractile apparatus in SMCs Morano et al. (2000) generated *Myh11*$^{-/-}$ knockout mice. The mice were born at the expected Mendelian ratio at a normal weight, indicating normal foetal development, but died 24-72 hours later (Morano et al., 2000). They determined that although lack of SM-MHC was not required for foetal development it was essential for the initial high force generation created during smooth muscle contraction in order for long-term survival post-birth (Morano et al., 2000). This results in several key physiological processes being affected such as closure of the ductus arteriosus, development of normal blood pressure and micturition (Morano et al., 2000).

In relation to human disease, mutations in the *MYH11* gene are a common cause of familial thoracic aortic aneurysm/aortic dissection (TAAD) associated with PDA (Zhu et al., 2006, Pannu et al., 2007). These include splice site mutations, exonic deletions and missense substitutions (Zhu et al., 2006, Pannu et al., 2007). Pannu et al. (2007) suggested that the molecular basis of dysfunction caused by *MYH11* mutations is the result of altered cross-bridge elasticity (Pannu et al., 2007). This is caused by disrupted communication between the myosin motor domain and the regulatory domain/ lever arm.

To date a large number of genes that result in dysfunctional SMC contractility, like *MYH11*, are associated with non-inflammatory vasculopathies, in particular TAAD (Table 2-7) (Milewicz et al., 2008, Guo et al., 2007, Zhu et al., 2006, Renard et al., 2013). Herein I identified for the first time that the vasculopathy associated with mutations in *MYH11* might involve the cerebral circulation and therefore extend beyond the aorta.

In the proband a missense alteration, R1535Q, was revealed in exon 33 of *MYH11*, which resides in the coiled-coil domain of SM-MHC. Two further examples of missense substitutions from arginine (R) to glutamine (Q) have been observed at residues 712 (Pannu et al., 2007) and 1758 (Zhu et al., 2006) of SM-MHC in association with a vascular pathology. The amino acid alteration in all three instances is from a charged to an uncharged amino acid indicative of likely deleterious functional effects. The change at residue 712 was revealed in a proband from a family where at least one member had been previously diagnosed with PDA (Pannu et al., 2007). The mutation at this residue was located in the ATPase head region and was

associated with an occlusive arterial disease resulting in coronary artery disease (CAD) and peripheral vasculopathy (Pannu et al., 2007). It was thought that this mutation caused disease by disrupting communication between the motor domain and the lever arm resulting in reduced myosin motor elasticity and aortic stiffness (Pannu et al., 2007). The alteration at residue 1758 was identified in an American kindred diagnosed with aortic dissection and/or PDA (Glancy et al., 2001) and was located in the coiled-coil domain. It was hypothesized that this substitution would affect structure of the coiled-coil domain and consequently myosin thick filament assembly (Zhu et al., 2006). In addition to the effect on SM-MHC structure and function, mutations in *MYH11* have been observed to play a role in causing SMC hyperplasia by the cells switching to a proliferative state in response to cellular cues (Pannu et al., 2007). As previously mentioned, the R1535Q (4604G>A) mutation I have identified is located in the coiled-coil domain of SM-MHC. It is likely that a similar molecular mechanism is affected in the pathogenesis of the cerebral arteriopathy present in my patient (A-III-3) i.e. altered structure of the coiled-coil domain arising in modified communication between it and the motor domain of SM-MHC. Whether an external influence or additional factor is required for disease to develop is uncertain. In addition, how modified communication between the domains can cause an occlusive phenotype is not clear but nevertheless my finding expands the phenotype associated with heterozygous mutations in *MYH11* to include an occlusive cerebral arteriopathy.

There are similarities between my discovery in *MYH11* and the *ACTA2* story (Guo et al., 2007, Milewicz et al., 2010). *ACTA2* was first identified as a causative gene for TAAD in several families with each family harbouring a different novel missense substitution (Guo et al., 2007). The mutations perturbed the dynamics of actin assembly and/or stability and thus aortic structural integrity (Guo et al., 2007). More specifically aortas from affected individuals showed characteristic traits of aortic medial degeneration such as loss of elastic fibers, increased proteoglycan deposition and decreased number of smooth muscle cells (Guo et al., 2007, Milewicz et al., 2010). Stenosis due to SMC proliferation was also evident in the vasa vasorum causing occlusion in focal areas (Guo et al., 2007, Milewicz et al., 2010). Following these findings a subsequent publication noted that in addition to TAAD, carriers of *ACTA2*-mutations also presented with premature onset of CADnand/or ischaemic strokes, which in some cases were classified as MMD (Guo et al., 2009). The authors

concluded that some *ACTA2* mutations segregate with occlusive vascular disease caused by increased SMC proliferation in the medial layers of the arteries (Guo et al., 2009). It is thought *ACTA2* may play a role in SMC proliferation because polymerization of α-actin modulates SMCs between a quiescent cell that expresses high levels of contractile proteins to a proliferating cell that does not express any (Parmacek, 2007, Owens, 1995). Therefore, any null/missense mutations in *ACTA2* would cause SMCs to proliferate uncontrollably (Guo et al., 2009). The *ACTA2* mutation associated with MMD was R212Q (635G>A) with histopathologic studies of the internal carotid arteries showing increased SMC proliferation in the intimal layer leading to vessel occlusion (Guo et al., 2009). Interestingly, *ACTA2* mutations appear to cause dilatation of the aorta but stenosis of smaller arteries indicating the gene may have a differential effect depending on the vessel involved (Guo et al., 2009). There may a similar mechanistic link in A-III-3 regarding *MYH11* mutations. That is the mutation may cause a stenotic phenotype in smaller vessels but result in aneurysms in large vessels.

It should be noted that there are differences in the radiological phenotype between the arteriopathy of the proband described in this chapter and that associated with *ACTA2*. In the *ACTA2* arteriopathy the proximal branches of the circle of Willis are unusually straight, with occlusive characteristics and lack of basal collaterals (Munot et al., 2012). In my patient the arterial vasculature is similarly straight but, in contrast, there is a profuse basal collateral network distinctive to MMD (Starosolski et al., 2015). Whilst the radiological phenotype is well recognised in *ACTA2* patients (Starosolski et al., 2015, Munot et al., 2012), the one associated with *MYH11* has yet to be established. It may be that a distinctive morphological signature is waiting to be defined.

My findings have potential implications for vascular screening to include the cerebrovascular circulation in patients with *MYH11* mutations. Currently only the aorta is screened. In addition, there are significant clinical consequences as beta-blockade can be a potential therapy prescribed for TAAD patients but such a treatment could adversely affect systemic blood pressure and thus brain perfusion in the presence of cerebral vasculopathy, with a potential fatal outcome. Whilst *MYH11* patients should receive cerebrovascular screening, in cases such as the one discussed

here, who present with predominantly neurological symptoms, it is also important to perform a detailed cardiac assessment with echocardiography and other aortic imaging. For patients with no established definitive vascular changes, screening for subclinical vascular involvement, such as measuring arterial stiffness with pulse wave velocity may have a role. It may be that a similar approach should be considered for all patients with a moyamoya arteriopathy who are misleadingly thought to have only cerebral vasculature involvement. *MYH11* testing could also be done in children with MMD who have an atypical cerebral angiographic presentation or poor response to pial synangiosis. My findings also highlight a need for establishing the relevance/importance of *MYH11* screening by looking at a larger cohort of children with stroke and arteriopathy and assessing potential *MYH11* variant frequency.

3.7 Conclusion

In summary, I have expanded the phenotype associated with heterozygous mutations in *MYH11* to include cerebrovascular disease similar to moyamoya arteriopathy. My findings have the following implications:

1. Children with arterial ischaemic stroke and vasculopathy should be screened for mutations in *MYH11* particularly if they have an atypical cerebral angiographic presentation or poor response to pial synangiosis.
2. Patients with established *MYH11* mutations should be screened for cerebrovascular involvement and vascular surveillance should extend beyond the aorta.

I published my findings in Neurology (Keylock et al., 2018).

Chapter 4 Moyamoya-like cerebrovascular disease associated with heterozygous mutations in *c-CBL*

4.1 Summary

Moyamoya arteriopathy is characterised by progressive stenosis of the terminal part of the internal carotid arteries and the development of abnormal collateral deep vessels. Its pathophysiology is unknown. Moyamoya arteriopathy can be the sole manifestation of the disease (moyamoya disease) or be associated with various conditions (moyamoya syndrome) including some Mendelian diseases. In this chapter I investigated the genetic basis of moyamoya in 3 families using a WES approach. WES was performed in four early-onset moyamoya sporadic cases and their parents (trios). I identified heterozygous mutations in *c-CBL* in all affected cases. c-CBL is an E3 ubiquitin ligase that down regulates various receptor tyrosine kinases. Detailed *in vitro* functional expression studies were undertaken in the patients with mutations in *c-CBL* that showed impaired c-CBL-mediated degradation of cell-surface receptors in a dominant-negative fashion. These results were compatible with dysregulated intracellular signalling through RAS, which contributed to the development of this novel genetic cause of cerebral vasculopathy in these patients. These data suggest that *c-CBL* gene screening should be considered in early-onset moyamoya, even in the absence of obvious signs of a RASopathy.

4.2 Introduction

This chapter focuses on three families: one family under the care of the neurovascular service at GOSH (lead clinician Dr Ganesan) where the index case presented with a moyamoya-like arteriopathy; another family with two affected siblings and their mother with moyamoya-like cerebrovascular disease; and a third family where the index case (now deceased) presented with a similar arteriopathy phenotype. For the purposes of this thesis I will refer to these families as family B, C and D.

4.3 c-CBL function and structure

c-CBL encodes the Casitas B-cell lymphoma protein (CBL or c-CBL), which functions as an E3 ubiquitin ligase and multi-adaptor protein. There are three mammalian isoforms of CBL: c-CBL, CBL-b and CBL-c. For the purpose of this report I have focused on the c-CBL isoform.

c-CBL is involved in the regulation of signal transduction in various cell types by altering growth factor receptor signaling cascades (Schmidt and Dikic, 2005). More specifically it negatively regulates various receptor protein tyrosine kinase-signaling pathways via receptor degradation and acts as an adaptor protein in tyrosine phosphorylation-dependent signaling (Thien et al., 2001, Fu et al., 2003).

c-CBL has five functionally distinct protein domains: an N-terminal tyrosine kinase binding (TKB) domain, a linker domain, a zinc binding RING finger domain, a proline-rich region and a C-terminal ubiquitin-associated (UBA) domain (Thien and Langdon, 2005) (see Figure 4-1). The TKB domain determines substrate specificity and is joined to the RING finger domain by the linker region (Thien and Langdon, 2005). The RING finger domain regulates the E3 ubiquitin ligase activity, which is essential to the ubiquitin transfer process (Pickart, 2001). Through this domain c-CBL directs monoubiquitination of receptors, which in turn promotes their lysosomal-mediated degradation (Schmidt and Dikic, 2005). The proline-rich region is the site of interaction between c-CBL and cytosolic proteins involved in the adaptor functions of c-CBL (Thien and Langdon, 2005). The UBA domain is the site of interaction

between c-CBL and the ubiquitin domains of other proteins (Thien and Langdon, 2005).

Historically mutations in *c-CBL* have primarily been associated with acute myeloid leukaemia (Caligiuri et al., 2007, Sargin et al., 2007), myeloproliferative neoplasms (Grand et al., 2009, Dunbar et al., 2008) and juvenile myelomonocytic leukaemia (JMML) (Niemeyer et al., 2010, Loh et al., 2009). Deletion of the essential Y371 residue in the *c-CBL* linker region has been reported to induce oncogenicity by disrupting the integrity of the α-helical structure of the linker region (Andoniou et al., 1994). Due to the oncogenic effect, it is unsurprising that mutation of this residue is observed in ~50% of JMML patients (Niemeyer et al., 2010, Perez et al., 2010). Germline mutations have now been proven to cause a Noonan-like syndrome with or without JMML (Niemeyer et al., 2010, Perez et al., 2010). Patients display phenotypic characteristics similar to the RASopathy Noonan syndrome such as facial dysmorphia, cognitive deficit and musculoskeletal anomalies. Pertinent to my study is the observation that some of these patients also display symptoms consistent with a vascular pathology (Niemeyer et al., 2010). One patient was diagnosed with a large vessel vasculitis consistent with TA whilst others presented with arterial hypertension, optic atrophy and acquired cardiomyopathy (Niemeyer et al., 2010). More recently several patients with MMD have been found to harbour mutations in *c-CBL* that affect the protein's E3 ubiquitin ligase activity (Guey et al., 2017a, Hyakuna et al., 2015).

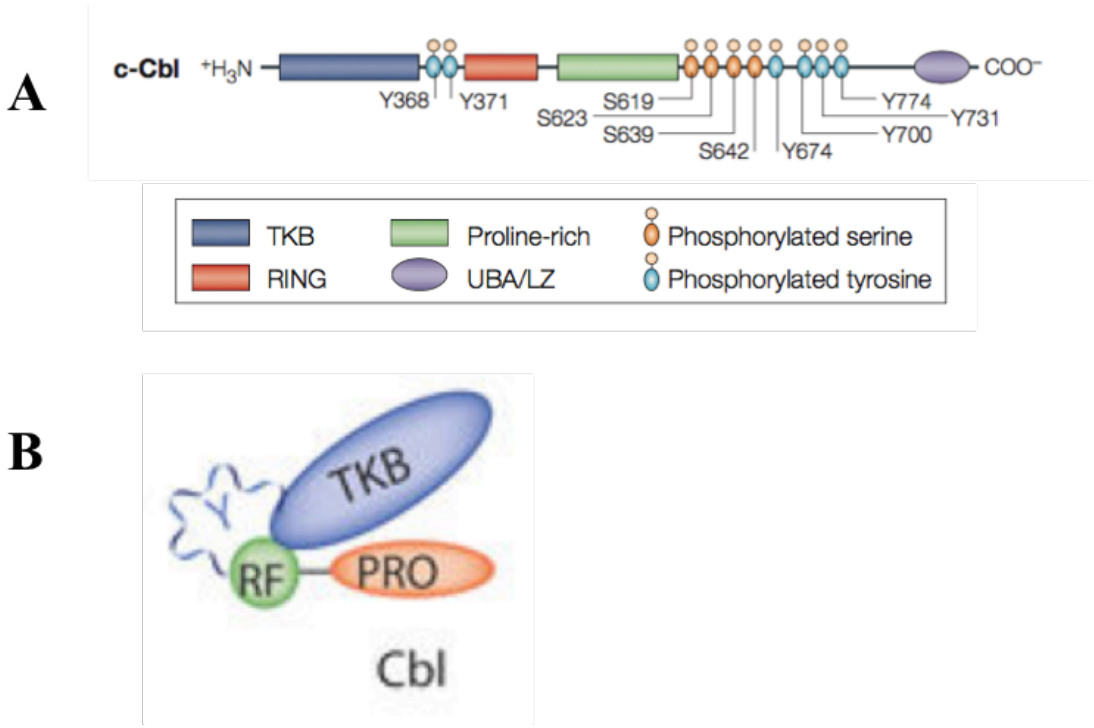

Figure 4-1 The domain structure of c-CBL. Adapted from references (Schmidt and Dikic, 2005, Polo, 2012).

(A) A schematic representation of the structure of c-CBL or CBL. The region between the tyrosine kinase binding (TKB) and RING domains is known as the linker region. (B) Globular representation c-CBL.

4.4 Ubiquitin E3 ligase mechanism

Ubiquitin (Ub), a small 8 kDa protein, can be covalently attached to a vast range of substrates to aid in the regulation of numerous eukaryotic processes (Komander and Rape, 2012). Substrate modification can be achieved through the addition of a single Ub to a lysine residue (monoubiquitination), multiple Ubs to numerous substrate lysines (multi-monoubiquitination) or a polyubiquitin chain to one substrate lysine (polyubiquitination) (Sadowski and Sarcevic, 2010). Attachment of Ub involves three classes of enzymes, an E1 Ub-activating enzyme, an E2 Ub-conjugating enzyme and an E3 Ub ligase. The E1 enzyme activates Ub in an ATP-dependent reaction forming a thioester bond between the Ub C-terminus and the E1 catalytic cysteine. Ub is then transferred to the catalytic cysteine of the E2 enzyme forming an E2/Ub intermediate. Finally, the E3 binds both the E2/Ub intermediate and the substrate to catalyze transfer of the Ub to a substrate lysine (Sadowski and Sarcevic, 2010, Berndsen and

Wolberger, 2014). The purpose of the E3 enzymes is thus twofold: firstly, to catalyze Ub transfer and secondly, to match E2/Ub constructs with their complementary substrates (Berndsen and Wolberger, 2014).

There are over 600 human E3 ligases (Li et al., 2008) that can be split into three families depending on certain conserved structural domains and the mechanism by which they transfer Ub from the E2 to the substrate (Pickart and Eddins, 2004, Smit and Sixma, 2014). The first and largest family is that of the RING family. E3 enzymes that belong to this family can catalyze direct transfer of Ub from an E2 to a substrate (Deshaies and Joazeiro, 2009). This is done by simultaneously binding the E2/Ub and the substrate. The other two families are smaller and ubiquitinate substrates using a two-step process. They are the homology to E6AP C terminus (HECT) family and the RING-between-RING (RBR) family. E3 enzymes from these families initially transfer Ub from an E2 to an active cysteine residue on an E3 and then from the E3 to a substrate (Smit and Sixma, 2014, Scheffner and Kumar, 2014).

c-CBL is a RING E3 ligase and, to date, is known to interact with at least 150 proteins (Schmidt and Dikic, 2005). These range from tyrosine kinases and growth factor receptors (Thien and Langdon, 2001) to adaptor proteins (Loreto et al., 2002) and cell adhesion molecules (Kaabeche et al., 2005). Of particular interest is its role in controlling proliferative signals by ubiquitinating various receptor tyrosine kinases (RTKs) such as epidermal growth factor receptor (EGFR) and platelet-derived growth factor receptor (PDGFR) (Thien and Langdon, 2001) (Figure 4-2). Ubiquitination of RTKs and their subsequent downregulation are mediated by the E3 ubiquitin ligase activity of c-CBL. As already mentioned the linker and RING finger domains are crucial to this process (Schmidt and Dikic, 2005, Thien and Langdon, 2001).

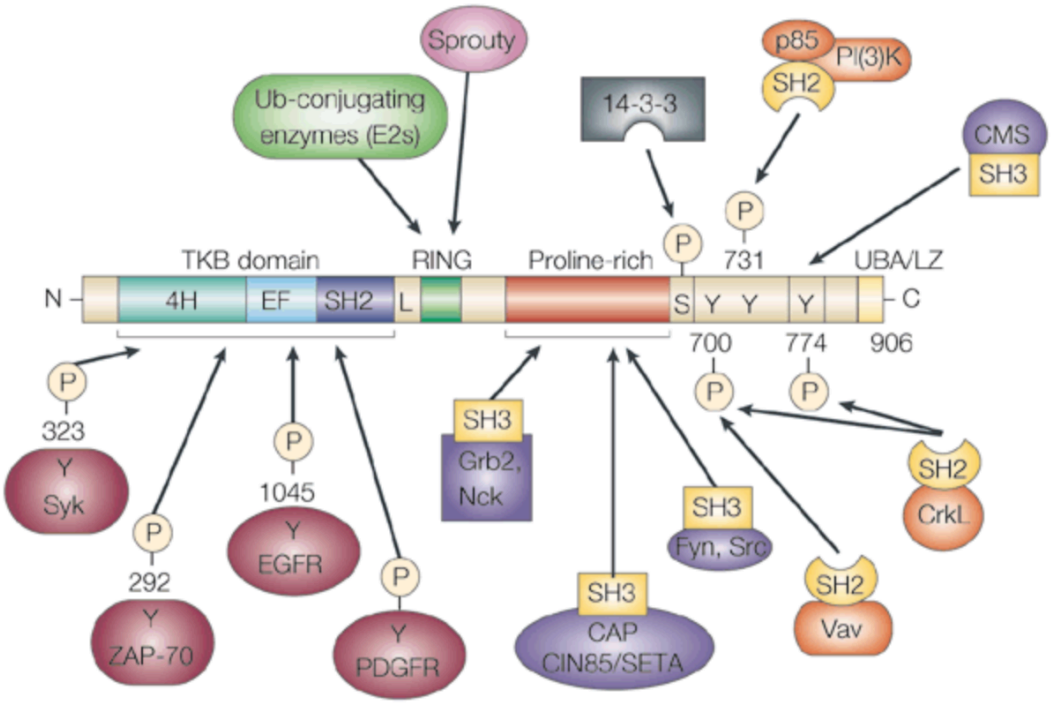

Figure 4-2 c-CBL interacts with many different signaling proteins. *Adapted from reference (Thien and Langdon, 2001).*

4.5 c-CBL and regulation of EGFR and PDGFR

It is well documented that c-CBL is involved in the pathway involving EGFR degradation (Figure 4-3) (Levkowitz et al., 1998, Pennock and Wang, 2008, Joazeiro et al., 1999). Briefly, epidermal growth factor (EGF) binds to the extracellular portion of EGFR. This stimulates the tyrosine kinase domain of the receptor, which in turn results in phosphorylation of several C-terminal tyrosine residues. An EGFR- c-CBL complex can then form either directly or indirectly. Direct association occurs when tyrosine-1045 is phosphorylated which serves as a docking site for the TKB domain of c-CBL (Levkowitz et al., 1998). Indirect association happens when the adaptor protein GRB2 (growth factor receptor-bound protein 2) binds to the proline region of c-CBL after either tyrosine-1068 or tyrosine-1086 on EGFR is phosphorylated (Figure 4-3 B) (Pennock and Wang, 2008). c-CBL is phosphorylated allowing E2 enzyme recruitment to the RING finger of c-CBL and Ub addition at various sites on

the receptor. In a similar fashion c-CBL is a negative regulator of PDGFR and thus PDGF-induced cell proliferation (Miyake et al., 1999, Reddi et al., 2007).

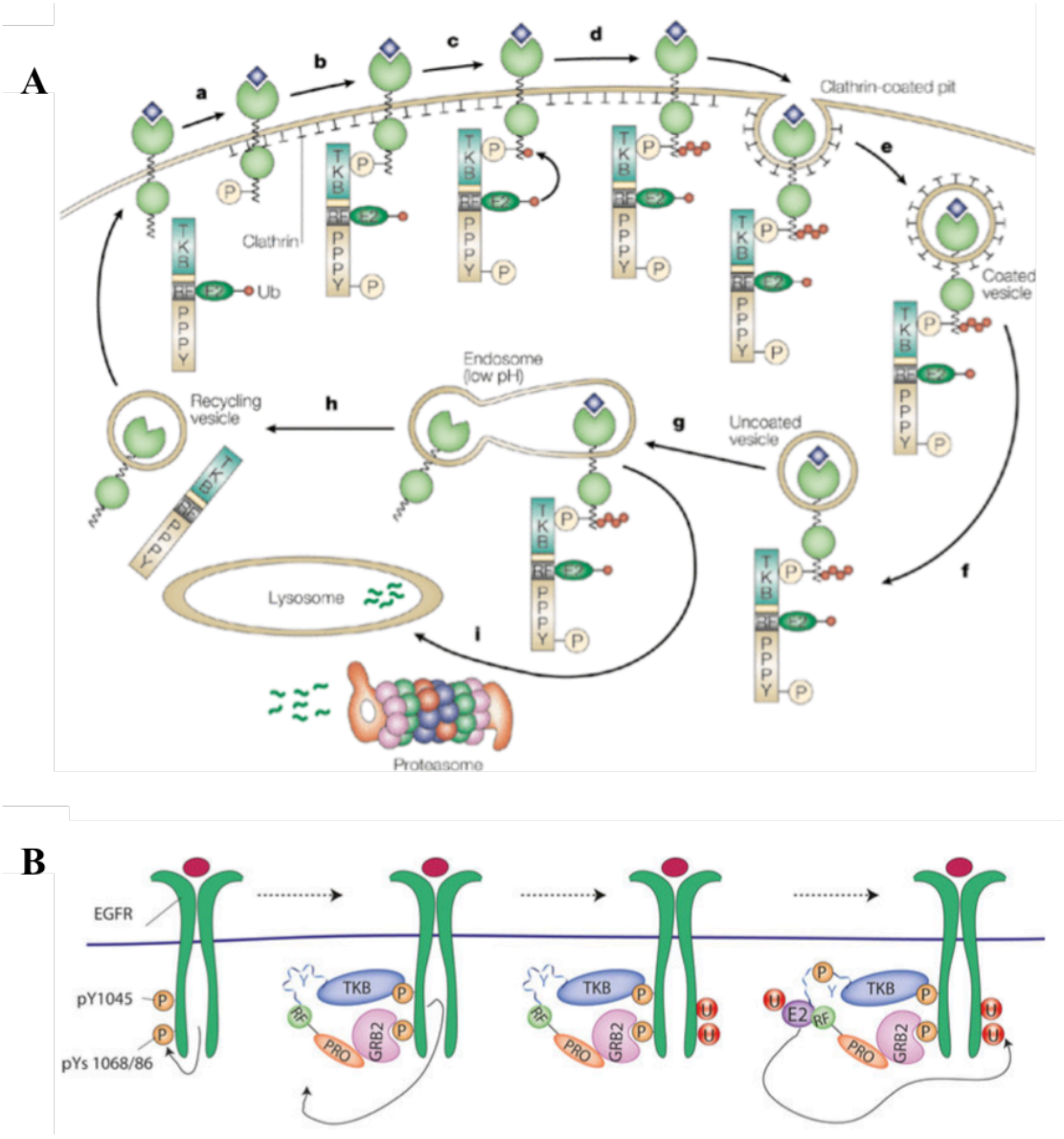

Figure 4-3 EGFR downregulation via c-CBL mediated ubiquitination.

(A) Direct association between EGFR and c-CBL. (Thien and Langdon, 2001) a) EGF binding induces phosphorylation (P) of EGFR. b) Cbl is recruited to EGFR binding through its TKB domain. c-CBL becomes phosphorylated. c) The E3 ubiquitin ligase function of c-CBL catalyzes transfer of Ub to EGFR. d) Continued addition of Ub results in multiubiquitination. e-f) EGFR-c-CBL complex is internalized. g) Ligand dissociates and EGFR is recycled back to the cell surface membrane. (B) Indirect association between EGFR and c-CBL via growth factor receptor-bound protein 2 (GRB2). (Pennock and Wang, 2008).

4.6 EGFR and induction of the Ras-Raf-mitogen activated protein kinase pathway

The Ras-Raf-mitogen activated protein kinase (MAPK) pathway is one of the major signaling cascades stimulated by EGFR and other similar RTKs (Alroy and Yarden, 1997). This pathway couples signals from membrane bound receptors to downstream effectors to regulate numerous biological processes including cell proliferation, apoptosis inhibition, gene expression and angiogenesis (Herbst, 2004, McCubrey et al., 2007). In summary, Ras recruits and activates Raf, a protein kinase, which in turn promotes MEK1/2 and activates ERK1/2. Activated ERK1/2 can phosphorylate various different substrates and control different transcription factors (Li et al., 2016).

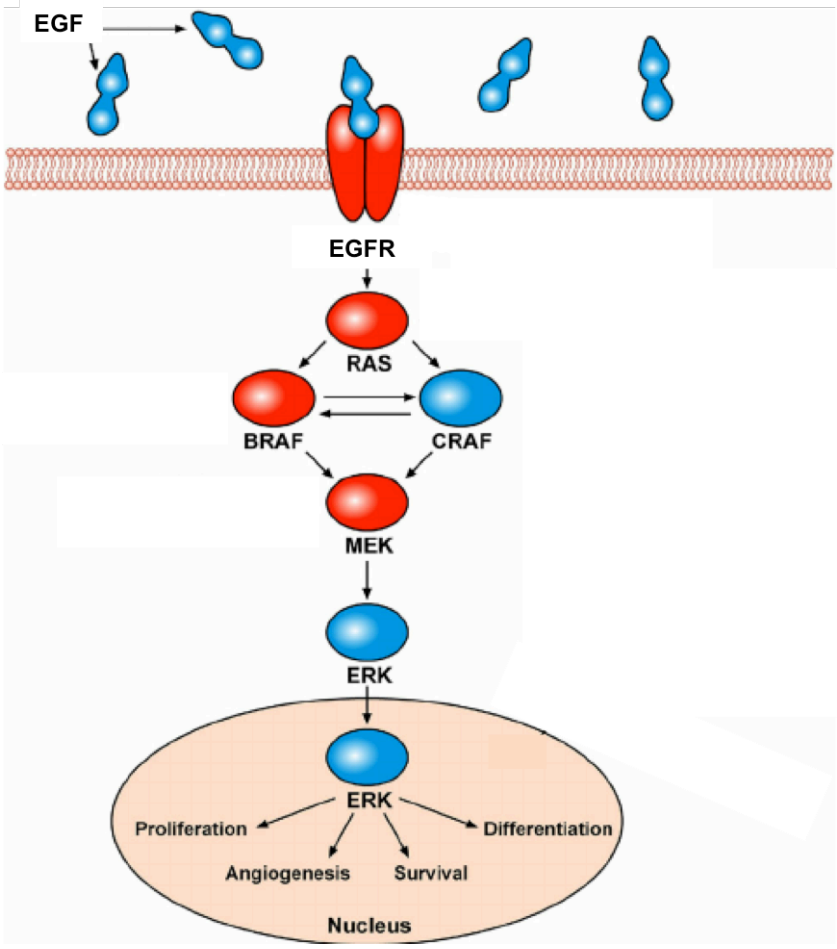

Figure 4-4 Schematic representation of MAPK/ERK signaling pathway. *Adapted from reference (Carlomagno and Chiariello, 2014).*

4.7 c-CBL and regulation of PLCγ1

In endothelial cells pro-angiogenic signaling is in part controlled by activation of phospholipase Cγ1 (PLCγ1) by vascular endothelial growth factor 2 (VEGFR-2) (Meyer et al., 2003) (Figure 4-5). VEGFR-2 also activates c-CBL, which mediates the anti-angiogenic function of VEGFR-2 by targeting PLCγ1 for ubiquitination (Figure 4-5). In porcine aortic endothelial cells (PAECs) an E3 ligase deficient form of c-CBL was found to cause increased PAEC sprouting indicating an inhibitory role of c-CBL in angiogenesis (Singh et al., 2007).

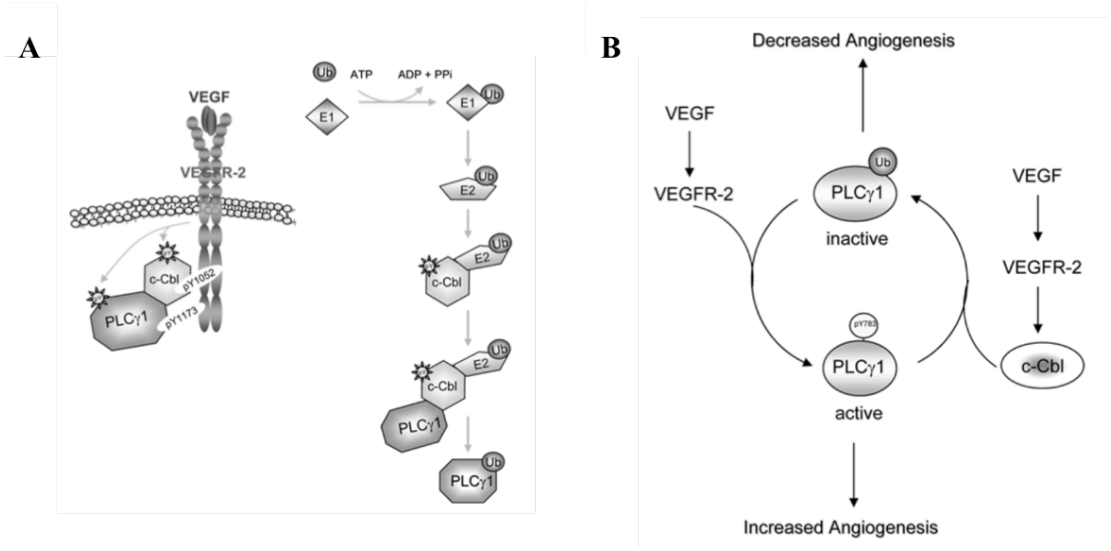

Figure 4-5 c-CBL and PLCγ1 activation by VEGFR2 and c-CBL mediated ubiquitination of PLCγ1 and involvement of c-CBL in angiogenesis. *Adapted from reference (Rahimi, 2009).*

4.8 Family tree for family B

The index case of family B was an Asian male from non-consanguineous parents, referred to as B-II-3 from now on. The family tree is presented in Figure 4-6.

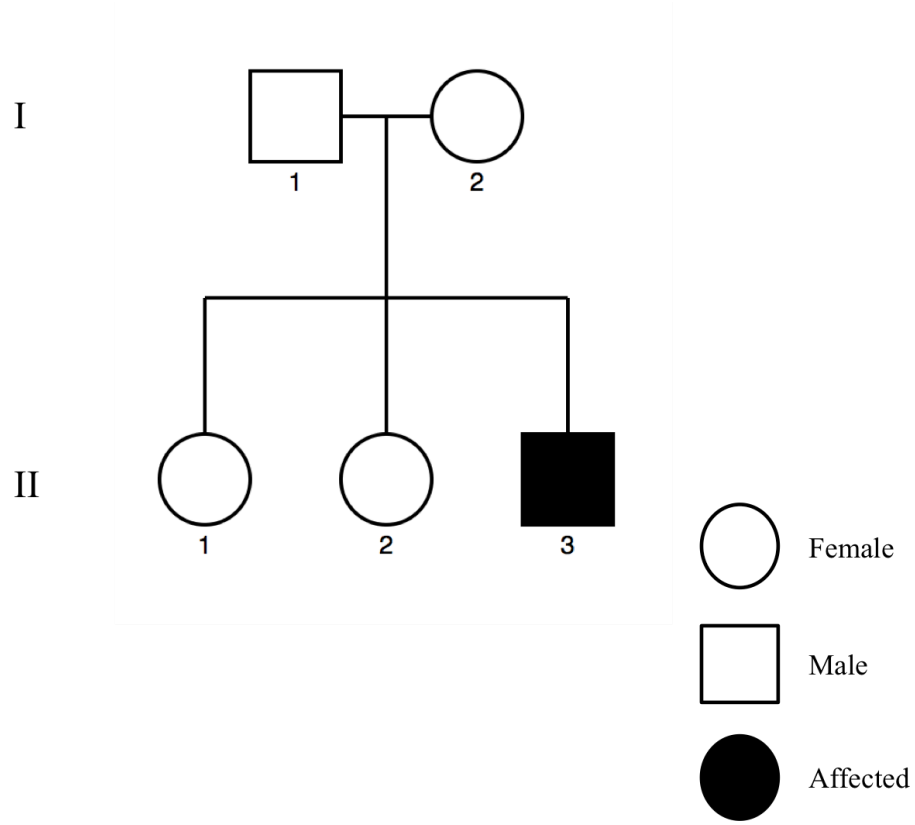

Figure 4-6 Family tree for family B

4.9 Clinical presentation of B-II-3

The initial presentation of the index case of family B was at the age of 2 ½ years old when he was found to have left sided leg and arm weakness and left sided facial weakness. There were no clear precipitants to this presentation. He did not report any fevers, skin rashes, respiratory, musculoskeletal or gastrointestinal symptoms of note. Brain MRI revealed an acute infarct in the right MCA territory involving the right frontal, temporal and parietal lobe cortex and some right anterior cerebral artery frontal lobe cortical involvement (Figure 4-7). Brain MRI also showed evidence of a past left sided infarct in the periventricular white matter. In addition, brain MRA and catheter angiography of the cerebral circulation revealed bilateral occlusive vasculopathy involving the ICA with established collaterals in keeping with a moyamoya radiological pattern (Figure 4-7). Visceral digital subtraction angiography was normal. Echocardiography was normal. There was no acute phase response (ESR 5 mm/h; normal range < 10 mm/h and CRP5 mg/L; normal range< 20 mg/L);

ANCA/ANA testing was negative and broad metabolic and infectious disease screen were negative (see Appendix 1 for stroke protocol investigations). As he was noted to have two café-au-lait spots genetic screening of *NF1* gene mutations was undertaken and was negative whilst array CGH did not detect any copy number variants. Of note, he was also identified to have factor XII deficiency (factor XII levels 32 IU/L; normal range 50-150 IU/L) but he did not experience any bleeding episodes and had no evidence of intracerebral haemorrhage. He was considered to have moyamoya arteriopathy with no evidence of a systemic vasculopathy and was started on aspirin (5 mg/kg/day). At 4 years of age he underwent bilateral ECIC bypass and is currently doing well with no further events. As an aside he suffered from an unexplained right-sided skull fracture and related soft tissue swelling at the age of 4 ½ years that healed with no complications. There was no evidence of osteopenia as assessed by a lumbar spine dexa scan and there were no psychosocial concerns.

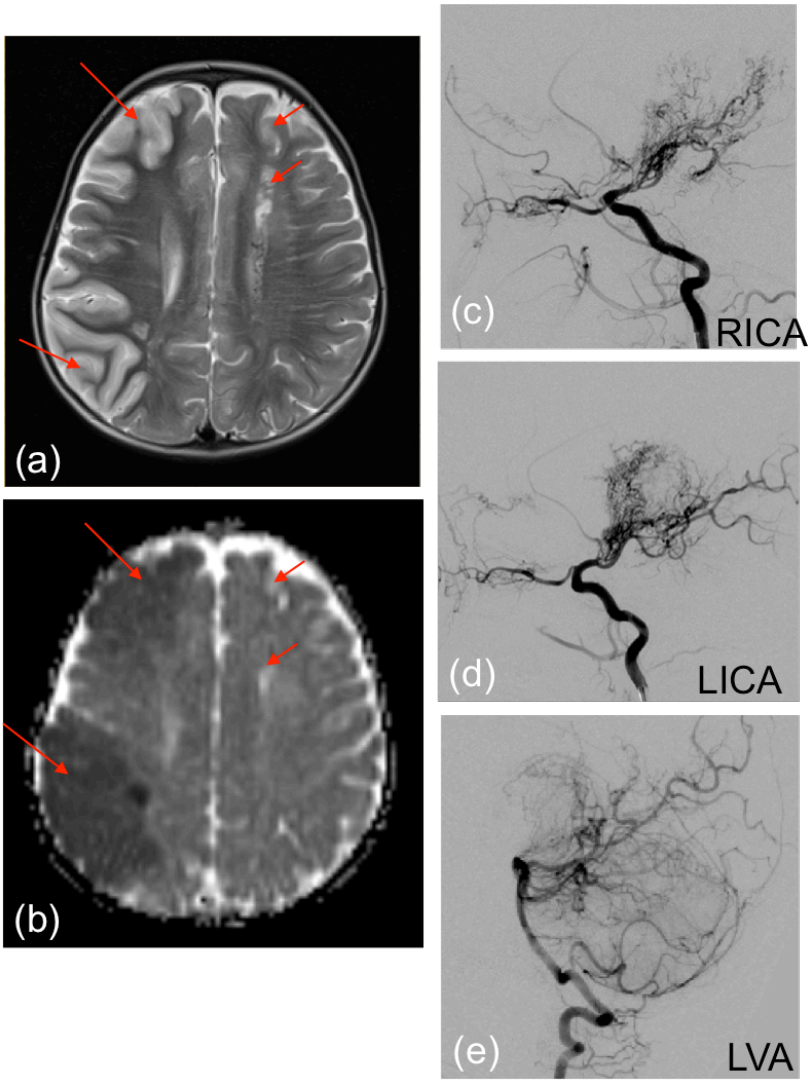

Figure 4-7 Brain magnetic resonance imaging (MRI) and cerebral catheter angiography images for B-II-3.

(a) Axial T2- and (b) ADC map from the diffusion-weighted images (DWI) shows an acute right largely cortically based right MCA territory infarct (long red arrows). Left mature deep and cortical ACA/MCA watershed infarcts indicate previous left hemispheric injury (short red arrows). (c) Catheter angiography of the cerebral circulation shows a right ICA stenosis with some filling of a narrow right MCA branch and occluded right ACA and multiple moyamoya, ethmoidal and ophthalmic collateral vessels. (d) The left ICA is occluded just beyond the left PCA and ACA branch can be seen to fill via collaterals. The collateral pattern is similar to the right with additional pial collaterals from the left PCA. (e) The posterior circulation vessels are normal and fill the cerebral hemispheres via collateral pial vessels. RICA = right internal carotid artery, LICA = left internal carotid artery, LVA = left vertebral artery, ADC = apparent diffusion coefficient, ACA = anterior cerebral artery, ICA = internal carotid artery, MCA = middle cerebral artery, MM = moyamoya, PCA = posterior cerebral artery, tICA = terminal internal carotid artery, VA = vertebral artery.

4.10 Family tree for family C

The index case of family C was a Caucasian female from non-consanguineous parents, referred to as C-III-2 from now on. The family tree is shown in Figure 4-8.

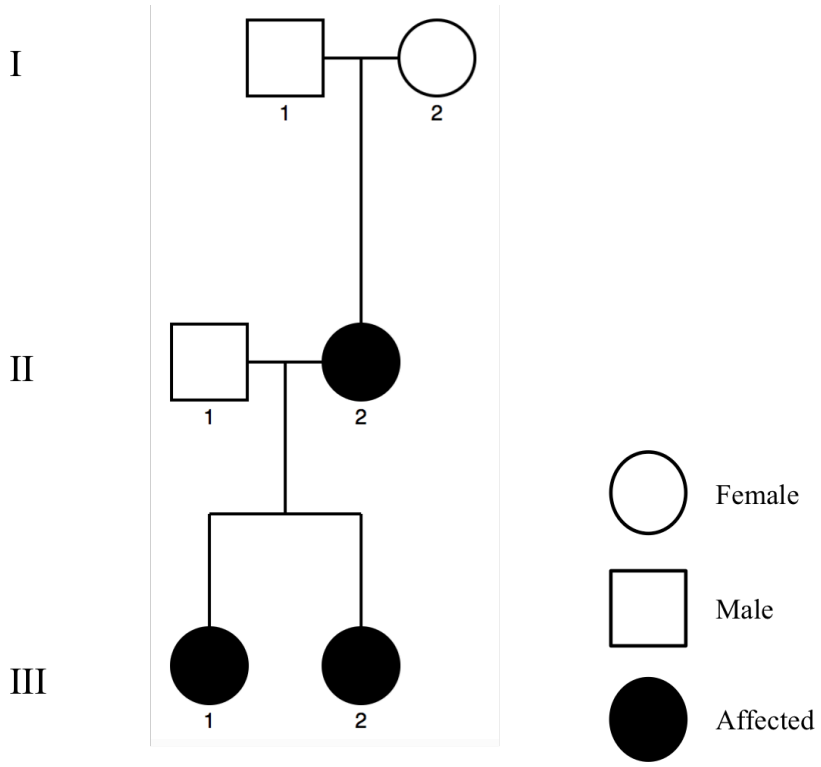

Figure 4-8 Family tree for family C

4.11 Clinical presentation of C-III-2

C-III-2 who had a history of pulmonary valve stenosis diagnosed at birth presented to the neurovascular services at GOSH (Dr Ganesan/Dr Eleftheriou) and Bristol (Dr Mallick) at the age of 4 months with acute dehydration followed by encephalopathy and a left sided focal seizure. Brain MRI at the time revealed acute swelling and signal change with restricted diffusion of the whole right hemisphere, other than the basal ganglia structures. Subsequent MRA and catheter angiography of the cerebral circulation showed an occlusive arteriopathy of the terminal ICAs, the MCA and the anterior cerebral arteries (Figure 4-9). The ICA occlusion was found to be worse on the right hand side in comparison to the left with a profuse basal collateral network. Contrast brain computed tomography (CT) showed no intracerebral calcification.

Extensive screening for infectious, metabolic and rheumatological causes was found to be negative. She was thus diagnosed with an unclassified cerebral vasculopathy with a moyamoya-like pattern and was started on aspirin (5 mg/kg/day). She remained stable over time with no stroke recurrence but progressive white matter disease over time (Figure 4-10). Intriguingly, her mother and sister also had cerebrovascular events and were identified to have a similar pattern of arteriopathy (Figure 4-11 & Figure 4-12). Both affected siblings have undergone ECIC bypass with good results. WES was undertaken for this family in collaboration with Hywell Williams (GOSHgene).

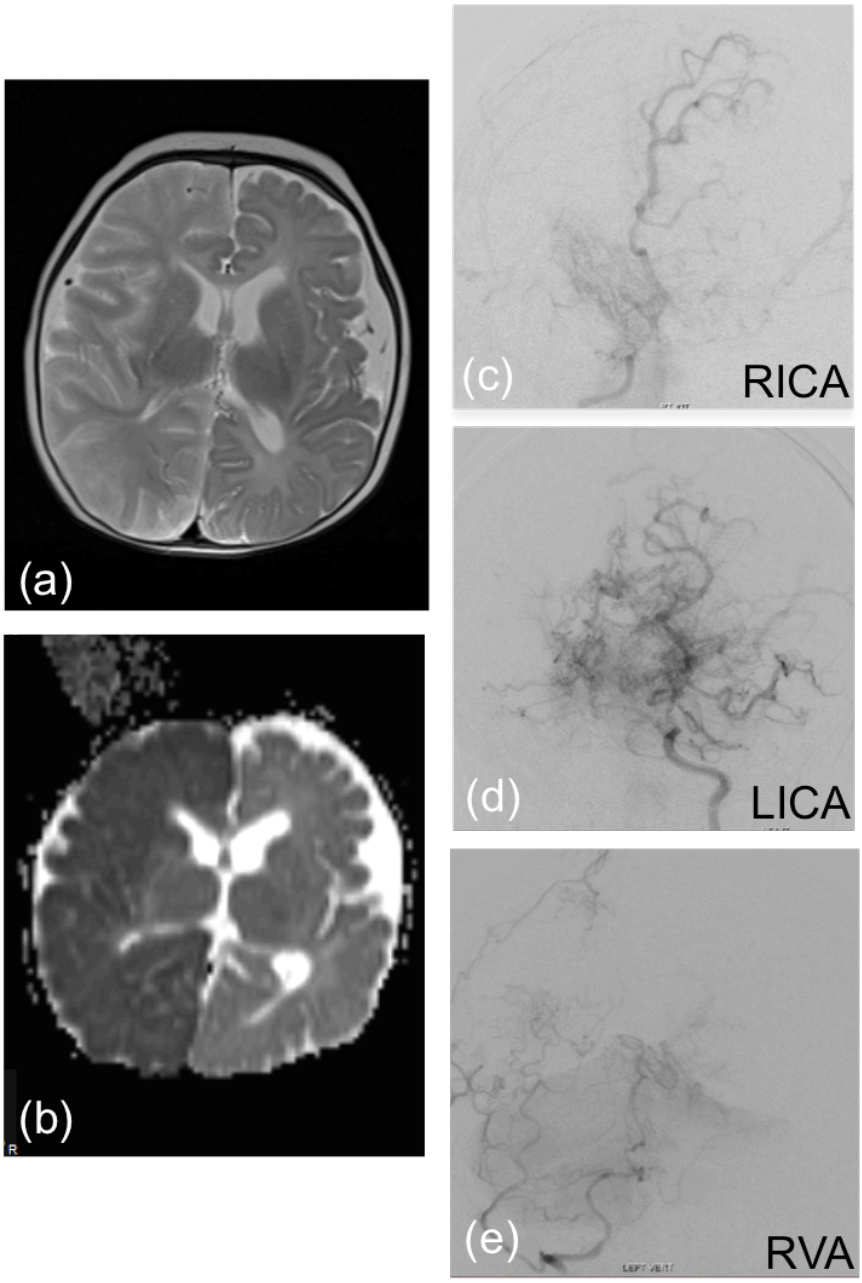

Figure 4-9 Brain MRI and catheter cerebral angiography images of the cerebral circulation for C-III-2 during initial presentation.

(a, b) Brain MRI showing an acute right hemispheric infarction sparing the deep grey structures. (c) The CA demonstrates a small and poorly filling RICA, stenosed at the skull base and occluded at the cavernous segment. The hemisphere is filled via moyamoya collaterals and a foetal right PCA. (d) The left tICA is severely stenosed and fills only a stenosed left MCA and multiple moyamoya collaterals. (e) The right VA and basilar artery are small and do not fill the PCAs. RICA = right internal carotid artery, LICA = left internal carotid artery, RVA = right vertebral artery, CA = catheter angiogram, MCA = middle cerebral artery, PCA = posterior cerebral artery, tICA = terminal internal carotid artery, VA = vertebral artery.

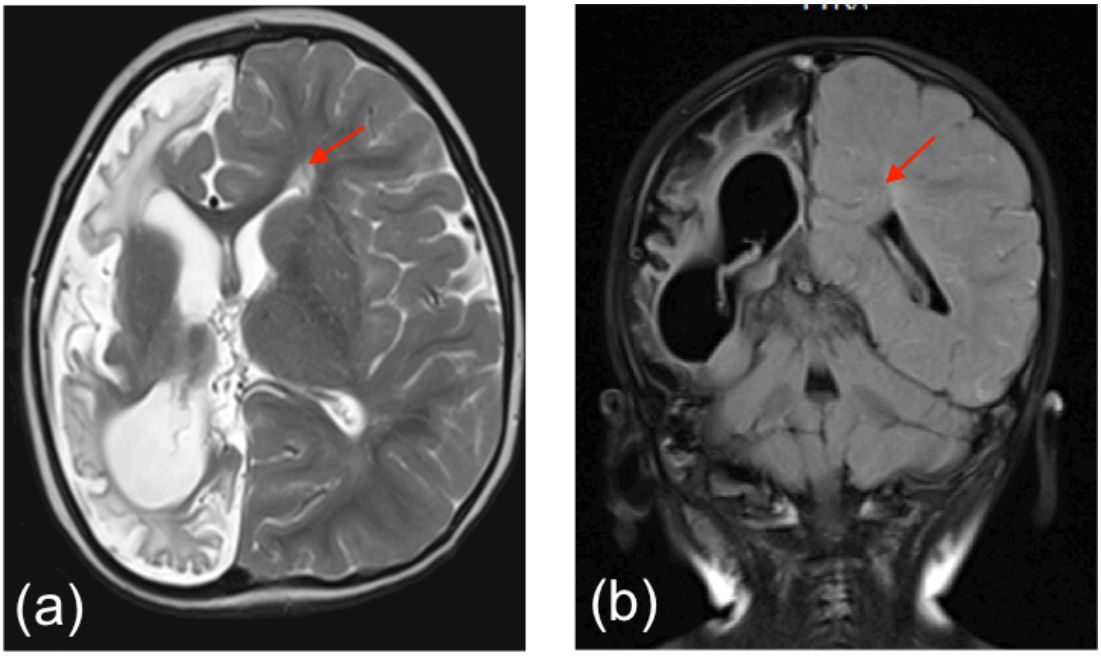

Figure 4-10 Follow up brain MRI for C-III-2.

(a) 12 months following initial presentation showed maturation of the old infarct and (b) new white matter disease.

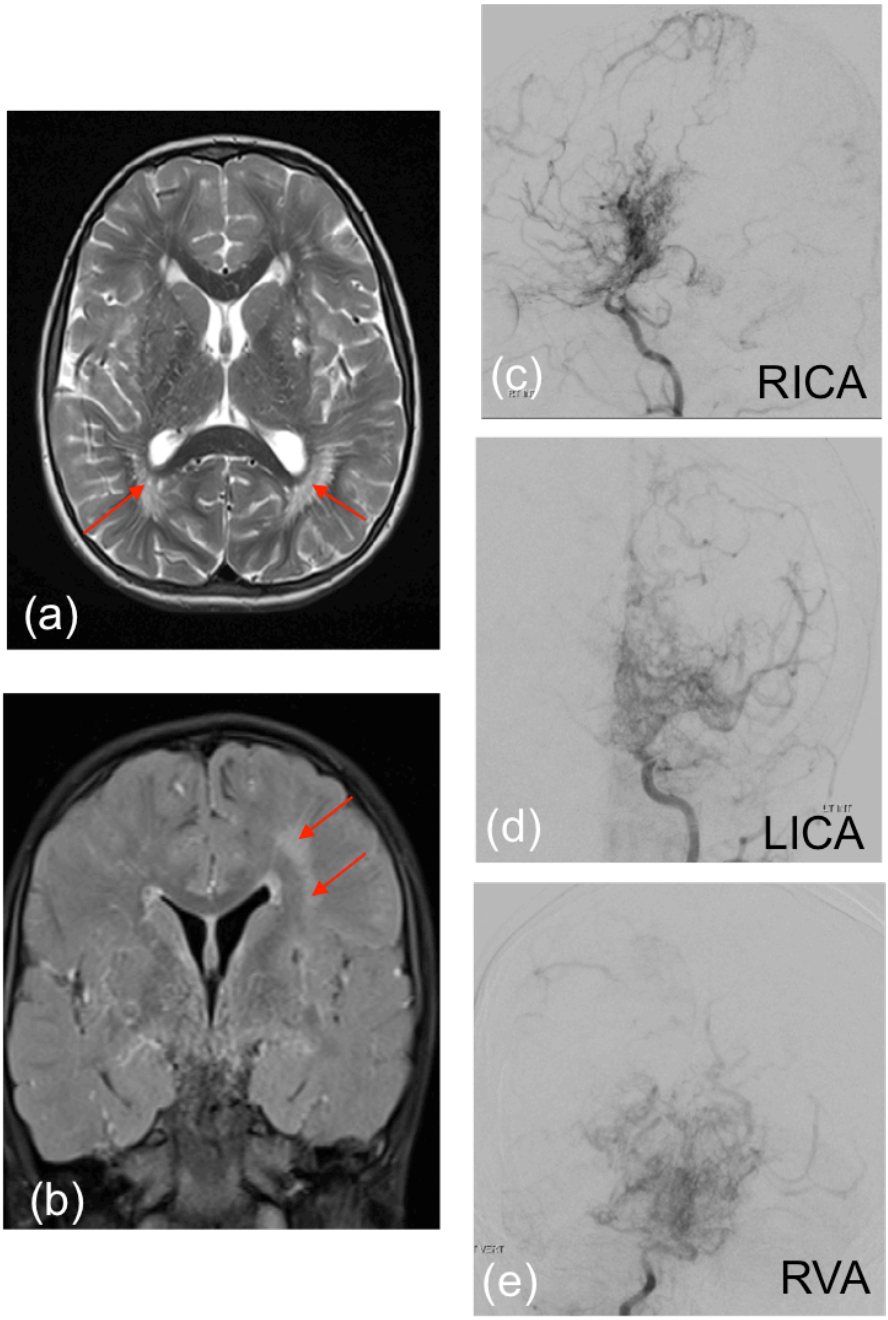

Figure 4-11 Brain MRI and catheter angiography of the cerebral circulation for C-III-1.

(a, b) C-III-1 had both subcortical white matter lesions in both hemispheres with large perivascular spaces (long red arrows). (c) The RICA is occluded at the cavernous segment with filling of some vessels via multiple moyamoya collaterals. (d) The LICA is occluded at the cavernous segment with severe stenosis of proximal ACA and MCA and multiple moyamoya collaterals. (e) The LVA is occluded and the RVA is stenosed shortly before forming the basilar artery which is small and which is occluded at it terminus with no filling of the PCAs. Multiple pial collaterals are visible. RICA = right internal carotid artery, LICA = left internal carotid artery, R/LVA = right/left vertebral artery, ACA = anterior cerebral artery, MCA = middle cerebral artery, PCA = posterior cerebral artery.

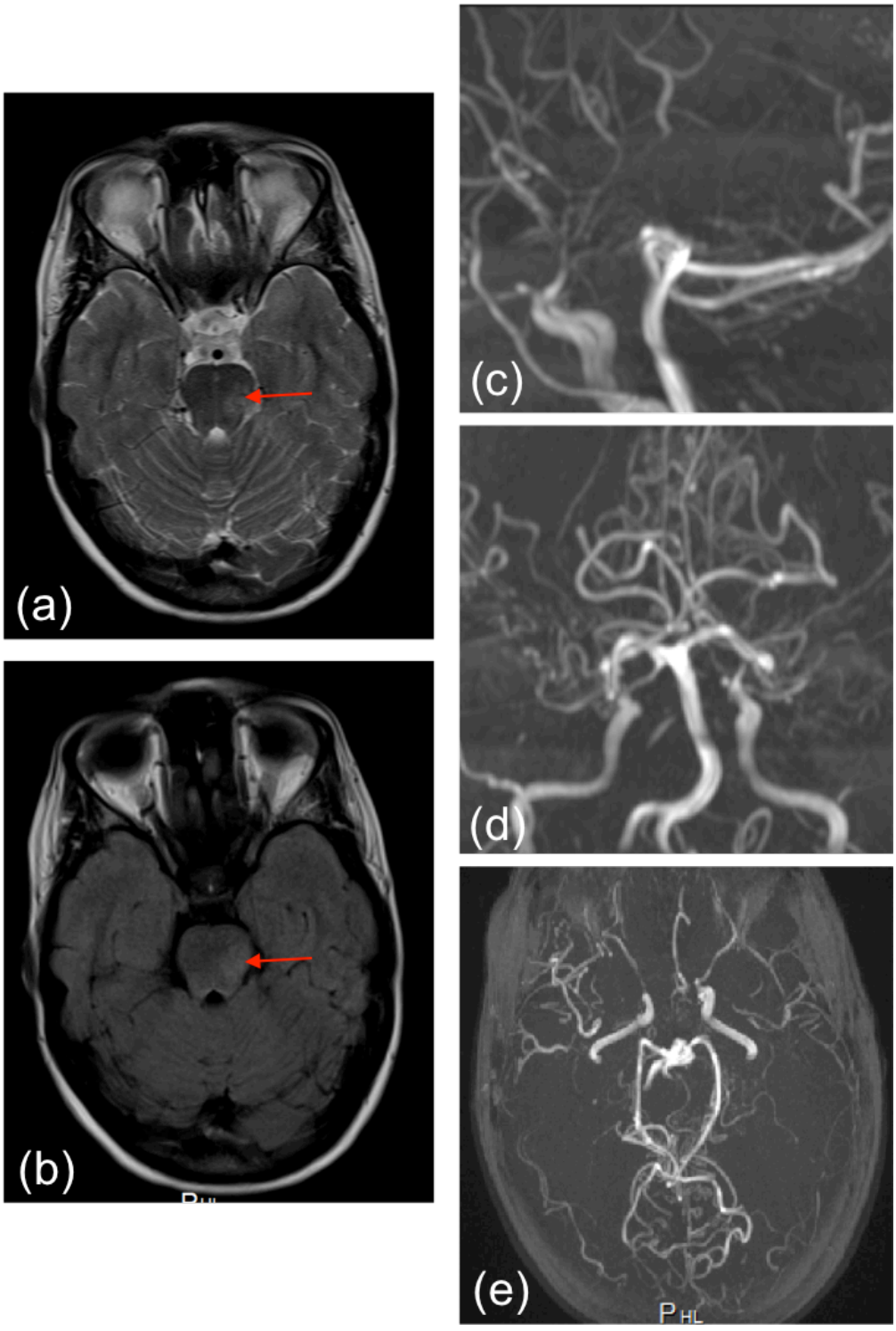

Figure 4-12 Brain MRI and MRA images for C-II-2.

(a, b) C-II-2 was found to have a signal abnormality in the left mid pons of uncertain significance (long red arrows). (c, d) Her MRA revealed bilateral occlusion of the tICAs with filling of distal vessels via moyamoya collaterals. (e) The posterior circulation appears patent but attenuated with pial collateral formation. tICA = terminal internal carotid artery.

4.12 Family tree for family D

The index case of family D was a Caucasian male from non-consanguineous parents, referred to as D-II-6 from now on. The family tree is shown in Figure 4-13.

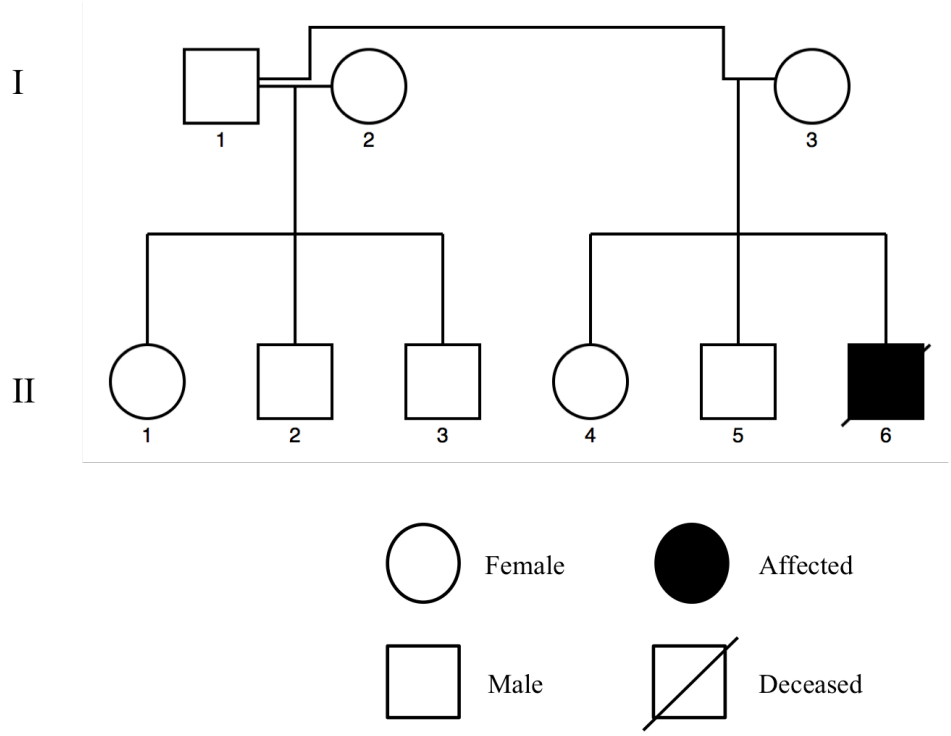

Figure 4-13 Family tree for family D

4.13 Clinical presentation of D-II-6

D-II-6 was born following a normal pregnancy and delivery, with a birth weight of 3.37kg (50th percentile). During the first year of life he was noted to be quite floppy and his motor skill and fine skill development was delayed. He began sitting at around two, and walked independently at around 4 years of age. He was found to have an enlarged liver and spleen when he was seven months old after being referred to his local paediatric team for pneumonia. Despite numerous investigations at that stage, no clear cause for his poor development and hepatosplenomegaly was identified. Throughout childhood, he continued to show slow development and attended a school for children with special needs. Apart from his learning difficulties, he had no other

health problems in childhood. He was very short sighted in his right eye and slightly short sighted in his left. Over the last three years, he developed progressive swelling in his legs, which was worse on the left. His cardiology assessment including ECG and echocardiography were normal. At the age of 5.5 years old he presented with left-sided focal seizures and left-sided hemiplegia and was subsequently found to have an acute intracranial haemorrhage with ventricular extension and vascular changes consistent with moyamoya arteriopathy (Figure 4-14). He had further intracranial haemorrhage into the right lentiform nucleus during this episode (intraventricular and subarachnoid haemorrhage) that was difficult to control and he subsequently died. His array CGH did not find any copy number variants.

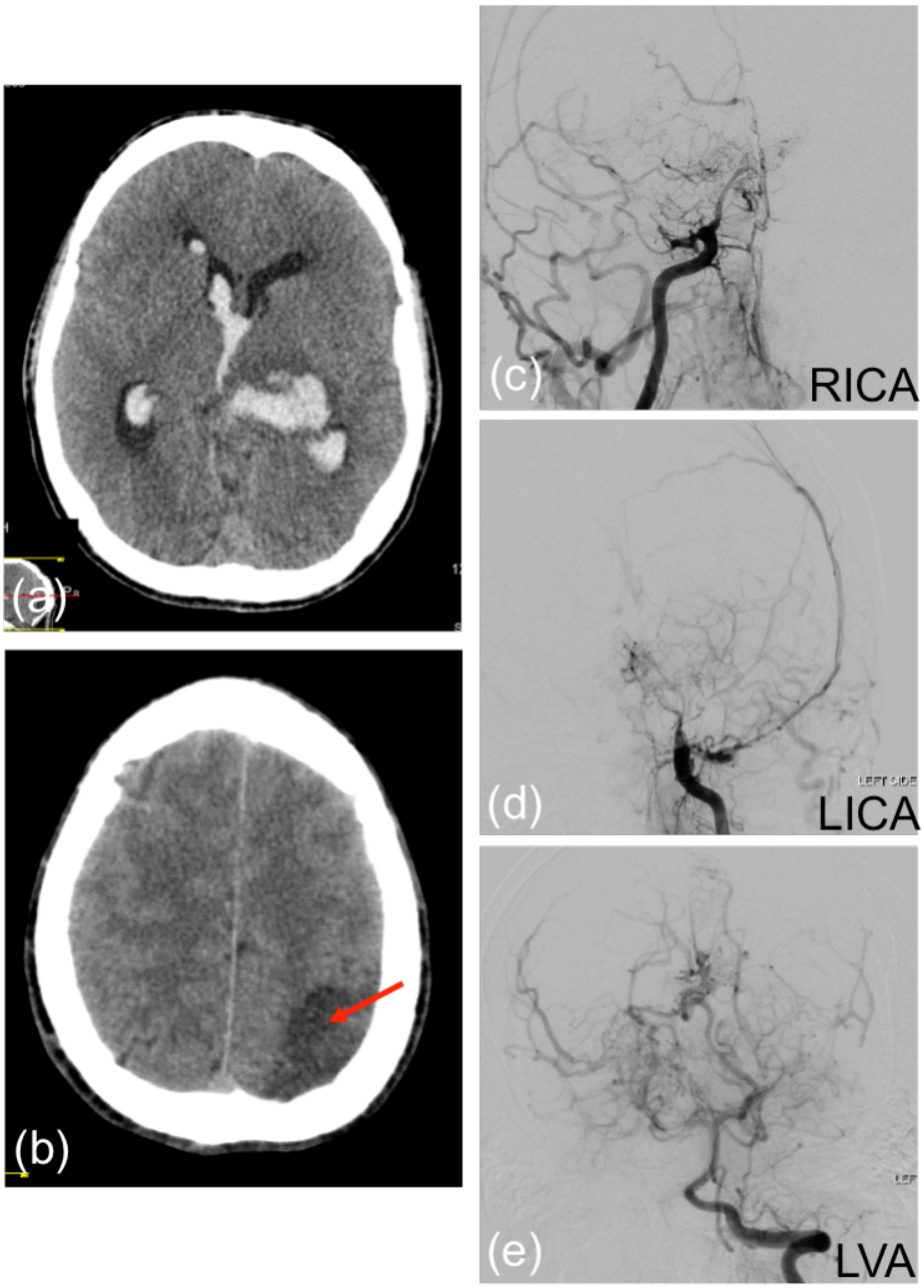

Figure 4-14 Brain MRI and catheter angiography of the cerebra circulation images for D-II-6.

(a, b) An acute left MCA infarct (long red arrow) is seen in D-II-6 who presented with a left capsular, thalamic, intraventricular and subarachnoid haemorrhage (see in a). (c, d) The CA reveals bilateral occlusion of the terminal ICAs with no distal filling via normal intracranial vasculature but some filling of the hemispheres from EC-IC and skull base collaterals. (e) The P1 segment of the right PCA is occluded but multiple pial collaterals are seen filling the hemispheres. RICA = right internal carotid artery, LICA = left internal carotid artery, LVA = left vertebral artery, CA = catheter angiogram, ICA = internal carotid artery, MCA = middle cerebral artery, PCA = posterior cerebral artery, tICA = terminal internal carotid artery.

4.14 Methods

The general methods used in the experiments outlined in this chapter are described in Chapter 2 General materials and methods. The specific methods used to investigate the functional relevance of the identified *c-CBL* mutations are discussed here.

4.14.1 Human dermal fibroblast cell transdifferentiation

For transdifferentiation of human dermal fibroblast cells (HDFCs), the culture plates were pre-coated with matrigel (BD Biosciences). To begin with, 400 µl of matrigel was mixed with 25 ml of cold medium. 1 ml of this diluted matrigel solution was then added to each well of a 6-well plate and incubated for 30 minutes. The matrigel was then aspirated with the removal of as much fluid as possible. HDFCs were evenly seeded on the matrigel pre-coated plates. After overnight incubation, cells were treated with 2% heat-inactivated horse serum and 5 ng/mL TGFβ1 to induce fibroblast transdifferentiation into smooth muscle cell (SMC)-like cells referred to as SMC-myofibroblasts. The cells were harvested on day 14 for RNA isolation or alpha-smooth muscle cell actin staining for FACS analysis. qPCR analysis was performed to analyse mRNA expression of a SMC marker gene (*ACTA2*).

4.14.2 siRNA transfection in human umbilical vein endothelial cells

c-CBL siRNA (CBLHSS101416, Invitrogen) was reconstituted with RNAse free water to a concentration of 13.3 µg/nmol. Two negative siRNA controls were used: Stealth RNAi™ siRNA Negative Control Med GC and Stealth RNAi™ siRNA Negative Control Lo GC (Thermo Fisher Scientific).

Cells were plated the day before transfection to ensure ~90-100% confluency at the time of transfection. On the day of transfection cells were washed twice with Opti-MEM® (Thermo Fisher Scientific) to remove any FBS-containing media. Volumes were calculated for 1 well of a 6-well plate. Firstly, 150 µl of Opti-MEM® and 6 µl of Lipofectamine® (Thermo Fisher Scientific) were combined in a 1.5 ml eppendorf. In a separate 1.5 ml eppendorf, 150 µl of Opti-MEM® and 7.5 µl of siRNA were combined. The diluted Lipofectamine® and diluted siRNA were then mixed in a 1:1

ratio and incubated at room temperature for 5 minutes to allow formation of a DNA-lipid complex. To each well was added 250 µl of this DNA-lipid complex. After a 4 hour incubation at 37°C, 1 ml of the cell's normal media was added and the cells were incubated for an additional 48 hours at 37°C. Volumes were halved if cells were plated in a 12-well plate.

4.14.3 Cell stimulation

Three different cell types were used in a number of experiments detailed in this chapter: HUVECs, PBMCs and HDFCs. Prior to stimulation, HUVECs and transformed HDFCs were washed with sterile PBS and put in quiescent media for 24 hours; PBMCs were left in normal media overnight after being extracted or thawed. HUVECs were stimulated with 20 ng/ml recombinant human vascular endothelial growth factor (VEGF) 165 protein (R&D systems); PBMCs were stimulated with 20 ng/ml EGF recombinant human protein (Thermo Fisher Scientific); and transformed HDFCs were stimulated with 20 ng/ml PDGF A/B (PeproTech).

4.14.4 Immunoprecipitation

Protein was extracted from PBMCs using M-PER® mammalian protein extraction reagent (Thermo Fisher Scientific), supplemented with protease inhibitor cocktail, instead of RIPA buffer. Samples were centrifuged (6,500 x *g* for 20 minutes) at 4°C and the supernatant transferred to a fresh 1.5 ml eppendorf. 1 ml M-PER® reagent and 10 µl primary antibody were added and tubes were rotated overnight at 4°C.

Protein A beads (Thermo Fisher Scientific) were washed three times with M-PER® reagent before being added to each sample; 70 µl of beads per sample were used. The samples were rotated for 4 hours at 4°C. The beads were washed with 500 µl M-PER® reagent and centrifuged briefly (18,000 x *g* for 2 minutes) at 4°C. This was repeated three times.

4.14.5 Ubiquitination

An ubiquitination assay kit (Abcam) was used. In brief, assay reagents were added to a 1.5 ml eppendorf in the order indicated in Table 4-1. The contents were mixed

gently and incubated at 37°C for 60 minutes. The assay was then quenched by adding 50 µl 5X SDS loading buffer. Samples were either immediately analysed using Western Blot or stored at -20°C for later analysis.

Table 4-1 Ubiquitylation assay reagents

Reagent	E2-Ub	E2-Ub –ve control
Distilled water	21.5 µl	19 µl
10X ubiquitinylation buffer	5 µl	5 µl
Inorganic pyrophophatase solution (100U/mL in 20mM Tris-HCl, pH 7.5)	10 µl	10 µl
Dithiothreitol solution (50mM in 20mM Tris-Cl, pH7.5)	1 µl	1 µl
Mg-ATP	2.5 µl	-
EDTA (50mM)	-	5 µl
20X E1 (2 µM)	2.5 µl	2.5 µl
10X E2 (Ubch5a) (25 µM)	5 µl	5 µl
20X Ub (50 µM)	2.5 µl	2.5 µl

4.14.6 Vasculogenesis assay

A number of studies have explored the ability of endothelial cells to form vascular networks on extracellular matrix formulations (Matrigel^{TM}) as means of recapitulating vasculogenesis events happening *in vivo* (Tepper et al., 2002, Montanez et al., 2002). Plating endothelial cells onto a layer of gel matrix is a well-established assay that mimics capillary-like tubule formation, a process that is representative of the later stage of angiogenesis (Lawley and Kubota, 1989). Matrigel is a mixture of extracellular and basement membrane proteins that allows tubules to form after only 1 hour (Lawley and Kubota, 1989). An aliquot of frozen growth factor reduced matrigel without phenol red (BD Biosciences) was left to thaw in the refrigerator for approximately 3 hours. A flat-bottomed 96-well plate and p200 pipette tips were pre-cooled in the freezer for a similar length of time. The defrosted matrigel was briefly centrifuged to remove any bubbles and 50 µl pipetted into each well, approximately 12 per aliquot. The plate was incubated at 37°C for 30 min to allow the matrix solution to solidify. HUVEC cell concentration was adjusted to 100,000 cells/ml in EGM-2 and 200 µl was added per well. The plate was incubated at 37°C for 18-24 hours and then inspected under an inverted microscope for tube formation. The

number of tubules formed was counted in 5 random fields for each condition; each condition was run in duplicate (Figure 4-15).

The number of tubules was counted using ImageJ in each picture taken. The average number of tubules was calculated and divided by the area of the well to give the number of tubules per mm. Results were displayed as mean of five images taken per well.

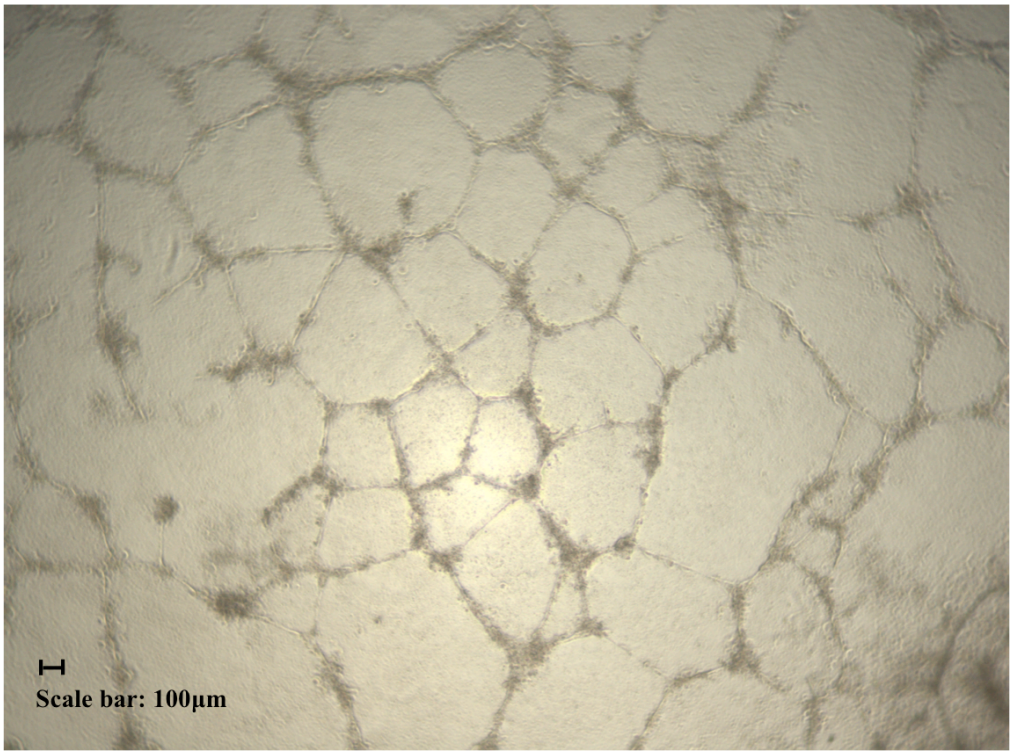

Figure 4-15 Human umbilical vein endothelial cell (HUVEC) capillary network (tubule) formation on matrigel.

HUVECs grown overnight were treated with trypsin and re-suspended in EGM-2 at 10000 cells per 100µl prior to being seeded onto a matrigel coated 96-well plate. The formation of HUVEC vascular networks was examined with light microscopy at after 12 hours. Images were captured using an inverted microscope. 40 x magnification.

4.14.7 FACS analysis of EGFR, MAPK and phosphorylated-MAPK expression in PBMCs, HUVECs and HDFCs

For PBMCs, primary antibodies for EGFR, MAPK and phosphorylated-MAPK were used (Table 4-2). The secondary antibody was a goat anti-rabbit Alexa 488 (LifeTechnologies). Regarding detection of EGFR, cells were permeabilised. For

permeabilised cells, cells were fixed using 200 µl 4% PFA and permeabilised with BD Phosflow™ Perm Buffer III (BD Biosciences). The wash buffer used for permeabilised cells was BD Perm/Wash™ Buffer (BD Biosciences).

For HUVECs, primary antibodies for PLCγ1 and phosphorylated-PLCγ1 were used (Table 4-2). The secondary antibody was a goat anti-rabbit Alexa 488 (LifeTechnologies). Before the addition of any antibodies, cells were fixed and permeabilised using the BD Cytofix/Cytoperm™ fixation/permeabilization solution (BD Biosciences). The wash buffer used for permeabilised cells was BD Perm/Wash™ Buffer (BD Biosciences).

For transformed HDFCs (smooth muscle cell-like cells), primary antibody for phosphorylated-MAPK was used (Table 4-2). The secondary antibody was a goat anti-rabbit Alexa 488 (LifeTechnologies). Before the addition of any antibodies, cells were fixed and permeabilised. For staining with phosphorylated-MAPK, cells were fixed using 200 µl cytofix (BD Biosciences) and permeabilised with BD Phosflow™ Perm Buffer III (BD Biosciences). A staining buffer (BD Biosciences) was used for wash steps.

A summary of the method is shown in Figure 4-16.

Table 4-2 FACS antibodies used to examine the RAS pathway in different cell types.

Antibody	Company	Clone
c-CBL (C-3)	Santa Cruz Biotechnology	Mouse monoclonal
Epidermal growth factor receptor (A-10)	Santa Cruz Biotechnology	Mouse monoclonal
Phospho-p44/42 MAPK (Erk1/2)	Cell signaling technology	Rabbit polyclonal
PLCγ1	Cell signaling technology	Rabbit polyclonal
Phospho-PLCγ1 (Tyr783)	Cell signaling technology	Rabbit polyclonal
Goat anti-rabbit alexa 488	Life Technologies	Goat polyclonal

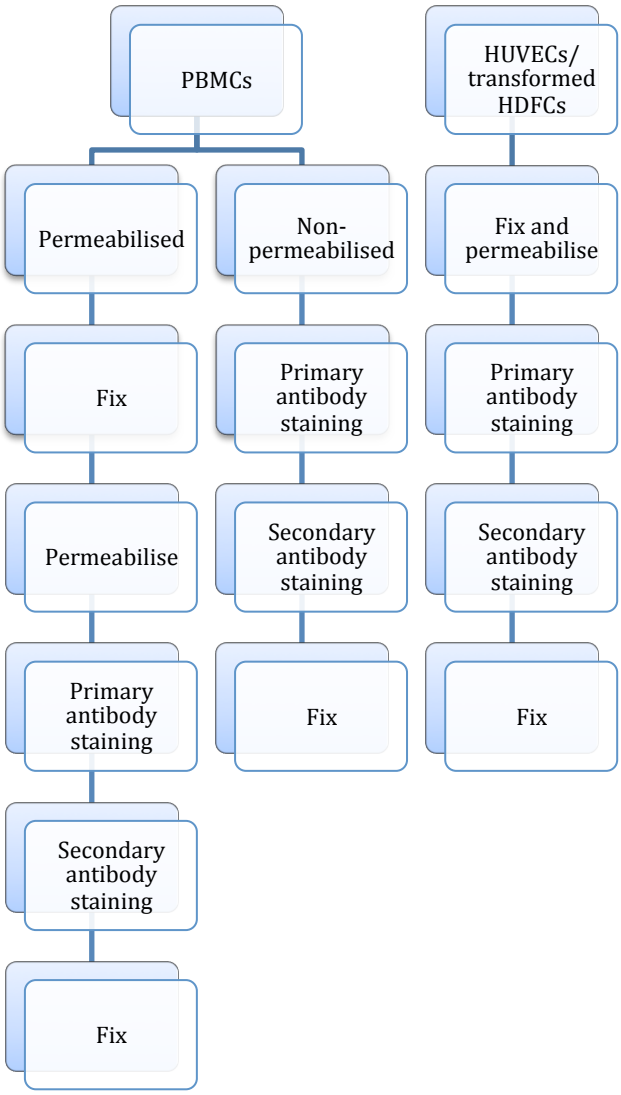

Figure 4-16 Flow diagram of staining method for PBMCs, HUVECs and transformed HDFCs for FACS assays to explore the RAS signaling pathway.

4.14.8 Analysis of FACS assays to explore the RAS signaling pathway

For EGFR and MPAK staining, gating of the monocyte population was carried out first before relative fluorescence intensity for EGFR and MAPK was identified (Figure 4-17). Representative flow cytometric plots are shown in Figure 4-17 below.

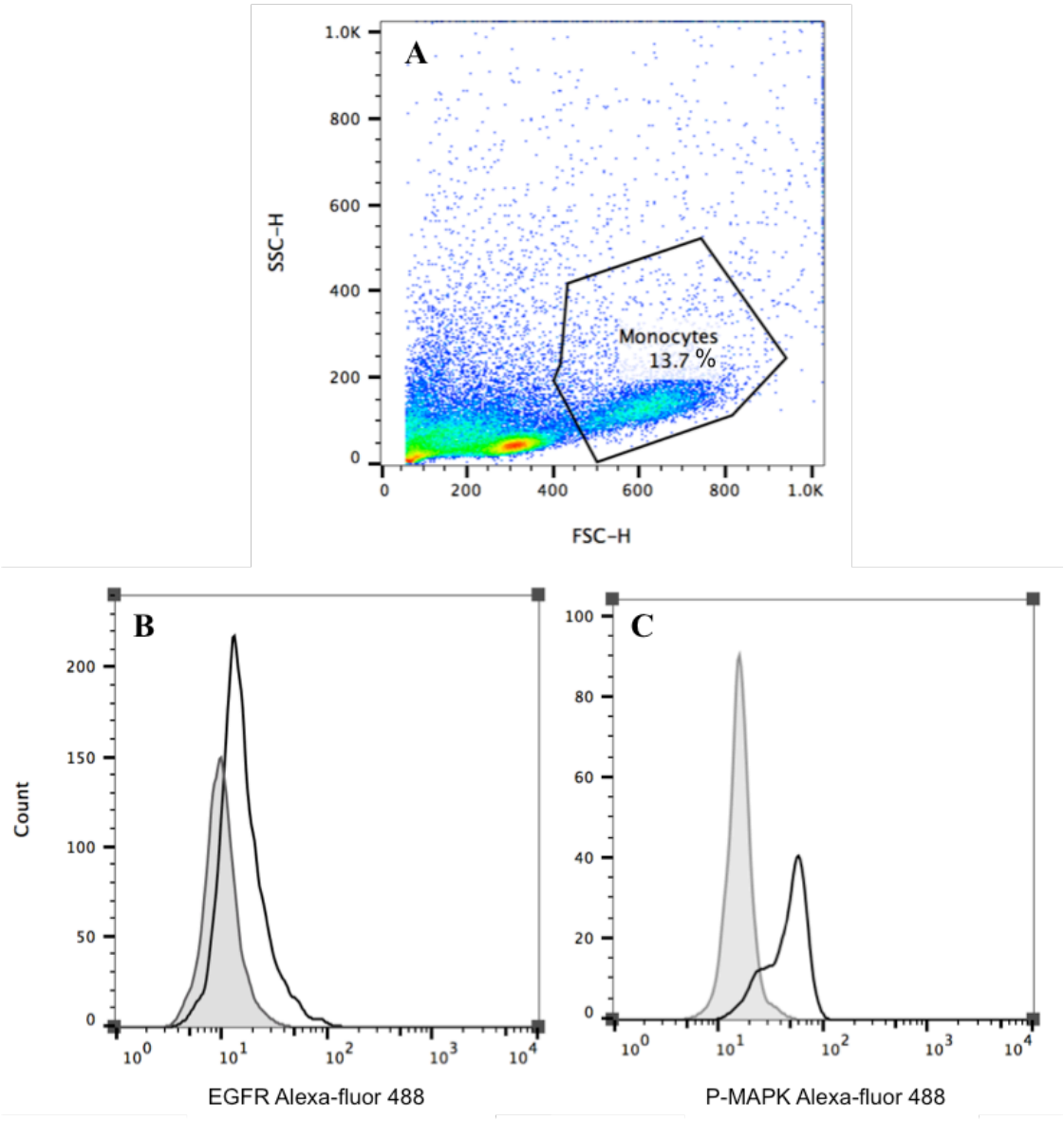

Figure 4-17 Flow cytometry gating strategy for monocyte EGFR and phosphorylated-MAPK staining.

(A) Gating on monocytes population was based on forward (x-axis) and side (y-axis) scatter properties. (B) Indicative FACS histogram showing positive EGFR staining (black line). Alexa-fluor 488 stained monocytes were used as an isotype control (grey shaded). (C) Representative histogram showing cells positive for phosphorylated-MAPK (black line). Alexa-fluor 488 stained monocytes were used as an isotype control (grey shaded).

For HUVECs and HDFCs live and dead cells were first identified prior to gating on positive cells for each specific antibody. Representative flow cytometric plots are shown in Figure 4-18 and Figure 4-19 for HUVECs and HDFCs, respectively.

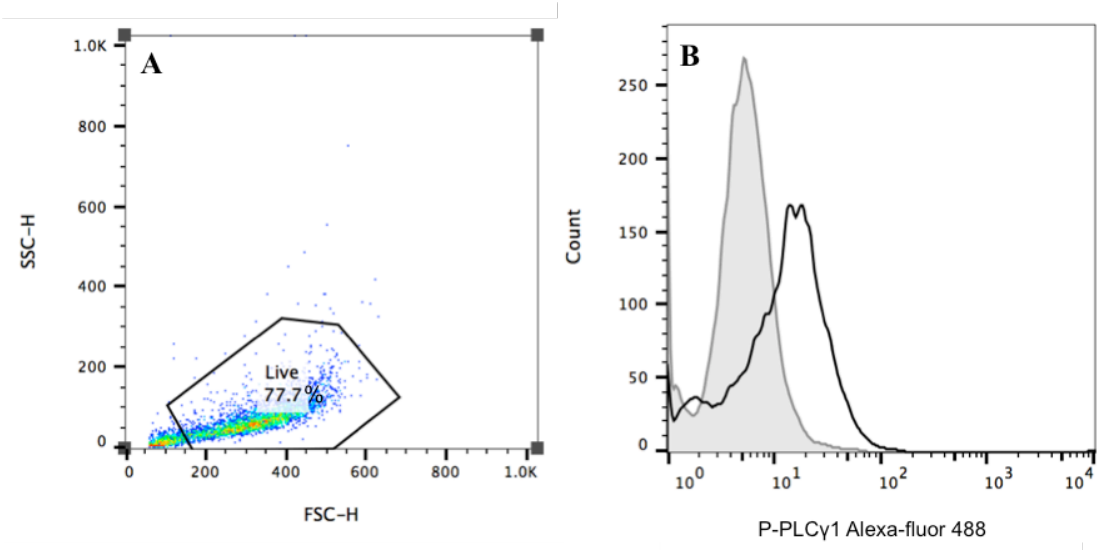

Figure 4-18 Flow cytometry gating strategy for phosphorylated-PLCγ1 staining on HUVECs.

(A) A live HUVEC gate was first identified using forward (x-axis) and side (y-axis) scatter. (B) Cells positive for phosphorylated-PLCγ1 were identified (black line). Alexa-fluor 488 stained HUVECs were used as an isotype control (grey shaded).

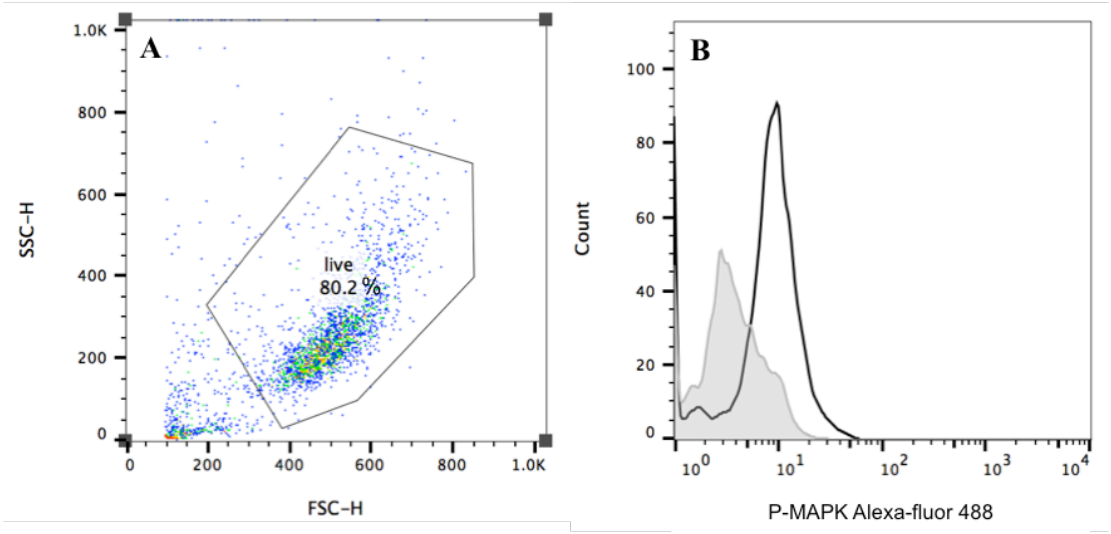

Figure 4-19 Flow cytometry gating strategy for phosphorylated-MAPK staining on HDFCs.

(A) A live gate was first identified using forward (x-axis) and side (y-axis) scatter. (B) Cells positive for phosphorylated-MAPK were identified (black line). Alexa-fluor 488 stained HDFCs were used as an isotype control (grey shaded).

All experiments were carried out in triplicate unless otherwise stated. Data are expressed as mean and SEM. Comparisons between groups were analysed using t-test, $P < 0.05$ was considered significant.

4.15 Identifying a causal allele: Whole Exome Sequencing

WES was performed on B-II-3 and both of his parents (see General methods and materials section 2.16). As only B-II-3 was affected a dominant heterozygous model was assumed as a possible mode of inheritance. WES identified 24,949 variants. As a first filter the WES output was initially compared to the vasculopathy candidate gene list (Table 2-7). Variants were found in five candidate genes: *COL5A2, MYH11, NOTCH1, SKI* and *c-CBL*. These were investigated further.

4.15.1 Verification of candidate gene variants

These candidate genes were verified using Sanger sequencing (see General methods and materials 2.15). The primers used are listed in Table 4-3.

Table 4-3 Primer sequences used for Sanger sequencing.

Primer name	Primer sequence
c-CBL exon 8 F	AACCATATCACTGGACACAAGC
c-CBL exon 8 R	CAGCCCTGACCTTCTGATTC
c-CBL exon 11 F	TTCTTTGCTGTGTACTAGTGGG
c-CBL exon 11 R	CTCACTGAAAGCTTGGCCTC
COL5A2 exon 44 F	CAAAACAGTTTGGCAACAGC
COL5A2 exon 44 R	ATGCAAATTCCAGAAGGGC
MYH11 exon 9 F	AGCCAGCTCGGGTTACTTG
MYH11 exon 9 R	CAGTGCACAACCTGCACC
MYH11 exon 37 F	GCTGGAAAATGAGACACTGC
MYH11 exon 37 R	CAATCCCAGCTTTGCTGAC
NOTCH1 exon 17 F	ATCCTCGGCTCAGTGAAGAG

NOTCH1 exon 17 R	CTTTGAAGAGGAGCTGGTGG
SKI exon 6 F	TCAGATAGATGACCCCACGG
SKI exon 6 R	TCTTCGATCTGAAAGGGAGC

The variants in *NOTCH1* and *SKI* were found to be false positives; however the variants in *MYH11, COL5A2* and *c-CBL* were confirmed to be potential novel heterozygous missense mutations.

4.15.1.1 Candidate gene: *MYH11*

The variant in *MYH11* was a non-synonymous substitution NM_002474:c.914A>G (p.N305S) (Figure 4-20), which causes an amino acid change from asparagine to serine. Both are polar amino acids with uncharged side chains, which means there was unlikely to be a change in the protein structure and consequently function. This was supported by the SIFT, MutationTaster and PolyPhen-2 programs that predicted the change to be benign.

The role of *MYH11* and the diseases associated with known mutations have been discussed previously (see Chapter 3). As the variant was predicted to be benign I decided to investigate the variants observed in the other genes first.

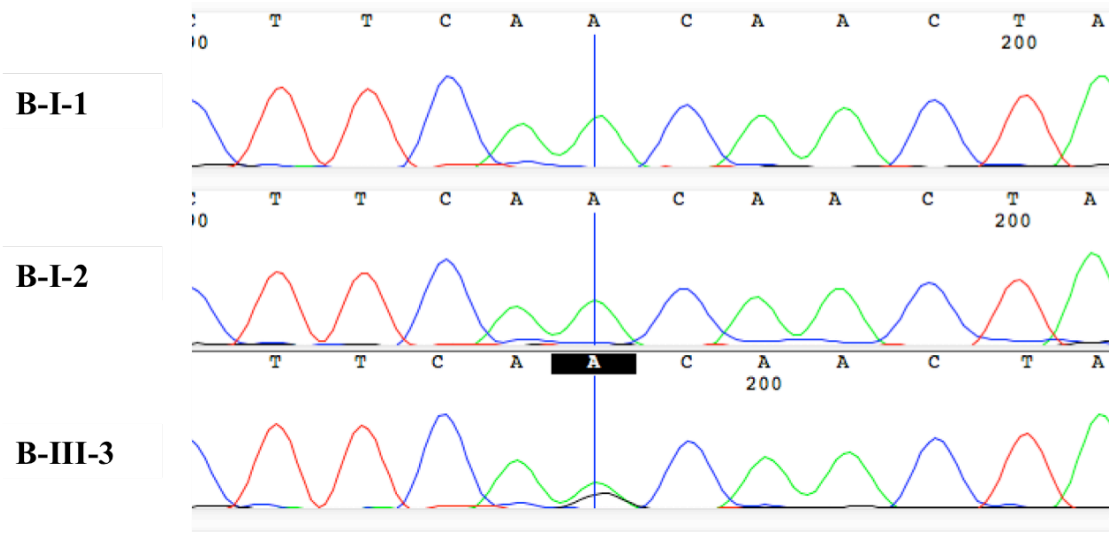

Figure 4-20 Sanger sequencing chromatogram of MYH11 for the parents (B-I-1 and B-I-2) and proband (B-II-3) of family B.

Aligned to the reference sequence exon 9 of MYH11 (NM_002474). Blue line indicates a heterozygous non-synonymous missense substitution present in the proband but not in either parent (c.914A>G:p.N305S).

4.15.1.2 Candidate gene: *COL5A2*

The mutation in *COL5A2* was a non-synonymous substitution NM_000393:c.3098C>T (p.P1033L) (Figure 4-21) that caused an amino acid change from proline to leucine. Conserved between species, the differences in structural and chemical properties between the two amino acids were predicted to have a deleterious effect by several different algorithms: SFIT, MutationTaster and PolyPhen-2.

COL5A2 encodes type V collagen alpha chain 2. Unlike collagen type I, which is abundant in tissues such as the dermis, cornea and bone, type V collagen, is a minor component of connective tissues (Kadler et al., 1996, Birk et al., 1990). It is proposed to play a role in defining the diameter of heterotypic collagen fibrils in connective tissue. Mutations in *COL5A2* are associated with the classical form of EDS and result in functional changes to the dermal and bone collagens (Michalickova et al., 1998). Reports so far indicate that these mutations are mainly located in the triple-helix domain of the gene and cause structural alterations to the α2(V)-chains resulting in abnormally formed heterotrimers (Malfait et al., 2005, Symoens et al., 2012). Although there is a vascular form of EDS, this type is associated with *COL3A1,* which encodes collagen type III alpha chain 1 (Kontusaari et al., 1990). Collagen type

III is a major component of the extracellular matrix in skin and various organs as well as playing a role in cardiovascular development (Liu et al., 1997). Taking this into account it seemed unlikely that the mutation in *COL5A2* alone would result in the observed stenotic occlusive cerebrovascular phenotype. In addition the patient did not demonstrate the typical classical EDS features. Therefore, I considered this variant unlikely to be causative of the vascular phenotype.

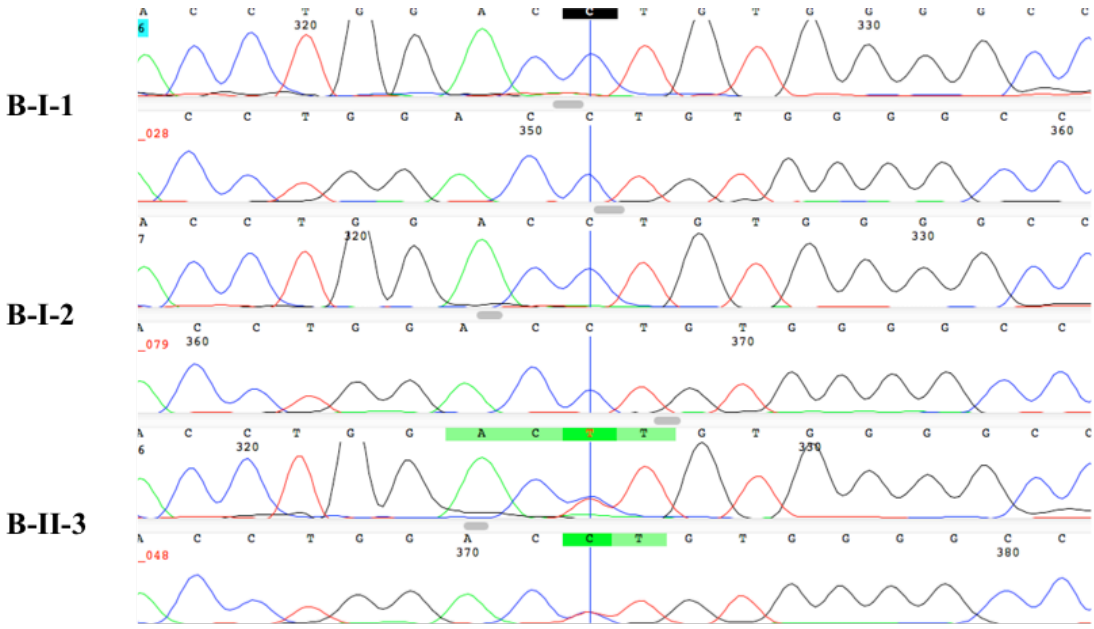

Figure 4-21 Sanger sequencing chromatogram of COL5A2 for the parents (B-I-1 and B-I-2) and proband (B-II-3) of family B.

Aligned to the reference sequence exon 44 of COL5A2 (NM_000393). Blue line indicates a heterozygous non-synonymous missense substitution present in the proband but not in the parents (c.3098C>T:p.P1033L).

4.15.1.3 Candidate gene: c-*CBL*

Two mutations were observed in *c-CBL*: a non-synonymous substitution (Figure 4-22) and a non-frameshift deletion (Figure 4-23). The non-synonymous missense substitution NM_005188:c.1858C>T (p.L620F) resulted in an amino acid change from leucine to phenylalanine. This was predicted to be damaging by the SIFT, MutationTaster and PolyPhen-2 programs. However, its minor allele frequency was 1.1% according to the 1000 Genome database, which would suggest it is not very rare and therefore unlikely to be pathogenic. The non-frameshift deletion NM_005188:c.1110_1112del (p.370_371del) resulted in the deletion of two residues:

a leucine and a tyrosine in the linker region of c-CBL. No information was available as to whether this deletion would be deleterious or not and this genetic variant had not been previously reported.

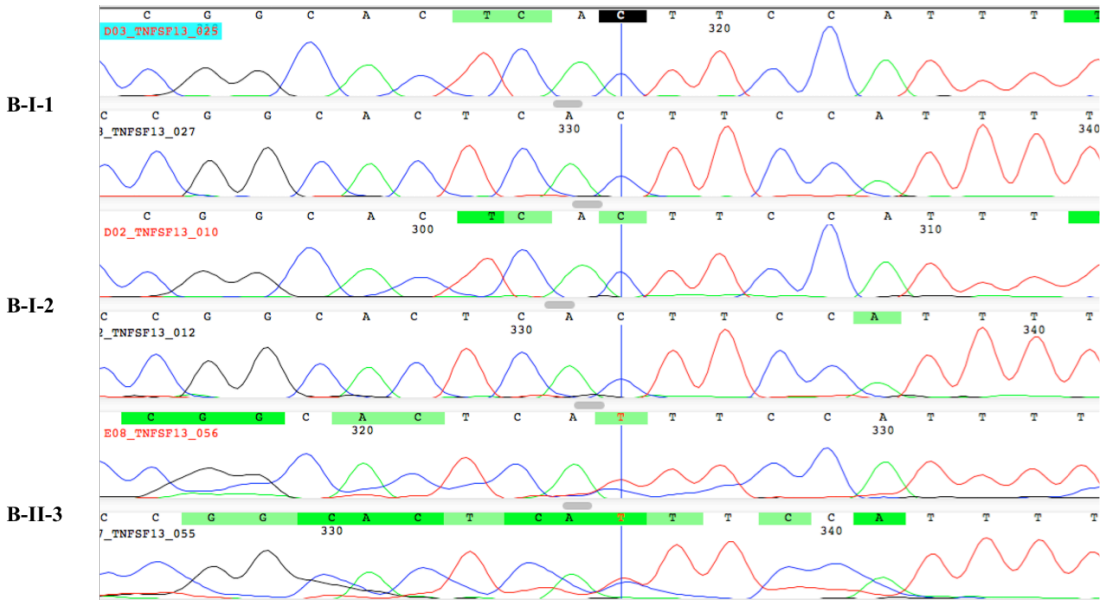

Figure 4-22 Sanger sequencing chromatogram of c-CBL for the parents (B-I-1 and B-I-2) and proband (B-II-3) of family B.

Aligned to reference sequence exon 11 of c-CBL (NM_005188). Blue line indicates a heterozygous non-synonymous missense substitution present in the proband but not in the parents (c.1858C>T:p.L620F).

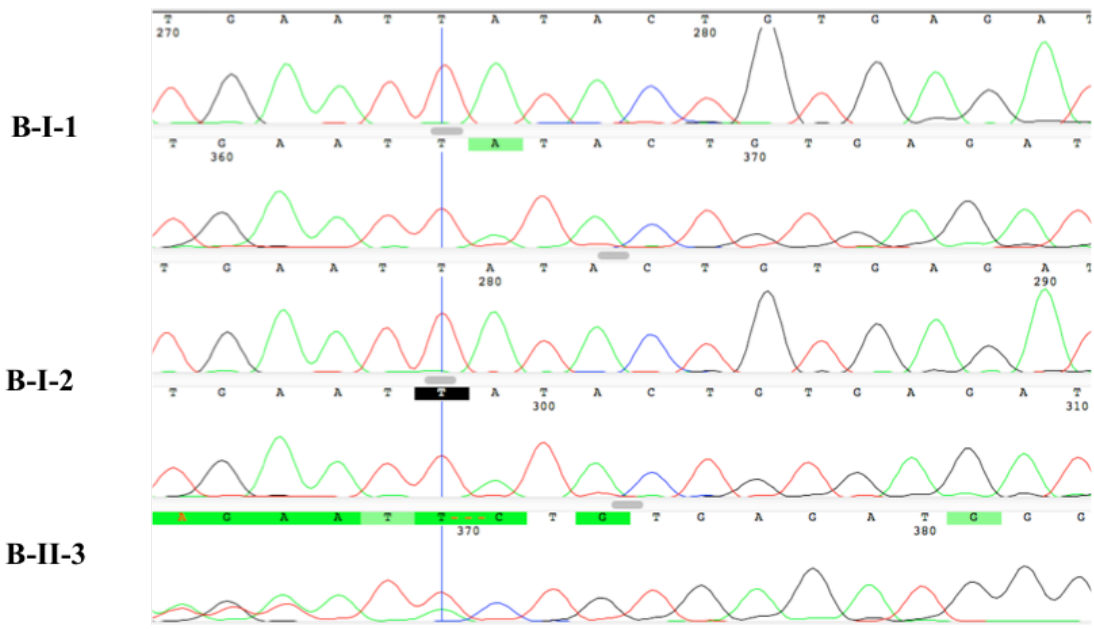

Figure 4-23 Sanger sequencing chromatogram of c-CBL for the parents (B-I-1 and B-I-2) and proband (B-II-3) of family B.

Aligned to reference sequence exon 8 of c-CBL (NM_005188). Blue line indicates a non-frameshift deletion present in the proband but not in the parents (c.1110_1112del:p.370_371del).

4.16 Effect of p.370_371del *c-CBL* variant on protein and RNA levels

4.16.1 Protein expression of wild-type c-CBL

c-CBL is a ubiquitously expressed protein (Schmidt and Dikic, 2005) so as a preliminary experiment I looked at c-CBL expression in several different cell lines to confirm this. Three cell types were investigated: an EBV transformed B cell line, a Jurkat cell line and dermal fibroblasts from a healthy control (Figure 4-24). Protein expression was adjusted relative to actin showing that, compared to the EBV transformed cells, c-CBL expression is 48% lower in Jurkat cells and 10% lower in dermal fibroblasts (Table 4-4). This provides preliminary evidence that *c-CBL* is ubiquitously expressed.

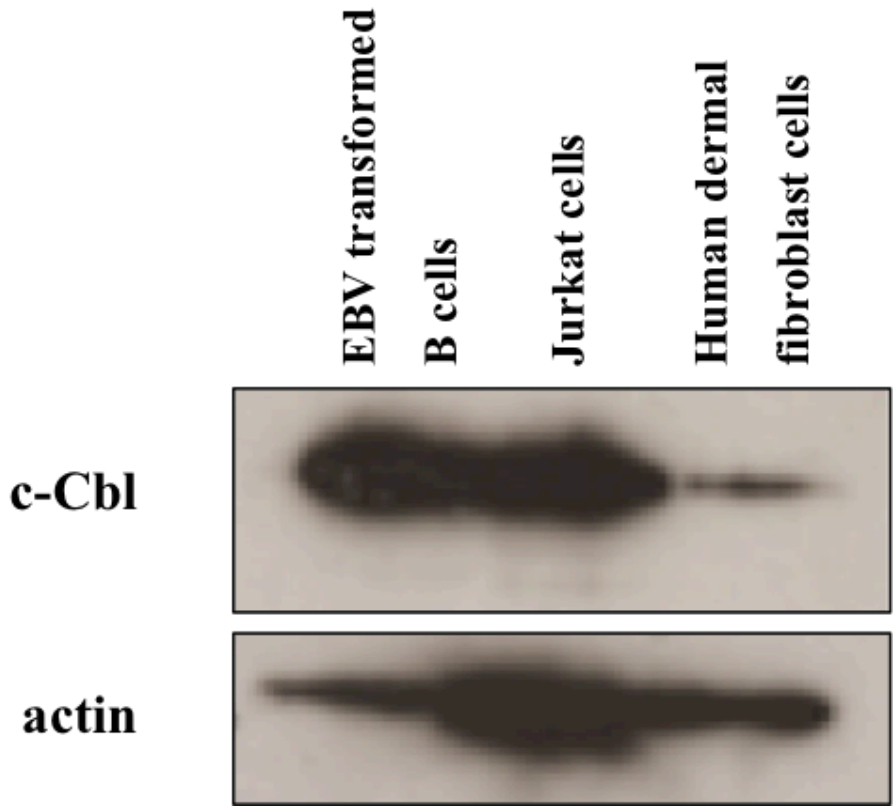

Figure 4-24 c-CBL protein expression.

A preliminary assay investigating expression of wild type c-CBL in EBV transformed B cells, Jurkat cells and Human dermal fibroblast cells.

Table 4-4 Adjusted protein expression of c-CBL relative to actin in EBV transformed B cells, jurkat cells and human dermal fibroblast cells.

	Cell Type	Area under curve	% (relative to others of same gene)	Relative Density	Adjusted Density
Actin	B Cell	44102.818	18.842	1	
	Jurkat Cell	117208.855	50.075	2.6576	
	Fibroblast	72757.257	31.084	1.6497	
c-CBL	B Cell	106492.349	43.627	1	**1**
	Jurkat Cell	119158.624	48.816	1.1189	**0.4210**
	Fibroblast	18444.442	7.556	0.1732	**0.1050**

4.16.2 c-CBL variant does not affect protein or mRNA expression levels in B-II-3.

As the deletion of a residue (p.370_371del) may affect protein expression and/or function I first examined whether c-CBL protein expression was affected in PBMCs derived from B-II-3. PBMC *c-CBL* mRNA expression was also examined (Figure 4-26). Protein expression of c-CBL in B-II-3 PBMCs (Figure 4-25, lane A) was comparable to that of a healthy control (Figure 4-25, lane C). After adjusting c-CBL protein expression relative to actin, relative band density was 0.7112 for control PBMCs compared to B-II-3 PBMCs. Expression of c-CBL in human dermal fibroblasts was lower than in PBMCs: relative band density of 0.43 compared to 0.7112. The relative mean *c-CBL* mRNA expression in B-II-3 PBMCs was 18.7 (SEM=0.2), which was not significantly different from the relative mean expression in control PBMCs of 18.455 (SEM=0.375, *P*=0.7304) (Figure 4-26). This finding would suggest that the detected gene deletion in *c-CBL* is likely to affect protein function rather than protein expression.

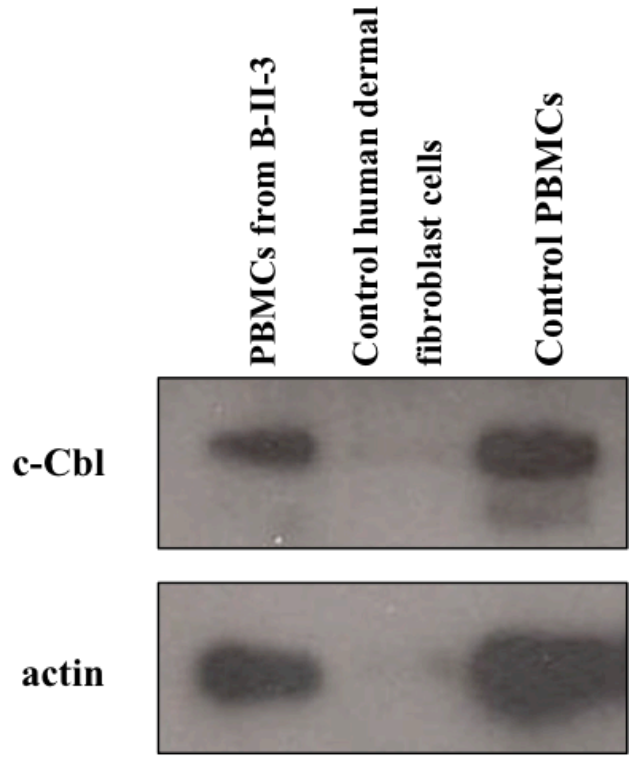

Figure 4-25 c-CBL protein expression in control and B-II-3 PBMCs.

Table 4-5 Adjusted protein expression of c-CBL relative to actin.

	Cell Type	Area under curve	% (relative to others of same gene)	Relative Density	Adjusted Density
Actin	B-II-3 PBMCs	28147.877	37.9650732	1	
	Control HDFCs	3730.518	5.031618861	0.13253284	
	Control PBMCs	32263.111	57.00330797	1.14620051	
c-CBL	B-II-3 PBMCs	15114.815	45.9957228	1	**1**
	Control HDFCs	860.598	2.61887605	0.05693738	**0.430**
	Control PBMCs	16885.936	37.4961276	0.81520901	**0.7112**

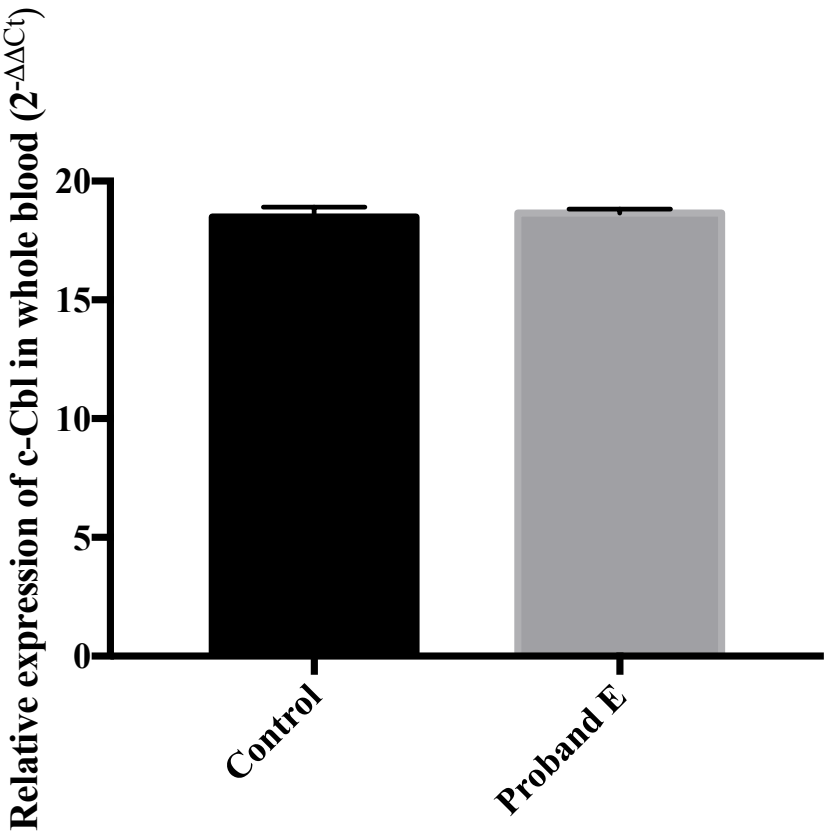

Figure 4-26 c-CBL mRNA expression in PBMCs from B-II-3 and healthy controls.

c-CBL expression was analysed by qPCR and was comparable between B-II-3 and a control. A T-test was performed: t=0.396, df=2, P=0.7304.

4.17 Functional effect of p.370_371del *c-CBL* variant in PBMCs

4.17.1 Reduced EGF-induced EGFR degradation

Mutation of the Y371 residue in the linker region of c-CBL is crucial to E3 ligase activity (Perez et al., 2010, Kassenbrock and Anderson, 2004, Swaminathan and Tsygankov, 2006). Therefore I investigated whether deletion of this residue affected downregulation of a well-known RTK: EGFR. After stimulation with EGF, relative EGFR expression appeared to be higher in PBMCs from B-II-3 compared to control PBMCs across the whole time course, although it did not reach statistical significance (*P*=0.0768) (Figure 4-27). Although unstimulated cells from B-II-3 had a lower initial relative EGFR expression level of 0.953, SEM=0.114 at 0 minutes compared to the control (mean=1, SEM=0.103), stimulation induced a greater response in B-II-3 PBMCs compared to the control across all time points (Figure 4-27). Interestingly, at 30 minutes post-stimulation fold change in relative EGFR expression was decreasing in control PBMCs (mean=0.951, SEM=0.081) whilst still increasing in B-II-3 PBMCs (mean=1.228, SEM=0.11) (Figure 4-27). This is consistent with the hypothesis that deletion of this crucial tyrosine residue (Y371) affects the E3 ligase activity of c-CBL. At 60 minutes, fold change in relative EGFR expression did start to decrease in B-II-3 PBMCs (mean=1.143) suggesting that some E3 ligase activity is retained. It appears efficiency of EGFR degradation is affected leading to a higher sustained response to EGF, which is eventually downregulated.

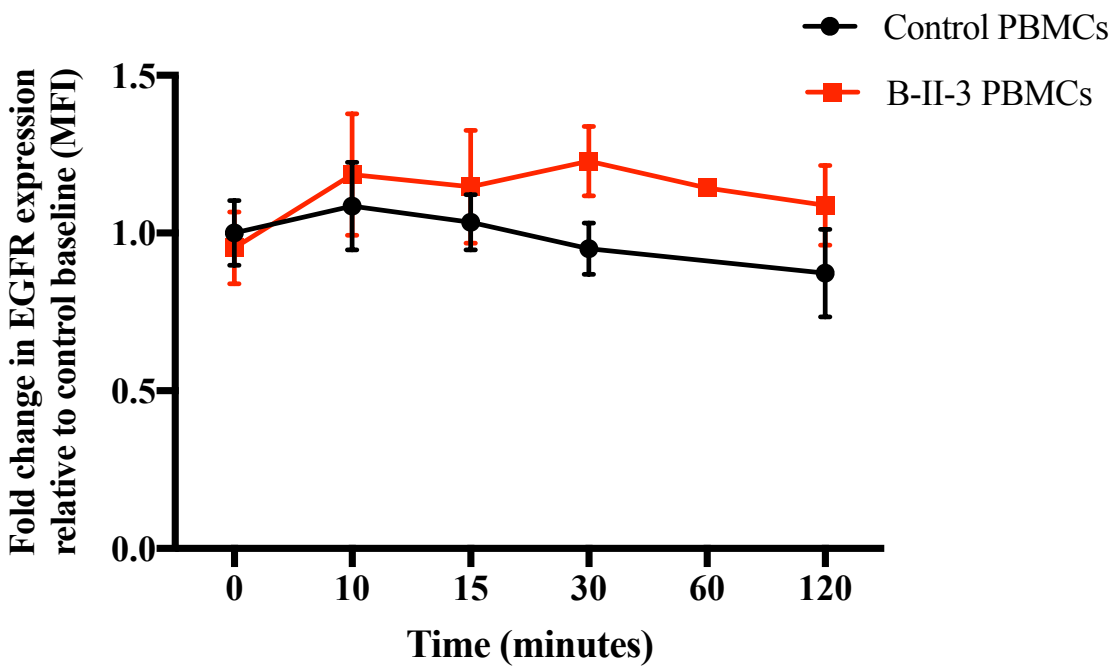

Figure 4-27 Fold change in relative EGFR expression in permeabilised PBMCs from B-II-3 and healthy controls.

PBMCs were stimulated with 20 ng/ml EGF for the indicated periods of time, permeabilised, and stained. Cells were analysed using FACS for EGFR expression. Data are expressed as fold change relative to mean baseline of the control at 0 minutes and plotted as mean of triplicate samples, where possible, with one standard error of mean indicated.

To further explore the consequence of the mutated c-CBL protein I decided to investigate the downstream signaling pathway in PBMCs. One of the pathways activated by EGFR is the MAPK/ERK pathway (Figure 4-4). This pathway is essential to normal cell development and regulates processes such as cell cycle regulation, differentiation, growth and cell senescence (Tidyman and Rauen, 2009). Using FACS I investigated the expression level of the activated form of MAPK i.e. phosphorylated MAPK (P-MAPK). Baseline relative expression level of P-MAPK was higher at 1.263 (SEM=0.131) in B-II-3 PBMCs compared to the control which was 0.868 (SEM=0.147). Although there was a similar trend in the upregulation and subsequent downregulation of P-MAPK expression between the control and B-II-3 PBMCs, the fold change in relative expression level was higher in B-II-3 PBMCs at all time points (P=0.01) (Figure 4-28). In addition, a peak fold change in P-MAPK expression of 1.577 (SEM=0.096) in the B-II-3 PBMCs occurred at 30 minutes post-stimulation whilst the peak fold change in relative P-MAPK expression in the control

PBMCs occurred at 10 minutes post-stimulation and was 1.027 (SEM=0.12). Downregulation did not happen until 60 minutes post-stimulation in the B-II-3 PBMCs (mean=1.212, SEM=0.12) compared to 30 minutes in the control (mean=0.839, SEM=0.108) (Figure 4-28). At 30 minutes, the fold change in relative expression level of P-MAPK appeared to still be increasing in B-II-3 PBMCs whilst the response was plateauing in the control. Statistical analysis for individual time points indicated that the most significant difference in the relative P-MAPK expression level between B-II-3 and the control was seen at 30 minutes (P=0.007). This provides additional evidence that there is a sustained period of EGFR stimulation in B-II-3 PBMCs due to reduced c-CBL E3 ubiquitin ligase activity.

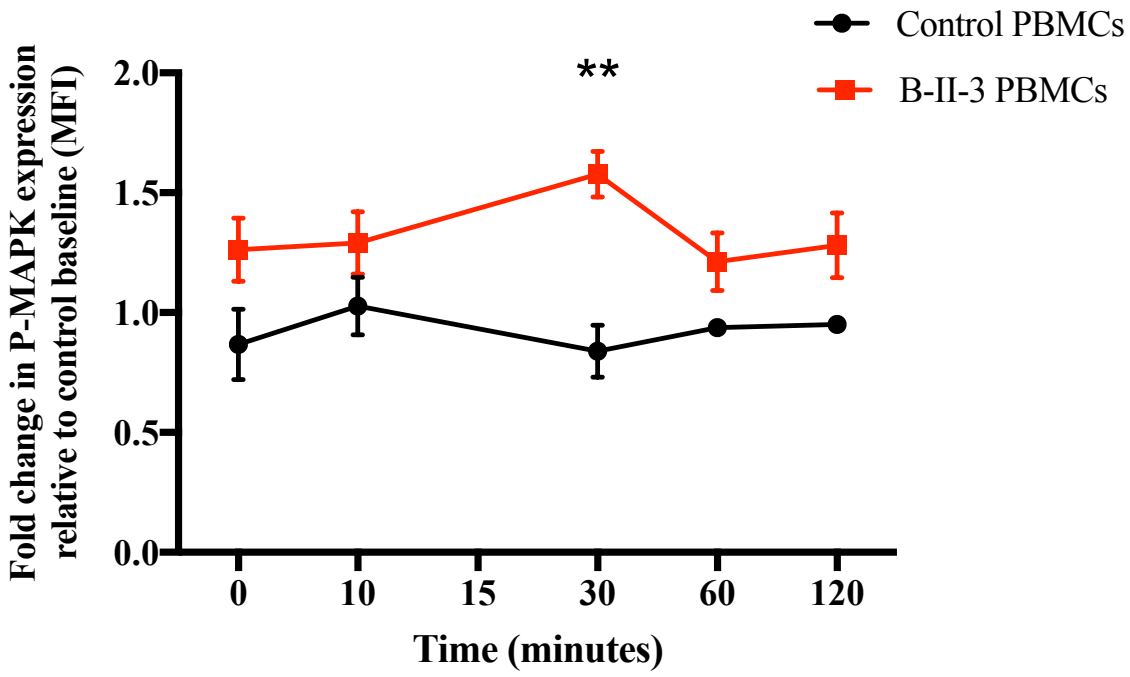

Figure 4-28 Fold change in relative phosphorylated-MAPK expression in permeabilised PBMCs from B-II-3 and healthy controls.

*PBMCs were stimulated with 20 ng/ml EGF for the indicated periods of time, permeabilised, and stained. Cells were analysed using FACS for Phosphorylated-MAPK expression. Data are expressed as fold change relative to mean baseline of the control at 0 minutes and plotted as mean of triplicate samples, where possible, with one standard error of mean indicated. T-tests were performed ** <0.01. There was a significantly higher change in relative P-MAPK expression between the control and B-II-3 PBMCs at all time points, P=0.01.*

4.17.2 No detectable ubiquitination activity after EGF stimulation

To explore whether the reduced degradation of EGFR is a direct consequence of the lack of E3 ubiquitin ligase activity of c-CBL, I performed an immunoprecipitation assay of the targeted protein (c-CBL) followed by an ubiquitination experiment. Using PBMCs from B-I-1 (father with a wild-type genotype for *c-CBL*) and B-II-3 I immunoprecipitated c-CBL to eliminate the possibility of any other molecule ubiquitinating EGFR. EGFR was then added as a substrate and ubiquitination of EGFR assessed. c-CBL protein was detected in both samples with a relative density of 1 in B-I-1 PBMCs and 0.551 in B-II-3 PBMCs (Table 4-6). However, ubiquitination of EGFR was only detectable in B-I-1 but not in B-II-3 PBMCs (Figure 4-29 and Table 4-6). These observations confirm that c-CBL is measureable in B-II-3 PBMCs but its function appears to be altered/reduced so that it is unable to ubiquitinate EGFR. This is evidence of a direct link between c-CBL and its inability to function as an E3 ubiquitin ligase.

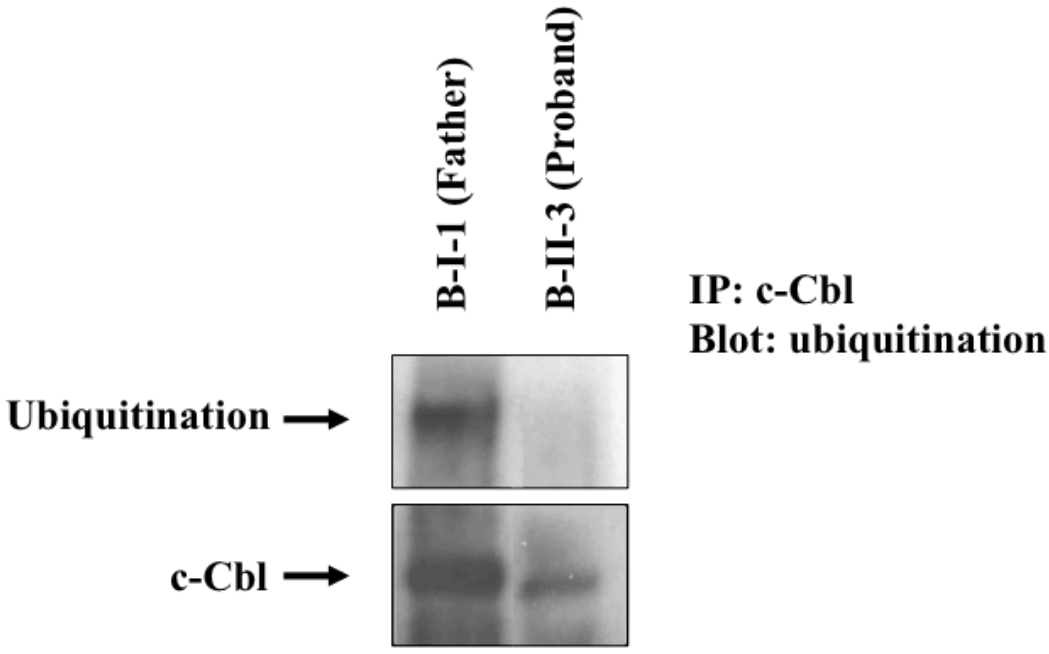

Figure 4-29 Ubiquitination assay using PBMCs from B-I-1 (Father) and B-II-3 (Proband). *To begin with c-CBL was immunoprecipitated. EGFR was then added as a substrate and assessed for ubiquitination.*

Table 4-6 Adjusted protein expression of ubiquitinated EGFR relative to c-CBL.

	Lane	Area under curve	% (relative to others of same gene)	Relative Density	Adjusted Density
c-CBL	B-I-1 (Father)	6240.803	64.4673492	1	
	B-II-3 (Proband)	3439.761	35.5326508	0.55117282	
Ub	B-I-1 (Father)	9036.966	100	1	**1**
	B-II-3 (Proband)	0	0	0	**0**

4.18 Functional effect of siRNA *c-CBL* in HUVECs

To assess whether the mutated c-CBL protein affected endothelial cell function and angiogenesis I then transfected HUVECs with *c-CBL* siRNA. Endothelial cells line the inside of all vessel walls and have been found, in MMD patients, to exhibit an active angiogenic process (Chmelova et al., 2010). In endothelial cells pro-angiogenic signaling is in part controlled by activation of phospholipase Cγ1 (PLCγ1) via vascular endothelial growth factor 2 (VEGFR-2) (Meyer et al., 2003). To mimic the genotype of B-II-3 I transfected HUVECs with siRNA targeted to *c-CBL.* Transfection with *c-CBL* siRNA resulted in a significant decrease of *c-CBL* expression by 68.43% (SEM=8.4%, *P*=0.0002) compared to the control and 49.2% compared to the SCR *c-CBL* siRNA (*P*=0.0021) (Figure 4-30).

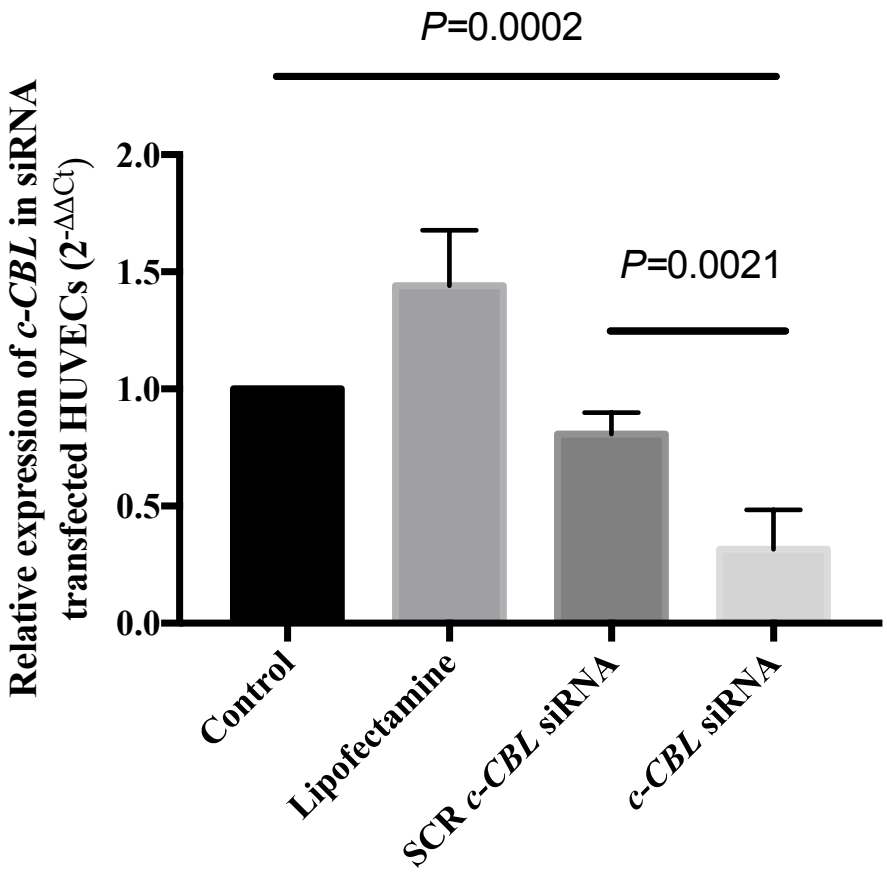

Figure 4-30 c-CBL mRNA expression in HUVECs transfected with lipofectamine, SCR c-CBL siRNA and c-Cbl siRNA.

c-CBL expression was analysed by qPCR and was comparable between the conditions. A T-test was performed between the control and c-CBL siRNA conditions: t=8.139, df=6, P=0.0002; and the SCR c-CBL siRNA and c-CBL siRNA conditions: t=5.134, df=6, P=0.0021.

Once I had confirmed successful knockdown of *c-CBL,* I looked at phosphorylated PLCγ1 (P-PLCγ1) expression. There was significant upregulation of relative P-PLCγ1 expression in siRNA c-CBL transfected cells compared to control SCR transfected HUVECs at all time points, *P*=0.0005. Stimulation via VEGF caused an upregulation of mean relative P-PLCγ1 expression from 0.689 (SEM=0.258) in the SCR *c-CBL* siRNA transfected negative control HUVECs to 2.615 (SEM=1.565) after 30 minutes (Table 4-31). A similar pattern was observed in the *c-CBL* siRNA transfected HUVECs from 3.445 (SEM=0.937) at baseline to 4.871 (SEM=1.711) at 30 minutes (Table 4-31). Interestingly, at baseline there was already a significant difference in P-PLCγ1 levels between the negative control HUVECs and those transfected with *c-CBL* siRNA (*P*=0.04706) suggesting an inability of the silenced *c-CBL* cells to

regulate P-PLCγ1 even before VEGF stimulation. After 60 minutes relative mean expression of P-PLCγ1 was 0.590 (SEM=0.285) in the negative control HUVECs indicative of a c-CBL mediated downregulation process (Table 4-31). However, silencing of *c-CBL* appeared to dampen the downregulation response in the *c-CBL* siRNA transfected HUVECs, as P-PLCγ1 expression had still not returned to its baseline level after 60 minutes (mean=5.473, SEM=1.68) (Table 4-31). In fact, at 60 minutes the mean expression level of P-PLCγ1 between the negative control HUEVCs and the *c-CBL* siRNA transfected HUVECs was significantly different (*P*=0.03332). This data would suggest c-CBL is a key mediator in the downregulation of P-PLCγ1 expression after VEGF stimulation. These results support what has previously been reported which is that lack of E3 ubiquitin ligase activity in c-CBL affects its ability to ubiquitinate PLCγ1 causing sustained upregulation of activated PLCγ1. The functional consequence of sustained increased PLCγ1 expression should be increased pro-angiogenic signaling. I then therefore performed a vasculogenesis assay using matrigel to investigate the rate of angiogenesis. HUVECs transfected with *c-CBL* siRNA formed a significantly greater number of tubule branches (mean=20.14, SEM=2.675) compared to the control SCR transfected HUVECs (mean=13.37, SEM=1.495) (*P*=0.0198) (Figure 4-32). This difference in number of tubule branches is evident in Figure 4-33.

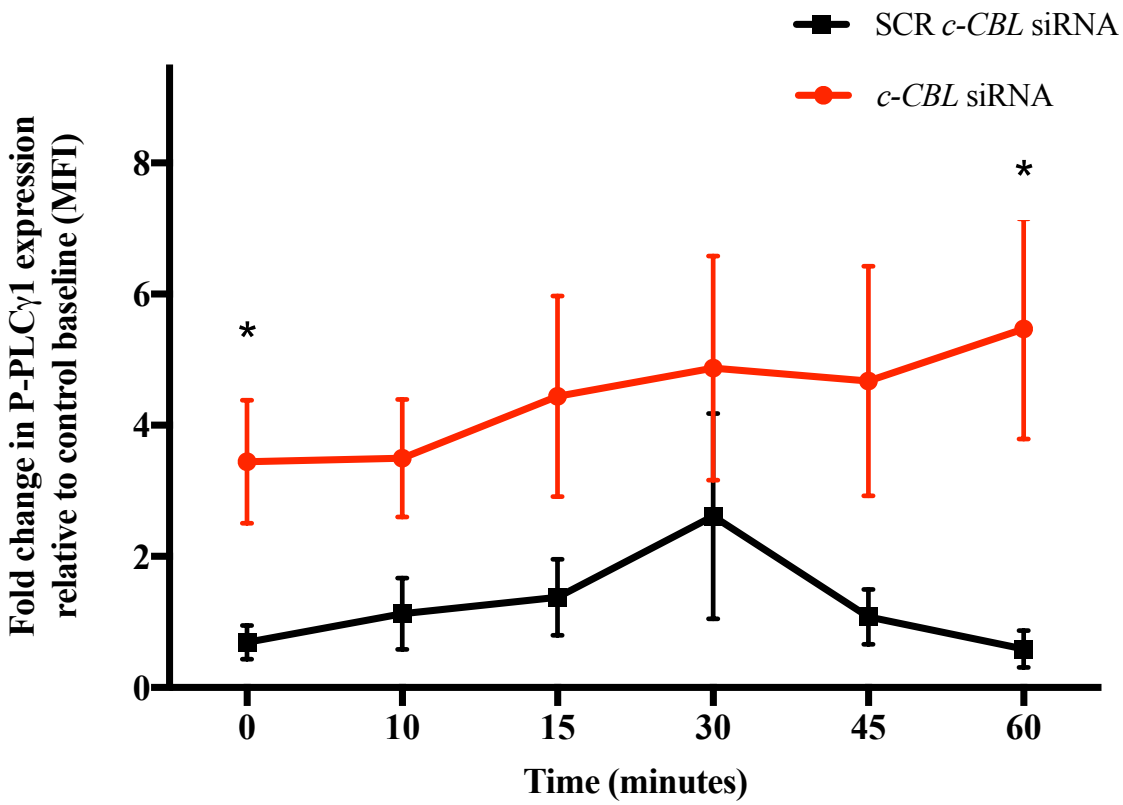

Figure 4-31 Fold change in relative phosphorylated-PLCγ1 expression in siRNA c-CBL transfected HUVECs. HUVECs were transfected with siRNA targeting c-CBL or a negative control (SCR).

*They were stimulated with 20 ng/ml VEGF for the indicated periods of time, permeabilised, and stained. Cells were analysed using FACS for Phosphorylated-PLCγ1 expression. Data are expressed as relative fold change compared to the mean control baseline at 0 minutes and plotted as mean of triplicate samples with one standard error of mean indicated. T-tests were performed * <0.05. There was significant upregulation of relative P-PLCγ1 expression in siRNA c-CBL transfected cells compared to control SCR transfected HUVECs at all time points, P=0.0005.*

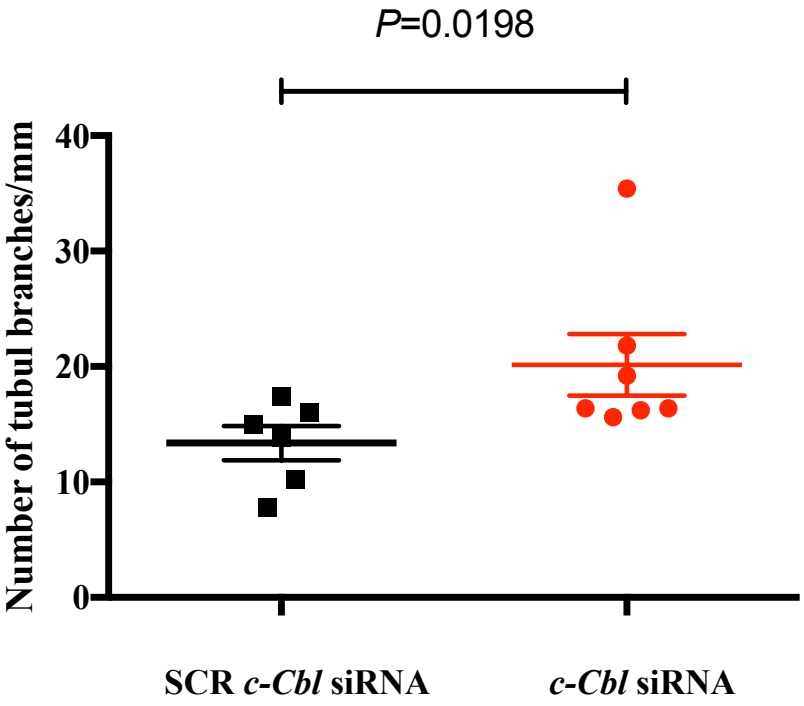

Figure 4-32 siRNA c-CBL HUVEC tubule formation using a matrigel assay.

HUVECs were either transfected with siRNA targeting c-CBL or a negative control (SCR). Experiment was repeated in triplicate. A Mann-Whitney U test was performed. HUVECs transfected with c-CBL siRNA formed a significantly greater number of tubule branches compared to the control SCR transfected HUVECs, P=0.0198.

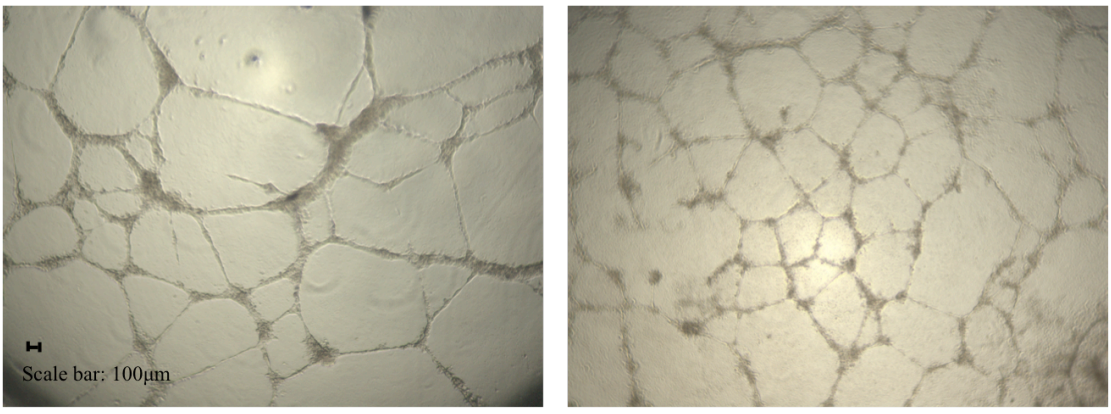

Figure 4-33 Human umbilical vein endothelial cell (HUVEC) capillary network (tubule) formation on matrigel for SCR c-CBL siRNA and c-CBL siRNA transfected HUVECs.

HUVECs grown overnight were treated with trypsin and re-suspended in EGM-2 at 10000 cells per 100µl prior to being seeded onto a matrigel coated 96-well plate. The formation of HUVEC vascular networks was examined with light microscopy at after 12 hours. Images were captured using an inverted microscope. 40 x magnification.

4.19 Additional patients

Two additional families diagnosed with a moyamoya arteriopathy were identified with a variant in *c-CBL.* The first was family C where WES, which was carried out in collaboration with Hywell Williams, revealed an intronic mutation: NM_005188:c.1228-2A>G. This mutation, predicted to affect splicing, occurs upstream of exon 9 which encodes part of the RING finger domain. A gel image showed the presence of smaller fragments in C-III-2 suggesting the mutation created an alternate transcript by splicing out an exon (Table 4-34). In family D a heterozygous missense mutation was identified posthumously: NM_005188:c.1100C>A (p.Q367P). This residue is located in the linker region of c-CBL. For family D I was unable to perform any functional experiments as no samples were available.

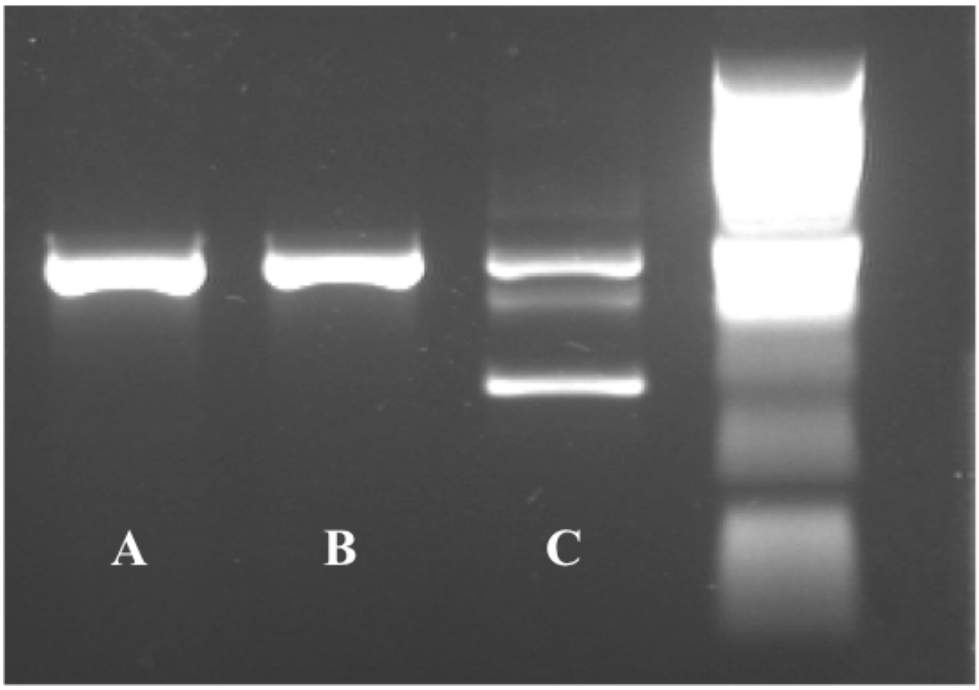

Figure 4-34 Agarose gel image of amplified c-CBL cDNA.
(A-B) Control. (C) C-III-2.

4.20 Functional effect of *c-CBL* mutations in HDFCs and SMC-myofibroblasts

4.20.1 Sustained PDGF-induced activation of the MAPK pathway

Taking into account previous studies that have demonstrated abnormal SMC function contributes to the vasculopathy associated with moyamoya arteriopathy and that c-CBL is expressed in SMCs, I then chose to explore whether mutant c-CBL affected SMC function (Reid et al., 2010). I was able to acquire HDFCs from B-II-3, C-III-1 and C-III-2, which I transformed into SMC-myofibroblasts (Desmouliere et al., 1993). To determine whether the HDFCs had transdifferentiated into SMC-myofibroblasts relative expression of *ACTA2* at day 0 and day 14 were analysed (Figure 4-35). Mean *ACTA2* expression at day 14 had increased 31-fold (SEM=3) compared to day 0 confirming successful transdifferentiation into SMC-myofibroblasts (Figure 4-35).

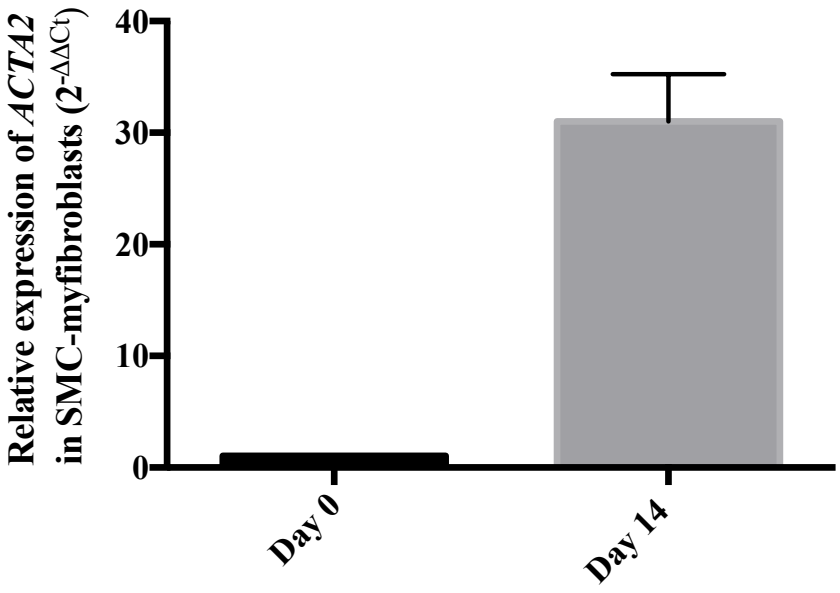

Figure 4-35 Relative expression of ACTA2 in HDFCs and SMC-myofibroblasts derived from B-II-3 patient.

HDFCs were treated with TGFβ1 for 14 days to induce transdifferentiation into SMC-myofibroblasts.

In SMCs MAPK is upregulated/activated by PDGF via PDGFR, which in turn is downregulated by c-CBL (Cho et al., 2000). To establish whether the mutations in B-II-3, C-III-1 and C-III-2 affected regulation of the MAPK pathway, HDFCs and SMC-myofibroblasts were stimulated with PDGF and P-MAPK expression was measured. In control HDFCs, upregulation of P-MAPK expression was fairly rapid occurring during the first 10 minutes post-stimulation from 1 to 1.832 (Figure 4-37). This was followed by an efficient downregulation returning relative P-MAPK expression to approximately baseline levels by 30 minutes (1.09) (Figure 4-37). In contrast, the patient HDFCs had a higher baseline expression level at 1.628 (SEM=0.474), which peaked post-stimulation after 45 minutes (mean=1.842, SEM=0.665) (Figure 4-37). These results would suggest that in the patients there is a dysregulation of P-MAPK following PDGF stimulation. In SMC-myofibroblasts the difference in the fold change of P-MAPK expression was not so pronounced as in HDFCs. Fold change in P-MAPK expression peaked after 10 minutes in both the control SMC-myofibroblasts (1.832) and patient SMC-myofibroblasts (mean=1.562, SEM=0.089) (Figure 4-37). However, downregulation in patient SMC-myofibroblasts was delayed and did not return to baseline levels until 60 minutes post-stimulation. In control SMC-myofibroblasts fold change in relative P-MAPK expression was back to baseline levels after 30 minutes (1.09) (Figure 4-37). At this same time point fold change in relative P-MAPK expression was still at 1.496 (SEM=0.156) in patient SMC-myofibroblasts. There also appears to be some form of reduced/delayed downregulation of P-MAPK in SMC-myofibroblasts in the patients compared to the control indicative of an aberrant functioning c-CBL protein. This however needs to be further explored.

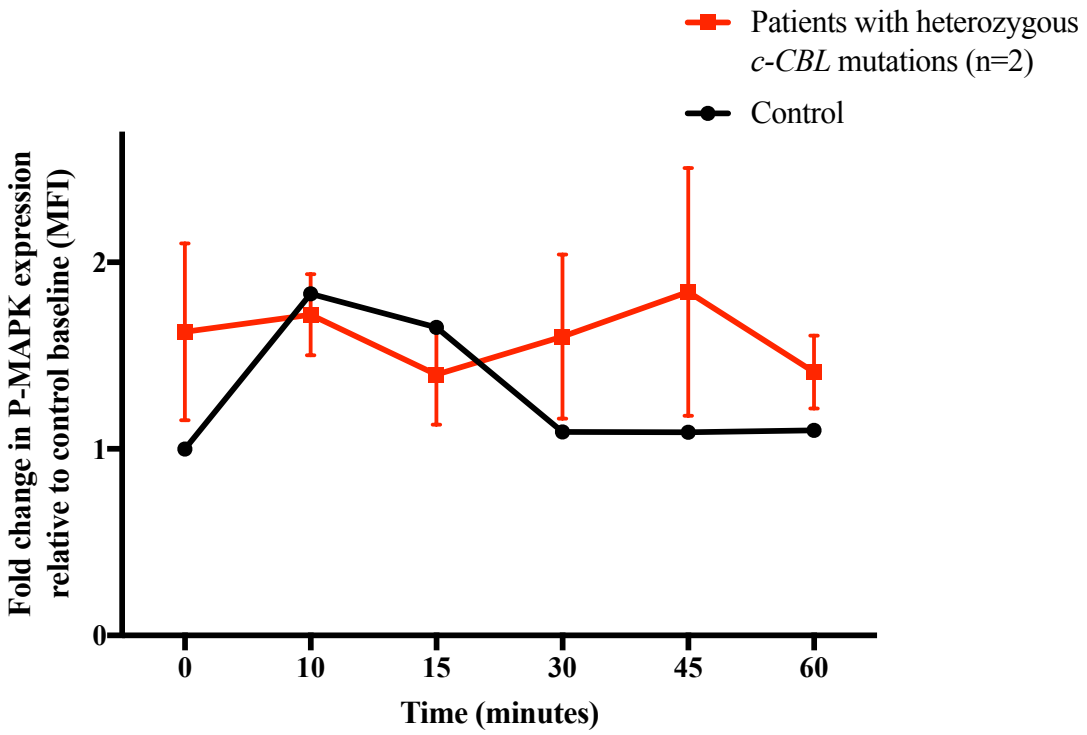

Figure 4-36 Fold change in relative phosphorylated-MAPK expression in B-II-3, C-III-1 and control HDFCs.

HDFCs were stimulated with 20 ng/ml PDGF for the indicated periods of time, permeabilised, and stained. Cells were analysed using FACS for Phosphorylated-MAPK expression. Data are expressed as relative fold change compared to the mean control baseline at 0 minutes and plotted, where possible, as mean of triplicate samples with one standard error of mean indicated.

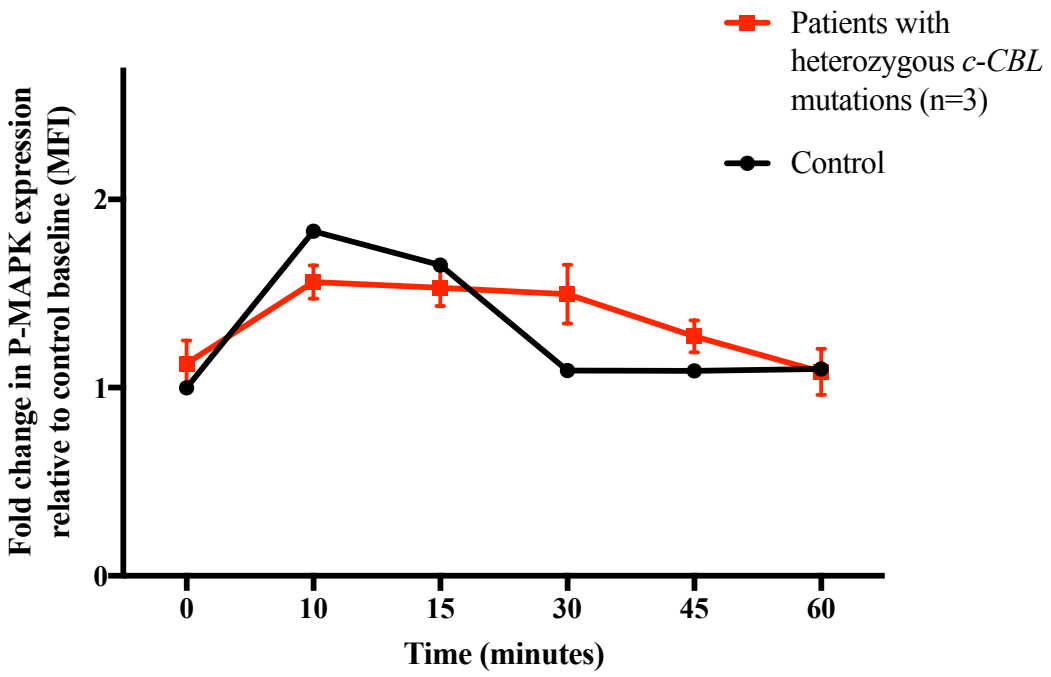

Figure 4-37 Phosphorylated-MAPK expression in B-II-3, C-III-1, C-III-2 and control SMC-myofibroblasts.

SMC-myofibroblasts were stimulated with 20 ng/ml PDGF for the indicated periods of time, permeabilised, and stained. Cells were analysed using FACS for Phosphorylated-MAPK expression. Data are expressed as relative fold change compared to the mean control baseline at 0 minutes and plotted, where possible, as mean of triplicate samples with one standard error of mean indicated.

4.21 Discussion

I have identified two different germline heterozygous mutations in *c-CBL* in different patients presenting with an early-onset moyamoya-like arteriopathy in line with some other recently published cases (Seaby et al., 2017, Guey et al., 2017a). I have advanced the field in two ways. Firstly, one of the mutations I have found is a novel deletion and has yet to be reported in relation to this disease. Secondly, my work has for the first time provided insight into how c-CBL could mechanistically cause a moyamoya-like vasculopathy. My findings may have wider implications for the understanding of the disease mechanisms implicated in moyamoya arteriopathy.

I found a de novo mutation in B-II-3: a non-frameshift deletion in *c-CBL*. The deletion resulted in the loss of p.370_371, which incorporated the functionally

sensitive Y371 residue (Niemeyer et al., 2010, Perez et al., 2010). In addition to the oncogenic properties conferred by Y371, other alterations to this residue result in various structural abnormalities to the TKB domain and consequently affect substrate interactions (Perez et al., 2010, Kassenbrock and Anderson, 2004, Swaminathan and Tsygankov, 2006). For example, Y371F mutants lose their E3 ligase activity and Y371E mutants possess constitutive E3 activity independent of tyrosine phosphorylation (Perez et al., 2010, Kassenbrock and Anderson, 2004, Swaminathan and Tsygankov, 2006). The literature all points to the fact that the linker region is essential to the E3 ligase activity of c-CBL (Schmidt and Dikic, 2005). Therefore I surmised that deletion of the Y371 residue was likely to be deleterious. I also discovered a family with three affected members (C-II-2, C-III-1 and C-III-2) all harbouring a previously documented splice site mutation: NM_005188:c.1228-2A>G (Guey et al., 2017a, Niemeyer et al., 2010). This mutation is known to excise a portion of exon 9 that encodes part of the RING finger domain. Like B-II-3, the *c-CBL* mutations in family C affect the E3 ubiquitin ligase activity of c-CBL.

Here, I show that using patient PBMCs and a siRNA transfected primary cell line mutant c-CBL protein has inhibited E3 ubiquitin ligase activity. This affects its ability to down regulate RTKs, such as EGFR and PDGR, thus enhancing downstream pathways like the Ras-Raf-MAPK pathway. As moyamoya arteriopathy is an occlusive vascular disease, the occlusions observed in the cerebral and renal vessels could be due to increased cellular proliferation caused by this aberrant RTK signaling. In line with previous studies, I also found evidence to suggest that mutant c-CBL function abrogates downregulation of active PLCγ1 subsequently increasing angiogenesis. Ubiquitination of PLCγ1 by c-CBL serves as an inhibitory mechanism to VEGFR-2 induced angiogenesis (Singh et al., 2007). This is relevant to the development of the basal collateral network, which characterises the moyamoya arteriopathy phenotype. Finally, in some preliminary experiments, I was also able to show evidence of aberrant upregulation of the Ras-Raf-MAPK signaling pathway in SMC-myofibroblasts derived from patient HDFCs. Proliferation of intimal SMCs are a characteristic feature of the steno-occlusive arteries observed in MMD patients (Fukui et al., 2000) Sustained upregulation of this pathway due to the reduced E3 ubiquitin ligase activity of c-CBL could thus provide a significant link between the observed phenotype and a potential pathogenic mechanism in patients with a

moyamoya-like arteriopathy. The Ras-Raf-MAPK signaling pathway was originally identified as a growth-promoting pathway key in cell growth and proliferation (Katz et al., 2007). Upregulation of this pathway due to overexpression or aberrant activity of RTKs, such as EGFR, has an established association with uncontrolled proliferation (De Luca et al., 2012). Normally associated with various forms of cancer, mutations in these RTKs have various effects ranging from the activation of intrinsic tyrosine kinase catalytic domains to altering substrate specificity (Katz et al., 2007). However, in this study I am proposing that a defect in the negative-feedback mechanism, rather than a mutated RTK, causes uncontrolled cell proliferation. Abnormal E3 ubiquitin ligase activity has been previously linked to cancer development through deregulation of crucial cellular processes, such as cell cycle progression and cell proliferation (Sun, 2006, Ciechanover and Iwai, 2004). I believe that a similar mechanism is responsible for the excessive cell proliferation and resulting vascular occlusion seen in moyamoya arteriopathy with the difference being that cancer development is a multistep process requiring the accumulation of a number of mutations as opposed to the presence of a singular mutation (Vogelstein and Kinzler, 1993). I propose that the presence of a heterozygous mutation is enough to cause a deregulation in cell proliferation via the Ras-Raf-MAPK pathway but not enough to result in the development of any malignancy. Interestingly, homozygous mutations in *c-CBL* have been linked to JMML (Niemeyer et al., 2010, Loh et al., 2009) and although heterozygous mutations have been observed in some patients, the crucial target tissues (i.e. haematopoietic cells) demonstrate loss of this heterozygosity. This would indicate that a homozygous state or a 'two hit' process, in line with the Knudson hypothesis, is necessary for oncogenicity (Knudson, 1971). To support this theory is the fact that none of the patients recruited to my study have developed JMML to date. Several heterozygous *c-CBL* mutations have also been identified in association with Noonan-syndrome like disorder (NS) (Martinelli et al., 2010, Perez et al., 2010). In NS the mutations primarily affect residues located in the RING finger domain and are also hypothesized to dysregulate RTK metabolism and the Ras-Raf-MAPK pathway (Martinelli et al., 2010). None of the affected individuals from families B and C displayed any features consistent with this disorder, which would suggest *c-CBL* mutations could have a wide range of phenotypic consequences with the specific affected residue having a profound effect on the clinical condition observed. Interestingly, D-II-6 had the same mutation as one of the

probands described by Martinelli et al. (2010). Although the proband had some features suggestive of NS they were not given a definitive diagnosis, as they did not fulfill all the diagnostic criteria (Martinelli et al., 2010). Like this proband, D-II-6 also displayed some features similar to those characterising NS such as developmental delay. This would add further weight to the idea that there is a large degree of clinical variability in the disorders associated with *c-CBL* mutations with moyamoya arteriopathy being another phenotype to add to this ever-growing list.

Although my data provides preliminary evidence as to how *c-CBL* could be a causative gene for MMD, there were several limitations to my work. Firstly, a couple of the experiments did not approach significance: the expression level of EGFR in PBMCs and the expression level of P-MAPK in the HDFC and SMC-myofibroblast assays. Regarding the PBMCs, I was unable to obtain any PBMCs for any affected individuals in family C during my PhD, but repeat experiments exploring the EGFR and MAPK pathways in these additional patients are now planned. There appeared to be a tendency towards a significant difference in regulation of EGFR between patient and control cells when all the time points were considered together (Figure 4-27). Repeating the assay in additional patients could cause this difference to become significant for the whole time course as well as for all individual time points. Regarding the HDFC/SMC-myofibroblast assays, these experiments were preliminary and need to be repeated. There appeared to be a difference between control and patient samples, which I would assume would become significant once repeats were carried out. Secondly, downregulation may have been easier to assess via immunoprecipitation and then western blotting. However, as expression of EGFR in PBMCs was very low and difficult to detect I chose to analyse the expression level using FACS. The other alternative would be to transfect a relevant cell line to mimic the heterozygous state observed in the patients. In this instance, creating a stable transfection line harbouring the exact mutation I wished to imitate would be fairly difficult I decided to study the patient cells themselves. This has the obvious caveat that I could only look at populations that were easily accessible i.e. PBMCs and HDFCs.

My data suggest that clinicians should consider *c-CBL* screening in patients with early-onset moyamoya arteriopathy even in the absence of obvious developmental

abnormalities, or malignant haematological manifestations suggestive of a RASopathy. Importantly, similarities were observed in the clinical presentation of these cases. All these patients had a very-early-onset moyamoya arteriopathy, with silent infarcts observable on initial imaging, suggesting an even earlier onset of the disease. The radiological appearances are typical of moyamoya with extensive collateral formation present. This is in contrast with other moyamoya-like syndromes without collateral formation such as the ACTA2 related arteriopathies. Three of the cohort presented with acute infarction, which was associated with thalamic, capsular and intraventricular haemorrhage. The initial course of the disease was very severe with a widespread arteriopathy requiring revascularization.

The identification of these heterozygous mutations in *c-CBL*, a major RAS pathway gene, strongly reinforces the involvement of this pathway in moyamoya pathophysiology. NF1 and NS are classical causes of moyamoya, which are both caused by mutated proteins involved in the RAS pathway (Ganesan and Kirkham, 1997, Vargiami et al., 2014). In addition, moyamoya has recently been reported in two patients presenting with a Noonan-like syndrome related to heterozygous mutations in the *SHOC2* gene, which also belongs to the RAS pathway (Choi et al., 2015, Lo et al., 2015). Altogether, these data lead me to consider the RAS pathway as a key pathway in the moyamoya pathophysiology and the experiments presented here add weight to this theory. The identification of a pathogenic *c-CBL* mutation in this context also raises questions regarding the haematological follow-up to be proposed for such patients given the absence of haematological malignancy to date.

4.22 Conclusion

In summary I have identified various different *c-CBL* germline mutations in several patients diagnosed with a cerebrovascular disease similar to a moyamoya arteriopathy. I have also started to delineate the mechanism behind how these mutations could contribute to the observed phenotype. My findings have the following implications:

1. The occlusive vasculopathic phenotype of MMD may be the result of aberrant RTK signaling due to reduced E3 ubiquitin ligase activity of c-CBL and this

provides interesting clues for the underlying pathophysiology of the disease in addition to possible therapeutic targets.

2. Children with arterial ischaemic stroke and vasculopathy should be screened for mutations in *c-CBL* particularly those with early onset MMD even in the absence of obvious developmental abnormalities, or malignant haematological manifestations suggestive of a RASopathy.

Chapter 5 Systemic and cerebral vasculopathy associated with heterozygous mutations in *RNF213*

5.1 Summary

The *RNF213* gene is a known susceptibility gene for moyamoya disease. In this chapter, I investigated 3 families with a vascular phenotype and employed whole exome sequencing and a targeted gene panel to identify several previously reported and one novel missense heterozygous mutations in *RNF213*. The proband from the first family displayed symptoms typically found in patients with a moyamoya arteriopathy and so this data adds to the body of evidence supporting the hypothesis that *RNF213* is associated with MMD. The other two probands appeared to display a phenotype similar to that of a large vessel vasculitis resembling Takayasu arteritis (TA). Therefore, my data would expand the phenotype associated with *RNF213* and would suggest that *RNF213* could also contribute to some large vessel diseases.

5.2 Introduction

This chapter focuses on patients identified through international collaborations via vasculitis research networks (international collaborations with Professor Ozen (Ankara, Turkey); Professor Dolezalova (Prague, the Czech Republic); and Dr Kamphuis (Amsterdam, Netherlands). All patients had an early onset unclassified vasculopathy.

5.3 Family tree for family E

Index case of family E was a Czech male from non-consanguineous parents, referred to as E-III-2 from now on (Figure 5-1).

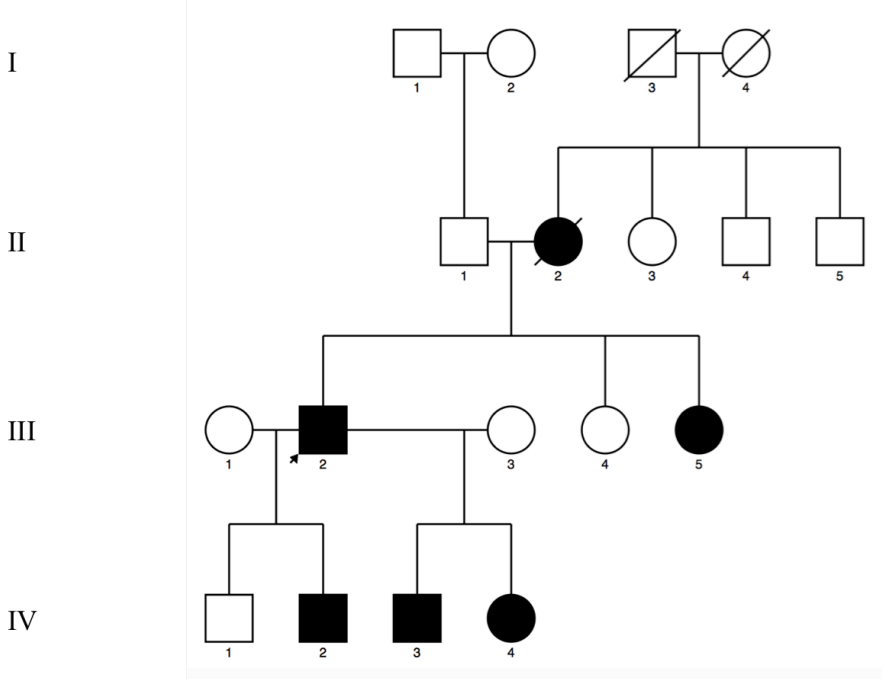

Figure 5-1 Family tree for family E

5.4 E-III-2 clinical presentation

Initial presentation for E-III-2 was at the age of 40 years old with arterial ischaemic stroke and bilateral knee effusions. Digital subtraction angiography showed bilateral occlusion of the ICA with multiple collaterals. One month after this first relatively mild stroke he had a second stroke. This time he was also found to have systemic arterial hypertension of unknown aetiology. He subsequently recovered in terms of neurological findings but still suffered with recurrent headaches. Of note he reported no fevers or other systemic symptoms and had normal renal function

E-IV-3 presented at the age of 9 years with a right shoulder girdle myoclonus and focal dystonia of his right hand. MRA showed multiple stenotic lesions of the ICA, ACA and MCA bilaterally with collaterals between the posterior and anterior

circulation. He subsequently had a second short lasting episode of one-sided myoclonus triggered by stress or exertion. His last brain MRA scan showed stable appearances. He however developed significant systemic arterial hypertension requiring multiple anti hypertensive agents. E-IV-4 presented at age 2.5 with her first arterial ischaemic stroke and right-sided hemiparesis. Her MRA showed multiple stenoses of the ICA and MCA and ACA bilaterally with collaterals. She had two subsequent strokes: one a month later and one a year after initial presentation but this time it was left-sided. Brain MRA showed progression of the arteriopathy with further stenosis of the ACA and MCA. She then had an EC-IC revascularisation procedure. She also developed systemic hypertension requiring several antihypertensive medicines. She was treated with corticosteroids, methotrexate and LMWH, aspirin and antihypertensives.

Relevant family history included a maternal grandmother who died at the age of 37 (E-I-4) from stroke and a sister (E-III-5) who presented at age 13 with stroke-like episodes.

5.5 Family tree for family F

Index case of family F was a Turkish female from consanguineous parents, referred to as F-II-1 from now on (Figure 5-2)

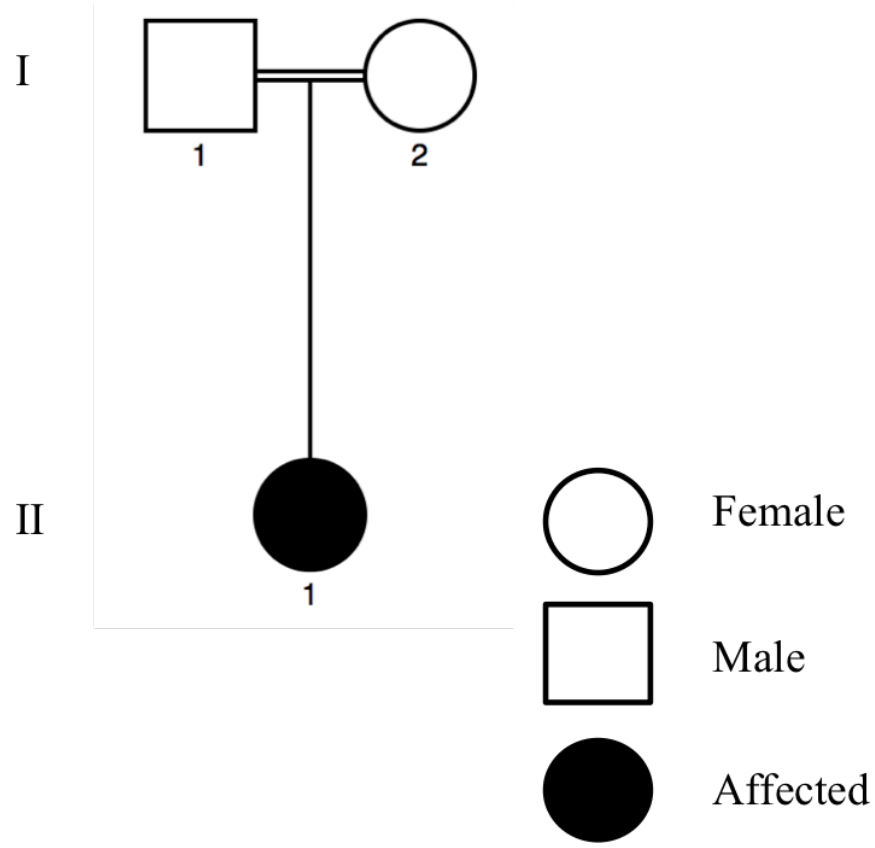

Figure 5-2 Family tree for family F.

5.6 F-II-1 clinical presentation

Initial presentation of F-II-1 was at the age of 4 years when she presented with arterial hypertension and four limb BP discrepancy. To establish whether the arterial hypertension was secondary to a vasculopathy she had a CT-angio, which showed severe stenotic lesions of the thoracic and abdominal aortas brachio-cephalic artery, bilateral carotid arteries and renal artery. She was thought to have a large vessel vasculitis, TA-like, and was treated with oral steroids and methotrexate. Her hypertension remains well controlled at her latest follow up. Annual MR-angiography however showed persistent narrowing at multiple sites of the aorta, with no obvious target for revascularisation.

5.7 Family tree for family G

Index case of family G was a Dutch female from non-consanguineous parents, referred to as G-II-1 from now on (Figure 5-3).

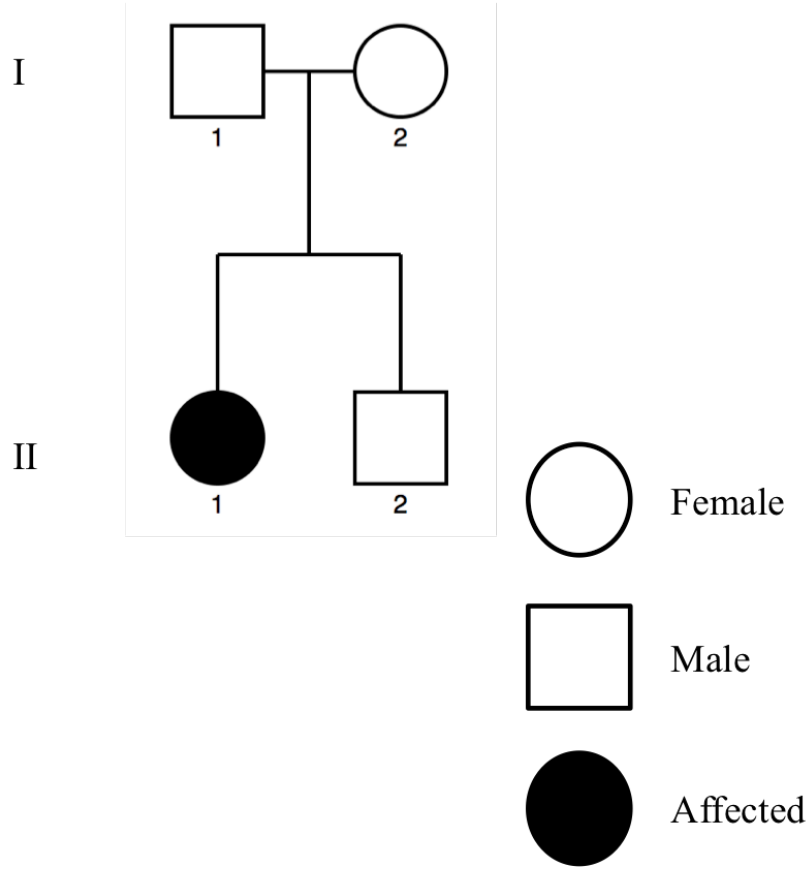

Figure 5-3 Family tree for family G.

5.8 G-II-1 clinical presentation

G-II-1 initially presented with persistent pyrexia, arterial hypertension, raised ESR and CRP, anaemia and elevated platelet count (ranging from 650-800 x 10*9/l; normal range 150-450 x 10*9/l). Renal function was impaired with creatinine ranging between 40 micromol/l and 60 micromol/l), and proteinuria (raised urine:albumin creatinine ratio of 400 micromol/L; normal range < 10 micromol/L). Renal biopsy was normal.

Catheter angiography demonstrated a widespread vascular disease affecting the cerebral vasculature, intestinal and renal arteries. A PET-CT scan showed no avid uptake. She was considered to have an early onset large vessel vasculopathy, TA-like. She was therefore started on corticosteroids and methotrexate treatment. Several antihypertensives were also required to control her hypertension including captopril, amlodipine, labetalol, clonidine and a thiazide diuretic.

5.9 Identifying a causal allele: Whole Exome Sequencing

5.9.1 E-III-2

A targeted approach of sequencing genes known to cause vasculopathy was applied in the case of E-III-2. DNA was isolated and sequenced using the "Vasculitis and Inflammation Panel" (VIP): a targeted gene panel (Omoyinmi et al., 2017). This panel restricts the list of genes for analysis to ones that have been implicated in vasculitic and vasculopathic phenotypes and is updated periodically as new genes are discovered. The version used for E-III-2 was VIP2 and the list of genes included on the panel can be found in Appendix 2. A causative mutation in *RNF213* was identified and confirmed using Sanger sequencing: p.D4013N (Figure 5-4). It was identified in the proband as well as in E-IV-3 and E-IV-4.

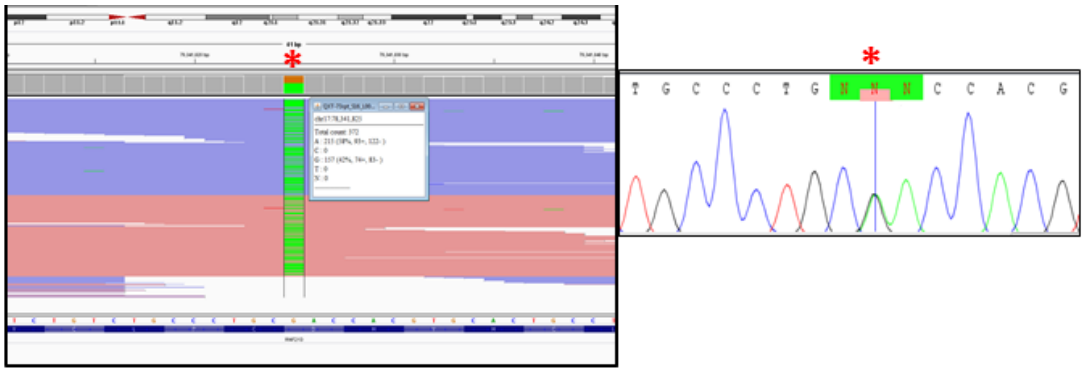

Figure 5-4 Mutation in RNF213 identified by VIP targeted gene panel and confirmed by Sanger sequencing. *Adapted from reference (Omoyinmi et al., 2017)*

5.9.2 F-II-1

WES was performed on F-II-1 (see General methods and materials 2.16). Before the filters were applied the WES output was initially compared to the candidate gene list (Table 2-7). Variants were found in four candidate genes: *COL5A1, NOTCH1, RNF213* and *SKI*. These were investigated further.

5.9.2.1 Verification of candidate gene variants

The candidate genes were verified using Sanger sequencing. The primers used are listed in Table 5-1. The variants in *COL5A1, NOTCH1,* and *SKI* were found to be false positives; however, the variant in *RNF213* was confirmed to be a novel heterozygous missense mutation NM_001256071:c.15007C>G (p.L5003V). Predicted to be deleterious by the SIFT, MutationTaster and PolyPhen-2 programs, the non-synonymous substitution results in an amino acid change from leucine to valine (p. L5003V).

Table 5-1 Primer sequences used for Sanger sequencing

Primer name	Primer sequence
COL5A1 exon 46 F	TGTCTCTGTCTTGTTCCCCG
COL5A1 exon 46 R	CTTCCAGTTGGAATGAGGAG
NOTCH1 exon 18 F	CGTAGCCATCGATCTTGTCC
NOTCH1 exon 18 R	TCAGCCCCAATCCTGAGTAG
RNF213 exon 65 F	GCCCAAGTGTCAGCTGTTAG
RNF213 exon 65 R	TCTACTGTCCCTGGTGTGTCC
SKI exon 6 F	GTCTGAAAAGCCTTTGTGGG
SKI exon 6 R	ACCTGCTAGGACACAGGCTC

F-II-1

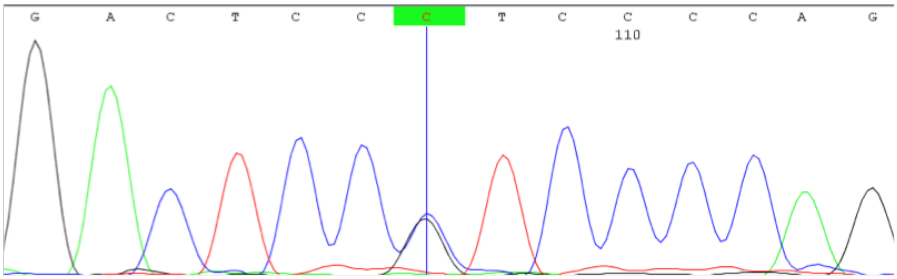

Figure 5-5 Sanger sequencing chromatogram of RNF213 for the proband (F-II-1).

Aligned to reference sequence exon 65 of RNF213 (NM_001256071). Blue line indicates a heterozygous non-synonymous missense substitution present in the proband (c.15007C>G:p.L5003V).

5.9.3 G-II-1

WES was performed on G-II-1 (see General methods and materials section 2.16). Before the filters were applied the WES output was initially compared to the candidate gene list (Table 2-7). Two heterozygous missense variants were found in *RNF213*: NM_001256071:c.516C>T(p.P1721L) and NM_001256071:c.1419A>G(p.K4732E).

5.10 Discussion

The *RNF213* gene encodes the ubiquitously expressed ring finger protein 213 (RNF213) whose exact function is as yet unknown but is thought to possess ATPase and ubiquitin ligase activity (Kamada et al., 2011, Liu et al., 2011). RNF213 has a C3HC4-type RING finger domain, which is a specialised zinc finger domain that can bind two zinc atoms and is thought to play a role in protein-protein interactions. It also has an AAA domain that is responsible for ATP binding and hydrolysis (Lupas and Martin, 2002). In general, proteins with these domains are involved in mechanical cell processes such as molecule transportation, DNA unwinding and protein folding.

RNF213 is known as a susceptibility gene for MMD (Kamada et al., 2011, Liu et al., 2011). Two founder mutations were originally recognized in association with MMD (p.R4810K and p.R4859K) in Japanese/East Asian populations (Kamada et al., 2011, Liu et al., 2011) which were swiftly followed by the identification of multiple other

mutations in various different populations (Cecchi et al., 2014, Guey et al., 2017b, Kobayashi et al., 2016, Miyatake et al., 2012a). Although numerous mutations have been discovered in connection with MMD, the mechanism behind disease development has yet to be elucidated. Mutations do not seem to affect ubiquitin ligase activity or protein expression and it is not even clear whether mutations have haploinsufficient, dominant negative or gain-of-function mechanistic effects (Liu et al., 2011). To attempt to delineate the physiological role of *RNF213 in vivo* the gene was knocked down in zebrafish, which caused abnormal vessel sprouting in the head region indicative of a role in intracranial angiogenesis (Liu et al., 2011). Given the fact that the animal model demonstrated a convincing angiogenic role for *RNF213* whilst the functional consequences of any *RNF213* mutations are yet to be determined, it may be that environmental factors, such as infection or autoimmune conditions, are necessary, in combination with a genetic predisposition, for MMD pathogenesis (Ogawa et al., 2003, Czartoski et al., 2005, Tanigawara et al., 1997, Ueno et al., 2002). In fact, *RNF213* has been found to be upregrulated by inflammatory interferon signaling with a concomitant reduction in angiogenesis (Kobayashi et al., 2015, Ohkubo et al., 2015). More specifically, the p.R4810K *RNF213* mutation allows antiangiogenic signaling in the presence of environmental stimuli such as hypoxia and interferon exposure whereas wild-type *RNF213* can only inhibit angiogenesis in the interferon-signaling pathway (Kobayashi et al., 2015). More recent data has suggested that *RNF213* has cell-cycle dependent and independent effects, which could contribute to the MMD phenotype. This data has found, firstly, that RNF213 promotes endothelial cell proliferation by positively regulating PI3K-AKT activity. Therefore loss-of-function mutations in *RNF213* may induce angiopathy by causing persistently low PI3K-AKT activity (Ohkubo et al., 2015). Secondly, it discovered that matrix metalloproteinases (MMPs) were significantly up regulated in the absence of *RNF213* compounding the poor angiogenic response of siRNA *RNF213* transfected endothelial cells (Ohkubo et al., 2015). This evidence has led to the hypothesis that MMD patients might produce higher quantities of MMPs which at excessive levels are known to have deleterious consequences on vascular structure maintenance (Kovacic et al., 2012). In keeping with this idea *RNF213* is also thought to play a part in vascular construction due to reported associations with systolic blood pressure, intracranial aneurysms and coronary artery disease (Zhou et al., 2016, Akagawa et al., 2018). However,

regardless of these recent discoveries any functional link between the *RNF213* mutations documented and MMD has still not been found. For example although the p.R4810K *RNF213* mutation can lead to reduced angiogenesis it is not known how this pathological process is related to the crucial hallmark of MMD: abnormal SMC proliferation.

This current case series has looked at three families in which different *RNF213* variants were discovered. The proband from the first family (E-III-2) harboured a missense mutation that has previously been reported in association with MMD (Cecchi et al., 2014, Liu et al., 2011). Like the previously reported cases, E-III-2 also has a cerebral vasculopathy with vessel occlusion and collateral formation. This case therefore increases the body of evidence linking *RNF213* to MMD. The proband from the second family (F-II-1) was found to have a novel missense mutation NM_001256071:c.15007C>G(p.L5003V). The mutation was not listed in the Exome Aggregation Consortium (http://exac.broadinstitute.org/) version 0.3.1 or the Human Genetic Variation Database (http://www.hgvd.genome.med.kyoto-u.ac.jp/) (Lek et al., 2016, Higasa et al., 2016) and was predicted to be deleterious. As the 3D structure of *RNF213* has yet to be resolved, it is not known how this mutation could structurally affect the protein. According to the InterPro database (http://www.ebi.ac.uk/interpro/) this residue (p.L5003V) falls outside the known domains of *RNF213* (Figure 5-6). Unlike E-III-2, F-II-1 has no cerebral involvement instead her phenotype resembles that of TA, a large vessel vasculitis affecting the aorta. This finding therefore expands the phenotype associated with heterozygous mutations in *RNF213* to include a large vessel vasculitis. Other vascular diseases that have been linked with *RNF213* mutations so far include premature CAD, stroke, subarachnoid haemorrhage, aortic coarctation and thoracic aortic aneurysm (TAA) (Cecchi et al., 2014). The last proband (G-II-1) had two heterozygous missense variants in *RNF213*: NM_001256071:c.5162C>T (p.P1721L) and NM_001256071:c.14194A>G (p.K4732E). The p.P1721L mutation has previously been reported in a Caucasian MMD cohort and is predicted to be damaging by PolyPhen2 and PROVEAN (Guey et al., 2017b). The p.K4732E variant on the other hand is predicted to be benign by PolyPhen2, SIFT and MutationTaster. This case provides additional evidence to the potential causality of an *RNF213* mutation in the pathogenesis of an early onset large vessel vasculopathy, TA-like.

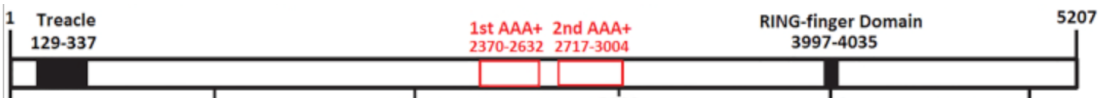

Figure 5-6 The domain structure of RNF213. *Adapted from reference (Zhou et al., 2016).*

My findings have potential implications for screening of *RNF213* in patients suspected with large vessel vasculitis such as TA particularly in cases where the disease starts early in life or there are familial cases. My findings also provide supporting evidence to the fact that *RNF213* plays a significant role in vessel development irrespective of the size of vessel affected.

5.11 Conclusion

In summary, I have identified various different *RNF213* germline mutations in several patients diagnosed with different vascular diseases; one similar to a moyamoya arteriopathy and the others indicative of a large vessel vasculitis. My findings have the following implications:

1. Children with moyamoya arteriopathy and mutations in *RNF213* and/or particularly those with early onset moyamoya arteriopathy should have broad vascular imaging to look for other vascular bed involvement.
2. For children with suspected large vessel vasculitis and vasculopathy with onset early in life and/or if there are familial cases, screening for mutations in *RNF213* should be considered.

Chapter 6 General discussion

This study was initiated to identify novel genetic causes of cerebral and systemic vasculopathies. As outlined in the preceding chapters the results of this study have been:

- The expansion of the phenotype associated with heterozygous mutations in *MYH11* to include moyamoya-like cerebrovascular disease.
- The identification of a novel heterozygous mutation in *c-CBL* in a patient with a moyamoya-like arteriopathy.
- The proposal of a likely and relevant pathogenic mechanism for MMD involving the RAS pathway.
- The expansion of the phenotype associated with heterozygous mutations in *RNF213* to include a systemic large vessel vasculopathy.

MMD is an occlusive cerebrovascular disease with an elusive pathogenic mechanism. Genetic factors appear to play an important role as approximately 10% of MMD cases are familial whilst an additional number of cases are associated with other genetic diseases such as neurofibromatosis 1, Down syndrome and Noonan syndrome (Bang et al., 2016). Currently, *RNF213* is known to be a susceptibility gene whilst *ACTA2* is a recognised cause of familial MMD (Guo et al., 2009, Kamada et al., 2011). Environmental factors such as autoimmune diseases or inflammation are also thought to play a role in the aetiopathogenesis of this condition (Panegyres et al., 1993, Phi et al., 2015, Tanigawara et al., 1997, Yamada et al., 1997). Identification of two genes for a familial moyamoya-like arteriopathy is a significant step forward in this field. My data provide support for the idea that MMD is a proliferative disease of endothelial and smooth muscle cells as well as identify exciting avenues of future research into the exact mechanisms behind disease pathogenesis. From what I have found it appears that a dysregulation in the Ras-Raf-MAPK signaling pathway with a concomitant upregulation in angiogenesis could neatly explain the MMD phenotype of steno-occlusive vessels and collateral formation.

This study has also demonstrated several interesting points about the genetics surrounding vasculopathies. Firstly, it provides clear evidence that, with regards to

certain systemic and cerebral vasculopathies, there appears to be a spectrum in the phenotypic characteristics displayed by affected individuals. *MYH11* is known to cause familial thoracic aortic aneurysm (Zhu et al., 2006) but also results in a cerebral vasculopathy whilst *RNF213* is a recognised susceptibility gene for MMD (Kamada et al., 2011) but could also cause a large vessel vasculitis. It is entirely feasible that the genes have differential consequences depending on the vessel size. Previous studies support the idea that vascular-disease genes can present as vascular occlusion or enlargement as well as affecting different arteries within the same disease (Guo et al., 2009, Friedman et al., 2002). Secondly, there are still undiscovered genetic causes of vasculopathy and vasculitis out there. Although these disorders are rare, the burden of disease is high and any insights into their pathogenesis and/or aetiology could significantly aid treatment and thus improve the overall care and welfare of patients. Identification of new genes and how they cause disease ultimately informs clinical practice, aids diagnosis of diseases and highlights pathways for potential drug development. However, as a scientist I do realize this is easier said than done, as highlighting a potential therapeutic pathway is a far cry from identifying how this can be translated into viable and accepted medical treatment. Lastly, sequencing of early-onset cases, be they sporadic or not, is a valid and fruitful method of discovering new genetic causes of vasculopathy. However what method of sequencing is best? As stated previously, these diseases are rare affecting less than 1 in 10,000 people so is the cost-benefit of WES or WGS and the accompanying data analysis practical? An efficient alternative to WES/WGS could be the vasculitis and inflammation panel developed by Omoyinmi et al. (2017), the design of which I contributed to from work contained in this thesis. My discoveries would suggest that a targeted panel like this one is an extremely powerful and valuable tool in routine clinical care and research, in identifying new diseases associated with known candidate genes and expanding the phenotypes of established gene-disease associations. The ability to quickly and easily identify variants from a list of mechanistically and aetiologically relevant genes is extremely important in expediting the sequencing process in clinical care, and also in research.

6.1 Future work

This study has generated exciting data but due to the time frame there were several avenues left unexplored.

I identified a new phenotype linked to *MYH11* but was unable to perform any functional work due to lack of time and availability of relevant patient cells. Ideally I would have liked to simultaneously study the effect of the mutation I discovered *in vitro* and *in vivo*. It would be useful to initially look at two cell populations relevant to the MMD phenotype: SMCs and myofibroblasts. I would then assess cell proliferation and migration in them. For the myofibroblasts I would transform A-III-3 HDFCs using TGFβ1 as I did for families B and C. For the SMCs, as it is highly unlikely I would be able to explant SMCs from A-III-3, I would need to create a cell line. As the mutation is a heterozygous substitution rather than a deletion a knockout gene approach is not appropriate. Instead using the CRISPR Nickase system, which allows precise editing of site-specific bases, I would suggest creating a SMC line with the mutation found in A-III-3. It would also be interesting to study the mutation's effect in an animal model. The CRISPR Nickase system has been demonstrated as an efficient and powerful gene-editing tool in animal models (Shen et al., 2014, Zhang et al., 2017) whilst mouse and zebrafish models have previously been used to study MMD (Sonobe et al., 2014, Liu et al., 2011). Creating a model using the CRISPR Nickase system would help to delineate the pathogenic mechanism regarding *MYH11* and a moyamoya-like arteriopathy.

Regarding the c-CBL story, I would like to repeat the PBMC assays I did in B-II-3 in the three affected members of family C. This should provide a clear statistically significant difference in the expression levels of EGFR and P-MAPK across the whole time course. The myofibroblast experiments were only preliminary so I would like to expand this body of work. Firstly, I would repeat the myofibroblast assays in all patients to assess P-MAPK expression as well as the effect on PDGFR degradation. This would increase the power and hopefully result in a statistically significant difference. Secondly, I would assess the proliferation and migration characteristics of the cells. I would expect there to be a higher rate of proliferation in the patient myofibroblasts compared to control myofibroblasts. Thirdly, I would like

to look at the effect of the mutant c-CBL on ubiquitination of PDGFR and EGFR. I have carried out a similar assay in B-II-3 PBMCs but I would like to repeat it in this cell line for all the affected individuals from families B and C. I was able to look at the effect of siRNA transfected HUVECs on tubule formation but it would be interesting to create an animal model to observe the effects of the mutated c-CBL protein on vascular development *in vivo*.

6.2 Publications

1. Keylock, A., Hong, Y., Saunders, D., Omoyinmi, E., Mulhern, C., Roebuck, D., Brogan, P., Ganesan, V. & Eleftheriou, D. 2018. Moyamoya-like cerebrovascular disease in a child with a novel mutation in myosin heavy chain 11. *Neurology,* 90**,** 136-138.

   Images from this paper were chosen to be on the cover of the February 2018 issue of the Neurology journal.

2. Omoyinmi, E., Standing, A., Keylock, A., Price-Kuehne, F., Melo Gomes, S., Rowczenio, D., Nanthapisal, S., Cullup, T., Nyanhete, R., Ashton, E., Murphy, C., Clarke, M., Ahlfors, H., Jenkins, L., Gilmour, K., Eleftheriou, D., Lachmann, H. J., Hawkins, P. N., Klein, N. & Brogan, P. A. 2017. Clinical impact of a targeted next-generation sequencing gene panel for autoinflammation and vasculitis. *PLoS One,* 12**,** e0181874.

References

Akagawa, H., Mukawa, M., Nariai, T., Nomura, S., Aihara, Y., Onda, H., Yoneyama, T., Kudo, T., Sumita, K., Maehara, T., Kawamata, T. & Kasuya, H. 2018. Novel and recurrent RNF213 variants in Japanese pediatric patients with moyamoya disease. *Hum Genome Var,* 5**,** 17060.

Alroy, I. & Yarden, Y. 1997. The ErbB signaling network in embryogenesis and oncogenesis: signal diversification through combinatorial ligand-receptor interactions. *FEBS Lett,* 410**,** 83-6.

Amlie-Lefond, C., Bernard, T. J., Sebire, G., Friedman, N. R., Heyer, G. L., Lerner, N. B., Deveber, G., Fullerton, H. J. & International Pediatric Stroke Study, G. 2009. Predictors of cerebral arteriopathy in children with arterial ischemic stroke: results of the International Pediatric Stroke Study. *Circulation,* 119**,** 1417-23.

Andoniou, C. E., Thien, C. B. & Langdon, W. Y. 1994. Tumour induction by activated abl involves tyrosine phosphorylation of the product of the cbl oncogene. *EMBO J,* 13**,** 4515-23.

Bang, O. Y., Fujimura, M. & Kim, S. K. 2016. The Pathophysiology of Moyamoya Disease: An Update. *J Stroke,* 18**,** 12-20.

Barbier, M., Gross, M. S., Aubart, M., Hanna, N., Kessler, K., Guo, D. C., Tosolini, L., Ho-Tin-Noe, B., Regalado, E., Varret, M., Abifadel, M., Milleron, O., Odent, S., Dupuis-Girod, S., Faivre, L., Edouard, T., Dulac, Y., Busa, T., Gouya, L., Milewicz, D. M., Jondeau, G. & Boileau, C. 2014. MFAP5 loss-of-function mutations underscore the involvement of matrix alteration in the pathogenesis of familial thoracic aortic aneurysms and dissections. *Am J Hum Genet,* 95**,** 736-43.

Batu, E. D., Karadag, O., Taskiran, E. Z., Kalyoncu, U., Aksentijevich, I., Alikasifoglu, M. & Ozen, S. 2015. A Case Series of Adenosine Deaminase 2-deficient Patients Emphasizing Treatment and Genotype-phenotype Correlations. *J Rheumatol,* 42**,** 1532-4.

Belostotsky, V. M., Shah, V. & Dillon, M. J. 2002. Clinical features in 17 paediatric patients with Wegener granulomatosis. *Pediatr Nephrol,* 17**,** 754-61.

Berlit, P. 1994. The spectrum of vasculopathies in the differential diagnosis of vasculitis. *Semin Neurol,* 14**,** 370-9.

Berndsen, C. E. & Wolberger, C. 2014. New insights into ubiquitin E3 ligase mechanism. *Nat Struct Mol Biol,* 21**,** 301-7.

Bersano, A., Baron, P., Lanfranconi, S., Trobia, N., Sterzi, R., Motto, C., Comi, G., Sessa, M., Martinelli-Boneschi, F., Micieli, G., Ferrarese, C., Santoro, P.,

Parati, E., Boncoraglio, G., Padovani, A., Pezzini, A., Candelise, L. & Lombardia, G. G. 2012. Lombardia GENS: a collaborative registry for monogenic diseases associated with stroke. *Funct Neurol,* 27**,** 107-17.

Birk, D. E., Fitch, J. M., Babiarz, J. P., Doane, K. J. & Linsenmayer, T. F. 1990. Collagen fibrillogenesis in vitro: interaction of types I and V collagen regulates fibril diameter. *J Cell Sci,* 95 (Pt 4)**,** 649-57.

Blankenberg, D., Von Kuster, G., Coraor, N., Ananda, G., Lazarus, R., Mangan, M., Nekrutenko, A. & Taylor, J. 2010. Galaxy: a web-based genome analysis tool for experimentalists. *Curr Protoc Mol Biol,* Chapter 19**,** Unit 19 10 1-21.

Boileau, C., Guo, D. C., Hanna, N., Regalado, E. S., Detaint, D., Gong, L., Varret, M., Prakash, S. K., Li, A. H., D'indy, H., Braverman, A. C., Grandchamp, B., Kwartler, C. S., Gouya, L., Santos-Cortez, R. L., Abifadel, M., Leal, S. M., Muti, C., Shendure, J., Gross, M. S., Rieder, M. J., Vahanian, A., Nickerson, D. A., Michel, J. B., National Heart, L., Blood Institute Go Exome Sequencing, P., Jondeau, G. & Milewicz, D. M. 2012. TGFB2 mutations cause familial thoracic aortic aneurysms and dissections associated with mild systemic features of Marfan syndrome. *Nat Genet,* 44**,** 916-21.

Bollag, G., Clapp, D. W., Shih, S., Adler, F., Zhang, Y. Y., Thompson, P., Lange, B. J., Freedman, M. H., Mccormick, F., Jacks, T. & Shannon, K. 1996. Loss of NF1 results in activation of the Ras signaling pathway and leads to aberrant growth in haematopoietic cells. *Nat Genet,* 12**,** 144-8.

Boyd, K. P., Korf, B. R. & Theos, A. 2009. Neurofibromatosis type 1. *J Am Acad Dermatol,* 61**,** 1-14; quiz 15-6.

Brogan, P. & Eleftheriou, D. 2017. Vasculitis update: pathogenesis and biomarkers. *Pediatr Nephrol*.

Brogan, P., Eleftheriou, D. & Dillon, M. 2010. Small vessel vasculitis. *Pediatr Nephrol,* 25**,** 1025-35.

Brogan, P. A., Shah, V., Klein, N. & Dillon, M. J. 2004. Vbeta-restricted T cell adherence to endothelial cells: a mechanism for superantigen-dependent vascular injury. *Arthritis Rheum,* 50**,** 589-97.

Brunner, J., Feldman, B. M., Tyrrell, P. N., Kuemmerle-Deschner, J. B., Zimmerhackl, L. B., Gassner, I. & Benseler, S. M. 2010. Takayasu arteritis in children and adolescents. *Rheumatology (Oxford),* 49**,** 1806-14.

Burgner, D., Davila, S., Breunis, W. B., Ng, S. B., Li, Y., Bonnard, C., Ling, L., Wright, V. J., Thalamuthu, A., Odam, M., Shimizu, C., Burns, J. C., Levin, M., Kuijpers, T. W., Hibberd, M. L. & International Kawasaki Disease Genetics, C. 2009. A genome-wide association study identifies novel and functionally related susceptibility Loci for Kawasaki disease. *PLoS Genet,* 5**,** e1000319.

Cabral, D. A., Canter, D. L., Muscal, E., Nanda, K., Wahezi, D. M., Spalding, S. J., Twilt, M., Benseler, S. M., Campillo, S., Charuvanij, S., Dancey, P., Eberhard, B. A., Elder, M. E., Hersh, A., Higgins, G. C., Huber, A. M., Khubchandani, R., Kim, S., Klein-Gitelman, M., Kostik, M. M., Lawson, E. F., Lee, T., Lubieniecka, J. M., Mccurdy, D., Moorthy, L. N., Morishita, K. A., Nielsen, S. M., O'neil, K. M., Reiff, A., Ristic, G., Robinson, A. B., Sarmiento, A., Shenoi, S., Toth, M. B., Van Mater, H. A., Wagner-Weiner, L., Weiss, J. E., White, A. J., Yeung, R. S. & Initiative, A. R. I. N. w. t. P. 2016. Comparing Presenting Clinical Features in 48 Children With Microscopic Polyangiitis to 183 Children Who Have Granulomatosis With Polyangiitis (Wegener's): An ARChiVe Cohort Study. *Arthritis Rheumatol,* 68**,** 2514-26.

Caligiuri, M. A., Briesewitz, R., Yu, J., Wang, L., Wei, M., Arnoczky, K. J., Marburger, T. B., Wen, J., Perrotti, D., Bloomfield, C. D. & Whitman, S. P. 2007. Novel c-CBL and CBL-b ubiquitin ligase mutations in human acute myeloid leukemia. *Blood,* 110**,** 1022-4.

Callewaert, B., Malfait, F., Loeys, B. & De Paepe, A. 2008. Ehlers-Danlos syndromes and Marfan syndrome. *Best Pract Res Clin Rheumatol,* 22**,** 165-89.

Caorsi, R., Penco, F., Grossi, A., Insalaco, A., Omenetti, A., Alessio, M., Conti, G., Marchetti, F., Picco, P., Tommasini, A., Martino, S., Malattia, C., Gallizi, R., Podda, R. A., Salis, A., Falcini, F., Schena, F., Garbarino, F., Morreale, A., Pardeo, M., Ventrici, C., Passarelli, C., Zhou, Q., Severino, M., Gandolfo, C., Damonte, G., Martini, A., Ravelli, A., Aksentijevich, I., Ceccherini, I. & Gattorno, M. 2017. ADA2 deficiency (DADA2) as an unrecognised cause of early onset polyarteritis nodosa and stroke: a multicentre national study. *Ann Rheum Dis,* 76**,** 1648-1656.

Carlomagno, F. & Chiariello, M. 2014. Growth factor transduction pathways: paradigm of anti-neoplastic targeted therapy. *J Mol Med (Berl),* 92**,** 723-33.

Carlson, J. A. & Chen, K. R. 2006. Cutaneous vasculitis update: small vessel neutrophilic vasculitis syndromes. *Am J Dermatopathol,* 28**,** 486-506.

Carlson, J. A. & Chen, K. R. 2007. Cutaneous vasculitis update: neutrophilic muscular vessel and eosinophilic, granulomatous, and lymphocytic vasculitis syndromes. *Am J Dermatopathol,* 29**,** 32-43.

Carmona, F. D., Martin, J. & Gonzalez-Gay, M. A. 2015. Genetics of vasculitis. *Curr Opin Rheumatol,* 27**,** 10-7.

Cecchi, A. C., Guo, D., Ren, Z., Flynn, K., Santos-Cortez, R. L., Leal, S. M., Wang, G. T., Regalado, E. S., Steinberg, G. K., Shendure, J., Bamshad, M. J., University of Washington Center for Mendelian, G., Grotta, J. C., Nickerson, D. A., Pannu, H. & Milewicz, D. M. 2014. RNF213 rare variants in an ethnically diverse population with Moyamoya disease. *Stroke,* 45**,** 3200-7.

Chang, L. Y., Chang, I. S., Lu, C. Y., Chiang, B. L., Lee, C. Y., Chen, P. J., Wang, J. T., Ho, H. N., Chen, D. S., Huang, L. M. & Kawasaki Disease Research, G.

2004. Epidemiologic features of Kawasaki disease in Taiwan, 1996-2002. *Pediatrics,* 114**,** e678-82.

Chatterjee, S., Flamm, S. D., Tan, C. D. & Rodriguez, E. R. 2014. Clinical diagnosis and management of large vessel vasculitis: Takayasu arteritis. *Curr Cardiol Rep,* 16**,** 499.

Chmelova, J., Kolar, Z., Prochazka, V., Curik, R., Dvorackova, J., Sirucek, P., Kraft, O. & Hrbac, T. 2010. Moyamoya disease is associated with endothelial activity detected by anti-nestin antibody. *Biomed Pap Med Fac Univ Palacky Olomouc Czech Repub,* 154**,** 159-62.

Cho, A., Graves, J. & Reidy, M. A. 2000. Mitogen-activated protein kinases mediate matrix metalloproteinase-9 expression in vascular smooth muscle cells. *Arterioscler Thromb Vasc Biol,* 20**,** 2527-32.

Choi, J. H., Oh, M. Y., Yum, M. S., Lee, B. H., Kim, G. H. & Yoo, H. W. 2015. Moyamoya syndrome in a patient with Noonan-like syndrome with loose anagen hair. *Pediatr Neurol,* 52**,** 352-5.

Ciechanover, A. & Iwai, K. 2004. The ubiquitin system: from basic mechanisms to the patient bed. *IUBMB Life,* 56**,** 193-201.

Cleves, C., Friedman, N. R., Rothner, A. D. & Hussain, M. S. 2010. Genetically confirmed CADASIL in a pediatric patient. *Pediatrics,* 126**,** e1603-7.

Crow, Y. J. 1993. Aicardi-Goutieres Syndrome. *In:* ADAM, M. P., ARDINGER, H. H., PAGON, R. A., WALLACE, S. E., BEAN, L. J. H., STEPHENS, K. & AMEMIYA, A. (eds.) *GeneReviews((R)).* Seattle (WA).

Crow, Y. J., Hayward, B. E., Parmar, R., Robins, P., Leitch, A., Ali, M., Black, D. N., Van Bokhoven, H., Brunner, H. G., Hamel, B. C., Corry, P. C., Cowan, F. M., Frints, S. G., Klepper, J., Livingston, J. H., Lynch, S. A., Massey, R. F., Meritet, J. F., Michaud, J. L., Ponsot, G., Voit, T., Lebon, P., Bonthron, D. T., Jackson, A. P., Barnes, D. E. & Lindahl, T. 2006a. Mutations in the gene encoding the 3'-5' DNA exonuclease TREX1 cause Aicardi-Goutieres syndrome at the AGS1 locus. *Nat Genet,* 38**,** 917-20.

Crow, Y. J., Leitch, A., Hayward, B. E., Garner, A., Parmar, R., Griffith, E., Ali, M., Semple, C., Aicardi, J., Babul-Hirji, R., Baumann, C., Baxter, P., Bertini, E., Chandler, K. E., Chitayat, D., Cau, D., Dery, C., Fazzi, E., Goizet, C., King, M. D., Klepper, J., Lacombe, D., Lanzi, G., Lyall, H., Martinez-Frias, M. L., Mathieu, M., Mckeown, C., Monier, A., Oade, Y., Quarrell, O. W., Rittey, C. D., Rogers, R. C., Sanchis, A., Stephenson, J. B., Tacke, U., Till, M., Tolmie, J. L., Tomlin, P., Voit, T., Weschke, B., Woods, C. G., Lebon, P., Bonthron, D. T., Ponting, C. P. & Jackson, A. P. 2006b. Mutations in genes encoding ribonuclease H2 subunits cause Aicardi-Goutieres syndrome and mimic congenital viral brain infection. *Nat Genet,* 38**,** 910-6.

Curtis, N., Zheng, R., Lamb, J. R. & Levin, M. 1995. Evidence for a superantigen mediated process in Kawasaki disease. *Arch Dis Child,* 72**,** 308-11.

Czartoski, T., Hallam, D., Lacy, J. M., Chun, M. R. & Becker, K. 2005. Postinfectious vasculopathy with evolution to moyamoya syndrome. *J Neurol Neurosurg Psychiatry,* 76**,** 256-9.

D'arco, F., D'amico, A., Caranci, F., Di Paolo, N., Melis, D. & Brunetti, A. 2014. Cerebrovascular stenosis in neurofibromatosis type 1 and utility of magnetic resonance angiography: our experience and literature review. *Radiol Med,* 119**,** 415-21.

De Luca, A., Maiello, M. R., D'alessio, A., Pergameno, M. & Normanno, N. 2012. The RAS/RAF/MEK/ERK and the PI3K/AKT signalling pathways: role in cancer pathogenesis and implications for therapeutic approaches. *Expert Opin Ther Targets,* 16 Suppl 2**,** S17-27.

Dergun, M., Kao, A., Hauger, S. B., Newburger, J. W. & Burns, J. C. 2005. Familial occurrence of Kawasaki syndrome in North America. *Arch Pediatr Adolesc Med,* 159**,** 876-81.

Deshaies, R. J. & Joazeiro, C. A. 2009. RING domain E3 ubiquitin ligases. *Annu Rev Biochem,* 78**,** 399-434.

Desmouliere, A., Geinoz, A., Gabbiani, F. & Gabbiani, G. 1993. Transforming growth factor-beta 1 induces alpha-smooth muscle actin expression in granulation tissue myofibroblasts and in quiescent and growing cultured fibroblasts. *J Cell Biol,* 122**,** 103-11.

Dillon, P. F., Aksoy, M. O., Driska, S. P. & Murphy, R. A. 1981. Myosin phosphorylation and the cross-bridge cycle in arterial smooth muscle. *Science,* 211**,** 495-7.

Dowling, M. M. & Kirkham, F. J. 2017. Stroke in sickle cell anaemia is more than stenosis and thrombosis: the role of anaemia and hyperemia in ischaemia. *Br J Haematol,* 176**,** 151-153.

Doyle, A. J., Doyle, J. J., Bessling, S. L., Maragh, S., Lindsay, M. E., Schepers, D., Gillis, E., Mortier, G., Homfray, T., Sauls, K., Norris, R. A., Huso, N. D., Leahy, D., Mohr, D. W., Caulfield, M. J., Scott, A. F., Destree, A., Hennekam, R. C., Arn, P. H., Curry, C. J., Van Laer, L., Mccallion, A. S., Loeys, B. L. & Dietz, H. C. 2012. Mutations in the TGF-beta repressor SKI cause Shprintzen-Goldberg syndrome with aortic aneurysm. *Nat Genet,* 44**,** 1249-54.

Du Moulin, M., Nurnberg, P., Crow, Y. J. & Rutsch, F. 2011. Cerebral vasculopathy is a common feature in Aicardi-Goutieres syndrome associated with SAMHD1 mutations. *Proc Natl Acad Sci U S A,* 108**,** E232; author reply E233.

Dunbar, A. J., Gondek, L. P., O'keefe, C. L., Makishima, H., Rataul, M. S., Szpurka, H., Sekeres, M. A., Wang, X. F., Mcdevitt, M. A. & Maciejewski, J. P. 2008.

250K single nucleotide polymorphism array karyotyping identifies acquired uniparental disomy and homozygous mutations, including novel missense substitutions of c-Cbl, in myeloid malignancies. *Cancer Res,* 68**,** 10349-57.

Eleftheriou, D., Batu, E. D., Ozen, S. & Brogan, P. A. 2015a. Vasculitis in children. *Nephrol Dial Transplant,* 30 Suppl 1**,** i94-103.

Eleftheriou, D., Dillon, M. J., Tullus, K., Marks, S. D., Pilkington, C. A., Roebuck, D. J., Klein, N. J. & Brogan, P. A. 2013. Systemic polyarteritis nodosa in the young: a single-center experience over thirty-two years. *Arthritis Rheum,* 65**,** 2476-85.

Eleftheriou, D., Varnier, G., Dolezalova, P., Mcmahon, A. M., Al-Obaidi, M. & Brogan, P. A. 2015b. Takayasu arteritis in childhood: retrospective experience from a tertiary referral centre in the United Kingdom. *Arthritis Res Ther,* 17**,** 36.

Ewart, A. K., Jin, W., Atkinson, D., Morris, C. A. & Keating, M. T. 1994. Supravalvular aortic stenosis associated with a deletion disrupting the elastin gene. *J Clin Invest,* 93**,** 1071-7.

Freitas, D. S., Camargo, C. Z., Mariz, H. A., Arraes, A. E. & De Souza, A. W. 2012. Takayasu arteritis: assessment of response to medical therapy based on clinical activity criteria and imaging techniques. *Rheumatol Int,* 32**,** 703-9.

Friedman, J. M., Arbiser, J., Epstein, J. A., Gutmann, D. H., Huot, S. J., Lin, A. E., Mcmanus, B. & Korf, B. R. 2002. Cardiovascular disease in neurofibromatosis 1: report of the NF1 Cardiovascular Task Force. *Genet Med,* 4**,** 105-11.

Fu, J. F., Hsu, J. J., Tang, T. C. & Shih, L. Y. 2003. Identification of CBL, a proto-oncogene at 11q23.3, as a novel MLL fusion partner in a patient with de novo acute myeloid leukemia. *Genes Chromosomes Cancer,* 37**,** 214-9.

Fukui, M., Kono, S., Sueishi, K. & Ikezaki, K. 2000. Moyamoya disease. *Neuropathology,* 20 Suppl**,** S61-4.

Gallione, C. J., Richards, J. A., Letteboer, T. G., Rushlow, D., Prigoda, N. L., Leedom, T. P., Ganguly, A., Castells, A., Ploos Van Amstel, J. K., Westermann, C. J., Pyeritz, R. E. & Marchuk, D. A. 2006. SMAD4 mutations found in unselected HHT patients. *J Med Genet,* 43**,** 793-7.

Gallo, E. M., Loch, D. C., Habashi, J. P., Calderon, J. F., Chen, Y., Bedja, D., Van Erp, C., Gerber, E. E., Parker, S. J., Sauls, K., Judge, D. P., Cooke, S. K., Lindsay, M. E., Rouf, R., Myers, L., Ap Rhys, C. M., Kent, K. C., Norris, R. A., Huso, D. L. & Dietz, H. C. 2014. Angiotensin II-dependent TGF-beta signaling contributes to Loeys-Dietz syndrome vascular pathogenesis. *J Clin Invest,* 124**,** 448-60.

Ganesan, V. & Kirkham, F. J. 1997. Noonan syndrome and moyamoya. *Pediatr Neurol,* 16**,** 256-8.

Gardner-Medwin, J. M., Dolezalova, P., Cummins, C. & Southwood, T. R. 2002. Incidence of Henoch-Schonlein purpura, Kawasaki disease, and rare vasculitides in children of different ethnic origins. *Lancet,* 360**,** 1197-202.

Garg, N., Kasapcopur, O., Foster, J., 2nd, Barut, K., Tekin, A., Kizilkilic, O. & Tekin, M. 2014. Novel adenosine deaminase 2 mutations in a child with a fatal vasculopathy. *Eur J Pediatr,* 173**,** 827-30.

Garg, V., Muth, A. N., Ransom, J. F., Schluterman, M. K., Barnes, R., King, I. N., Grossfeld, P. D. & Srivastava, D. 2005. Mutations in NOTCH1 cause aortic valve disease. *Nature,* 437**,** 270-4.

Germain, D. P. & Herrera-Guzman, Y. 2004. Vascular Ehlers-Danlos syndrome. *Ann Genet,* 47**,** 1-9.

Giardine, B., Riemer, C., Hardison, R. C., Burhans, R., Elnitski, L., Shah, P., Zhang, Y., Blankenberg, D., Albert, I., Taylor, J., Miller, W., Kent, W. J. & Nekrutenko, A. 2005. Galaxy: a platform for interactive large-scale genome analysis. *Genome Res,* 15**,** 1451-5.

Glancy, D. L., Wegmann, M. & Dhurandhar, R. W. 2001. Aortic dissection and patent ductus arteriosus in three generations. *Am J Cardiol,* 87**,** 813-5, A9.

Goecks, J., Nekrutenko, A., Taylor, J. & Galaxy, T. 2010. Galaxy: a comprehensive approach for supporting accessible, reproducible, and transparent computational research in the life sciences. *Genome Biol,* 11**,** R86.

Goutieres, F. 2005. Aicardi-Goutieres syndrome. *Brain Dev,* 27**,** 201-6.

Grand, F. H., Hidalgo-Curtis, C. E., Ernst, T., Zoi, K., Zoi, C., Mcguire, C., Kreil, S., Jones, A., Score, J., Metzgeroth, G., Oscier, D., Hall, A., Brandts, C., Serve, H., Reiter, A., Chase, A. J. & Cross, N. C. 2009. Frequent CBL mutations associated with 11q acquired uniparental disomy in myeloproliferative neoplasms. *Blood,* 113**,** 6182-92.

Granild-Jensen, J., Jensen, U. B., Schwartz, M. & Hansen, U. S. 2009. Cerebral autosomal dominant arteriopathy with subcortical infarcts and leukoencephalopathy resulting in stroke in an 11-year-old male. *Dev Med Child Neurol,* 51**,** 754-7.

Gray, J. R. & Davies, S. J. 1996. Marfan syndrome. *J Med Genet,* 33**,** 403-8.

Guey, S., Grangeon, L., Brunelle, F., Bergametti, F., Amiel, J., Lyonnet, S., Delaforge, A., Arnould, M., Desnous, B., Bellesme, C., Herve, D., Schwitalla, J. C., Kraemer, M., Tournier-Lasserve, E. & Kossorotoff, M. 2017a. De novo mutations in CBL causing early-onset paediatric moyamoya angiopathy. *J Med Genet,* 54**,** 550-557.

Guey, S., Kraemer, M., Herve, D., Ludwig, T., Kossorotoff, M., Bergametti, F., Schwitalla, J. C., Choi, S., Broseus, L., Callebaut, I., Genin, E., Tournier-Lasserve, E. & Consortium, F. 2017b. Rare RNF213 variants in the C-terminal region encompassing the RING-finger domain are associated with moyamoya angiopathy in Caucasians. *Eur J Hum Genet,* 25**,** 995-1003.

Guillevin, L., Durand-Gasselin, B., Cevallos, R., Gayraud, M., Lhote, F., Callard, P., Amouroux, J., Casassus, P. & Jarrousse, B. 1999. Microscopic polyangiitis: clinical and laboratory findings in eighty-five patients. *Arthritis Rheum,* 42**,** 421-30.

Guo, D. C., Pannu, H., Tran-Fadulu, V., Papke, C. L., Yu, R. K., Avidan, N., Bourgeois, S., Estrera, A. L., Safi, H. J., Sparks, E., Amor, D., Ades, L., Mcconnell, V., Willoughby, C. E., Abuelo, D., Willing, M., Lewis, R. A., Kim, D. H., Scherer, S., Tung, P. P., Ahn, C., Buja, L. M., Raman, C. S., Shete, S. S. & Milewicz, D. M. 2007. Mutations in smooth muscle alpha-actin (ACTA2) lead to thoracic aortic aneurysms and dissections. *Nat Genet,* 39**,** 1488-93.

Guo, D. C., Papke, C. L., Tran-Fadulu, V., Regalado, E. S., Avidan, N., Johnson, R. J., Kim, D. H., Pannu, H., Willing, M. C., Sparks, E., Pyeritz, R. E., Singh, M. N., Dalman, R. L., Grotta, J. C., Marian, A. J., Boerwinkle, E. A., Frazier, L. Q., Lemaire, S. A., Coselli, J. S., Estrera, A. L., Safi, H. J., Veeraraghavan, S., Muzny, D. M., Wheeler, D. A., Willerson, J. T., Yu, R. K., Shete, S. S., Scherer, S. E., Raman, C. S., Buja, L. M. & Milewicz, D. M. 2009. Mutations in smooth muscle alpha-actin (ACTA2) cause coronary artery disease, stroke, and Moyamoya disease, along with thoracic aortic disease. *Am J Hum Genet,* 84**,** 617-27.

Guo, D. C., Regalado, E., Casteel, D. E., Santos-Cortez, R. L., Gong, L., Kim, J. J., Dyack, S., Horne, S. G., Chang, G., Jondeau, G., Boileau, C., Coselli, J. S., Li, Z., Leal, S. M., Shendure, J., Rieder, M. J., Bamshad, M. J., Nickerson, D. A., Gen, T. A. C. R. C., National Heart, L., Blood Institute Grand Opportunity Exome Sequencing, P., Kim, C. & Milewicz, D. M. 2013. Recurrent gain-of-function mutation in PRKG1 causes thoracic aortic aneurysms and acute aortic dissections. *Am J Hum Genet,* 93**,** 398-404.

Guo, X. & Chen, S. Y. 2012. Transforming growth factor-beta and smooth muscle differentiation. *World J Biol Chem,* 3**,** 41-52.

Habashi, J. P., Judge, D. P., Holm, T. M., Cohn, R. D., Loeys, B. L., Cooper, T. K., Myers, L., Klein, E. C., Liu, G., Calvi, C., Podowski, M., Neptune, E. R., Halushka, M. K., Bedja, D., Gabrielson, K., Rifkin, D. B., Carta, L., Ramirez, F., Huso, D. L. & Dietz, H. C. 2006. Losartan, an AT1 antagonist, prevents aortic aneurysm in a mouse model of Marfan syndrome. *Science,* 312**,** 117-21.

Hanley, W. B. & Jones, N. B. 1967. Familial dissecting aortic aneurysm. A report of three cases within two generations. *Br Heart J,* 29**,** 852-8.

Hara, K., Shiga, A., Fukutake, T., Nozaki, H., Miyashita, A., Yokoseki, A., Kawata, H., Koyama, A., Arima, K., Takahashi, T., Ikeda, M., Shiota, H., Tamura, M., Shimoe, Y., Hirayama, M., Arisato, T., Yanagawa, S., Tanaka, A., Nakano, I., Ikeda, S., Yoshida, Y., Yamamoto, T., Ikeuchi, T., Kuwano, R., Nishizawa, M., Tsuji, S. & Onodera, O. 2009. Association of HTRA1 mutations and familial ischemic cerebral small-vessel disease. *N Engl J Med,* 360**,** 1729-39.

Haritunians, T., Boulter, J., Hicks, C., Buhrman, J., Disibio, G., Shawber, C., Weinmaster, G., Nofziger, D. & Schanen, C. 2002. CADASIL Notch3 mutant proteins localize to the cell surface and bind ligand. *Circ Res,* 90**,** 506-8.

Herbst, R. S. 2004. Review of epidermal growth factor receptor biology. *Int J Radiat Oncol Biol Phys,* 59**,** 21-6.

Herve, D., Philippi, A., Belbouab, R., Zerah, M., Chabrier, S., Collardeau-Frachon, S., Bergametti, F., Essongue, A., Berrou, E., Krivosic, V., Sainte-Rose, C., Houdart, E., Adam, F., Billiemaz, K., Lebret, M., Roman, S., Passemard, S., Boulday, G., Delaforge, A., Guey, S., Dray, X., Chabriat, H., Brouckaert, P., Bryckaert, M. & Tournier-Lasserve, E. 2014. Loss of alpha1beta1 soluble guanylate cyclase, the major nitric oxide receptor, leads to moyamoya and achalasia. *Am J Hum Genet,* 94**,** 385-94.

Higasa, K., Miyake, N., Yoshimura, J., Okamura, K., Niihori, T., Saitsu, H., Doi, K., Shimizu, M., Nakabayashi, K., Aoki, Y., Tsurusaki, Y., Morishita, S., Kawaguchi, T., Migita, O., Nakayama, K., Nakashima, M., Mitsui, J., Narahara, M., Hayashi, K., Funayama, R., Yamaguchi, D., Ishiura, H., Ko, W. Y., Hata, K., Nagashima, T., Yamada, R., Matsubara, Y., Umezawa, A., Tsuji, S., Matsumoto, N. & Matsuda, F. 2016. Human genetic variation database, a reference database of genetic variations in the Japanese population. *J Hum Genet,* 61**,** 547-53.

Hoffman, G. S. & Calabrese, L. H. 2014. Vasculitis: determinants of disease patterns. *Nat Rev Rheumatol,* 10**,** 454-62.

Howard, J. 1997. Molecular motors: structural adaptations to cellular functions. *Nature,* 389**,** 561-7.

Hyakuna, N., Muramatsu, H., Higa, T., Chinen, Y., Wang, X. & Kojima, S. 2015. Germline mutation of CBL is associated with moyamoya disease in a child with juvenile myelomonocytic leukemia and Noonan syndrome-like disorder. *Pediatr Blood Cancer,* 62**,** 542-4.

Iwahashi, Y., Kawasaki, A., Hirano, F., Sada, K., Kobayashi, S., Yamada, H., Furukawa, H., Yamagata, K., Sumida, T., Miyasaka, N., Tohma, S., Ozaki , S., Matsuo, S., Hashimoto, H., Makino, H., Arimura, Y., Harigai, M. & Tsuchiya, N. 2017. Association of TNFSF4 Polymorphism with Proteinase 3 - ANCA Positive Vasculitis in a Japanese Population. *Rheumatology* 56**,** iii109-iii110.

Jayne, D. 2010. Rituximab treatment for vasculitis. *Clin J Am Soc Nephrol,* 5**,** 1359-62.

Jennette, J. C., Falk, R. J., Andrassy, K., Bacon, P. A., Churg, J., Gross, W. L., Hagen, E. C., Hoffman, G. S., Hunder, G. G., Kallenberg, C. G. & Et Al. 1994. Nomenclature of systemic vasculitides. Proposal of an international consensus conference. *Arthritis Rheum,* 37**,** 187-92.

Jennette, J. C., Xiao, H. & Falk, R. J. 2006. Pathogenesis of vascular inflammation by anti-neutrophil cytoplasmic antibodies. *J Am Soc Nephrol,* 17**,** 1235-42.

Jeremiah, N., Neven, B., Gentili, M., Callebaut, I., Maschalidi, S., Stolzenberg, M. C., Goudin, N., Fremond, M. L., Nitschke, P., Molina, T. J., Blanche, S., Picard, C., Rice, G. I., Crow, Y. J., Manel, N., Fischer, A., Bader-Meunier, B. & Rieux-Laucat, F. 2014. Inherited STING-activating mutation underlies a familial inflammatory syndrome with lupus-like manifestations. *J Clin Invest,* 124**,** 5516-20.

Joazeiro, C. A., Wing, S. S., Huang, H., Leverson, J. D., Hunter, T. & Liu, Y. C. 1999. The tyrosine kinase negative regulator c-Cbl as a RING-type, E2-dependent ubiquitin-protein ligase. *Science,* 286**,** 309-12.

Johnston, S. L., Lock, R. J. & Gompels, M. M. 2002. Takayasu arteritis: a review. *J Clin Pathol,* 55**,** 481-6.

Joutel, A., Corpechot, C., Ducros, A., Vahedi, K., Chabriat, H., Mouton, P., Alamowitch, S., Domenga, V., Cecillion, M., Marechal, E., Maciazek, J., Vayssiere, C., Cruaud, C., Cabanis, E. A., Ruchoux, M. M., Weissenbach, J., Bach, J. F., Bousser, M. G. & Tournier-Lasserve, E. 1996. Notch3 mutations in CADASIL, a hereditary adult-onset condition causing stroke and dementia. *Nature,* 383**,** 707-10.

Joutel, A., Corpechot, C., Ducros, A., Vahedi, K., Chabriat, H., Mouton, P., Alamowitch, S., Domenga, V., Cecillion, M., Marechal, E., Maciazek, J., Vayssiere, C., Cruaud, C., Cabanis, E. A., Ruchoux, M. M., Weissenbach, J., Bach, J. F., Bousser, M. G. & Tournier-Lasserve, E. 1997. Notch3 mutations in cerebral autosomal dominant arteriopathy with subcortical infarcts and leukoencephalopathy (CADASIL), a mendelian condition causing stroke and vascular dementia. *Ann N Y Acad Sci,* 826**,** 213-7.

Kaabeche, K., Guenou, H., Bouvard, D., Didelot, N., Listrat, A. & Marie, P. J. 2005. Cbl-mediated ubiquitination of alpha5 integrin subunit mediates fibronectin-dependent osteoblast detachment and apoptosis induced by FGFR2 activation. *J Cell Sci,* 118**,** 1223-32.

Kadler, K. E., Holmes, D. F., Trotter, J. A. & Chapman, J. A. 1996. Collagen fibril formation. *Biochem J,* 316 (Pt 1)**,** 1-11.

Kamada, F., Aoki, Y., Narisawa, A., Abe, Y., Komatsuzaki, S., Kikuchi, A., Kanno, J., Niihori, T., Ono, M., Ishii, N., Owada, Y., Fujimura, M., Mashimo, Y.,

Suzuki, Y., Hata, A., Tsuchiya, S., Tominaga, T., Matsubara, Y. & Kure, S. 2011. A genome-wide association study identifies RNF213 as the first Moyamoya disease gene. *J Hum Genet,* 56**,** 34-40.

Kamphans, T., Sabri, P., Zhu, N., Heinrich, V., Mundlos, S., Robinson, P. N., Parkhomchuk, D. & Krawitz, P. M. 2013. Filtering for compound heterozygous sequence variants in non-consanguineous pedigrees. *PLoS One,* 8**,** e70151.

Kassenbrock, C. K. & Anderson, S. M. 2004. Regulation of ubiquitin protein ligase activity in c-Cbl by phosphorylation-induced conformational change and constitutive activation by tyrosine to glutamate point mutations. *J Biol Chem,* 279**,** 28017-27.

Katz, M., Amit, I. & Yarden, Y. 2007. Regulation of MAPKs by growth factors and receptor tyrosine kinases. *Biochim Biophys Acta,* 1773**,** 1161-76.

Kawasaki, A., Yamashita, K., Hirano, F., Sada, K., Kobayashi, S., Yamada, H., Furukawa, H., Yamagata, K., Sumida, T., Miyasaka, N., Tohma, S., Ozaki , S., Matsuo, S., Hashimoto, H., Makino, H., Arimura, Y., Harigai, M. & Tsuchiya, N. 2017. Association of ETS1 polymorphism in 3' untranslated region with granulomatosis with polyangiitis and PR3-ANCA-positive vasculitis in a Japanese population.

Kerr, G. S., Hallahan, C. W., Giordano, J., Leavitt, R. Y., Fauci, A. S., Rottem, M. & Hoffman, G. S. 1994. Takayasu arteritis. *Ann Intern Med,* 120**,** 919-29.

Keylock, A., Hong, Y., Saunders, D., Omoyinmi, E., Mulhern, C., Roebuck, D., Brogan, P., Ganesan, V. & Eleftheriou, D. 2018. Moyamoya-like cerebrovascular disease in a child with a novel mutation in myosin heavy chain 11. *Neurology,* 90**,** 136-138.

Khor, C. C., Davila, S., Breunis, W. B., Lee, Y. C., Shimizu, C., Wright, V. J., Yeung, R. S., Tan, D. E., Sim, K. S., Wang, J. J., Wong, T. Y., Pang, J., Mitchell, P., Cimaz, R., Dahdah, N., Cheung, Y. F., Huang, G. Y., Yang, W., Park, I. S., Lee, J. K., Wu, J. Y., Levin, M., Burns, J. C., Burgner, D., Kuijpers, T. W., Hibberd, M. L., Hong Kong-Shanghai Kawasaki Disease Genetics, C., Korean Kawasaki Disease Genetics, C., Taiwan Kawasaki Disease Genetics, C., International Kawasaki Disease Genetics, C., Consortium, U. S. K. D. G. & Blue Mountains Eye, S. 2011. Genome-wide association study identifies FCGR2A as a susceptibility locus for Kawasaki disease. *Nat Genet,* 43**,** 1241-6.

Kiezun, A., Garimella, K., Do, R., Stitziel, N. O., Neale, B. M., Mclaren, P. J., Gupta, N., Sklar, P., Sullivan, P. F., Moran, J. L., Hultman, C. M., Lichtenstein, P., Magnusson, P., Lehner, T., Shugart, Y. Y., Price, A. L., De Bakker, P. I., Purcell, S. M. & Sunyaev, S. R. 2012. Exome sequencing and the genetic basis of complex traits. *Nat Genet,* 44**,** 623-30.

Kim, J. J., Hong, Y. M., Sohn, S., Jang, G. Y., Ha, K. S., Yun, S. W., Han, M. K., Lee, K. Y., Song, M. S., Lee, H. D., Kim, D. S., Lee, J. E., Shin, E. S., Jang, J. H., Lee, Y. S., Kim, S. Y., Lee, J. Y., Han, B. G., Wu, J. Y., Kim, K. J., Park, Y. M., Seo, E. J., Park, I. S., Lee, J. K. & Korean Kawasaki Disease Genetics, C. 2011. A genome-wide association analysis reveals 1p31 and 2p13.3 as susceptibility loci for Kawasaki disease. *Hum Genet,* 129**,** 487-95.

Kim, J. S. 2016. Moyamoya Disease: Epidemiology, Clinical Features, and Diagnosis. *J Stroke,* 18**,** 2-11.

Kim, S. & Dedeoglu, F. 2005. Update on pediatric vasculitis. *Curr Opin Pediatr,* 17**,** 695-702.

Kim, S. K., Seol, H. J., Cho, B. K., Hwang, Y. S., Lee, D. S. & Wang, K. C. 2004. Moyamoya disease among young patients: its aggressive clinical course and the role of active surgical treatment. *Neurosurgery,* 54**,** 840-4; discussion 844-6.

Knudson, A. G., Jr. 1971. Mutation and cancer: statistical study of retinoblastoma. *Proc Natl Acad Sci U S A,* 68**,** 820-3.

Kobayashi, H., Brozman, M., Kyselova, K., Viszlayova, D., Morimoto, T., Roubec, M., Skoloudik, D., Petrovicova, A., Juskanic, D., Strauss, J., Halaj, M., Kurray, P., Hranai, M., Harada, K. H., Inoue, S., Yoshida, Y., Habu, T., Herzig, R., Youssefian, S. & Koizumi, A. 2016. RNF213 Rare Variants in Slovakian and Czech Moyamoya Disease Patients. *PLoS One,* 11**,** e0164759.

Kobayashi, H., Matsuda, Y., Hitomi, T., Okuda, H., Shioi, H., Matsuda, T., Imai, H., Sone, M., Taura, D., Harada, K. H., Habu, T., Takagi, Y., Miyamoto, S. & Koizumi, A. 2015. Biochemical and Functional Characterization of RNF213 (Mysterin) R4810K, a Susceptibility Mutation of Moyamoya Disease, in Angiogenesis In Vitro and In Vivo. *J Am Heart Assoc,* 4.

Komander, D. & Rape, M. 2012. The ubiquitin code. *Annu Rev Biochem,* 81**,** 203-29.

Kontusaari, S., Tromp, G., Kuivaniemi, H., Ladda, R. L. & Prockop, D. J. 1990. Inheritance of an RNA splicing mutation (G+ 1 IVS20) in the type III procollagen gene (COL3A1) in a family having aortic aneurysms and easy bruisability: phenotypic overlap between familial arterial aneurysms and Ehlers-Danlos syndrome type IV. *Am J Hum Genet,* 47**,** 112-20.

Kovacic, J. C., Mercader, N., Torres, M., Boehm, M. & Fuster, V. 2012. Epithelial-to-mesenchymal and endothelial-to-mesenchymal transition: from cardiovascular development to disease. *Circulation,* 125**,** 1795-808.

Kryukov, G. V., Pennacchio, L. A. & Sunyaev, S. R. 2007. Most rare missense alleles are deleterious in humans: implications for complex disease and association studies. *Am J Hum Genet,* 80**,** 727-39.

Kuo, H. C., Yang, K. D., Juo, S. H., Liang, C. D., Chen, W. C., Wang, Y. S., Lee, C. H., Hsi, E., Yu, H. R., Woon, P. Y., Lin, I. C., Huang, C. F., Hwang, D. Y., Lee, C. P., Lin, L. Y., Chang, W. P. & Chang, W. C. 2011a. ITPKC single nucleotide polymorphism associated with the Kawasaki disease in a Taiwanese population. *PLoS One,* 6**,** e17370.

Kuo, H. C., Yu, H. R., Juo, S. H., Yang, K. D., Wang, Y. S., Liang, C. D., Chen, W. C., Chang, W. P., Huang, C. F., Lee, C. P., Lin, L. Y., Liu, Y. C., Guo, Y. C., Chiu, C. C. & Chang, W. C. 2011b. CASP3 gene single-nucleotide polymorphism (rs72689236) and Kawasaki disease in Taiwanese children. *J Hum Genet,* 56**,** 161-5.

Kuroda, S. & Houkin, K. 2008. Moyamoya disease: current concepts and future perspectives. *Lancet Neurol,* 7**,** 1056-66.

Lander, E. S., Linton, L. M., Birren, B., Nusbaum, C., Zody, M. C., Baldwin, J., Devon, K., Dewar, K., Doyle, M., Fitzhugh, W., Funke, R., Gage, D., Harris, K., Heaford, A., Howland, J., Kann, L., Lehoczky, J., Levine, R., Mcewan, P., Mckernan, K., Meldrim, J., Mesirov, J. P., Miranda, C., Morris, W., Naylor, J., Raymond, C., Rosetti, M., Santos, R., Sheridan, A., Sougnez, C., Stange-Thomann, N., Stojanovic, N., Subramanian, A., Wyman, D., Rogers, J., Sulston, J., Ainscough, R., Beck, S., Bentley, D., Burton, J., Clee, C., Carter, N., Coulson, A., Deadman, R., Deloukas, P., Dunham, A., Dunham, I., Durbin, R., French, L., Grafham, D., Gregory, S., Hubbard, T., Humphray, S., Hunt, A., Jones, M., Lloyd, C., Mcmurray, A., Matthews, L., Mercer, S., Milne, S., Mullikin, J. C., Mungall, A., Plumb, R., Ross, M., Shownkeen, R., Sims, S., Waterston, R. H., Wilson, R. K., Hillier, L. W., Mcpherson, J. D., Marra, M. A., Mardis, E. R., Fulton, L. A., Chinwalla, A. T., Pepin, K. H., Gish, W. R., Chissoe, S. L., Wendl, M. C., Delehaunty, K. D., Miner, T. L., Delehaunty, A., Kramer, J. B., Cook, L. L., Fulton, R. S., Johnson, D. L., Minx, P. J., Clifton, S. W., Hawkins, T., Branscomb, E., Predki, P., Richardson, P., Wenning, S., Slezak, T., Doggett, N., Cheng, J. F., Olsen, A., Lucas, S., Elkin, C., Uberbacher, E., Frazier, M., et al. 2001. Initial sequencing and analysis of the human genome. *Nature,* 409**,** 860-921.

Lawley, T. J. & Kubota, Y. 1989. Induction of morphologic differentiation of endothelial cells in culture. *J Invest Dermatol,* 93**,** 59S-61S.

Lee, B., Godfrey, M., Vitale, E., Hori, H., Mattei, M. G., Sarfarazi, M., Tsipouras, P., Ramirez, F. & Hollister, D. W. 1991. Linkage of Marfan syndrome and a phenotypically related disorder to two different fibrillin genes. *Nature,* 352**,** 330-4.

Lee, Y. C., Kuo, H. C., Chang, J. S., Chang, L. Y., Huang, L. M., Chen, M. R., Liang, C. D., Chi, H., Huang, F. Y., Lee, M. L., Huang, Y. C., Hwang, B., Chiu, N. C., Hwang, K. P., Lee, P. C., Chang, L. C., Liu, Y. M., Chen, Y. J., Chen, C. H., Taiwan Pediatric, I. D. A., Chen, Y. T., Tsai, F. J. & Wu, J. Y. 2012. Two new susceptibility loci for Kawasaki disease identified through genome-wide association analysis. *Nat Genet,* 44**,** 522-5.

Leistritz, D. F., Pepin, M. G., Schwarze, U. & Byers, P. H. 2011. COL3A1 haploinsufficiency results in a variety of Ehlers-Danlos syndrome type IV with delayed onset of complications and longer life expectancy. *Genet Med,* 13**,** 717-22.

Lek, M., Karczewski, K. J., Minikel, E. V., Samocha, K. E., Banks, E., Fennell, T., O'donnell-Luria, A. H., Ware, J. S., Hill, A. J., Cummings, B. B., Tukiainen, T., Birnbaum, D. P., Kosmicki, J. A., Duncan, L. E., Estrada, K., Zhao, F., Zou, J., Pierce-Hoffman, E., Berghout, J., Cooper, D. N., Deflaux, N., Depristo, M., Do, R., Flannick, J., Fromer, M., Gauthier, L., Goldstein, J., Gupta, N., Howrigan, D., Kiezun, A., Kurki, M. I., Moonshine, A. L., Natarajan, P., Orozco, L., Peloso, G. M., Poplin, R., Rivas, M. A., Ruano-Rubio, V., Rose, S. A., Ruderfer, D. M., Shakir, K., Stenson, P. D., Stevens, C., Thomas, B. P., Tiao, G., Tusie-Luna, M. T., Weisburd, B., Won, H. H., Yu, D., Altshuler, D. M., Ardissino, D., Boehnke, M., Danesh, J., Donnelly, S., Elosua, R., Florez, J. C., Gabriel, S. B., Getz, G., Glatt, S. J., Hultman, C. M., Kathiresan, S., Laakso, M., Mccarroll, S., Mccarthy, M. I., Mcgovern, D., Mcpherson, R., Neale, B. M., Palotie, A., Purcell, S. M., Saleheen, D., Scharf, J. M., Sklar, P., Sullivan, P. F., Tuomilehto, J., Tsuang, M. T., Watkins, H. C., Wilson, J. G., Daly, M. J., Macarthur, D. G. & Exome Aggregation, C. 2016. Analysis of protein-coding genetic variation in 60,706 humans. *Nature,* 536**,** 285-91.

Leung, D. Y., Travers, J. B., Giorno, R., Norris, D. A., Skinner, R., Aelion, J., Kazemi, L. V., Kim, M. H., Trumble, A. E., Kotb, M. & Et Al. 1995. Evidence for a streptococcal superantigen-driven process in acute guttate psoriasis. *J Clin Invest,* 96**,** 2106-12.

Levkowitz, G., Waterman, H., Zamir, E., Kam, Z., Oved, S., Langdon, W. Y., Beguinot, L., Geiger, B. & Yarden, Y. 1998. c-Cbl/Sli-1 regulates endocytic sorting and ubiquitination of the epidermal growth factor receptor. *Genes Dev,* 12**,** 3663-74.

Li, H., Llera, A. & Mariuzza, R. A. 1998. Structure-function studies of T-cell receptor-superantigen interactions. *Immunol Rev,* 163**,** 177-86.

Li, L., Zhao, G. D., Shi, Z., Qi, L. L., Zhou, L. Y. & Fu, Z. X. 2016. The Ras/Raf/MEK/ERK signaling pathway and its role in the occurrence and development of HCC. *Oncol Lett,* 12**,** 3045-3050.

Li, W., Bengtson, M. H., Ulbrich, A., Matsuda, A., Reddy, V. A., Orth, A., Chanda, S. K., Batalov, S. & Joazeiro, C. A. 2008. Genome-wide and functional annotation of human E3 ubiquitin ligases identifies MULAN, a mitochondrial E3 that regulates the organelle's dynamics and signaling. *PLoS One,* 3**,** e1487.

Lie, J. T. 1998. Vasculopathies of Neurofibromatosis Type 1 (von Recklinghausen Disease). *Cardiovasc Pathol,* 7**,** 97-108.

Liu, W., Morito, D., Takashima, S., Mineharu, Y., Kobayashi, H., Hitomi, T., Hashikata, H., Matsuura, N., Yamazaki, S., Toyoda, A., Kikuta, K., Takagi,

Y., Harada, K. H., Fujiyama, A., Herzig, R., Krischek, B., Zou, L., Kim, J. E., Kitakaze, M., Miyamoto, S., Nagata, K., Hashimoto, N. & Koizumi, A. 2011. Identification of RNF213 as a susceptibility gene for moyamoya disease and its possible role in vascular development. *PLoS One,* 6**,** e22542.

Liu, X., Wu, H., Byrne, M., Krane, S. & Jaenisch, R. 1997. Type III collagen is crucial for collagen I fibrillogenesis and for normal cardiovascular development. *Proc Natl Acad Sci U S A,* 94**,** 1852-6.

Liu, Y., Jesus, A. A., Marrero, B., Yang, D., Ramsey, S. E., Sanchez, G. A. M., Tenbrock, K., Wittkowski, H., Jones, O. Y., Kuehn, H. S., Lee, C. R., Dimattia, M. A., Cowen, E. W., Gonzalez, B., Palmer, I., Digiovanna, J. J., Biancotto, A., Kim, H., Tsai, W. L., Trier, A. M., Huang, Y., Stone, D. L., Hill, S., Kim, H. J., Hilaire, C. S., Gurprasad, S., Plass, N., Chapelle, D., Horkayne-Szakaly, I., Foell, D., Barysenka, A., Candotti, F., Holland, S. M., Hughes, J. D., Mehmet, H., Issekutz, A. C., Raffeld, M., Mcelwee, J., Fontana, J. R., Minniti, C. P., Moir, S., Kastner, D. L., Gadina, M., Steven, A. C., Wingfield, P. T., Brooks, S. R., Rosenzweig, S. D., Fleisher, T. A., Deng, Z., Boehm, M., Paller, A. S. & Goldbach-Mansky, R. 2014. Activated STING in a vascular and pulmonary syndrome. *N Engl J Med,* 371**,** 507-518.

Livingston, J. H. & Crow, Y. J. 2016. Neurologic Phenotypes Associated with Mutations in TREX1, RNASEH2A, RNASEH2B, RNASEH2C, SAMHD1, ADAR1, and IFIH1: Aicardi-Goutieres Syndrome and Beyond. *Neuropediatrics,* 47**,** 355-360.

Lo, F. S., Wang, C. J., Wong, M. C. & Lee, N. C. 2015. Moyamoya disease in two patients with Noonan-like syndrome with loose anagen hair. *Am J Med Genet A,* 167**,** 1285-8.

Loeys, B. L., Chen, J., Neptune, E. R., Judge, D. P., Podowski, M., Holm, T., Meyers, J., Leitch, C. C., Katsanis, N., Sharifi, N., Xu, F. L., Myers, L. A., Spevak, P. J., Cameron, D. E., De Backer, J., Hellemans, J., Chen, Y., Davis, E. C., Webb, C. L., Kress, W., Coucke, P., Rifkin, D. B., De Paepe, A. M. & Dietz, H. C. 2005. A syndrome of altered cardiovascular, craniofacial, neurocognitive and skeletal development caused by mutations in TGFBR1 or TGFBR2. *Nat Genet,* 37**,** 275-81.

Loeys, B. L., Schwarze, U., Holm, T., Callewaert, B. L., Thomas, G. H., Pannu, H., De Backer, J. F., Oswald, G. L., Symoens, S., Manouvrier, S., Roberts, A. E., Faravelli, F., Greco, M. A., Pyeritz, R. E., Milewicz, D. M., Coucke, P. J., Cameron, D. E., Braverman, A. C., Byers, P. H., De Paepe, A. M. & Dietz, H. C. 2006. Aneurysm syndromes caused by mutations in the TGF-beta receptor. *N Engl J Med,* 355**,** 788-98.

Loh, M. L., Sakai, D. S., Flotho, C., Kang, M., Fliegauf, M., Archambeault, S., Mullighan, C. G., Chen, L., Bergstraesser, E., Bueso-Ramos, C. E., Emanuel, P. D., Hasle, H., Issa, J. P., Van Den Heuvel-Eibrink, M. M., Locatelli, F., Stary, J., Trebo, M., Wlodarski, M., Zecca, M., Shannon, K. M. & Niemeyer,

C. M. 2009. Mutations in CBL occur frequently in juvenile myelomonocytic leukemia. *Blood,* 114**,** 1859-63.

Loreto, M. P., Berry, D. M. & Mcglade, C. J. 2002. Functional cooperation between c-Cbl and Src-like adaptor protein 2 in the negative regulation of T-cell receptor signaling. *Mol Cell Biol,* 22**,** 4241-55.

Lupas, A. N. & Martin, J. 2002. AAA proteins. *Curr Opin Struct Biol,* 12**,** 746-53.

Lyons, P. A., Rayner, T. F., Trivedi, S., Holle, J. U., Watts, R. A., Jayne, D. R., Baslund, B., Brenchley, P., Bruchfeld, A., Chaudhry, A. N., Cohen Tervaert, J. W., Deloukas, P., Feighery, C., Gross, W. L., Guillevin, L., Gunnarsson, I., Harper, L., Hruskova, Z., Little, M. A., Martorana, D., Neumann, T., Ohlsson, S., Padmanabhan, S., Pusey, C. D., Salama, A. D., Sanders, J. S., Savage, C. O., Segelmark, M., Stegeman, C. A., Tesar, V., Vaglio, A., Wieczorek, S., Wilde, B., Zwerina, J., Rees, A. J., Clayton, D. G. & Smith, K. G. 2012. Genetically distinct subsets within ANCA-associated vasculitis. *N Engl J Med,* 367**,** 214-23.

Maksimowicz-Mckinnon, K., Clark, T. M. & Hoffman, G. S. 2007. Limitations of therapy and a guarded prognosis in an American cohort of Takayasu arteritis patients. *Arthritis Rheum,* 56**,** 1000-9.

Maksimowicz-Mckinnon, K. & Hoffman, G. S. 2007. Takayasu arteritis: what is the long-term prognosis? *Rheum Dis Clin North Am,* 33**,** 777-86, vi.

Malfait, F., Coucke, P., Symoens, S., Loeys, B., Nuytinck, L. & De Paepe, A. 2005. The molecular basis of classic Ehlers-Danlos syndrome: a comprehensive study of biochemical and molecular findings in 48 unrelated patients. *Hum Mutat,* 25**,** 28-37.

Malfait, F., Francomano, C., Byers, P., Belmont, J., Berglund, B., Black, J., Bloom, L., Bowen, J. M., Brady, A. F., Burrows, N. P., Castori, M., Cohen, H., Colombi, M., Demirdas, S., De Backer, J., De Paepe, A., Fournel-Gigleux, S., Frank, M., Ghali, N., Giunta, C., Grahame, R., Hakim, A., Jeunemaitre, X., Johnson, D., Juul-Kristensen, B., Kapferer-Seebacher, I., Kazkaz, H., Kosho, T., Lavallee, M. E., Levy, H., Mendoza-Londono, R., Pepin, M., Pope, F. M., Reinstein, E., Robert, L., Rohrbach, M., Sanders, L., Sobey, G. J., Van Damme, T., Vandersteen, A., Van Mourik, C., Voermans, N., Wheeldon, N., Zschocke, J. & Tinkle, B. 2017. The 2017 international classification of the Ehlers-Danlos syndromes. *Am J Med Genet C Semin Med Genet,* 175**,** 8-26.

Manganelli, P., Giacosa, R., Fietta, P., Zanetti, A. & Neri, T. M. 2003. Familial vasculitides: Churg-Strauss syndrome and Wegener's granulomatosis in 2 first-degree relatives. *J Rheumatol,* 30**,** 618-21.

Marian, A. J. 2012. Challenges in medical applications of whole exome/genome sequencing discoveries. *Trends Cardiovasc Med,* 22**,** 219-23.

Markovic, A. 2012. [Vasculitis and vasculopathy]. *Acta Med Croatica,* 66 Suppl 1**,** 19-24.

Markus, H. S., Martin, R. J., Simpson, M. A., Dong, Y. B., Ali, N., Crosby, A. H. & Powell, J. F. 2002. Diagnostic strategies in CADASIL. *Neurology,* 59**,** 1134-8.

Martinelli, S., De Luca, A., Stellacci, E., Rossi, C., Checquolo, S., Lepri, F., Caputo, V., Silvano, M., Buscherini, F., Consoli, F., Ferrara, G., Digilio, M. C., Cavaliere, M. L., Van Hagen, J. M., Zampino, G., Van Der Burgt, I., Ferrero, G. B., Mazzanti, L., Screpanti, I., Yntema, H. G., Nillesen, W. M., Savarirayan, R., Zenker, M., Dallapiccola, B., Gelb, B. D. & Tartaglia, M. 2010. Heterozygous germline mutations in the CBL tumor-suppressor gene cause a Noonan syndrome-like phenotype. *Am J Hum Genet,* 87**,** 250-7.

Mason, J. C. 2010. Takayasu arteritis--advances in diagnosis and management. *Nat Rev Rheumatol,* 6**,** 406-15.

Mason, J. C., Cowie, M. R., Davies, K. A., Schofield, J. B., Cambridge, J., Jackson, J., So, A., Allard, S. A. & Walport, M. J. 1994. Familial polyarteritis nodosa. *Arthritis Rheum,* 37**,** 1249-53.

Mccrindle, B. W., Rowley, A. H., Newburger, J. W., Burns, J. C., Bolger, A. F., Gewitz, M., Baker, A. L., Jackson, M. A., Takahashi, M., Shah, P. B., Kobayashi, T., Wu, M. H., Saji, T. T., Pahl, E., American Heart Association Rheumatic Fever, E., Kawasaki Disease Committee of the Council on Cardiovascular Disease in The, Y., Council On, C., Stroke, N., Council on Cardiovascular, S., Anesthesia, Council On, E. & Prevention 2017. Diagnosis, Treatment, and Long-Term Management of Kawasaki Disease: A Scientific Statement for Health Professionals From the American Heart Association. *Circulation,* 135**,** e927-e999.

Mccubrey, J. A., Steelman, L. S., Chappell, W. H., Abrams, S. L., Wong, E. W., Chang, F., Lehmann, B., Terrian, D. M., Milella, M., Tafuri, A., Stivala, F., Libra, M., Basecke, J., Evangelisti, C., Martelli, A. M. & Franklin, R. A. 2007. Roles of the Raf/MEK/ERK pathway in cell growth, malignant transformation and drug resistance. *Biochim Biophys Acta,* 1773**,** 1263-84.

Metzker, M. L. 2010. Sequencing technologies - the next generation. *Nat Rev Genet,* 11**,** 31-46.

Meyer, R. D., Latz, C. & Rahimi, N. 2003. Recruitment and activation of phospholipase Cgamma1 by vascular endothelial growth factor receptor-2 are required for tubulogenesis and differentiation of endothelial cells. *J Biol Chem,* 278**,** 16347-55.

Michalickova, K., Susic, M., Willing, M. C., Wenstrup, R. J. & Cole, W. G. 1998. Mutations of the alpha2(V) chain of type V collagen impair matrix assembly and produce ehlers-danlos syndrome type I. *Hum Mol Genet,* 7**,** 249-55.

Milewicz, D. M., Guo, D. C., Tran-Fadulu, V., Lafont, A. L., Papke, C. L., Inamoto, S., Kwartler, C. S. & Pannu, H. 2008. Genetic basis of thoracic aortic aneurysms and dissections: focus on smooth muscle cell contractile dysfunction. *Annu Rev Genomics Hum Genet,* 9**,** 283-302.

Milewicz, D. M., Ostergaard, J. R., Ala-Kokko, L. M., Khan, N., Grange, D. K., Mendoza-Londono, R., Bradley, T. J., Olney, A. H., Ades, L., Maher, J. F., Guo, D., Buja, L. M., Kim, D., Hyland, J. C. & Regalado, E. S. 2010. De novo ACTA2 mutation causes a novel syndrome of multisystemic smooth muscle dysfunction. *Am J Med Genet A,* 152A**,** 2437-43.

Milewicz, D. M., Pyeritz, R. E., Crawford, E. S. & Byers, P. H. 1992. Marfan syndrome: defective synthesis, secretion, and extracellular matrix formation of fibrillin by cultured dermal fibroblasts. *J Clin Invest,* 89**,** 79-86.

Milewicz, D. M., Regalado, E. S., Shendure, J., Nickerson, D. A. & Guo, D. C. 2014. Successes and challenges of using whole exome sequencing to identify novel genes underlying an inherited predisposition for thoracic aortic aneurysms and acute aortic dissections. *Trends Cardiovasc Med,* 24**,** 53-60.

Milewicz, D. M., Witz, A. M., Smith, A. C., Manchester, D. K., Waldstein, G. & Byers, P. H. 1993. Parental somatic and germ-line mosaicism for a multiexon deletion with unusual endpoints in a type III collagen (COL3A1) allele produces Ehlers-Danlos syndrome type IV in the heterozygous offspring. *Am J Hum Genet,* 53**,** 62-70.

Miyake, S., Mullane-Robinson, K. P., Lill, N. L., Douillard, P. & Band, H. 1999. Cbl-mediated negative regulation of platelet-derived growth factor receptor-dependent cell proliferation. A critical role for Cbl tyrosine kinase-binding domain. *J Biol Chem,* 274**,** 16619-28.

Miyatake, S., Miyake, N., Touho, H., Nishimura-Tadaki, A., Kondo, Y., Okada, I., Tsurusaki, Y., Doi, H., Sakai, H., Saitsu, H., Shimojima, K., Yamamoto, T., Higurashi, M., Kawahara, N., Kawauchi, H., Nagasaka, K., Okamoto, N., Mori, T., Koyano, S., Kuroiwa, Y., Taguri, M., Morita, S., Matsubara, Y., Kure, S. & Matsumoto, N. 2012a. Homozygous c.14576G>A variant of RNF213 predicts early-onset and severe form of moyamoya disease. *Neurology,* 78**,** 803-10.

Miyatake, S., Touho, H., Miyake, N., Ohba, C., Doi, H., Saitsu, H., Taguri, M., Morita, S. & Matsumoto, N. 2012b. Sibling cases of moyamoya disease having homozygous and heterozygous c.14576G>A variant in RNF213 showed varying clinical course and severity. *J Hum Genet,* 57**,** 804-6.

Mohammad, A. J., Jacobsson, L. T., Mahr, A. D., Sturfelt, G. & Segelmark, M. 2007. Prevalence of Wegener's granulomatosis, microscopic polyangiitis, polyarteritis nodosa and Churg-Strauss syndrome within a defined population in southern Sweden. *Rheumatology (Oxford),* 46**,** 1329-37.

Montanez, E., Casaroli-Marano, R. P., Vilaro, S. & Pagan, R. 2002. Comparative study of tube assembly in three-dimensional collagen matrix and on Matrigel coats. *Angiogenesis,* 5**,** 167-72.

Morales, E., Pineda, C. & Martinez-Lavin, M. 1991. Takayasu's arteritis in children. *J Rheumatol,* 18**,** 1081-4.

Morano, I., Chai, G. X., Baltas, L. G., Lamounier-Zepter, V., Lutsch, G., Kott, M., Haase, H. & Bader, M. 2000. Smooth-muscle contraction without smooth-muscle myosin. *Nat Cell Biol,* 2**,** 371-5.

Morgan, A. J. & Schwartz, R. A. 2010. Cutaneous polyarteritis nodosa: a comprehensive review. *Int J Dermatol,* 49**,** 750-6.

Morgan, M. D., Harper, L., Williams, J. & Savage, C. 2006. Anti-neutrophil cytoplasm-associated glomerulonephritis. *J Am Soc Nephrol,* 17**,** 1224-34.

Morishita, K. A., Rosendahl, K. & Brogan, P. A. 2011. Familial Takayasu arteritis - a pediatric case and a review of the literature. *Pediatr Rheumatol Online J,* 9**,** 6.

Moritani, T., Hiwatashi, A., Shrier, D. A., Wang, H. Z., Numaguchi, Y. & Westesson, P. L. 2004. CNS vasculitis and vasculopathy: efficacy and usefulness of diffusion-weighted echoplanar MR imaging. *Clin Imaging,* 28**,** 261-70.

Munot, P., Saunders, D. E., Milewicz, D. M., Regalado, E. S., Ostergaard, J. R., Braun, K. P., Kerr, T., Lichtenbelt, K. D., Philip, S., Rittey, C., Jacques, T. S., Cox, T. C. & Ganesan, V. 2012. A novel distinctive cerebrovascular phenotype is associated with heterozygous Arg179 ACTA2 mutations. *Brain,* 135**,** 2506-14.

Nanthapisal, S., Murphy, C., Omoyinmi, E., Hong, Y., Standing, A., Berg, S., Ekelund, M., Jolles, S., Harper, L., Youngstein, T., Gilmour, K., Klein, N. J., Eleftheriou, D. & Brogan, P. A. 2016. Deficiency of Adenosine Deaminase Type 2: A Description of Phenotype and Genotype in Fifteen Cases. *Arthritis Rheumatol,* 68**,** 2314-22.

Navon Elkan, P., Pierce, S. B., Segel, R., Walsh, T., Barash, J., Padeh, S., Zlotogorski, A., Berkun, Y., Press, J. J., Mukamel, M., Voth, I., Hashkes, P. J., Harel, L., Hoffer, V., Ling, E., Yalcinkaya, F., Kasapcopur, O., Lee, M. K., Klevit, R. E., Renbaum, P., Weinberg-Shukron, A., Sener, E. F., Schormair, B., Zeligson, S., Marek-Yagel, D., Strom, T. M., Shohat, M., Singer, A., Rubinow, A., Pras, E., Winkelmann, J., Tekin, M., Anikster, Y., King, M. C. & Levy-Lahad, E. 2014. Mutant adenosine deaminase 2 in a polyarteritis nodosa vasculopathy. *N Engl J Med,* 370**,** 921-31.

Newburger, J. W. & Fulton, D. R. 2004. Kawasaki disease. *Curr Opin Pediatr,* 16**,** 508-14.

Newburger, J. W., Takahashi, M., Gerber, M. A., Gewitz, M. H., Tani, L. Y., Burns, J. C., Shulman, S. T., Bolger, A. F., Ferrieri, P., Baltimore, R. S., Wilson, W.

R., Baddour, L. M., Levison, M. E., Pallasch, T. J., Falace, D. A., Taubert, K. A., Committee on Rheumatic Fever, E., Kawasaki, D., Council on Cardiovascular Disease in The, Y., American Heart, A. & American Academy Of, P. 2004. Diagnosis, treatment, and long-term management of Kawasaki disease: a statement for health professionals from the Committee on Rheumatic Fever, Endocarditis and Kawasaki Disease, Council on Cardiovascular Disease in the Young, American Heart Association. *Circulation,* 110**,** 2747-71.

Ng, P. C. & Kirkness, E. F. 2010. Whole genome sequencing. *Methods Mol Biol,* 628**,** 215-26.

Ng, S. B., Turner, E. H., Robertson, P. D., Flygare, S. D., Bigham, A. W., Lee, C., Shaffer, T., Wong, M., Bhattacharjee, A., Eichler, E. E., Bamshad, M., Nickerson, D. A. & Shendure, J. 2009. Targeted capture and massively parallel sequencing of 12 human exomes. *Nature,* 461**,** 272-6.

Niemeyer, C. M., Kang, M. W., Shin, D. H., Furlan, I., Erlacher, M., Bunin, N. J., Bunda, S., Finklestein, J. Z., Sakamoto, K. M., Gorr, T. A., Mehta, P., Schmid, I., Kropshofer, G., Corbacioglu, S., Lang, P. J., Klein, C., Schlegel, P. G., Heinzmann, A., Schneider, M., Stary, J., Van Den Heuvel-Eibrink, M. M., Hasle, H., Locatelli, F., Sakai, D., Archambeault, S., Chen, L., Russell, R. C., Sybingco, S. S., Ohh, M., Braun, B. S., Flotho, C. & Loh, M. L. 2010. Germline CBL mutations cause developmental abnormalities and predispose to juvenile myelomonocytic leukemia. *Nat Genet,* 42**,** 794-800.

Numano, F., Okawara, M., Inomata, H. & Kobayashi, Y. 2000. Takayasu's arteritis. *Lancet,* 356**,** 1023-5.

Oda, H., Nakagawa, K., Abe, J., Awaya, T., Funabiki, M., Hijikata, A., Nishikomori, R., Funatsuka, M., Ohshima, Y., Sugawara, Y., Yasumi, T., Kato, H., Shirai, T., Ohara, O., Fujita, T. & Heike, T. 2014. Aicardi-Goutieres syndrome is caused by IFIH1 mutations. *Am J Hum Genet,* 95**,** 121-5.

Ogawa, K., Nagahiro, S., Arakaki, R., Ishimaru, N., Kobayashi, M. & Hayashi, Y. 2003. Anti-alpha-fodrin autoantibodies in Moyamoya disease. *Stroke,* 34**,** e244-6.

Ohkubo, K., Sakai, Y., Inoue, H., Akamine, S., Ishizaki, Y., Matsushita, Y., Sanefuji, M., Torisu, H., Ihara, K., Sardiello, M. & Hara, T. 2015. Moyamoya disease susceptibility gene RNF213 links inflammatory and angiogenic signals in endothelial cells. *Sci Rep,* 5**,** 13191.

Omoyinmi, E., Standing, A., Keylock, A., Price-Kuehne, F., Melo Gomes, S., Rowczenio, D., Nanthapisal, S., Cullup, T., Nyanhete, R., Ashton, E., Murphy, C., Clarke, M., Ahlfors, H., Jenkins, L., Gilmour, K., Eleftheriou, D., Lachmann, H. J., Hawkins, P. N., Klein, N. & Brogan, P. A. 2017. Clinical impact of a targeted next-generation sequencing gene panel for autoinflammation and vasculitis. *PLoS One,* 12**,** e0181874.

Onouchi, Y., Gunji, T., Burns, J. C., Shimizu, C., Newburger, J. W., Yashiro, M., Nakamura, Y., Yanagawa, H., Wakui, K., Fukushima, Y., Kishi, F., Hamamoto, K., Terai, M., Sato, Y., Ouchi, K., Saji, T., Nariai, A., Kaburagi, Y., Yoshikawa, T., Suzuki, K., Tanaka, T., Nagai, T., Cho, H., Fujino, A., Sekine, A., Nakamichi, R., Tsunoda, T., Kawasaki, T., Nakamura, Y. & Hata, A. 2008. ITPKC functional polymorphism associated with Kawasaki disease susceptibility and formation of coronary artery aneurysms. *Nat Genet,* 40**,** 35-42.

Onouchi, Y., Ozaki, K., Buns, J. C., Shimizu, C., Hamada, H., Honda, T., Terai, M., Honda, A., Takeuchi, T., Shibuta, S., Suenaga, T., Suzuki, H., Higashi, K., Yasukawa, K., Suzuki, Y., Sasago, K., Kemmotsu, Y., Takatsuki, S., Saji, T., Yoshikawa, T., Nagai, T., Hamamoto, K., Kishi, F., Ouchi, K., Sato, Y., Newburger, J. W., Baker, A. L., Shulman, S. T., Rowley, A. H., Yashiro, M., Nakamura, Y., Wakui, K., Fukushima, Y., Fujino, A., Tsunoda, T., Kawasaki, T., Hata, A., Nakamura, Y. & Tanaka, T. 2010. Common variants in CASP3 confer susceptibility to Kawasaki disease. *Hum Mol Genet,* 19**,** 2898-906.

Onouchi, Y., Ozaki, K., Burns, J. C., Shimizu, C., Terai, M., Hamada, H., Honda, T., Suzuki, H., Suenaga, T., Takeuchi, T., Yoshikawa, N., Suzuki, Y., Yasukawa, K., Ebata, R., Higashi, K., Saji, T., Kemmotsu, Y., Takatsuki, S., Ouchi, K., Kishi, F., Yoshikawa, T., Nagai, T., Hamamoto, K., Sato, Y., Honda, A., Kobayashi, H., Sato, J., Shibuta, S., Miyawaki, M., Oishi, K., Yamaga, H., Aoyagi, N., Iwahashi, S., Miyashita, R., Murata, Y., Sasago, K., Takahashi, A., Kamatani, N., Kubo, M., Tsunoda, T., Hata, A., Nakamura, Y., Tanaka, T., Japan Kawasaki Disease Genome, C. & Consortium, U. S. K. D. G. 2012. A genome-wide association study identifies three new risk loci for Kawasaki disease. *Nat Genet,* 44**,** 517-21.

Onouchi, Y., Tamari, M., Takahashi, A., Tsunoda, T., Yashiro, M., Nakamura, Y., Yanagawa, H., Wakui, K., Fukushima, Y., Kawasaki, T., Nakamura, Y. & Hata, A. 2007. A genomewide linkage analysis of Kawasaki disease: evidence for linkage to chromosome 12. *J Hum Genet,* 52**,** 179-90.

Owens, G. K. 1995. Regulation of differentiation of vascular smooth muscle cells. *Physiol Rev,* 75**,** 487-517.

Ozen, S. 2017. The changing face of polyarteritis nodosa and necrotizing vasculitis. *Nat Rev Rheumatol,* 13**,** 381-386.

Ozen, S., Anton, J., Arisoy, N., Bakkaloglu, A., Besbas, N., Brogan, P., Garcia-Consuegra, J., Dolezalova, P., Dressler, F., Duzova, A., Ferriani, V. P., Hilario, M. O., Ibanez-Rubio, M., Kasapcopur, O., Kuis, W., Lehman, T. J., Nemcova, D., Nielsen, S., Oliveira, S. K., Schikler, K., Sztajnbok, F., Terreri, M. T., Zulian, F. & Woo, P. 2004. Juvenile polyarteritis: results of a multicenter survey of 110 children. *J Pediatr,* 145**,** 517-22.

Ozen, S., Bakkaloglu, A., Dusunsel, R., Soylemezoglu, O., Ozaltin, F., Poyrazoglu, H., Kasapcopur, O., Ozkaya, O., Yalcinkaya, F., Balat, A., Kural, N., Donmez, O., Alpay, H., Anarat, A., Mir, S., Gur-Guven, A., Sonmez, F., Gok, F. &

Turkish Pediatric Vasculitis Study, G. 2007. Childhood vasculitides in Turkey: a nationwide survey. *Clin Rheumatol,* 26**,** 196-200.

Ozen, S., Pistorio, A., Iusan, S. M., Bakkaloglu, A., Herlin, T., Brik, R., Buoncompagni, A., Lazar, C., Bilge, I., Uziel, Y., Rigante, D., Cantarini, L., Hilario, M. O., Silva, C. A., Alegria, M., Norambuena, X., Belot, A., Berkun, Y., Estrella, A. I., Olivieri, A. N., Alpigiani, M. G., Rumba, I., Sztajnbok, F., Tambic-Bukovac, L., Breda, L., Al-Mayouf, S., Mihaylova, D., Chasnyk, V., Sengler, C., Klein-Gitelman, M., Djeddi, D., Nuno, L., Pruunsild, C., Brunner, J., Kondi, A., Pagava, K., Pederzoli, S., Martini, A., Ruperto, N. & Paediatric Rheumatology International Trials, O. 2010. EULAR/PRINTO/PRES criteria for Henoch-Schonlein purpura, childhood polyarteritis nodosa, childhood Wegener granulomatosis and childhood Takayasu arteritis: Ankara 2008. Part II: Final classification criteria. *Ann Rheum Dis,* 69**,** 798-806.

Ozen, S., Ruperto, N., Dillon, M. J., Bagga, A., Barron, K., Davin, J. C., Kawasaki, T., Lindsley, C., Petty, R. E., Prieur, A. M., Ravelli, A. & Woo, P. 2006. EULAR/PReS endorsed consensus criteria for the classification of childhood vasculitides. *Ann Rheum Dis,* 65**,** 936-41.

Pagnoux, C., Cohen, P. & Guillevin, L. 2006. Vasculitides secondary to infections. *Clin Exp Rheumatol,* 24**,** S71-81.

Panegyres, P. K., Morris, J. G., O'neill, P. J. & Balleine, R. 1993. Moyamoya-like disease with inflammation. *Eur Neurol,* 33**,** 260-3.

Pannu, H., Fadulu, V. T., Chang, J., Lafont, A., Hasham, S. N., Sparks, E., Giampietro, P. F., Zaleski, C., Estrera, A. L., Safi, H. J., Shete, S., Willing, M. C., Raman, C. S. & Milewicz, D. M. 2005. Mutations in transforming growth factor-beta receptor type II cause familial thoracic aortic aneurysms and dissections. *Circulation,* 112**,** 513-20.

Pannu, H., Tran-Fadulu, V., Papke, C. L., Scherer, S., Liu, Y., Presley, C., Guo, D., Estrera, A. L., Safi, H. J., Brasier, A. R., Vick, G. W., Marian, A. J., Raman, C. S., Buja, L. M. & Milewicz, D. M. 2007. MYH11 mutations result in a distinct vascular pathology driven by insulin-like growth factor 1 and angiotensin II. *Hum Mol Genet,* 16**,** 2453-62.

Papavasiliou, A., Bazigou-Fotopoulou, H. & Ikeda, H. 2007. Familial Moyamoya disease in two European children. *J Child Neurol,* 22**,** 1371-6.

Park, Y. W., Han, J. W., Park, I. S., Kim, C. H., Yun, Y. S., Cha, S. H., Ma, J. S., Lee, S. B., Kim, C. H., Lee, H. J. & Tockgo, Y. C. 2005. Epidemiologic picture of Kawasaki disease in Korea, 2000-2002. *Pediatr Int,* 47**,** 382-7.

Parmacek, M. S. 2007. Myocardin-related transcription factors: critical coactivators regulating cardiovascular development and adaptation. *Circ Res,* 100**,** 633-44.

Pendergraft, W. F., 3rd & Nachman, P. H. 2015. Recent pathogenetic advances in ANCA-associated vasculitis. *Presse Med,* 44**,** e223-9.

Pennock, S. & Wang, Z. 2008. A tale of two Cbls: interplay of c-Cbl and Cbl-b in epidermal growth factor receptor downregulation. *Mol Cell Biol,* 28**,** 3020-37.

Pepin, M. G., Murray, M. L. & Byers, P. H. 1993. Vascular Ehlers-Danlos Syndrome. *In:* PAGON, R. A., ADAM, M. P., ARDINGER, H. H., WALLACE, S. E., AMEMIYA, A., BEAN, L. J. H., BIRD, T. D., LEDBETTER, N., MEFFORD, H. C., SMITH, R. J. H. & STEPHENS, K. (eds.) *GeneReviews(R).* Seattle (WA).

Perez, B., Mechinaud, F., Galambrun, C., Ben Romdhane, N., Isidor, B., Philip, N., Derain-Court, J., Cassinat, B., Lachenaud, J., Kaltenbach, S., Salmon, A., Desiree, C., Pereira, S., Menot, M. L., Royer, N., Fenneteau, O., Baruchel, A., Chomienne, C., Verloes, A. & Cave, H. 2010. Germline mutations of the CBL gene define a new genetic syndrome with predisposition to juvenile myelomonocytic leukaemia. *J Med Genet,* 47**,** 686-91.

Phi, J. H., Wang, K. C., Lee, J. Y. & Kim, S. K. 2015. Moyamoya Syndrome: A Window of Moyamoya Disease. *J Korean Neurosurg Soc,* 57**,** 408-14.

Pickart, C. M. 2001. Mechanisms underlying ubiquitination. *Annu Rev Biochem,* 70**,** 503-33.

Pickart, C. M. & Eddins, M. J. 2004. Ubiquitin: structures, functions, mechanisms. *Biochim Biophys Acta,* 1695**,** 55-72.

Pinna, G. S., Kafetzis, D. A., Tselkas, O. I. & Skevaki, C. L. 2008. Kawasaki disease: an overview. *Curr Opin Infect Dis,* 21**,** 263-70.

Polo, S. 2012. Signaling-mediated control of ubiquitin ligases in endocytosis. *BMC Biol,* 10**,** 25.

Popa, E. R. & Tervaert, J. W. 2003. The relation between Staphylococcus aureus and Wegener's granulomatosis: current knowledge and future directions. *Intern Med,* 42**,** 771-80.

Punnoose, A. R., Lynm, C. & Golub, R. M. 2012. JAMA patient page. Henoch-Schonlein purpura. *JAMA,* 307**,** 742.

Putnam, E. A., Zhang, H., Ramirez, F. & Milewicz, D. M. 1995. Fibrillin-2 (FBN2) mutations result in the Marfan-like disorder, congenital contractural arachnodactyly. *Nat Genet,* 11**,** 456-8.

Rabbani, B., Tekin, M. & Mahdieh, N. 2014. The promise of whole-exome sequencing in medical genetics. *J Hum Genet,* 59**,** 5-15.

Rahimi, N. 2009. A role for protein ubiquitination in VEGFR-2 signalling and angiogenesis. *Biochem Soc Trans,* 37**,** 1189-92.

Ramesh, V., Bernardi, B., Stafa, A., Garone, C., Franzoni, E., Abinun, M., Mitchell, P., Mitra, D., Friswell, M., Nelson, J., Shalev, S. A., Rice, G. I., Gornall, H.,

Szynkiewicz, M., Aymard, F., Ganesan, V., Prendiville, J., Livingston, J. H. & Crow, Y. J. 2010. Intracerebral large artery disease in Aicardi-Goutieres syndrome implicates SAMHD1 in vascular homeostasis. *Dev Med Child Neurol,* 52**,** 725-32.

Rauen, K. A. 2013. The RASopathies. *Annu Rev Genomics Hum Genet,* 14**,** 355-69.

Rav-Acha, M., Plot, L., Peled, N. & Amital, H. 2007. Coronary involvement in Takayasu's arteritis. *Autoimmun Rev,* 6**,** 566-71.

Rea, D., Brandsema, J. F., Armstrong, D., Parkin, P. C., Deveber, G., Macgregor, D., Logan, W. J. & Askalan, R. 2009. Cerebral arteriopathy in children with neurofibromatosis type 1. *Pediatrics,* 124**,** e476-83.

Reddi, A. L., Ying, G., Duan, L., Chen, G., Dimri, M., Douillard, P., Druker, B. J., Naramura, M., Band, V. & Band, H. 2007. Binding of Cbl to a phospholipase Cgamma1-docking site on platelet-derived growth factor receptor beta provides a dual mechanism of negative regulation. *J Biol Chem,* 282**,** 29336-47.

Regalado, E. S., Guo, D. C., Villamizar, C., Avidan, N., Gilchrist, D., Mcgillivray, B., Clarke, L., Bernier, F., Santos-Cortez, R. L., Leal, S. M., Bertoli-Avella, A. M., Shendure, J., Rieder, M. J., Nickerson, D. A., Project, N. G. E. S. & Milewicz, D. M. 2011. Exome sequencing identifies SMAD3 mutations as a cause of familial thoracic aortic aneurysm and dissection with intracranial and other arterial aneurysms. *Circ Res,* 109**,** 680-6.

Reid, A. J., Bhattacharjee, M. B., Regalado, E. S., Milewicz, A. L., El-Hakam, L. M., Dauser, R. C. & Milewicz, D. M. 2010. Diffuse and uncontrolled vascular smooth muscle cell proliferation in rapidly progressing pediatric moyamoya disease. *J Neurosurg Pediatr,* 6**,** 244-9.

Reis-Filho, J. S. 2009. Next-generation sequencing. *Breast Cancer Res,* 11 Suppl 3**,** S12.

Renard, M., Callewaert, B., Baetens, M., Campens, L., Macdermot, K., Fryns, J. P., Bonduelle, M., Dietz, H. C., Gaspar, I. M., Cavaco, D., Stattin, E. L., Schrander-Stumpel, C., Coucke, P., Loeys, B., De Paepe, A. & De Backer, J. 2013. Novel MYH11 and ACTA2 mutations reveal a role for enhanced TGFbeta signaling in FTAAD. *Int J Cardiol,* 165**,** 314-21.

Renauer, P. A., Saruhan-Direskeneli, G., Coit, P., Adler, A., Aksu, K., Keser, G., Alibaz-Oner, F., Aydin, S. Z., Kamali, S., Inanc, M., Carette, S., Cuthbertson, D., Hoffman, G. S., Akar, S., Onen, F., Akkoc, N., Khalidi, N. A., Koening, C., Karadag, O., Kiraz, S., Langford, C. A., Maksimowicz-Mckinnon, K., Mcalear, C. A., Ozbalkan, Z., Ates, A., Karaaslan, Y., Duzgun, N., Monach, P. A., Ozer, H. T., Erken, E., Ozturk, M. A., Yazici, A., Cefle, A., Onat, A. M., Kisacik, B., Pagnoux, C., Kasifoglu, T., Seyahi, E., Fresko, I., Seo, P., Sreih, A. G., Warrington, K. J., Ytterberg, S. R., Cobankara, V., Cunninghame-Graham, D. S., Vyse, T. J., Pamuk, O. N., Tunc, S. E., Dalkilic,

E., Bicakcigil, M., Yentur, S. P., Wren, J. D., Merkel, P. A., Direskeneli, H. & Sawalha, A. H. 2015. Identification of Susceptibility Loci in IL6, RPS9/LILRB3, and an Intergenic Locus on Chromosome 21q22 in Takayasu Arteritis in a Genome-Wide Association Study. *Arthritis Rheumatol,* 67**,** 1361-8.

Rice, G., Newman, W. G., Dean, J., Patrick, T., Parmar, R., Flintoff, K., Robins, P., Harvey, S., Hollis, T., O'hara, A., Herrick, A. L., Bowden, A. P., Perrino, F. W., Lindahl, T., Barnes, D. E. & Crow, Y. J. 2007. Heterozygous mutations in TREX1 cause familial chilblain lupus and dominant Aicardi-Goutieres syndrome. *Am J Hum Genet,* 80**,** 811-5.

Rice, G. I., Bond, J., Asipu, A., Brunette, R. L., Manfield, I. W., Carr, I. M., Fuller, J. C., Jackson, R. M., Lamb, T., Briggs, T. A., Ali, M., Gornall, H., Couthard, L. R., Aeby, A., Attard-Montalto, S. P., Bertini, E., Bodemer, C., Brockmann, K., Brueton, L. A., Corry, P. C., Desguerre, I., Fazzi, E., Cazorla, A. G., Gener, B., Hamel, B. C., Heiberg, A., Hunter, M., Van Der Knaap, M. S., Kumar, R., Lagae, L., Landrieu, P. G., Lourenco, C. M., Marom, D., Mcdermott, M. F., Van Der Merwe, W., Orcesi, S., Prendiville, J. S., Rasmussen, M., Shalev, S. A., Soler, D. M., Shinawi, M., Spiegel, R., Tan, T. Y., Vanderver, A., Wakeling, E. L., Wassmer, E., Whittaker, E., Lebon, P., Stetson, D. B., Bonthron, D. T. & Crow, Y. J. 2009. Mutations involved in Aicardi-Goutieres syndrome implicate SAMHD1 as regulator of the innate immune response. *Nat Genet,* 41**,** 829-32.

Rice, G. I., Del Toro Duany, Y., Jenkinson, E. M., Forte, G. M., Anderson, B. H., Ariaudo, G., Bader-Meunier, B., Baildam, E. M., Battini, R., Beresford, M. W., Casarano, M., Chouchane, M., Cimaz, R., Collins, A. E., Cordeiro, N. J., Dale, R. C., Davidson, J. E., De Waele, L., Desguerre, I., Faivre, L., Fazzi, E., Isidor, B., Lagae, L., Latchman, A. R., Lebon, P., Li, C., Livingston, J. H., Lourenco, C. M., Mancardi, M. M., Masurel-Paulet, A., Mcinnes, I. B., Menezes, M. P., Mignot, C., O'sullivan, J., Orcesi, S., Picco, P. P., Riva, E., Robinson, R. A., Rodriguez, D., Salvatici, E., Scott, C., Szybowska, M., Tolmie, J. L., Vanderver, A., Vanhulle, C., Vieira, J. P., Webb, K., Whitney, R. N., Williams, S. G., Wolfe, L. A., Zuberi, S. M., Hur, S. & Crow, Y. J. 2014. Gain-of-function mutations in IFIH1 cause a spectrum of human disease phenotypes associated with upregulated type I interferon signaling. *Nat Genet,* 46**,** 503-509.

Rice, G. I., Kasher, P. R., Forte, G. M., Mannion, N. M., Greenwood, S. M., Szynkiewicz, M., Dickerson, J. E., Bhaskar, S. S., Zampini, M., Briggs, T. A., Jenkinson, E. M., Bacino, C. A., Battini, R., Bertini, E., Brogan, P. A., Brueton, L. A., Carpanelli, M., De Laet, C., De Lonlay, P., Del Toro, M., Desguerre, I., Fazzi, E., Garcia-Cazorla, A., Heiberg, A., Kawaguchi, M., Kumar, R., Lin, J. P., Lourenco, C. M., Male, A. M., Marques, W., Jr., Mignot, C., Olivieri, I., Orcesi, S., Prabhakar, P., Rasmussen, M., Robinson, R. A., Rozenberg, F., Schmidt, J. L., Steindl, K., Tan, T. Y., Van Der Merwe, W. G., Vanderver, A., Vassallo, G., Wakeling, E. L., Wassmer, E., Whittaker, E., Livingston, J. H., Lebon, P., Suzuki, T., Mclaughlin, P. J., Keegan, L. P., O'connell, M. A., Lovell, S. C. & Crow, Y. J. 2012. Mutations in ADAR1

cause Aicardi-Goutieres syndrome associated with a type I interferon signature. *Nat Genet,* 44**,** 1243-8.

Richards, B. L., March, L. & Gabriel, S. E. 2010. Epidemiology of large-vessel vasculidities. *Best Pract Res Clin Rheumatol,* 24**,** 871-83.

Rienhoff, H. Y., Jr., Yeo, C. Y., Morissette, R., Khrebtukova, I., Melnick, J., Luo, S., Leng, N., Kim, Y. J., Schroth, G., Westwick, J., Vogel, H., Mcdonnell, N., Hall, J. G. & Whitman, M. 2013. A mutation in TGFB3 associated with a syndrome of low muscle mass, growth retardation, distal arthrogryposis and clinical features overlapping with Marfan and Loeys-Dietz syndrome. *Am J Med Genet A,* 161A**,** 2040-6.

Ross, R. & Bornstein, P. 1969. The elastic fiber. I. The separation and partial characterization of its macromolecular components. *J Cell Biol,* 40**,** 366-81.

Runo, J. R., Vnencak-Jones, C. L., Prince, M., Loyd, J. E., Wheeler, L., Robbins, I. M., Lane, K. B., Newman, J. H., Johnson, J., Nichols, W. C. & Phillips, J. A., 3rd 2003. Pulmonary veno-occlusive disease caused by an inherited mutation in bone morphogenetic protein receptor II. *Am J Respir Crit Care Med,* 167**,** 889-94.

Ruperto, N., Ozen, S., Pistorio, A., Dolezalova, P., Brogan, P., Cabral, D. A., Cuttica, R., Khubchandani, R., Lovell, D. J., O'neil, K. M., Quartier, P., Ravelli, A., Iusan, S. M., Filocamo, G., Magalhaes, C. S., Unsal, E., Oliveira, S., Bracaglia, C., Bagga, A., Stanevicha, V., Manzoni, S. M., Pratsidou, P., Lepore, L., Espada, G., Kone-Paut, I., Zulian, F., Barone, P., Bircan, Z., Maldonado Mdel, R., Russo, R., Vilca, I., Tullus, K., Cimaz, R., Horneff, G., Anton, J., Garay, S., Nielsen, S., Barbano, G., Martini, A. & Paediatric Rheumatology International Trials, O. 2010. EULAR/PRINTO/PRES criteria for Henoch-Schonlein purpura, childhood polyarteritis nodosa, childhood Wegener granulomatosis and childhood Takayasu arteritis: Ankara 2008. Part I: Overall methodology and clinical characterisation. *Ann Rheum Dis,* 69**,** 790-7.

Sadowski, M. & Sarcevic, B. 2010. Mechanisms of mono- and poly-ubiquitination: Ubiquitination specificity depends on compatibility between the E2 catalytic core and amino acid residues proximal to the lysine. *Cell Div,* 5**,** 19.

Sargin, B., Choudhary, C., Crosetto, N., Schmidt, M. H., Grundler, R., Rensinghoff, M., Thiessen, C., Tickenbrock, L., Schwable, J., Brandts, C., August, B., Koschmieder, S., Bandi, S. R., Duyster, J., Berdel, W. E., Muller-Tidow, C., Dikic, I. & Serve, H. 2007. Flt3-dependent transformation by inactivating c-Cbl mutations in AML. *Blood,* 110**,** 1004-12.

Saruhan-Direskeneli, G., Hughes, T., Aksu, K., Keser, G., Coit, P., Aydin, S. Z., Alibaz-Oner, F., Kamali, S., Inanc, M., Carette, S., Hoffman, G. S., Akar, S., Onen, F., Akkoc, N., Khalidi, N. A., Koening, C., Karadag, O., Kiraz, S., Langford, C. A., Mcalear, C. A., Ozbalkan, Z., Ates, A., Karaaslan, Y., Maksimowicz-Mckinnon, K., Monach, P. A., Ozer, H. T., Seyahi, E., Fresko,

I., Cefle, A., Seo, P., Warrington, K. J., Ozturk, M. A., Ytterberg, S. R., Cobankara, V., Onat, A. M., Guthridge, J. M., James, J. A., Tunc, E., Duzgun, N., Bicakcigil, M., Yentur, S. P., Merkel, P. A., Direskeneli, H. & Sawalha, A. H. 2013. Identification of multiple genetic susceptibility loci in Takayasu arteritis. *Am J Hum Genet,* 93**,** 298-305.

Scheffner, M. & Kumar, S. 2014. Mammalian HECT ubiquitin-protein ligases: biological and pathophysiological aspects. *Biochim Biophys Acta,* 1843**,** 61-74.

Schmidt, M. H. & Dikic, I. 2005. The Cbl interactome and its functions. *Nat Rev Mol Cell Biol,* 6**,** 907-18.

Scott, R. M. & Smith, E. R. 2009. Moyamoya disease and moyamoya syndrome. *N Engl J Med,* 360**,** 1226-37.

Seaby, E. G., Gilbert, R. D., Andreoletti, G., Pengelly, R. J., Mercer, C., Hunt, D. & Ennis, S. 2017. Unexpected Findings in a Child with Atypical Hemolytic Uremic Syndrome: An Example of How Genomics Is Changing the Clinical Diagnostic Paradigm. *Front Pediatr,* 5**,** 113.

Shah, S., Kumar, Y., Mclean, B., Churchill, A., Stoodley, N., Rankin, J., Rizzu, P., Van Der Knaap, M. & Jardine, P. 2010. A dominantly inherited mutation in collagen IV A1 (COL4A1) causing childhood onset stroke without porencephaly. *Eur J Paediatr Neurol,* 14**,** 182-7.

Shen, B., Zhang, W., Zhang, J., Zhou, J., Wang, J., Chen, L., Wang, L., Hodgkins, A., Iyer, V., Huang, X. & Skarnes, W. C. 2014. Efficient genome modification by CRISPR-Cas9 nickase with minimal off-target effects. *Nat Methods,* 11**,** 399-402.

Singh, A. J., Meyer, R. D., Navruzbekov, G., Shelke, R., Duan, L., Band, H., Leeman, S. E. & Rahimi, N. 2007. A critical role for the E3-ligase activity of c-Cbl in VEGFR-2-mediated PLCgamma1 activation and angiogenesis. *Proc Natl Acad Sci U S A,* 104**,** 5413-8.

Singh, N., Hughes, M., Sebire, N. & Brogan, P. 2013. Takayasu arteritis in infancy. *Rheumatology (Oxford),* 52**,** 2093-5.

Smit, J. J. & Sixma, T. K. 2014. RBR E3-ligases at work. *EMBO Rep,* 15**,** 142-54.

Sonobe, S., Fujimura, M., Niizuma, K., Fujimura, T., Furudate, S., Nishijima, Y., Kure, S. & Tominaga, T. 2014. Increased vascular MMP-9 in mice lacking RNF213: moyamoya disease susceptibility gene. *Neuroreport,* 25**,** 1442-6.

Starosolski, Z., Villamizar, C. A., Rendon, D., Paldino, M. J., Milewicz, D. M., Ghaghada, K. B. & Annapragada, A. V. 2015. Ultra High-Resolution In vivo Computed Tomography Imaging of Mouse Cerebrovasculature Using a Long Circulating Blood Pool Contrast Agent. *Sci Rep,* 5**,** 10178.

Stenson, P. D., Ball, E. V., Howells, K., Phillips, A. D., Mort, M. & Cooper, D. N. 2009. The Human Gene Mutation Database: providing a comprehensive central mutation database for molecular diagnostics and personalized genomics. *Hum Genomics,* 4**,** 69-72.

Sun, Y. 2006. E3 ubiquitin ligases as cancer targets and biomarkers. *Neoplasia,* 8**,** 645-54.

Sun, Y., Ruivenkamp, C. A., Hoffer, M. J., Vrijenhoek, T., Kriek, M., Van Asperen, C. J., Den Dunnen, J. T. & Santen, G. W. 2015. Next-generation diagnostics: gene panel, exome, or whole genome? *Hum Mutat,* 36**,** 648-55.

Superti-Furga, A., Gugler, E., Gitzelmann, R. & Steinmann, B. 1988. Ehlers-Danlos syndrome type IV: a multi-exon deletion in one of the two COL3A1 alleles affecting structure, stability, and processing of type III procollagen. *J Biol Chem,* 263**,** 6226-32.

Suresh, E. 2006. Diagnostic approach to patients with suspected vasculitis. *Postgrad Med J,* 82**,** 483-8.

Suzuki, J. & Takaku, A. 1969. Cerebrovascular "moyamoya" disease. Disease showing abnormal net-like vessels in base of brain. *Arch Neurol,* 20**,** 288-99.

Swaminathan, G. & Tsygankov, A. Y. 2006. The Cbl family proteins: ring leaders in regulation of cell signaling. *J Cell Physiol,* 209**,** 21-43.

Symoens, S., Syx, D., Malfait, F., Callewaert, B., De Backer, J., Vanakker, O., Coucke, P. & De Paepe, A. 2012. Comprehensive molecular analysis demonstrates type V collagen mutations in over 90% of patients with classic EDS and allows to refine diagnostic criteria. *Hum Mutat,* 33**,** 1485-93.

Szudek, J., Evans, D. G. & Friedman, J. M. 2003. Patterns of associations of clinical features in neurofibromatosis 1 (NF1). *Hum Genet,* 112**,** 289-97.

Takayasu, M. 1908. A case with peculiar changes of the retinal central vessels (in Japanese). *Acta Soc Ophthal Jpn,* 12**,** 554-5.

Tanigawara, T., Yamada, H., Sakai, N., Andoh, T., Deguchi, K. & Iwamura, M. 1997. Studies on cytomegalovirus and Epstein-Barr virus infection in moyamoya disease. *Clin Neurol Neurosurg,* 99 Suppl 2**,** S225-8.

Tepper, O. M., Galiano, R. D., Capla, J. M., Kalka, C., Gagne, P. J., Jacobowitz, G. R., Levine, J. P. & Gurtner, G. C. 2002. Human endothelial progenitor cells from type II diabetics exhibit impaired proliferation, adhesion, and incorporation into vascular structures. *Circulation,* 106**,** 2781-6.

Terao, C., Yoshifuji, H., Kimura, A., Matsumura, T., Ohmura, K., Takahashi, M., Shimizu, M., Kawaguchi, T., Chen, Z., Naruse, T. K., Sato-Otsubo, A., Ebana, Y., Maejima, Y., Kinoshita, H., Murakami, K., Kawabata, D., Wada, Y., Narita, I., Tazaki, J., Kawaguchi, Y., Yamanaka, H., Yurugi, K., Miura, Y.,

Maekawa, T., Ogawa, S., Komuro, I., Nagai, R., Yamada, R., Tabara, Y., Isobe, M., Mimori, T. & Matsuda, F. 2013. Two susceptibility loci to Takayasu arteritis reveal a synergistic role of the IL12B and HLA-B regions in a Japanese population. *Am J Hum Genet,* 93**,** 289-97.

Thiele, H., Du Moulin, M., Barczyk, K., George, C., Schwindt, W., Nurnberg, G., Frosch, M., Kurlemann, G., Roth, J., Nurnberg, P. & Rutsch, F. 2010. Cerebral arterial stenoses and stroke: novel features of Aicardi-Goutieres syndrome caused by the Arg164X mutation in SAMHD1 are associated with altered cytokine expression. *Hum Mutat,* 31**,** E1836-50.

Thien, C. B. & Langdon, W. Y. 2001. Cbl: many adaptations to regulate protein tyrosine kinases. *Nat Rev Mol Cell Biol,* 2**,** 294-307.

Thien, C. B. & Langdon, W. Y. 2005. c-Cbl and Cbl-b ubiquitin ligases: substrate diversity and the negative regulation of signalling responses. *Biochem J,* 391**,** 153-66.

Thien, C. B., Walker, F. & Langdon, W. Y. 2001. RING finger mutations that abolish c-Cbl-directed polyubiquitination and downregulation of the EGF receptor are insufficient for cell transformation. *Mol Cell,* 7**,** 355-65.

Tidyman, W. E. & Rauen, K. A. 2009. The RASopathies: developmental syndromes of Ras/MAPK pathway dysregulation. *Curr Opin Genet Dev,* 19**,** 230-6.

Toshihiko, N. 1996. Current status of large and small vessel vasculitis in Japan. *Int J Cardiol,* 54 Suppl**,** S91-8.

Toth, J., Kovacs, M., Wang, F., Nyitray, L. & Sellers, J. R. 2005. Myosin V from Drosophila reveals diversity of motor mechanisms within the myosin V family. *J Biol Chem,* 280**,** 30594-603.

Tsai, F. J., Lee, Y. C., Chang, J. S., Huang, L. M., Huang, F. Y., Chiu, N. C., Chen, M. R., Chi, H., Lee, Y. J., Chang, L. C., Liu, Y. M., Wang, H. H., Chen, C. H., Chen, Y. T. & Wu, J. Y. 2011. Identification of novel susceptibility Loci for kawasaki disease in a Han chinese population by a genome-wide association study. *PLoS One,* 6**,** e16853.

Tsipouras, P., Byers, P. H., Schwartz, R. C., Chu, M. L., Weil, D., Pepe, G., Cassidy, S. B. & Ramirez, F. 1986. Ehlers-Danlos syndrome type IV: cosegregation of the phenotype to a COL3A1 allele of type III procollagen. *Hum Genet,* 74**,** 41-6.

Tulloh, R. M. R., Ramanan, A., Brogan, P., Tizard, J., Connolly, G.-M., Harnden, A., Mayon-White, R., Michie, C., Davidson, S., Craggs, P., Brown, K., Lynn, R. & Shingadia, D. 2016. Kawasaki disease. Results of the BPSU survey in UK and Ireland. *Archives of Disease in Childhood,* 101.

Uchino, K., Johnston, S. C., Becker, K. J. & Tirschwell, D. L. 2005. Moyamoya disease in Washington State and California. *Neurology,* 65**,** 956-8.

Ueno, M., Oka, A., Koeda, T., Okamoto, R. & Takeshita, K. 2002. Unilateral occlusion of the middle cerebral artery after varicella-zoster virus infection. *Brain Dev,* 24**,** 106-8.

Vale, R. D. & Milligan, R. A. 2000. The way things move: looking under the hood of molecular motor proteins. *Science,* 288**,** 88-95.

Van De Laar, I. M., Oldenburg, R. A., Pals, G., Roos-Hesselink, J. W., De Graaf, B. M., Verhagen, J. M., Hoedemaekers, Y. M., Willemsen, R., Severijnen, L. A., Venselaar, H., Vriend, G., Pattynama, P. M., Collee, M., Majoor-Krakauer, D., Poldermans, D., Frohn-Mulder, I. M., Micha, D., Timmermans, J., Hilhorst-Hofstee, Y., Bierma-Zeinstra, S. M., Willems, P. J., Kros, J. M., Oei, E. H., Oostra, B. A., Wessels, M. W. & Bertoli-Avella, A. M. 2011. Mutations in SMAD3 cause a syndromic form of aortic aneurysms and dissections with early-onset osteoarthritis. *Nat Genet,* 43**,** 121-6.

Vargiami, E., Sapountzi, E., Samakovitis, D., Batzios, S., Kyriazi, M., Anastasiou, A. & Zafeiriou, D. I. 2014. Moyamoya syndrome and neurofibromatosis type 1. *Ital J Pediatr,* 40**,** 59.

Vogelstein, B. & Kinzler, K. W. 1993. The multistep nature of cancer. *Trends Genet,* 9**,** 138-41.

Volpi, S., Picco, P., Caorsi, R., Candotti, F. & Gattorno, M. 2016. Type I interferonopathies in pediatric rheumatology. *Pediatr Rheumatol Online J,* 14**,** 35.

Wakai, K., Tamakoshi, A., Ikezaki, K., Fukui, M., Kawamura, T., Aoki, R., Kojima, M., Lin, Y. & Ohno, Y. 1997. Epidemiological features of moyamoya disease in Japan: findings from a nationwide survey. *Clin Neurol Neurosurg,* 99 Suppl 2**,** S1-5.

Waller, R., Ahmed, A., Patel, I. & Luqmani, R. 2013. Update on the classification of vasculitis. *Best Pract Res Clin Rheumatol,* 27**,** 3-17.

Wang, L., Guo, D. C., Cao, J., Gong, L., Kamm, K. E., Regalado, E., Li, L., Shete, S., He, W. Q., Zhu, M. S., Offermanns, S., Gilchrist, D., Elefteriades, J., Stull, J. T. & Milewicz, D. M. 2010. Mutations in myosin light chain kinase cause familial aortic dissections. *Am J Hum Genet,* 87**,** 701-7.

Watson, L., Brogan, P., Peart, I., Landes, C., Barnes, N. & Cleary, G. 2014. Diagnosis and assessment of disease activity in takayasu arteritis: a childhood case illustrating the challenge. *Case Rep Rheumatol,* 2014**,** 603171.

Watts, R., Al-Taiar, A., Mooney, J., Scott, D. & Macgregor, A. 2009. The epidemiology of Takayasu arteritis in the UK. *Rheumatology (Oxford),* 48**,** 1008-11.

Wennerberg, K., Rossman, K. L. & Der, C. J. 2005. The Ras superfamily at a glance. *J Cell Sci,* 118**,** 843-6.

Wetterstrand, K. *DNA Sequencing Costs: Data from the NHGRI Genome Sequencing Program (GSP)* [Online]. Available: http://www.genome.gov/sequencingcosts [Accessed 11 September 2015 2015].

Whiteman, P., Hutchinson, S. & Handford, P. A. 2006. Fibrillin-1 misfolding and disease. *Antioxid Redox Signal,* 8**,** 338-46.

Xie, G., Roshandel, D., Sherva, R., Monach, P. A., Lu, E. Y., Kung, T., Carrington, K., Zhang, S. S., Pulit, S. L., Ripke, S., Carette, S., Dellaripa, P. F., Edberg, J. C., Hoffman, G. S., Khalidi, N., Langford, C. A., Mahr, A. D., St Clair, E. W., Seo, P., Specks, U., Spiera, R. F., Stone, J. H., Ytterberg, S. R., Raychaudhuri, S., De Bakker, P. I., Farrer, L. A., Amos, C. I., Merkel, P. A. & Siminovitch, K. A. 2013. Association of granulomatosis with polyangiitis (Wegener's) with HLA-DPB1*04 and SEMA6A gene variants: evidence from genome-wide analysis. *Arthritis Rheum,* 65**,** 2457-68.

Xin, B., Jones, S., Puffenberger, E. G., Hinze, C., Bright, A., Tan, H., Zhou, A., Wu, G., Vargus-Adams, J., Agamanolis, D. & Wang, H. 2011. Homozygous mutation in SAMHD1 gene causes cerebral vasculopathy and early onset stroke. *Proc Natl Acad Sci U S A,* 108**,** 5372-7.

Yamada, H., Deguchi, K., Tanigawara, T., Takenaka, K., Nishimura, Y., Shinoda, J., Hattori, T., Andoh, T. & Sakai, N. 1997. The relationship between moyamoya disease and bacterial infection. *Clin Neurol Neurosurg,* 99 Suppl 2**,** S221-4.

Yamashiro, Y., Nagata, S., Oguchi, S. & Shimizu, T. 1996. Selective increase of V beta 2+ T cells in the small intestinal mucosa in Kawasaki disease. *Pediatr Res,* 39**,** 264-6.

Yang, Y. H., Hung, C. F., Hsu, C. R., Wang, L. C., Chuang, Y. H., Lin, Y. T. & Chiang, B. L. 2005. A nationwide survey on epidemiological characteristics of childhood Henoch-Schonlein purpura in Taiwan. *Rheumatology (Oxford),* 44**,** 618-22.

Zhang, Y., Qin, W., Lu, X., Xu, J., Huang, H., Bai, H., Li, S. & Lin, S. 2017. Programmable base editing of zebrafish genome using a modified CRISPR-Cas9 system. *Nat Commun,* 8**,** 118.

Zhou, Q., Yang, D., Ombrello, A. K., Zavialov, A. V., Toro, C., Zavialov, A. V., Stone, D. L., Chae, J. J., Rosenzweig, S. D., Bishop, K., Barron, K. S., Kuehn, H. S., Hoffmann, P., Negro, A., Tsai, W. L., Cowen, E. W., Pei, W., Milner, J. D., Silvin, C., Heller, T., Chin, D. T., Patronas, N. J., Barber, J. S., Lee, C. C., Wood, G. M., Ling, A., Kelly, S. J., Kleiner, D. E., Mullikin, J. C., Ganson, N. J., Kong, H. H., Hambleton, S., Candotti, F., Quezado, M. M., Calvo, K. R., Alao, H., Barham, B. K., Jones, A., Meschia, J. F., Worrall, B. B., Kasner, S. E., Rich, S. S., Goldbach-Mansky, R., Abinun, M., Chalom, E., Gotte, A. C., Punaro, M., Pascual, V., Verbsky, J. W., Torgerson, T. R., Singer, N. G., Gershon, T. R., Ozen, S., Karadag, O., Fleisher, T. A., Remmers, E. F., Burgess, S. M., Moir, S. L., Gadina, M., Sood, R., Hershfield, M. S., Boehm,

M., Kastner, D. L. & Aksentijevich, I. 2014. Early-onset stroke and vasculopathy associated with mutations in ADA2. *N Engl J Med,* 370**,** 911-20.

Zhou, S., Ambalavanan, A., Rochefort, D., Xie, P., Bourassa, C. V., Hince, P., Dionne-Laporte, A., Spiegelman, D., Gan-Or, Z., Mirarchi, C., Zaharieva, V., Dupre, N., Kobayashi, H., Hitomi, T., Harada, K., Koizumi, A., Xiong, L., Dion, P. A. & Rouleau, G. A. 2016. RNF213 Is Associated with Intracranial Aneurysms in the French-Canadian Population. *Am J Hum Genet,* 99**,** 1072-1085.

Zhu, L., Vranckx, R., Khau Van Kien, P., Lalande, A., Boisset, N., Mathieu, F., Wegman, M., Glancy, L., Gasc, J. M., Brunotte, F., Bruneval, P., Wolf, J. E., Michel, J. B. & Jeunemaitre, X. 2006. Mutations in myosin heavy chain 11 cause a syndrome associating thoracic aortic aneurysm/aortic dissection and patent ductus arteriosus. *Nat Genet,* 38**,** 343-9.

Zwerina, J., Eger, G., Englbrecht, M., Manger, B. & Schett, G. 2009. Churg-Strauss syndrome in childhood: a systematic literature review and clinical comparison with adult patients. *Semin Arthritis Rheum,* 39**,** 108-15.

Appendix

Appendix 1 Stroke protocol investigations

Great Ormond Street Hospital for Children NHS Foundation Trust Arterial Ischaemic Stroke: Clinical Checklist

This clinical checklist is not intended to be comprehensive; it is intended to supplement the conventional history and examination process by prompting the user to ask about or look for clinical factors which are potentially relevant to a child presenting with acute AIS. The aspects of the neurological examination which have been specifically highlighted are partly derived from items used in adult stroke severity scales but are not intended to replace more comprehensive clinical evaluation. If it is not possible to assess any of these parameters it is important to record this and the reasons for this (e.g. child was uncooperative or test was developmentally inappropriate).

History
Time of onset of symptoms
Prior events e.g. TIA
Seizures
Prior trauma to the head or neck
Chickenpox? If so, when?
History of recent infection
Head or neck pain?
Past medical history (incl. history of thrombosis)
Family history (incl. thrombosis, miscarriage)
Medication (& recreational drugs)
Development
Examination
Blood pressure
Peripheral pulses (check for radio-femoral delay)
Oxygen saturation
Temperature
Neurocutaneous signs
Cardiovascular examination
Conscious level (use modified Glasgow Coma Scale)
Neurological examination to include evaluation for:
Cranial nerve function including:
Eye movements (?gaze palsy)
Visual fields

Facial palsy
? Horner's syndrome
Motor deficit (if present specify location and severity using MRC scale)
Ataxia (if present specify location e.g. truncal or limb)
Sensory dysfunction (if present specify location)
Communication (including expressive and receptive language and articulation)
Swallowing
Neglect (if present specify location)Neurocognitive testing if applicable

Imaging

Brain MRI*
MRA circle of Willis*
MRA neck *
Transthoracic echocardiogram

Blood tests

Full blood count and blood film
Urea& electrolytes, liver function tests
ESR
CRP/hsCRP
Blood culture
Serum amyloid A
Haemoglobin electrophoresis if black or Mediterranean ethnicity
Clotting profile
Thrombophilia screen *(at GOSH this will include protein C, protein S, antithrombin, plasminogen, DRVVT, Exner, APC resistance ratio, FVL, MTHFR and PT20210 gene mutations)*
ANA/sdDNA/ENA/ANCA/C3 and C4
IgG/IgM/IgA
ACE
Anticardiolipin antibodies and b2 glycoprotein antibodies
Lupus anticoagulant
Plasma amino acids
Total plasma homocysteine
Plasma lactate
Ammonia
Cholesterol and triglycerides (random)
Plasma urate
Transferrin electrophoresis
Alpha galactosidase A if posterior circulation (to exclude Fabry disease)
Serum globotriaosylceramide if posterior circulation (to exclude Fabry disease)
Serology: mycoplasma, VZV, borellia, HSV1, HSV2
EBV VCA IgM, EBNA, EBV VCA IgG, CMV
Save serum
Save DNA

Urine

Organic acids
Urinary globotriaosylceramide (to exclude Fabry disease)

Saliva

VZV PCR viral load

CSF - Lumbar puncture is indicated in all patients.
Measure opening pressure

CSF MC&S
CSF protein and glucose (remember to check blood glucose at same time)
CSF VZV PCR
CSF VZV specific antibodies paired with serum, for calculation of intrathecal production)
CSF PCR HSV1, HSV2, PCR and CSF HSV specific antibodies
CSF PCR EBV, CMV
CSF mycoplasma IgM and IgG
CSF ACE
CSF lactate
CSF oligoclonal bands paired with serum
CSF save sample

Appendix 2 VIP2 gene list

Gene	Gene name	Chr	Transcript reference
ACTA2	Actin alpha 2	10	NM_001613
BMPR2	Bone morphogenetic protein type II receptor	2	NM_001204
FBN1	Fibrillin1	15	NM_000138
SLC2A10	Solute carrier family 2 (facilitated glucose transporter), member 10	20	NM_004612
TGBR1	Transforming growth factor-beta receptor, type 1	9	NM_001024847
MYH11	Myosin, Heavy Chain 11, Smooth Muscle	3	NM_001040113
RNF213	Ring finger protein 213	17	NM_001256071
GUCY1A3	Guanylate cyclase 1, soluble, alpha 3	4	NM_000856
MYLK	Myosin light chain kinase	3	NM_053025
PRKG1	Protein kinase, cGMP-dependent, type I	10	NM_001098512
SMAD3	SMAD family member 3	15	NM_005902
SMAD4	SMAD family member 4	18	NM_005359
TGFB2	Transforming growth factor, beta 2	1	NM_001135599
HFE	Hemochromatosis	6	NM_000410
RHOD	Ras homolog family member D	11	NM_014578
ELN	Elastin	7	NM_001278939
FBN2	Fibrillin 2	5	NM_001999
NOTCH1	Notch 1	9	NM_017617

ADAM17	ADAM Metallopeptidase Domain 17	2	NM_003183
AICDA	Activation-induced cytidine deaminase	12	NM_020661
BTK	Bruton's tyrosine kinase	X	NM_000061
CD40LG	CD40 antigen ligand	X	NM_000074
COL7A1	Collagen VII, Alpha-1 Polypeptide	3	NM_000094
CYBA	Cytochrome b alpha chain	16	NM_000101
CYBB	Cytochrome b beta chainp91-phox	X	NM_000397
DCLRE1C	DNA cross-link repair 1c	10	NM_001033855
DOCK8	Dedicator of cytokinesis 8	9	NM_203447
FERMT1	Ferritin family member 1	20	NM_017671
FOXP3	Forkhead box P3	X	NM_014009
G6PC3	Glucose-6-phosphatase 3	17	NM_138387
GUCY2C	Guanylate cyclase 2C	12	NM_004963
HPS1	Hermansky-Pudlak syndrome type 1	10	NM_000195
HPS4	Hermansky-Pudlak syndrome type 4	22	NM_022081
HPS6	Hermansky-Pudlak syndrome type 6	10	NM_024747
ICOS	Inducible T-cell co-stimulator	2	NM_012092
IKBKG	IKK-gamma	X	NM_003639
IL2RA	Interleukin 2 receptor, alpha chain	10	NM_000417
ITGB2	Beta-2 integrin chain	21	NM_000211
LRBA	Lipopolysaccharide-responsive and beige-like anchor brotein	4	NM_001199282
NCF1	Neutrophil cytosol factor 1	7	NM_000265
NCF2	Neutrophil cytosol factor 2	1	NM_000433
NCF4	Neutrophil cytosol factor 4	22	NM_000631
PIK3R1	Phosphatidylinositol 3-kinase regulatory subunit alpha	5	NM_181504
PTEN	Phosphatase and tensin homolog	10	NM_000314 (Sample 23) NM_001304717 (sample 29)
RET	Rearranged during transfection proto-oncogene	10	NM_020975
SKIV2L	Superkiller viralicidic activity 2-like	6	NM_006929
SLC37A4	Solute carrier family 37 (glucose-6-phosphate transporter), member 4	11	NM_001467
TTC37	Tetratricopeptide repeat domain 37	5	NM_014639
WAS	Wiskott-Aldrich syndrome	X	NM_000377

AP3B1	Adaptor-related protein complex 3, beta 1 subunit	5	NM_003664
CBL	Cbl Proto-Oncogene, E3 Ubiquitin Protein Ligase	11	NM_005188
CORO1A	Coronin, actin binding protein, 1A	16	NM_007074
CTPS1	Cytidine 5′ triphosphate synthase 1	1	NM_001905
IFNGR1	Interferon gamma receptor 1	6	NM_000416
IFNGR2	Interferon gamma receptor 2 (interferon gamma transducer 1)	21	NM_005534
MAGT1	Magnesium transporter 1	X	NM_032121
PIK3CD	Phosphatidylinositol-4,5-bisphosphate 3-kinase, catalytic subunit delta	1	NM_005026
SKI	v-ski avian sarcoma viral oncogene homolog	1	NM_003036
VPS13B	Vacuolar protein sorting 13 homolog B (yeast)	8	NM_017890
NF1	Neurofibromin 1	17	NM_000267
B2M	Beta-2-microglobulin	15	NM_004048
CTC1	CTS telomere maintenance complex component 1	17	NM_025099
STK4	Serine/threonine kinase 4	20	NM_006282
CASP10	Caspase 10	2	NM_032977
CASP8	Caspase 8	2	NM_033355
FAS	Tumour necrosis factor receptor superfamily member 6	10	NM_000043
FASLG	Tumor necrosis factor ligand superfamily member 6 (FAS ligand)	1	NM_000639
NRAS	Neuroblastoma ras	1	NM_002524
SH2D1A	SH2-domain protein 1a (Slam-associated protein)	X	NM_002351
XIAP	X-linked inhibitor of apoptosis	X	NM_001167
IL10	Interleukin 10	1	NM_000572
IL10RA	Interleukin 10 receptor, alpha	11	NM_001558
IL10RB	Interleukin 10 receptor, beta	21	NM_000628
IL1RN	Interleukin 1 receptor antagonist	2	NM_173842
IL36RN	Interleukin 36 receptor antagonist	2	NM_173170
LPIN2	Lipin 2	18	NM_014646
LYN	Tyrosine-Protein Kinase	8	NM_002350

MEFV	MEditerranean FeVer	16	NM_000243
MVK	Mevalonate Kinase	12	NM_000431
NLRP12	NLR pyrin domain containing protein 12	19	NM_144687
NLRP3	NLR pyrin domain containing protein 3	1	NM_001243133
NOD2	Nucleotide-binding oligomerization domain 2	16	NM_022162
PLCG2	Phospholipase C, Gamma-2	16	NM_002661
PSMB8	Proteasome Subunit, Beta-Type, 8	6	NM_148919
PSTPIP1	Proline-Serine-Threonine Phosphatase Interacting Protein 1	15	NM_003978
RBCK1	Ranbp-Type and C3HC4-Type Zinc Finger-Containing 1	20	NM_031229
TMEM173	Transmembrane protein 173	5	NM_198282
TNFRSF1A	Tumor Necrosis Factor Receptor Super Family 1A	12	NM_001065
TRNT1	tRNA nucleotidyl transferase, CCA-adding, 1	3	NM_182916
AP1S3	Adaptor-related protein complex 1, sigma 3 subunit	2	NM_001039569
CARD14	Caspase recruitment domain family, member 14	17	NM_024110
NLRC4	NLR family, CARD domain containing 4	2	NM_021209
NLRP7	NLR family, pyrin domain containing 7	19	NM_001127255
POMP	Proteasome maturation protein	13	NM_015932
PSMA3	Proteasome (prosome, macropain) subunit, alpha type, 3	14	NM_002788
PSMB4	proteasome (prosome, macropain) subunit, beta type, 4	1	NM_002796
PSMB9	proteasome (prosome, macropain) subunit, beta type, 9	6	NM_002800
SH3BP2	SH3-domain binding protein 2	4	NM_003023
TNFAIP3	tumor necrosis factor, α–induced protein 3	6	NM_001270507
TNFRSF11A	tumor necrosis factor receptor superfamily, member 11a	18	NM_003839
PYCARD	PYD and CARD domain containing	16	NM_013258
NLRP6	NLR family, pyrin domain containing 6	11	NM_138329
C1QA	Complement component 1, q subcomponent, A chain	1	NM_015991

C1QB	Complement component 1, q subcomponent, B chain	1	NM_000491
C1QC	Complement component 1, q subcomponent, C chain	1	NM_172369
C1R	Complement component 1r	12	NM_001733
C2	Complement component 2	6	NM_000063
C3	Complement component 3	19	NM_000064
C4A	Complement component 4A	6	NM_007293
C5	Complement component 5	9	NM_001735
C6	Complement component 6	5	NM_000065
C7	Complement component 7	5	NM_000587
C8A	Complement component 8 alpha	1	NM_000562
C8B	Complement component 8 beta	1	NM_000066
C9	Complement component 9	5	NM_001737
CFH	Complement factor H	1	NM_000186
CFHR5	Complement factor H-related protein 5	1	NM_030787
CFI	Complement factor 1	4	NM_000204
CFP	Complement Factor Properdin	X	NM_002621
MASP2	Mannose-binding lectin serine protease 2	1	NM_006610
MBL2	Mannose-binding lectin	10	NM_000242
SERPING1	Serpin Peptidase Inhibitor, Clade G (C1 Inhibitor), Member 1	11	NM_000062
COL3A1	Collagen, type III, alpha 1	2	NM_000090
COL5A1	Collagen, type V, alpha 1	9	NM_000093
COL5A2	Collagen, type V, alpha 2	2	NM_000393
PLOD1	Procollagen-lysine, 2-oxoglutarate 5-dioxygenase 1	1	NM_001316320
PRF1	Perforin	10	NM_005041
SLC29A3	Solute carrier family 29 (nucleoside transporter), member 3	10	NM_018344
STX11	Syntaxin 11	6	NM_003764
STXBP2	Syntaxin binding protein 2	19	NM_006949
UNC13D	Munc-13-4	17	NM_199242
DNASE2	deoxyribonuclease II, lysosomal	19	NM_001375
LYST	lysosomal trafficking regulator	1	NM_000081
RAB27A	RAB27A, member RAS oncogene family	15	NM_004580

APOA1	Apolipoprotein A1	11	NM_000039
APOA2	Apolipoprotein A2	1	NM_001643
FGA	Fibrinogen Alpha Chain	4	NM_000508
GSN	Gelsolin	9	NM_001127662
LYZ	Lysozyme	12	NM_000239
TTR	Transthyretin	18	NM_000371
APOE	apolipoprotein E	19	NM_000041
SAA1	serum amyloid A1	11	NM_000331
SAA2	serum amyloid A2	11	NM_030754
SAA4	serum amyloid A4, constitutive	11	NM_006512
APOC3	apolipoprotein C-III	11	NM_000040
APOA4	apolipoprotein A-IV	11	NM_000482
CBS	Cystathionine beta synthase	21	NM_000071
COL4A1	Alpha-1 chain of type IV collagen	13	NM_001845
CST3	Cystatin C3	20	NM_000099
GLA	Alpha-galactosidase A	X	NM_000169
HTRA1	HtrA serine peptidase-1 gene	10	NM_002775
NOTCH3	Neutrogenic locus notch homolog protein 3	19	NM_000435
ACP5	Acid phosphatase-5/tartrate-resistant phosphatase	19	NM_001111034
ADAR	Adenosine deaminase acting on RNA	1	NM_001111
DNASE1	Deoxyribonuclease 1	16	NM_005223
DNASE1L3	Deoxyribonuclease I-like 3	3	NM_004944
PRKCD	Protein Kinase C, Delta	3	NM_006254
RNASEH2A	Ribonuclease H2 subunit A	19	NM_006397
RNASEH2B	Ribonuclease H2 subunit B	13	NM_024570
RNASEH2C	Ribonuclease H2 subunit C	11	NM_032193
SAMHD1	SAM-domain and HD-containing protein 1	20	NM_015474
TREX1	Three prime repair exonuclease 1	3	NM_016381
CECR1	Cat eye syndrome chromosome region 1/Adenosine deaminase 2	22	NM_001282225
TRAP1	Tumour necrosis factor receptor-associated protein 1	16	NM_016292
WDR1	WD Repeat containing 1/Actin-interacting protein 1	4	NM_005112
UNC13D intron 1	Munc-13-4	17	NM_199242